TRACKING ARCTIC/SUBARCTIC EXPORT PRODUCTION VARIABILITY USING COMPOUND-SPECIFIC ISOTOPE ANALYSIS OF AMINO ACIDS

by

Shaomin Chen

Submitted in partial fulfilment of the requirements
for the degree of Doctor of Philosophy

at

Dalhousie University
Halifax, Nova Scotia
January, 2024

DEDICATION PAGE

To Mom and Dad,

for your unconditional trust, support, and love.

TABLE OF CONTENTS

LIST OF TABLES

LIST OF FIGURES

ABSTRACT

The Arctic and subarctic seas have been experiencing dramatic reductions in sea ice extent as a result of climate change. Changes in sea ice extent and surface primary production are expected to impact the timing, composition, and quality of export production that supports deep-water benthic food webs, having cascading effects on energy transfer, carbon (C) cycling, and food web functioning in Arctic and subarctic ecosystems. Enhanced understanding of primary production, export production, and carbon sequestration in sea-ice influenced regions is key to predict future productivity and community responses to the changing climate. The traditional approach to interpret stable isotope values of bulk organic materials has been widely used to study organic matter sources and cycling in different ecosystems. However, bulk stable isotopes can be difficult to interpret due to variations in source signatures and effects of metabolic processes, trophic transfer, and microbial alteration. Stable isotope values of carbon and nitrogen ($\delta^{13}C$ and $\delta^{15}N$) in amino acids (AAs) have been proven to provide specific information about C and N sources, shifts in nutrient sources, and physiological and heterotrophic processing of the organisms. Compound-specific isotope analysis (CSIA) of AAs has emerged as a powerful tool for tracing organic C and N in marine food webs, sinking particles, and ancient sediments, allowing for more accurate interpretation of stable isotope data.

With the novel CSIA-AA techniques, this thesis investigates different components of the biological pump in the Canadian Arctic and subarctic seas: sea ice algae and pelagic algae, exported sinking particles, and archived marine sediments. Chapter 2 explores differences in $\delta^{13}C$-AA and $\delta^{15}N$-AA signatures between sea ice and pelagic algae collected in Canadian Arctic and subarctic seas. For the first time, distinct $\delta^{13}C$-EAA fingerprints and different degrees of heterotrophic reworking are revealed between sea ice and pelagic algae. These results highlight the potential of CSIA-AA to trace C sources from sea ice and pelagic origins and to evaluate the efficiency of the biological pump in polar marine environments. Building on these findings, Chapter 3 applies CSIA-AA proxies on a two-year time-series of exported sinking particles collected in sediment traps in the northwestern Labrador Sea to explore the sources and composition of organic C and N in sinking OM. I reveal that sea ice algae and exported zooplankton fecal pellets can be a critical source of C and N for benthic fauna. Chapter 4 reports the first coupled AA $\delta^{13}C$ and $\delta^{15}N$ sediment core records spanning most of the Holocene period in northeastern Baffin Bay. I demonstrate robust long-term preservation of CSIA-AA proxies despite noticeable alteration in AA concentrations. These results expand limited existing CISA-AA data on multi-millennial sediments from temperate seas to polar regions and highlight the potential of AAs as reliable tracers to provide novel information for longer-term paleo-reconstruction. Together, this thesis paves the way for the use of a newly developed biomarker for sea ice algae and other existing CSIA-AA proxies that are proven to be reliable OM tracers across different sedimentary regimes and time scales in ice-covered Arctic and subarctic seas, which is essential for predicting future responses of Arctic/subarctic ecosystems to long-term climate change.

LIST OF ABBREVIATIONS USED

∑V	The Average Deviation of $\delta^{15}N$ Values of Trophic Amino Acids
AA	Amino Acid
BIC	Baffin Island Current
BP	Before the Present
C	Carbon
CCGS	Canadian Coast Guard Ship
CO_2	Carbon Dioxide
CSIA	Compound-Specific Isotope Analysis
DCM	Deep Chlorophyll Maximum
DI	Degradation Index
DIC	Dissolved Inorganic Carbon
DOM	Dissolved Organic Matter
EAA	Essential Amino Acid
GC-IRMS	Gas Chromatography-Isotope Ratio Mass Spectrometry
HBI	Highly Branched Isoprenoid
IP_{25}	Isoprenoid with 25 Carbon Atoms
LC	Labrador Current
LDA	Linear Discriminant Analysis
N	Nitrogen
N_2	Nitrogen Gas
NEAA	Non-Essential Amino Acid
NO_3	Nitrate
OM	Organic Matter
PCA	Principal Component Analysis
PN	Particulate Nitrogen
POC	Particulate Organic Carbon
POM	Particulate Organic Matter
SrcAA	Source Amino Acid
THAA	Total Hydrolysable Amino Acid
TP	Trophic Position

TPM	Total Particulate Matter
TrAA	Trophic Amino Acid
WGC	West Greenland Current

ACKNOWLEDGEMENTS

First and foremost, I would like to express my deepest gratitude to my supervisor, Dr. Owen Sherwood. Thank you so much for providing me with this incredible opportunity to work on this project. Your unfailing support and continuous encouragement have been invaluable throughout my academic journey. Your dedication to fostering an environment of intellectual curiosity and your willingness to share your wealth of knowledge have not only enriched my project but have also significantly contributed to my growth as a scholar.

I want to extend my heartfelt appreciation to the members of my committee, Dr. John Gosse, Dr. Markus Kienast, Dr. Zoe Finkel, and Dr. Peta J. Mudie. Your collective expertise and insightful advice have played a significant role in refining my research. I am truly grateful for the time and effort you have invested in this journey with me.

This work would not have been possible without my collaborators, Dr. Peta J. Mudie, Dr. Thibaud Dezutter, Dr. David Cote, Dr. Evan Edinger, Dr. Catherine Lalande, and Dr. Audrey Limoges. Special thanks go to Dr. C. J. Mundy from University of Manitoba for providing fast-ice algae samples and valuable insights on sea ice algae and statistics, Dr. Thomas Larsen, Dr. Matthew McCarthy, and Dr. Kelton McMahon for valuable discussions about the analyses and data, Shawn Meredyk from Amundsen Science for leading mooring deployments and recoveries, Dr. Maxime Geoffroy, Eugenie Jacobsen, and Jordan Sutton for helping with zooplankton sampling, Claire Normandeau for bulk stable isotope analyses, and Dr. Karen Stamieszkin for valuable discussion about zooplankton analyses.

I gratefully acknowledge the captain, officers, crew, and scientists onboard the Canadian Coast Guard Ship *Amundsen* for their professional support with sea ice, seawater, zooplankton sampling and the recovery of moorings and sediment core. I also want to thank current and past members of the Sherwood lab: Amy McAllister, Blake Tibert, Chelsea Fougère, Chukwuka Orji, Kerri J. Smith, Nina Golombek, Rachel N. Noddle, Simone Booker, and Wilder Greenman, for enthusiastic discussions, insightful feedback, technical assistance, and genuine support.

Last but not least, I would like to thank my family and friends for their love and support throughout the years. Mom, you stand as my ultimate inspiration, shaping my journey to become a resilient and empowered woman. Dad, your encouragement to embrace challenges and fearlessness has been a guiding force in my life. Jack, thanks for everything, for the tears, the laughs, and the memories we've made together. Words cannot describe how thankful I am to have you in my life. A special shout out goes to XG: your music and performances are a source of inspiration, filling my days with the power of hard work, courage, hope, and joy.

CHAPTER 1 INTRODUCTION

1.1 Overview

The overall goal of this thesis is to develop and apply a novel biogeochemical proxy to investigate the composition of export production in Arctic and subarctic seas.

Accelerating warming and sea ice reduction are expected to affect the timing, quantity, and quality of primary, secondary, and export production in the Arctic and subarctic seas. The thinning and loss of sea ice represents a habitat loss for sea-ice algae, which are a major contributor to primary production and important food sources to the sea ice, pelagic, and benthic food webs, and ultimately impacts human communities that rely on marine food resources in ice-covered regions.

To evaluate the role that sea ice algae play in export production, first, we need a biogeochemical proxy that can detect the presence of sea ice algae in detrital materials. Second, this proxy should be able to quantify the proportional contribution of sea ice algae versus other major components in export production (pelagic algae, zooplankton, and zooplankton fecal pellets). Finally, this proxy should be well preserved over long time scales in ancient marine sediments and biological archives such as long-lived deep-sea corals.

Here I leverage the novel technique of compound-specific isotope analysis of amino acids (CSIA-AA). CSIA-AA proxies have been extensively applied to cultured or field collected pelagic algae, zooplankton, and zooplankton fecal pellets from a wide range of geographical locations but never to sea ice algae, exported sinking particles, and ancient marine sediments from the eastern Canadian subarctic and Arctic seas.

The geographical focus of this thesis is the eastern Canadian subarctic and Arctic seas, from northwest Labrador Sea to Baffin Bay, driven largely by ship-time availability on the Canadian Coast Guard Ship *Amundsen.*

The research content of this thesis is organized into three chapters, each investigating the baseline signatures and the composition of 1) surface water primary

production, 2) exported sinking particles, and 3) a sediment core spanning the past ca. 9,000 years.

1.2 Biological Pump in the Arctic and Subarctic Seas

The ocean sequesters one-fourth to one-third anthropogenic carbon dioxide (CO_2) from the atmosphere each year (Sabine et al., 2004; Sabine and Tanhua, 2010). This is done by two principal mechanisms: the biological pump and the solubility pump (Fig. 1.1). The biological pump refers to biologically driven or mediated processes that transport photosynthetically fixed carbon (C) from the ocean's euphotic zone to deeper waters via passive sinking, advection or vertical mixing, and animal transport (Fig. 1.1; Turner, 2015). The solubility pump refers to air-sea exchange of atmospheric CO_2 into dissolved inorganic carbon (DIC) and the subsequent downwelling into the ocean interior (Fig. 1.1; Volk and Hoffert, 1985). The biological pump accounts for two thirds of oceanic CO_2 sequestration and the solubility pump accounts for the other third (Gruber and Sarmiento, 2002; Reid et al., 2009). The efficiency of the biological pump is quantified as the fraction of net primary production that leaves the euphotic zone (i.e., "export efficiency") multiplied by the fraction of exported production that makes it to a specified reference depth (i.e., "transfer efficiency"; Buesseler and Boyd, 2009; Buesseler et al., 2020). The total efficiency is controlled by a wide range of physical, chemical, and biological processes, such as nutrient availability, the composition of sinking particles, aggregation and disaggregation processes, microbial degradation, and zooplankton grazing and fecal pellet production (Fig. 1.1; De La Rocha and Passow, 2007). For most of the open ocean, biological pump efficiency is about 5–25% immediately below the euphotic zone and only about 1–3% in the deep sea (Buesseler, 1998; De La Rocha and Passow, 2007). There is considerable regional and temporal variability in the efficiency, with higher export and transfer during spring blooms and on productive shelves in polar seas (> 10–100%; Buesseler, 1998)

Rising anthropogenic CO_2, temperature, ocean stratification and acidification, and changing nutrient availability are predicted to impact the biological pump efficiency by altering surface phytoplankton abundance, composition, and phenology, and modifying the quantity, quality, and composition of exported organic matter (De La Rocha and

Passow, 2007; Finkel et al., 2010; Passow and Carlson, 2012; Arrigo and van Dijken, 2015; Turner, 2015; Durkin et al., 2016). However, sampling and accessibility challenges in the open ocean have left fundamental aspects of biological pump functioning under-constrained, especially over seasonal and longer timescales. These challenges are even greater in polar seas, which are particularly sensitive to climate change due to unique oceanographic conditions (sea ice, snow and solar dynamics, freshwater input, deep water convection, etc.; Wassmann, 2011, Passow and Carlson, 2012). An improved mechanistic understanding of different components in the biological pump, including the contribution of sea ice algae to export productivity and the role of bacterial heterotrophy in altering the composition of sinking particles is necessary to better predict future trends in global and regional biological pumping and to help inform climate mitigation and adaptation policies.

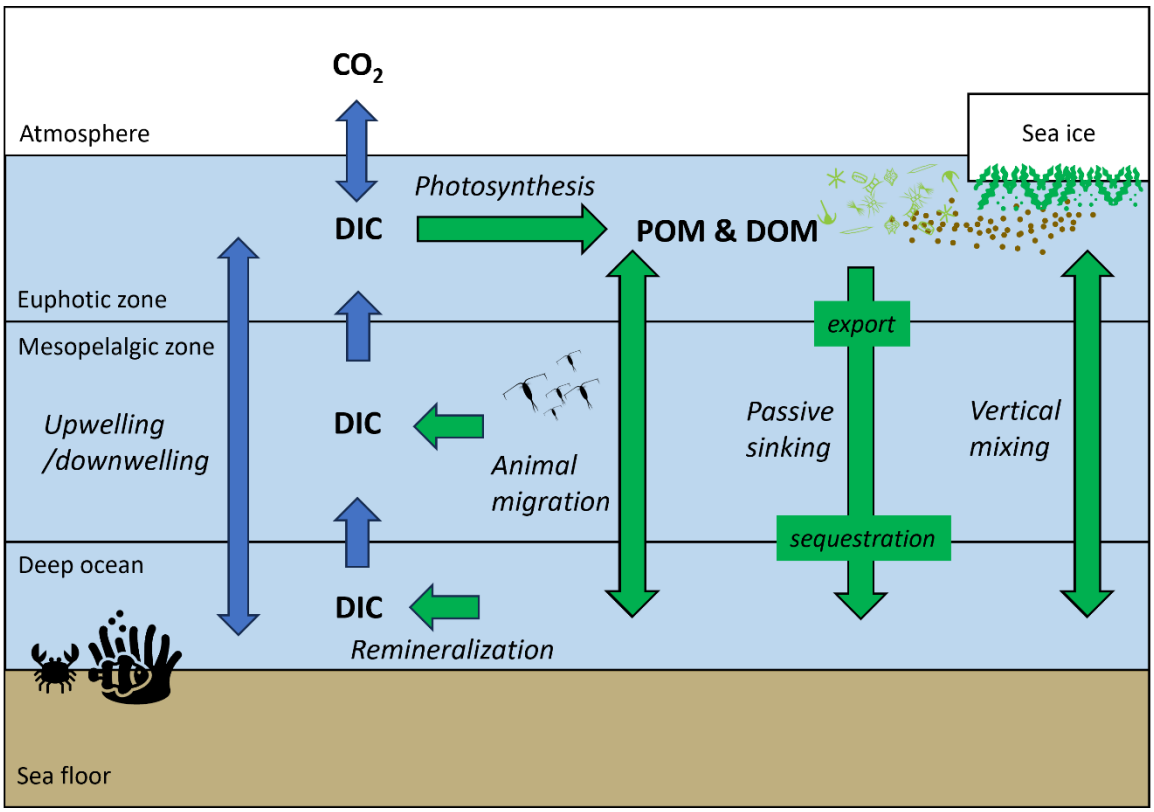

Figure 1.1 Simplified schematic of the biological (green arrows) and the solubility (blue arrows) pumps in Arctic/subarctic seas modified from Passow and Carlson, 2012. Particulate and dissolved organic matter (POM and DOM) produced via photosynthesis of carbon dioxide (CO_2) are transported to depth via migrating animals, passive sinking, and advection or vertical mixing. The sinking flux of POM and DOM decreases with depth with POM and DOM remineralized

back into dissolved inorganic carbon (DIC). Primary production transported below the euphotic zone is termed export production, whereas that transported below mesopelagic zone is called sequestration.

The Arctic and subarctic seas include the Arctic Ocean, comprising deep basins surrounding the north pole and encircled by broad continental shelves of Europe, Russia, Alaska, Canada, and Greenland (Coachman and Aagaard, 1974), and its marginal seas located between 50°N and 70°N (Fig. 1.2). Despite the relatively small size (3% of Earth's surface), the Arctic Ocean, as well as its marginal subarctic seas, plays an important role in global carbon uptake through surface water cooling, sea ice dynamics, and intense primary production on extensive shelf seas (Aagaard and Carmack, 1989; Kaltin et al., 2002; Anderson et al., 2004; Kaltin and Anderson, 2005; MacGilchrist et al., 2014). Cooling of low saline surface water increases CO_2 solubility, drawing down more CO_2 from the atmosphere whereas sea ice formation, cover, and melting affect air-sea exchange of CO_2 in different ways (Kaltin et al., 2002; Anderson et al., 2004). Intermediate and deep-water formation transports part of the dissolved CO_2 to deeper layers that have a longer residence time compared to surface and halocline layers in Baffin Bay (Top et al., 1980) and the Arctic shelves (Becker and Björk, 1996). The local and seasonal uptake of CO_2 is further amplified by the intense primary production on Arctic shelves: for example, the biological pump was found to be almost twice as effective as the solubility pump in drawing down CO_2 on the highly productive Bering-Chukchi shelves (Kaltin and Anderson, 2005).

The Arctic and subarctic seas are characterized by long, cold winters, short, cool summers, and permanent or seasonal sea ice covers due to seasonal extremes of solar radiation (Coachman and Aagaard, 1974; Hanna et al., 2021). Sea ice is formed by the freezing of seawater and is further modified by physical, chemical, and biological processes. Small ice crystals (frazil) first form in the water column when temperatures drop to the freezing point, and later float to the surface, accumulate and further freeze together into a contiguous ice sheet (Mundy and Meiners, 2021). Once ice sheets are formed, they can continue to grow in the winter as first-year ice and start to melt with increasing temperatures in spring and summer. If the ice is thick enough and survives the melt seasons, it is classified as multiyear ice (Mundy and Meiners, 2021). Both first-year

and multiyear ice provide a range of habitats for sea ice algae (Smith et al., 1990) and ice-associated grazers (e.g., amphipods and fish; Lønne and Gulliksen, 1991; Hop et al., 2000; Gradinger and Bluhm, 2004) and foraging, reproduction, and resting grounds for marine vertebrates (e.g., polar bears and ringed seals; Post et al., 2009, 2013).

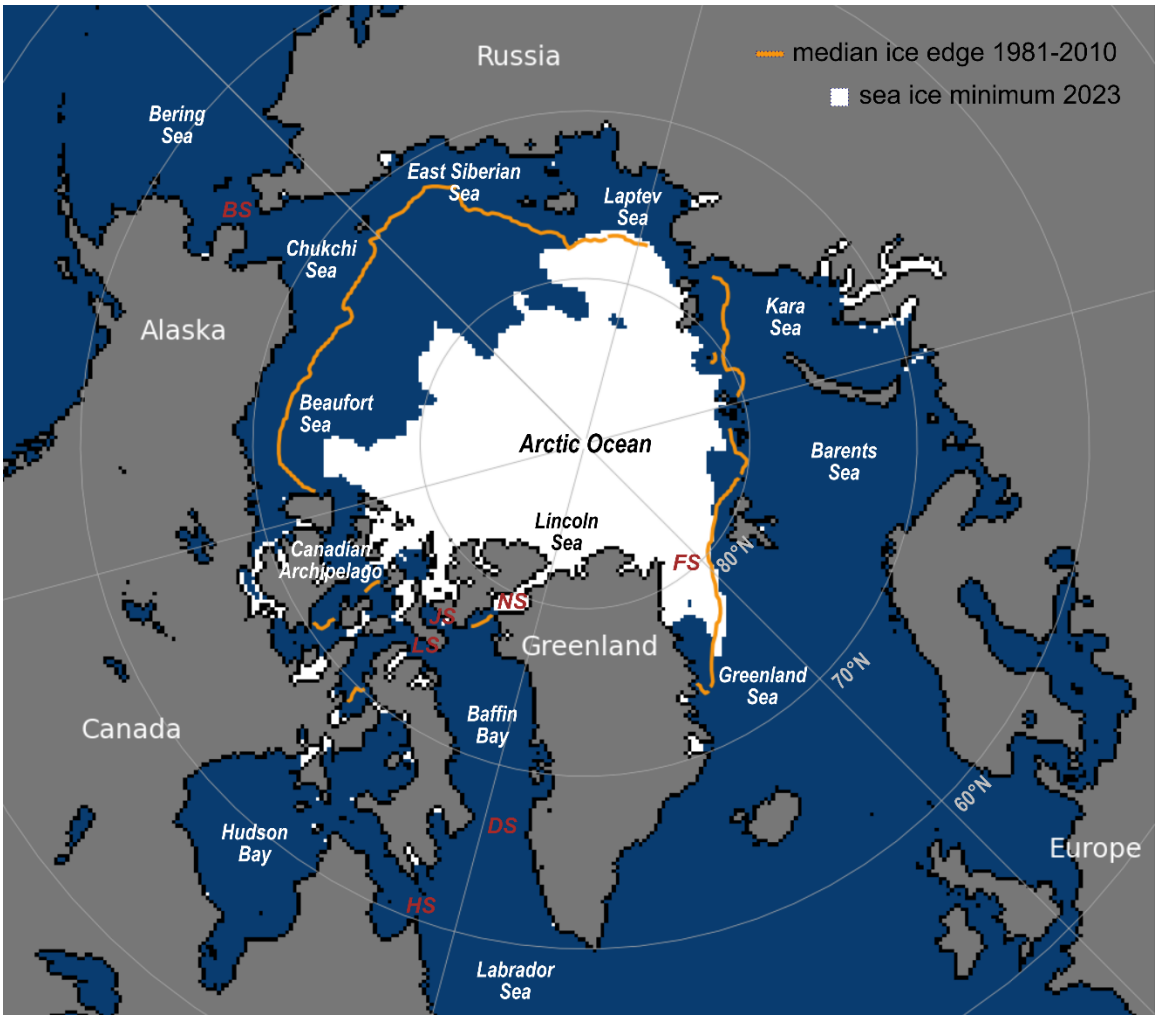

Figure 1.2 The Arctic Ocean and major subarctic seas. The white area shows Arctic sea ice extent for September 19, 2023 (sea ice minimum). The orange line shows the 1981 to 2010 average extent for that day. Figure modified from National Snow and Ice Data Center (Fetterer et al., 2017). BS, Bering Strait; DS, Davis Strait; FS, Fram Strait; HS, Hudson Strait; JS, Jones Sound; LS, Lancaster Sound; NS, Nares Strait.

Sea ice algae are a major contributor to primary production in Arctic and subarctic seas, especially in central Arctic Ocean with year-round multiyear ice (up to 60%; Legendre et al., 1992; Gosselin et al., 1997). Light is the main limiting factor of primary production in ice-covered Arctic/subarctic seas, which is not available (or very

limited) during late fall, winter, and early spring due to annual polar darkness and light attenuating snow and ice covers (Berge et al., 2015; Mundy and Meiners, 2021). Sea ice algae are adapted to grow at low-light conditions, freezing temperatures, and wide salinity gradients that fluctuates with ice melting and forming (Kirst and Wiencke, 1995; Lizotte, 2003; Janech et al., 2006; Bayer-Giraldi et al., 2011). In winter, sea ice algal biomass remains low due to low temperature and solar irradiance. With increase in day length and solar radiance and thinning of snow cover and sea ice, sea ice algal blooms occur first before phytoplankton (pelagic algae) blooms in the water column, mostly in the lower-most part of sea ice and in the ice-water interface (Fig. 1.3; Leu et al., 2015). The two most important representatives of sea ice algae in the Arctic and subarctic seas are *Nitzschia frigida*, a pennate diatom often dominating algal blooms in first-year ice, and *Melosira arctica*, a centric chain-forming diatom that can produce concentrated aggregates beneath multiyear ice and first-year ice (Leu et al., 2015; Mundy and Meiners, 2021). Towards summer, with further increase in air temperature and solar radiation, sea ice and snow cover begin to reduce, followed by the onset of pelagic algae blooms (Fig. 1.3; Leu et al., 2011, 2015). Sea ice algal biomass is either released to the water column by ice melting or maintained by the insulating snow layer that delays the melt process (Fig. 1.3; Fortier et al., 2002; Mundy et al., 2005; Campbell et al., 2015). During ice-free seasons, nutrients become limited due to the intense stratification of surface waters associated with freshwater discharge from sea-ice melt (Arrigo et al., 2008; MacGilchrist et al., 2014). The timing of sea ice algae and pelagic algae growth is critical for the quantity and quality of primary and secondary production, and for the energy transfer to higher trophic levels (Søreide et al., 2010). The production of sea ice algae is patchy and highly variable in the Arctic/subarctic seas, averaging 5–10 g C m^{-2} yr^{-1} while that of phytoplankton averages 12–50 g C m^{-2} yr^{-1}, depending on the latitude and the length of ice-free seasons (Legendre et al., 1992; Gosselin et al., 1997; Leu et al., 2011). In areas with extensive sea ice cover, sea ice algal production is of greater importance of the total primary production (Gosselin et al., 1997). Sea ice algae are important food sources for sea-ice, pelagic, and benthic grazers (Werner, 1997; Renaud et al., 2007; Søreide et al., 2010; Leu et al., 2011). Isoprenoid biomarkers have revealed a high contribution of ice-algae produced carbon to both pelagic and sea-ice food webs: 23–48% in pelagic

zooplankton, 58–92% in sea-ice associated zooplankton, and 72–100% in polar bears (Kohlbach et al., 2016). Taken together, changes in sea ice extent and dynamics are expected to impact the solubility pump by affecting air-sea exchange of CO_2, light and nutrient availability for primary production, timing, quantity, and quality of primary and secondary production, efficiency of biological pump (export production and sequestration), habitats and food sources for sea ice, pelagic, and benthic organisms, and thus have cascading effects on the overall Arctic/subarctic productivity and ecosystem functioning.

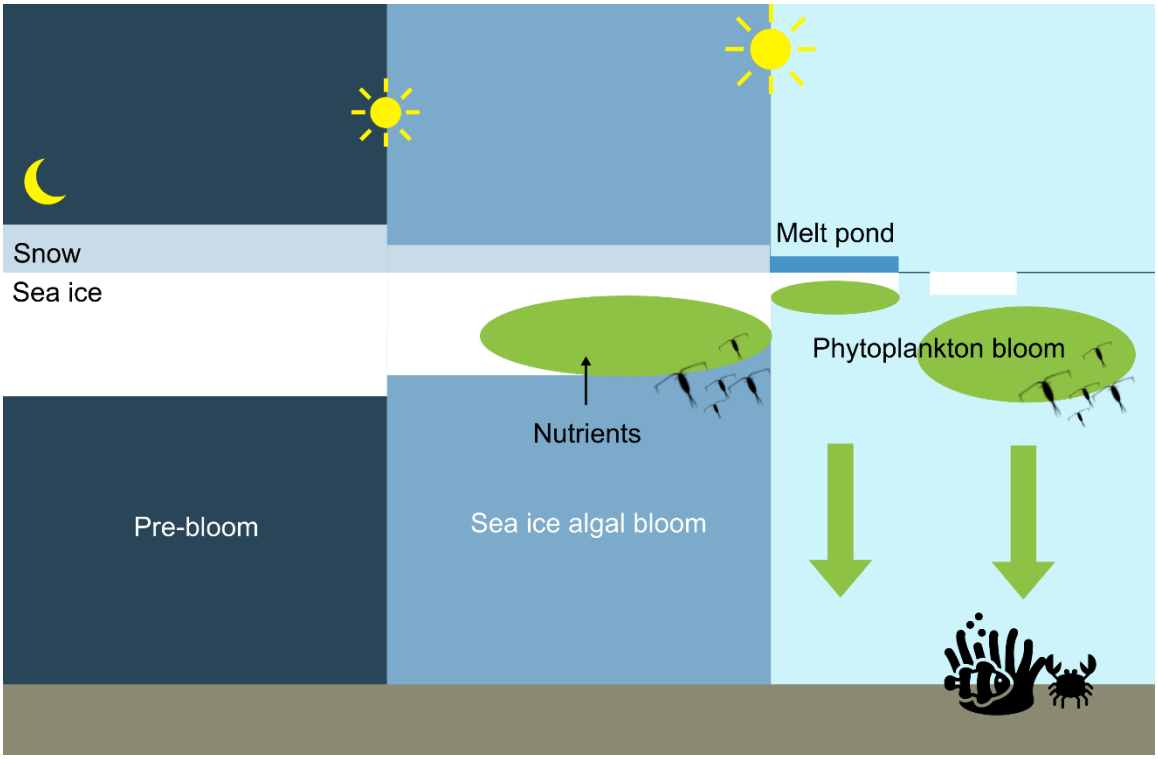

Figure 1.3 Simplified schematic of three developmental phases of sea ice algal and phytoplankton (pelagic algae) blooms from winter to spring in Arctic/subarctic seas. Figure modified from Leu et al., 2015.

The Arctic and subarctic oceans have been experiencing dramatic changes as a result of climate change since the industrial era. The average monthly sea ice extent in September has been declining on average at a rate of 12.5% per decade from 1979 to 2023 (Fig. 1.2; Sea Ice Index, Version 3. Fetterer et al., 2017). The reduction in sea ice extent is accompanied by younger and thinner ice, freshening surface water, and less ice-covered area in the Arctic, which affects light penetration, nutrient availability and

density stratification in the water column (Post et al. 2013; Meredith et al., 2019). As a result, the decline in sea ice has caused an increase in pelagic (open-sea) primary production, a reduced surface nutrient availability, and a shift in plankton community structure toward smaller-size picoplankton (Arrigo and van Dijken 2015; Li et al. 2009). Further, the loss of sea ice represents a habitat loss for highly productive sea-ice algae, which are a major contributor to primary production in the Arctic and subarctic seas (Legendre et al., 1992; Gosselin et al., 1997). Recent studies also pointed out that changes in timing, duration, and magnitude of sea ice and pelagic algal blooms due to the loss of sea ice may induce potential mismatches for the timing of zooplankton production and hence alter the quantity and quality of secondary production, biomass and energy transfer to higher trophic levels, and biological pump efficiency in the Arctic and subarctic seas (Post et al., 2013; Leu et al., 2011, 2015). Enhanced understanding of primary production, export production, and sequestration in sea-ice influenced regions is key to predict future productivity and community responses in the changing Arctic and subarctic seas.

1.3 Compound-specific Isotope Analysis of Amino Acids

The use of stable carbon and nitrogen isotopes ($\delta^{13}C$ and $\delta^{15}N$) on bulk organic matter (OM) is well established in marine biogeochemistry and ecology studies to explore source-sink and process information of C and N in marine primary production, export production, and sequestration (Peterson and Fry, 1987; Altabet et al., 1999). The δ notation describes the relative difference (in parts per thousand; reported in ‰ or per mil) of the isotopic ratios (e.g., $^{13}C/^{12}C$, $^{15}N/^{14}N$) of a sample and an internationally accepted standard (Vienna PeeDee Belemnite for $\delta^{13}C$ and the nitrogen gas (N_2) in air for $\delta^{15}N$; Peterson and Fry, 1987). $\Delta^{13}C$ and $\delta^{15}N$ of marine OM are primarily controlled by 1) source variability and the degree of utilization by autotrophs (Altabet and Francois, 1994; Waser et al., 1998), 2) trophic transfers (Fry, 1988), 3) biochemical composition (Abelson and Hoering, 1961; DeNiro and Epstein, 1977; Hayes, 2018), and 4) microbial degradation (Freudenthal et al., 2001). In food web studies, $\delta^{13}C$ and $\delta^{15}N$ values of primary producers are known as “baseline isotope values” and vary in space and time, influenced by physiological differences in species and environmental parameters such as

temperature, CO_2 and nitrate concentrations (Peterson and Fry, 1987; Altabet and Francois, 1994; Goericke and Fry, 1994; Needoba et al., 2003). When baseline C and N isotopes are integrated into consumer tissues through diet, mixing of various diet sources leads to alterations in $\delta^{13}C$, while metabolic fractionation causes enrichment in $\delta^{15}N$ (Peterson and Fry, 1987; Fry, 1988). Therefore, isotopic values of marine consumers and detrital materials record changes in source contribution and trophic transfers (Peterson and Fry, 1987; Altabet and Francois, 1994; Goericke and Fry, 1994). In marine environments, bulk stable isotope values of OM represent a mixture of sources and processes and thus are difficult to interpret (Boecklen et al., 2011). For example, it can be difficult to determine whether changes in the bulk stable isotope values in a consumer is caused by its trophic position or changes in the baseline level, or both (Post, 2002). Additional complications arise when the material is subject to microbial degradation (Harvey and Macko, 1997; Freudenthal et al., 2001). Microbes consume detrital OM through the release of extracellular hydrolytic enzymes, which favor the breakage of chemical bonds containing isotopically lighter isotopes (Silfer et al., 1992). To address the confounding issues in bulk stable isotope measurements, compound-specific isotope analysis (CSIA) is increasingly used in biogeochemical and ecological studies, which measures the isotope values of individual monomers that form a macromolecule (e.g., amino acids in protein).

Amino acids (AAs) are the major form of nitrogen (N) and organic C found in both living organisms and non-living organic matter (OM) and thus represent important fractions in plankton, bacteria, and marine sediments in the ocean (Cowie and Hedges, 1992; Hedges et al., 2001). For example, AAs typically comprise a dominating portion of the characterizable OM from surface plankton (> 60%) to deep sediments (> 50%) during progressive degradation with depth in the Pacific Ocean (Fig. 1.4; Wakeham et al., 1997; Middelburg, 2019). Recent advances in gas chromatography-isotope ratio mass spectrometry (GC-IRMS) have made CSIA-AA a powerful tool for tracing organic C and N in food webs (Larsen et al. 2013). Interpretation of $\delta^{13}C$ is based on the classification of AAs into essential and non-essential groups according to their dietary requirements by animals (Karasov and del Rio, 2007; Larsen et al., 2013; McMahon et al., 2013). Carbon skeletons of essential amino acids (EAAs: phenylalanine, threonine, isoleucine, leucine,

and valine) can only be synthesized by plants and bacteria de novo. Consumers cannot synthesize EAAs in adequate amounts to support growth and maintenance, and thus EAAs in consumer tissues are directly acquired from their diet with minimal changes to the C skeletons ("dietary routing"; O'Brien et al., 2002; Wu, 2009). Thus, $\delta^{13}C$ values of EAAs remain unchanged when EAAs are entirely incorporated into consumers' tissues (McMahon et al., 2010, 2013; Larsen et al., 2013), while non-EAAs can be synthesized de novo (e.g., from isotopically distinct carbohydrates or lipids) and their $\delta^{13}C$ values undergo large fractionations during de novo biosynthesis (McMahon et al., 2010, 2013). In autotrophs, the diverse biosynthetic pathways and associated isotopic effects between different phylogenic groups (e.g., terrestrial plants, fungi, eukaryotic microalgae, and bacteria) lead to distinct and consistent $\delta^{13}C$-EAA patterns, which are passed, unaltered, to higher trophic levels and eventually preserved in paleo-archives such as proteinaceous deep-sea corals and marine sediments (Larsen et al. 2015; McMahon et al. 2015). As a result, $\delta^{13}C$-EAA patterns in consumers record the isotopic signatures of primary producers fueling the food web.

Interpretation of $\delta^{15}N$ is based on different groupings that are independent of those based on $\delta^{13}C$. $\delta^{15}N$-AA values in autotrophs mainly derive from transamination of individual AA from the central glutamate pool (Macko et al., 1986). When incorporated into consumers or detrital OM, the autotrophic baseline signatures are altered due to trophic transfers or microbial degradation (Keil and Fogel, 2001; McCarthy et al., 2013). Different classes of AAs undergo different degrees of alteration: The $\delta^{15}N$ values of "source" AAs (SrcAAs: phenylalanine and lysine) undergo little or no $\delta^{15}N$ enrichment during trophic transfers and hence preserve baseline N values. $\delta^{15}N$-Phenylalanine is proven to be the most reliable baseline N proxy for not only animals (McClelland & Montoya, 2002; Chikaraishi et al., 2009), but for heterotrophic protists (Gutiérrez-Rodríguez et al., 2014; Décima et al., 2017), heterotrophic bacteria, fungi, and archaea (Yamaguchi et al., 2017), and plant materials (Fogel and Tuross, 1999). By contrast, the $\delta^{15}N$ values of "trophic" AAs (TrAAs: glutamine/glutamic acid, asparagine/aspartic acid, alanine, leucine, isoleucine, proline, and valine) become enriched with increasing trophic position or microbial processing (McClelland & Montoya, 2002). The decoupled changes in $\delta^{15}N$ of SrcAAs and TrAAs enable direct estimation of trophic position, and the

scattering patterns of TrAAs have been proposed as a new proxy for the extent of microbial resynthesis (McClelland and Montoya, 2002; McCarthy et al., 2007, 2013; Popp et al., 2007; Chikaraishi et al., 2009; Hannides et al., 2009, 2013; Nielsen et al., 2015). Hence, the complementary but fully independent δ^{13}C-AA and δ^{15}N-AA analyses provide detailed information about C and N sources, trophic changes, and microbial modification in marine OM and allow for more accurate interpretation of stable isotope data (McMahon et al., 2013; McMahon & McCarthy, 2016).

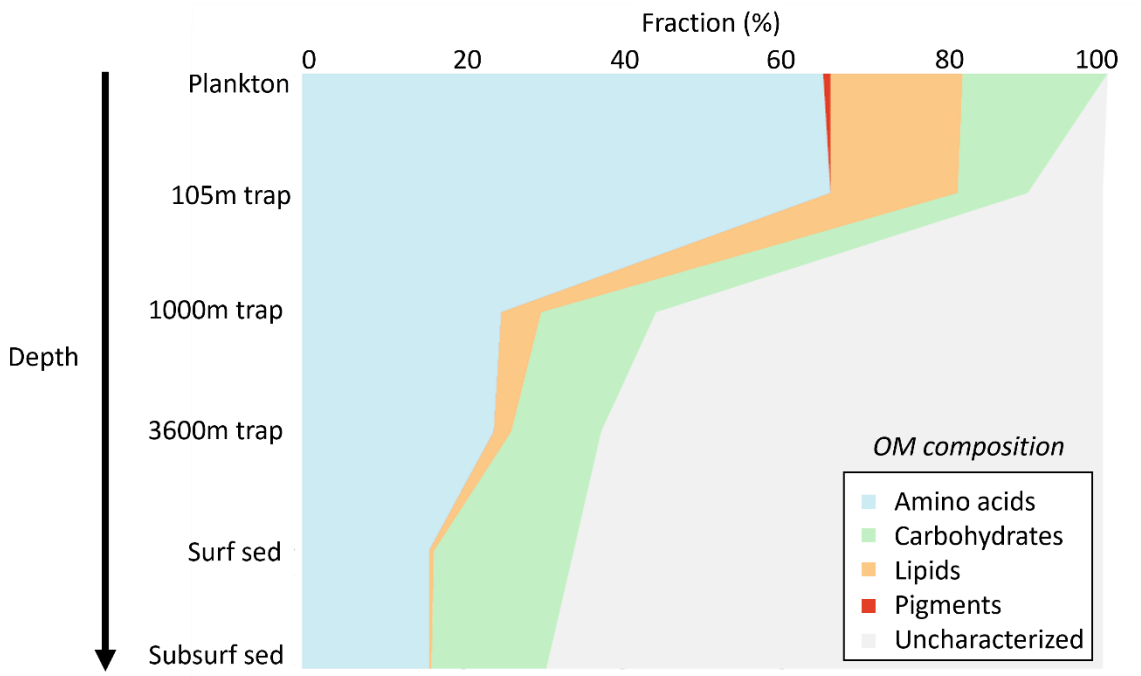

Figure 1.4 Changes in the biochemical composition of organic matter (OM) during progressive degradation from surface plankton and sediment traps at different depths to surface and subsurface sediments in the Pacific Ocean (Wakeham et al., 1997). Figure modified from Middelburg, 2019.

Compared to bulk stable isotopes, CSIA-AA requires a larger sample size for analysis: approximately 5–10 mg of organic carbon per sample was required for δ^{13}C-AA and δ^{15}N-AA analyses versus only about 0.1–0.3 mg for bulk stable isotope analysis. AAs are extracted from the samples and purified by acid hydrolysis and cation-exchange chromatography (Ohkouchi et al., 2017). The extracted AAs are converted into volatile derivatives by derivatization, which includes esterification and acylation using isopropanol and trifluoroacetic acid anhydride respectively (Silfer et al., 1991; Ohkouchi

et al., 2017). The volatile derivatives are then separated by the Gas Chromatography (GC) and converted into CO_2 or N_2 gas by combustion, allowing for continuous flow measurement of $^{13}C/^{12}C$ on the CO_2 gas or $^{15}N/^{14}N$ on the N_2 gas by the Isotope Ratio Mass Spectrometry (IRMS; Meier-Augenstein 1999). A total of twelve AAs is typically resolved: alanine (Ala), glycine (Gly), proline (Pro), valine (Val), leucine (Leu), isoleucine (Ile), asparagine + aspartic acid (Asx), threonine (Thr), serine (Ser), glutamine + glutamic acid (Glx), phenylalanine (Phe), and lysine (Lys). Final $\delta^{13}C$ values are corrected for the isotopic fractionation and the introduction of C atoms during derivatization according to Silfer et al. (1991) and normalized against instrument drift between successive triplicate injections of the AA standard by applying linear regression. Final $\delta^{15}N$ values are calibrated based on the offset between known and measured values of calibrated standards and normalized against instrument drift by applying linear regression (Yarnes and Herszage, 2017). In this thesis, the reproducibility of AA calibration standards ranges from 0.2‰ to 0.8‰ for both $\delta^{13}C$ and $\delta^{15}N$.

1.4 Objectives

As a key component of Arctic and subarctic primary and export production, sea ice algae are relatively understudied compared to pelagic algae. Data on sea ice algal dynamics have become more widely available since the 1990s but the number of field studies are still limited due to the difficulties in accessing sea ice environments and sampling under-ice algae (Legendre et al., 1992; Gosselin et al., 1997). Current estimates on Arctic and subarctic productivity mainly rely on satellite observations, which cannot account for under-ice algal growth and phytoplankton blooms (Mundy et al., 2009; Arrigo et al., 2012; Arrigo and van Dijken, 2015; Ardyna et al., 2020), and thus Arctic productivity may be drastically underestimated. Existing biomarkers for sea ice algae are either confounded by high uncertainties (bulk $\delta^{13}C$; Pineault et al., 2013; Søreide et al., 2013; De La Vega et al., 2019) and rapid degradation (fatty acids; Søreide et al., 2013; Kohlbach et al., 2016; Middelburg, 2019), or cannot provide community-level information on sea ice algal production, as is the case for biomarkers that are species specific (highly branched isoprenoids; Belt et al., 2007; Belt and Müller, 2013; Brown et al., 2014). Hence, additional ice-algal specific and well-preserved biomarkers are needed

for enhancing understanding of sea ice algal dynamics in the changing Arctic and subarctic seas.

Exported sinking particles are typically collected, measured, and characterized using moored sediment traps (Honjo and Doherty, 1988). Extensive effort has led to an improved understanding of regional fluxes and composition of exported particles in Beaufort Sea (Carey, 1987; Forbes et al., 1992; Lalande et al., 2009a), Canadian Arctic Archipelago (Hargrave et a., 1989, 1994; Dezutter et al., 2021), northern Baffin Bay (Hargrave et al., 2002; Lalande et al., 2009a), Laptev Sea, and East Siberian Sea (Lalande et al., 2009a, b, 2019). Nevertheless, challenges remain to describe organic matter composition in sediment traps: microalgae and zooplankton counts are time-consuming and labour-intensive, which can be complicated by large morphological variability within and between species, lack of taxonomic expertise, and inconsistency in identification methods (McQuatters-Gollop et al., 2017). Applications of CSIA-AA on exported sinking particles collected by moored sediment traps are scarce (e.g., Shen et al., 2021). An improved quantification of exported sinking particles is key to predicting future responses of Arctic/subarctic biological pump, marine ecosystems, and benthic communities to a rapidly changing climate.

Baffin Bay is a semi-enclosed deep basin (> 2,300 m) that is almost completely covered by sea ice from December to April (as of 2023, National Snow & Ice Data Center; Tang et al., 2004), connecting the Arctic to the subarctic Labrador Sea and the North Atlantic (Fig. 1.1). Thus, it is a good location to study past biogeochemical and ecological changes in response to sea ice dynamics in a mid-Arctic region. A number of studies on sediment cores from northeastern Baffin Bay have been conducted to investigate changes in oceanic conditions over the Holocene (0–11,700 yrs) period (e.g., Levac et al., 2001; Mudie et al., 2005; Knudsen et al., 2008; St-Onge and St-Onge, 2014; Caron et al., 2019a, b; Giraudeau et al., 2020; Hansen et al., 2020; Limoges et al., 2020; Saini et al., 2020; Jackson et al., 2021). However, applications of CSIA-AA proxies on ancient marine sediments are scarce, from only a few locations (Peru margin: Larsen et al., 2015; eastern tropical Pacific: Sauthoff, 2016; North Pacific: Batista et al., 2014; North Pacific and Pacific Arctic: Choi et al., 2022), but never from Baffin Bay.

With the novel CSIA-AA techniques, this thesis investigates different components of the biological pump in the Canadian Arctic and subarctic seas: sea ice algae and pelagic algae, exported sinking particles, and archived marine sediments. The focus of the study is to develop a new biomarker for Arctic/subarctic sea ice algae using CSIA-AA and to evaluate the fidelity of the CSIA-AA proxies in exported sinking particles and ancient marine sediments by addressing the following questions: 1) Are δ^{13}C-AA and δ^{15}N-AA patterns of sea ice algae can be distinguished from pelagic algae? 2) What are the ultimate and proximal sources in exported sinking OM? and 3) What are the C and N baseline signatures, and trophic and microbial processing recorded in Holocene sediments?

In this thesis, each of chapters 2, 3, and 4 are presented as a stand-alone manuscript. Chapter 2 has been published at the time of writing and the others were prepared as manuscripts for publications in winter, 2023 and spring, 2024. The sequence of chapters maintains a cohesive and logically structured flow, commencing with surface primary production and moving on to the export of OM at greater depths, finally delving into the exploration of paleo-records in subsurface Holocene marine sediments. By exploring the differences in δ^{13}C-AA and δ^{15}N-AA patterns of sea ice algae and pelagic algae in Chapter 2, the diagnostic potential of δ^{13}C-EAA for sea ice algae was demonstrated, which were then applied to investigate the sea ice algal contribution to exported sinking particles in Chapter 3 and Holocene sediments in Chapter 4. Building on the findings of Chapter 2 and previous work of other CSIA-AA proxies, we constrained the sources and proportional contributions of sinking organic matter to export flux in the northern Labrador Sea in Chapter 3 and carry out the first CSIA-AA measurements on Holocene sediments in northeastern Baffin Bay in Chapter 4. Chapter 3 and 4 highlighted the potential of AAs as reliable tracers to document detailed information on C and N baseline levels, and trophic and microbial processing in different sedimentary regimes over different time scales.

Chapter 2, “Amino acid δ^{13}C and δ^{15}N fingerprinting of sea ice and pelagic algae in Canadian Arctic and Subarctic Seas” by myself, P. Mudie, and O. A. Sherwood was published in the journal Frontiers in Marine Science in October, 2022. This manuscript

explores differences in δ^{13}C-AA and δ^{15}N-AA signatures between sea ice and pelagic algae collected in Canadian Arctic and subarctic seas. For the first time, distinct δ^{13}C-EAA fingerprints and different degrees of heterotrophic reworking were revealed between sea ice and pelagic algae. These results highlight the potential of CSIA-AA to trace C sources from sea ice and pelagic origins and to evaluate the efficiency of biological pump in polar marine environments, paving the way for our next chapter on exported sinking OM. In this study, O. A. Sherwood and I contributed to conception and design of the study. I carried out the sampling. O. A. Sherwood and I contributed to sample processing, measurements, and data analysis. P. Mudie provided up-to-date references and taxonomic data from sea ice and phytoplankton studies in Frobisher Bay for comparison with our data. I wrote the manuscript with input from all the co-authors.

Chapter 3, "Sea ice algae and zooplankton fecal pellets fuel tight benthic-pelagic coupling in the northern Labrador Sea" by myself, T. Dezutter, D. Cote, E. Edinger, C. Lalande, and O. A. Sherwood was prepared as a manuscript, to be submitted in winter, 2023. Building on the findings of Chapter 2, this manuscript applies CSIA-AA proxies on two-year time-series of sinking particles collected in two sediment traps in the northwestern Labrador Sea to explore the sources and composition of organic C and N in sinking OM. The location of sediment traps was at ca. 60°N, the southern border of the Arctic Ocean, in the transition zone from the Canadian Arctic to Labrador Sea. Our findings revealed that sea ice algae and exported zooplankton fecal pellets can be a critical source of C and N for benthic fauna. In this study, D. Cote, E. Edinger, and O. A. Sherwood and I contributed to conception and design of the study. T. Dezutter and I contributed to sampling. T. Dezutter contributed to flux measurements and microalgal and zooplankton counts. O. A. Sherwood and I contributed to sample processing, CSIA-AA and bulk stable isotope measurements, and data analysis. D. Cote, E. Edinger, and C. Lalande contributed to data interpretation. I wrote the manuscript with input from all the co-authors.

Chapter 4, "Holocene preservation of amino acid δ^{13}C and δ^{15}N signals in a sediment core from off Northwest Greenland over the Holocene" by myself, A. Limoges, and O. A. Sherwood was prepared as a manuscript, to be submitted in spring, 2024. This

manuscript presents the first coupled AA $\delta^{13}C$ and $\delta^{15}N$ sediment core records spanning most of the Holocene period in northeastern Baffin Bay. Our measurements show robust long-term preservation of CSIA-AA proxies despite noticeable alteration in AA concentrations. These results expand limited existing CISA-AA data on multi-millennial sediments from temperate seas to polar regions and highlight the potential of AAs as reliable tracers to provide novel information for longer-term paleo-reconstruction. In this study, O. A. Sherwood and I contributed to conception and design of the study. A. Limoges contributed to measurements of bulk OM stable isotope analyses, diatoms, and sea-ice biomarkers. O. A. Sherwood and I contributed to CSIA-AA sample processing, measurements, and data analysis. I wrote the manuscript with input from all the co-authors.

CHAPTER 2 AMINO ACID $\delta^{13}C$ AND $\delta^{15}N$ FINGERPRINTING OF SEA ICE AND PELAGIC ALGAE IN CANADIAN ARCTIC AND SUBARCTIC SEAS[1]

Abstract

The on-going decline in Arctic sea ice represents a significant loss of habitat for sea ice algae, which are a major contributor to primary production in the Arctic. Data on sea ice algal production is limited due to difficulties in both accessing sea-ice and sampling under-ice algae. Compound-specific isotope analysis (CSIA) of amino acids (AAs) is emerging as a powerful tool to trace element origins and biogeochemical processes in marine food webs and may address the knowledge gaps in sea ice algal productivity dynamics. Here we measured $\delta^{13}C$-AA and $\delta^{15}N$-AA in natural communities of sea ice and pelagic algae collected from regions offshore Labrador and Nunavut, Canada. Significant difference in $\delta^{13}C$-AA patterns between sea ice and pelagic algae was observed in different size classes. This difference was further supported by multivariate analyses based on normalized $\delta^{13}C$ of essential amino acids (EAAs), which demonstrated a clear separation between sea ice and pelagic algae. Beta (β) values and trophic position (TP) calculated from $\delta^{15}N$ of Glutamic Acid and Phenylalanine (Phe) and $\sum V$ parameter for microbial resynthesis indicated a slightly higher heterotrophic biomass in pelagic and sea ice samples as compared to cultured samples. This finding is consistent with the Phe-normalized $\delta^{15}N$ of Alanine and Threonine, which provided better separations between sea ice/pelagic algae and other end-member groups. Overall, our study provides first insights into the potential differences in $\delta^{13}C$-AA and $\delta^{15}N$-AA patterns between sea ice and pelagic algae and suggests carbon of sea ice origins may be distinguished from pelagic sources using CSIA-AA approach. These observations highlight the potential of CSIA-AA to estimate proportional contributions of sea ice and pelagic algae to export production and efficiency of benthic-pelagic coupling in polar marine environments.

[1]Chen, S.M., Mudie, P. and Sherwood, O.A., 2022. Amino acid $\delta^{13}C$ and $\delta^{15}N$ fingerprinting of sea ice and pelagic algae in Canadian Arctic and Subarctic Seas. *Frontiers in Marine Science*, *9*, p.976908.

Student Contribution: I contributed to conception and design of the study. I carried out sampling, sample processing, measurements and data analysis. I wrote the manuscript with input from all the co-authors.

2.1 Introduction

The Arctic Ocean has been experiencing unprecedented reductions in sea ice extent as a result of climate change. The average monthly sea ice extent in September has been declining on average at a rate of 12.8 ± 2.3% per decade from 1979 to 2018 (Meredith et al., 2019). This reduction is accompanied by younger and thinner ice, freshening surface water, and less ice-covered area in the Arctic, which may alter ecosystem dynamics by affecting light penetration, nutrient availability, and density stratification in the water column (Post et al., 2013). The decline in sea ice has caused an increase in pelagic primary production, a reduced surface nutrient availability, and a shift in plankton community structure toward picoplankton (Li et al., 2009; Finkel et al., 2010; Arrigo & van Dijken, 2015; Gérikas Ribeiro et al., 2020; Dhifallah et al., 2022). Further, the loss of sea ice represents a loss of habitat for highly productive sea ice algae, which can be a major contributor to primary production in the Arctic (3–25% and up to 60% in the central Arctic; Legendre et al., 1992; Gosselin et al., 1997; Arrigo 2014). Therefore, changes in sea ice extent and sea ice algal production are likely to have cascading effects on energy transfer, carbon (C) cycling, and food web functioning in Arctic ecosystems. Since 1997, data on sea ice algal activity and biomass have become more available, but the number of field studies with a sufficient spatial and temporal resolution are still limited (Gosselin et al., 1997; Leu et al., 2015). Despite an increase in primary production being reported, current estimates on Arctic/subarctic productivity have been mainly based on satellite observations, which cannot account for under-ice algal growth and phytoplankton blooms (Mundy et al., 2009; Arrigo et al., 2012; Arrigo & van Dijken, 2015; Ardyna et al., 2020), and thus Arctic productivity may be drastically underestimated. Recent studies also pointed out that changes in timing, duration, and magnitude of the different types of algal blooms due to the loss of sea ice may induce potential mismatches for the timing of zooplankton production and hence alter the biomass and energy transfer to higher trophic levels (Post et al., 2013; Leu et al., 2015). Enhanced understanding of sea ice algae production and clear distinction of their dynamics from pelagic algae is essential to evaluate future productivity and community responses in the changing Arctic.

A key to improved understanding of sea ice algae is the use of highly specific biomarkers. Existing proxies include bulk stable carbon isotopes ($\delta^{13}C$), fatty acids, and highly branched isoprenoids (HBI; e.g., IP_{25}). Sea ice algae have been reported to be more enriched in $\delta^{13}C$ compared to phytoplankton, due to the C-limiting environment in the semi-closed sea ice system (Kohlbach et al., 2016; De La Vega et al., 2019). This difference in bulk $\delta^{13}C$ has been widely used to trace C from sea ice algae and pelagic phytoplankton, yet interpretation of bulk $\delta^{13}C$ can be complicated by the variations in source signatures, effects of metabolic processes and other environmental factors (Pineault et al., 2013; Søreide et al., 2013; Kohlbach et al., 2016). To account for the uncertainties in bulk $\delta^{13}C$, fatty acid proxies were often used along with stable isotope analyses to provide a more accurate estimate of ice algal production (Budge et al., 2008; Søreide et al., 2013; Kohlbach et al., 2016). As a common biomarker for marine primary producers, fatty acids alone are not able to distinguish sea ice algae from phytoplankton, because both communities consist of mainly diatoms which produce the same fatty acids (Søreide et al., 2013; Kohlbach et al., 2016). The small biomass (5–14% of the C biomass) in marine phytoplankton and rapid degradation in detrital materials, however, pose challenges to preservation of fatty acid proxies in marine sediments or bioarchive organisms (e.g., mussels and deep-sea corals; De Troch et al., 2012; Jónasdóttir, 2019). A HBI proxy, IP_{25} ("Ice Proxy with 25 carbons"), was discovered to be exclusively produced by a few Arctic sea-ice diatoms and has been used as a presence/absence indicator of sea ice taxa in marine sediments (Belt et al., 2007; Brown et al., 2014). However, being highly species specific, this biomarker may not provide community-level information on sea ice algal production (Belt & Müller, 2013). Hence, additional ice-algal specific and well-preserved biomarkers are needed for advancing knowledge of sea ice algal dynamics in the Arctic.

Compound-specific isotope analysis (CSIA) of amino acids (AAs) has emerged as a powerful tool for tracing organic C and nitrogen (N) in marine food webs and sediments (Larsen et al., 2009; Larsen et al., 2013; McMahon et al., 2013; Batista et al., 2014; Ohkouchi et al., 2017). The traditional approach to interpret stable isotope values of bulk organic materials has been widely used to study organic matter sources and cycling in different ecosystems (Fry 1998). However, bulk isotopes can be difficult to

interpret due to modification by a wide range of environmental factors, including variations in C or N sources, trophic transfer, and microbial alteration (Boecklen et al., 2011). With the emerging CSIA-AA approach, these confounding factors can be addressed by measuring stable isotope values of carbon ($\delta^{13}C$) or nitrogen ($\delta^{15}N$) atoms in individual compounds, e.g., amino acids, that provide specific information about their sources and the physiology of the organisms (Close, 2019). Isotopic fractionation of C in AAs is largely determined by their assimilation and biosynthesis. Amino acids are conventionally classified into essential and non-essential AAs based on their dietary requirements by animals (Karasov & del Rio, 2007; McMahon et al., 2013). Essential amino acids (EAAs) can only be synthesized by autotrophs or resynthesized by bacteria de novo and utilized directly by consumers with minor alteration to their C skeletons (Larsen et al., 2013; McMahon et al., 2013). Diverse biosynthetic pathways and associated isotopic effects lead to distinct and consistent $\delta^{13}C$ of EAAs in different functional groups of primary producers (Hayes, 1993; Larsen et al., 2009), which are transferred to higher trophic levels with little or no trophic discrimination (McMahon et al., 2013). Therefore, $\delta^{13}C$-EAA patterns of consumers reflect the isotopic signatures of primary producers at the base of the food web (McMahon et al., 2013). In the ocean, the $\delta^{13}C$-EAA signatures of primary producers are passed, unaltered, to higher trophic levels and eventually preserved in paleo-archives such as proteinaceous deep-sea corals and marine sediments (Schiff et al., 2014; Larsen et al., 2015; McMahon et al., 2015). Such stable isotope "fingerprints" have been developed for primary producers from terrestrial and aquatic ecosystems (Larsen et al., 2009; Larsen et al., 2013; McMahon et al., 2015) and used in Bayesian mixing models to reconstruct plankton community structure from archived materials (McMahon et al., 2015). The changes in $\delta^{15}N$ in AAs during trophic transfers lead to different groupings of AAs that are independent of those based on $\delta^{13}C$. The $\delta^{15}N$ values of source AAs (SrcAAs) remain basically unchanged while those of trophic AAs (TrAAs) become enriched with increasing trophic position (McClelland & Montoya, 2002). The scattering of $\delta^{15}N$-AA values has been used to investigate the relative contribution of heterotrophic biomass (the $\sum V$ parameter; McCarthy et al., 2007). Hence, the ability of $\delta^{15}N$-AA to provide specific information about trophic transfers, N sources and microbial biomass disentangles the confounding effects for bulk isotope

values and allow for more accurate interpretation of stable isotope data (McMahon et al., 2013; McMahon & McCarthy, 2016).

Sea ice algae are subject to extreme variations in light, temperature, and salinity during ice formation and melting, and are therefore adapted to a wide range of environmental conditions (Kirst & Wiencke, 1995). These adaptations include changing chlorophyll characteristics in response to low-light conditions (Kirst & Wiencke, 1995) and production of anti-freeze proteins (Janech et al., 2006; Bayer-Giraldi et al., 2011), which may impact the biosynthetic pathways of AAs and generate unique δ^{13}C-AA and δ^{15}N-AA patterns that can be distinguished from algae of pelagic origins. We therefore hypothesize that the δ^{13}C-AA and δ^{15}N-AA patterns of sea ice algae can be distinguished from those of pelagic algae. Here we present the first preliminary test of this hypothesis by determining δ^{13}C-AA and δ^{15}N-AA values of sea ice and pelagic algae collected offshore Labrador and Nunavut, Canada. By measuring δ^{13}C-AA and δ^{15}N-AA values and comparing with existing data of other end-member autotrophs (Larsen et al., 2013; McCarthy et al., 2013; Sauthoff, 2016; Doherty et al., 2021), we assess the potential to develop a new quantitative biomarker for sea ice algae. With this proxy, it may be possible to reconstruct the relative contribution of sea ice algae to export production recorded in deep-sea corals and marine sediments, which will enhance our understanding of sea ice algae dynamics and contributions to export productivity.

2.2 Materials and Methods

2.2.1 Sample collection and processing

Brash ice and pelagic algae were collected opportunistically during expeditions of the Canadian Coast Guard Ship *Amundsen* to the northern Labrador Sea and Baffin Bay during late June to early July in 2019 and during mid-July to mid-August in 2021 (Fig. 2.1, Table A1). Brash ice algae were collected in Frobisher Bay (Station: FB) in 2019 and Baffin Bay in 2021 (Station: SF and CF) while pelagic algae were collected on the Labrador Shelf (Station: NS and IC) in 2019 and Baffin Bay in 2021 (Station: SF and CF). Both regions are subject to seasonal sea ice cover (Yashayaev et al., 2021).

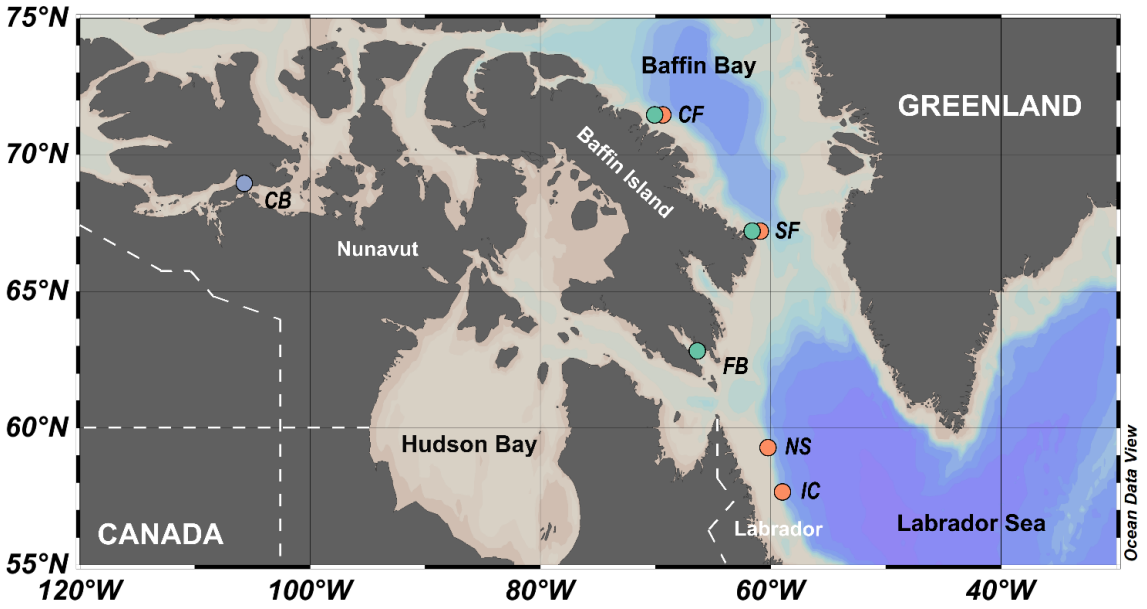

Figure 2.1 Map of sampling locations off Labrador and Nunavut, Canada. Light blue circles: sea ice algae collected by coring of spring fast ice; Green circles: sea ice algae collected by melting of late spring and early summer brash ice; Orange circles: pelagic algae collected by a CTD-Rosette. Location/station abbreviations: CB, Cambridge Bay; CF, Clark Fjord; SF, Southwind Fjord; FB, Frobisher Bay; NS, Non-sponge Site; IC, ISECOLD1-1500. Figure made with Ocean Data View, Schlitzer, 2021.

Pelagic algae were collected using a CTD-Rosette (Seabird SBE-911 plus) equipped with a fluorometer and 24 12-L Niskin bottles (Fig. 2.1). Fluorometer readings during the descent of the CTD were used to identify the depth of the deep chlorophyll maximum (DCM). Samples were then taken at depths at or above the DCM (Table A1). Seawater from each depth was then drawn directly from the Niskin bottles into a pre-rinsed 20-L plastic containers and kept in darkness before and during subsequent filtration. Algae were isolated by size-fractionated filtration through nylon filters of 180-µm and 20-µm pore size and polycarbonate filters of 3-µm and 0.2-µm pore size, respectively, using a peristaltic pump. Depending on the concentration of particulate organic matter (POM) in each sample, the volume of seawater filtered was between 10 and 20 L. Immediately following filtration, each filter was then packed into a piece of aluminum foil, placed in a plastic bag, and stored at -20°C until further analysis.

Sea ice algae were collected by scooping pieces of brash ice using a cage lowered by a crane from the bow of the ship. The ice was immediately placed in 0.2-µm filtered

seawater at an approximately 1:1 volume ratio and melted at room temperature in the dark upon collection. Melt water was filtered with the same size-fractionated system described above in 2021 (through 180-µm, 20-µm, 3-µm and 0.2-µm pore size filters). In 2019, due to time and equipment constraints, melt water was only filtered through 3-µm and 0.2-µm pore size filters. Every 0.5–1 L melted ice water was filtered through the size-fractionated system in a descending order for each sample.

Additional samples of sea ice algae were provided by Centre for Earth Observation Science, Manitoba. The samples were collected during the 2017 ICE-CAMPS field campaign (26 April to 12 May 2017) within a tidal strait area between the Finlayson Islands near Cambridge Bay, Nunavut (~69°00.033'N, 105°48.967'W; Fig. 2.1, Table A1), by filtration of landfast ice-core melt (30–100 ml) onto pre-combusted GF/F filters (Pogorzelec et al., in review).

Upon return to the laboratory, all the filters were freeze-dried and weighed to estimate the biomass collected on each filter by subtracting the average weight of blank filters (n = 10 for each type with a standard deviation up to 1.0 mg). Sea ice algae filters had approximate biomass ranging from < 0.1 to 12.2 mg while pelagic algae filters ranging from 0.7–11.9 mg. All the freeze-dried filters were stored at -20°C in dark again until further analysis.

2.2.2 Amino acid $\delta^{13}C$ and $\delta^{15}N$ analyses

Approximately 2–5 mg of biomass was required for $\delta^{13}C$-AA and $\delta^{15}N$-AA analyses per sample. For algae filters with a biomass < 1 mg, 2 or 3 filters of the same pore size from the same piece of ice or the same water depth were combined as one sample. Individual or combined filters of algae were transferred to Pyrex culture tubes in preparation for AA acid hydrolysis. Since some sea ice algae filters were collected through different pore sizes (only 3 and 0.2 µm), to make them comparable with pelagic algae, sea ice and pelagic algae filters with pore size of 180 µm, 20 µm and 3 µm collected from the same piece of ice or the same depth were combined to one sample. We found that nylon filters of 180-µm and 20-µm pore size reacted during AA derivatization and introduced contamination peaks during isotopic analyses. Therefore, biomass was

extracted from the nylon filters before hydrolysis. To carry out the extraction, 180-µm and 20-µm filters collected from the same depth were placed in 5 ml Milli-Q water in a Pyrex culture tube and ultrasonicated at 40 kHz for 45 min. Thereafter, the Pyrex tubes were centrifuged at 3000 rpm for 10 min, and the supernatant and the filters were removed from each tube. The 3-µm filter from the corresponding depth or the same piece of ice was then added to each Pyrex tube, so that each tube contained biomass from the 180-µm, 20-µm and 3-µm filters. The 0.2-µm filters from different depths or ice were treated as individual samples and transferred to Pyrex tubes for further hydrolysis. It is important to note that ultrasonic extraction may induce cell disruption which releases a portion of water-soluble proteins and free AAs (Rahman & Lamsal, 2021). The impact of ultrasonication on AA composition and CSIA values is discussed in the supplementary.

Individual or combined filters/biomass of sea ice algae and pelagic algae in Pyrex culture tubes were hydrolyzed in 2-ml 6-N HCl (Sigma-Aldrich) at 110 °C for 20 hours (Larsen et al., 2013; Batista et al., 2014; McMahon et al., 2015). Following hydrolysis, the liquid phase in each sample was transferred into a 4- or 7-ml dram vial (Sigma-Aldrich). Preparation was done in batches of 6–7 samples, two calibration standards of AA mixtures with known $\delta^{13}C$ and $\delta^{15}N$ values and a lab standard (homogenized Chlorella powder; Organika) processed in the same way as samples. Each sample was spiked with a norleucine (Nle) internal standard (Sigma-Aldrich) and purified using Dowex 50WX8 200-400 (H) cation exchange resin following Fábián et al. (1991) and Takano et al. (2010). To reduce polarity and increase volatility of AAs for GC-IRMS analysis, AAs were converted into volatile derivatives by esterification of carboxyl groups and subsequent acylation of amine groups using isopropanol and trifluoroacetic acid anhydride respectively (Silfer et al., 1991; McMahon et al., 2015). Derivatized samples were purified and extracted with a phosphate buffer (P-buffer) solution (Mixture of 1 M KH_2PO_4 and 1 M Na_2HPO_4 solution) prepared in deionized water (Millipore, Milli-Q; adjusted to pH = 7) and chloroform (Sigma-Aldrich) following the procedures described by Ueda et al. (1989), Carstens et al. (2013) and Broughton et al. (2015). Samples were well mixed with 2-ml P-buffer and 2-ml chloroform by shaking the vials for 30 sec and then centrifuged at 3000 rpm for 5 min. The P-buffer layer was removed followed by an addition of another 2-ml P-buffer solution to repeat the mixing and

centrifugation twice or three times. After the last centrifugation, the chloroform layer containing derivatized AAs was transferred to a new dram vial. The remaining P-buffer layer was washed by shaking and centrifugation with another 2-ml chloroform, which was pooled together with the previously obtained chloroform in the new dram vial. Purified samples in chloroform were acylated again, dried and dissolved in ethyl acetate (Sigma-Aldrich) for further analysis.

Samples were injected in triplicate or quadruplicate, bracketed by triplicate or quadruplicate injections of calibration standards, and analyzed for $\delta^{13}C$ or $\delta^{15}N$ using a Trace 1310 Gas Chromatograph (GC) coupled with a Delta V IRMS (Thermo Scientific). The following AAs were typically measured under our analytical conditions: alanine (Ala), glycine (Gly), proline (Pro), valine (Val), leucine (Leu), isoleucine (Ile), asparagine + aspartic acid (Asx), threonine (Thr), serine (Ser), glutamine + glutamic acid (Glx), phenylalanine (Phe), lysine (Lys) and tyrosine (Tyr). Measured $\delta^{13}C$ values were corrected for isotopic fractionation and introduction of C atoms during derivatization according to Silfer et al. (1991). Linear regression was used to normalize samples against instrument drift between successive triplicate injections of the amino acid standard (Yarnes & Herszage, 2017; denoted as calibrated $\delta^{13}C$). Measured $\delta^{15}N$ values were calibrated based on the offset between known and measured values of calibrated standards and normalized against instrument drift with linear regression (denoted as calibrated $\delta^{15}N$). The average reproducibility of $\delta^{13}C$ was ± 0.3‰ for the internal standard Nle, and from ± 0.2‰ (Asp) to ± 0.6‰ (Leu and Lys) for AA standards, respectively (n = 27 for each AA). The average reproducibility of $\delta^{15}N$ was ± 0.5‰ for the internal standard Nle, and from ± 0.3‰ (Pro) to ± 0.8‰ (Thr) for AA standards, respectively (n = 26 for each AA). The relative abundance (mol%) of amino acids was quantified by calibration of mass 44 peak areas measured during $\delta^{13}C$ analysis using relative response factors between each AA and the Nle internal standard, following Kaiser and Benner (2005).

2.2.3 Calculations and statistical analyses

To account for region-specific differences in baseline $\delta^{13}C$, calibrated $\delta^{13}C$ values were internally normalized by subtracting the mean of 5 EAAs (Phe, Leu, Ile, Thr and Val) for each sample (denoted as normalized $\delta^{13}C$). Normalization accounts for variations in inorganic C sources and other environmental parameters, whereas the internal variations between AAs are driven by the underlying biochemical mechanisms (Larsen et al., 2015; McMahon et al., 2015). Larsen et al. (2015) examined the $\delta^{13}C$-AA fingerprints of a cultured marine diatom (*Thalassiosira weissflogii*) under a wide range of environmental parameters (light, salinity, temperature, and pH). They found that despite natural variability in bulk $\delta^{13}C$ and absolute $\delta^{13}C$-AA values, the normalized $\delta^{13}C$-EAA values remained unaltered under different growing conditions, suggesting that internally-normalized $\delta^{13}C$-EAA signatures are diagnostic of the biosynthetic origins of AAs across environmental gradients (Larsen et al., 2015). This spatiotemporal consistency in $\delta^{13}C$-EAA signatures of marine primary producers was further validated by controlled experiments by Stahl (2021) and analyses of 135 field samples by Elliott Smith et al. (2022).

The trophic position (TP) of samples was estimated based on the calibrated $\delta^{15}N$ values of Glx and Phe, following the equation proposed by Chikaraishi et al. (2009) and modified by Nielsen et al. (2015):

$$TP = \frac{(\delta^{15}N_{Glx} - \delta^{15}N_{Phe} - 2.9‰)}{6.6‰} + 1 \quad (1)$$

Where 2.9‰ is the beta (β) value representing the difference between the trophic AA $\delta^{15}N$-Glx and the source AA $\delta^{15}N$-Phe in marine primary producers and 6.6‰ is the trophic enrichment factor representing the $\delta^{15}N$ enrichment in Glx relative to Phe with each trophic transfer (Chikaraishi et al., 2009; Nielsen et al., 2015). To compare with published β values, $\beta_{Glx/Phe}$ and $\beta_{Glx/Lys}$ values were calculated for sea ice and pelagic algae from the calibrated $\delta^{15}N$ values of Glx and Phe, and Glx and Lys, respectively.

To examine the degree of heterotrophic resynthesis, ∑V was calculated based on the deviation in calibrated $\delta^{15}N$ values of trophic AAs, following the formula McCarthy et al. (2007):

$$\sum V = \frac{1}{n} \sum ABS(\delta^{15}N_i - \delta^{15}N_{mean}) \quad (2)$$

Where n is the number of trophic AAs used in this calculation, $\delta^{15}N_i$ are the calibrated δ^{15}N values of each trophic AA (Ile, Leu, Asx, Glx, Pro and Ala) and $\delta^{15}N_{mean}$ is the average δ^{15}N value of these AAs. Higher ∑V values indicate a higher degree of heterotrophic resynthesis (McCarthy et al., 2007).

Prior to testing the differences between sea ice and pelagic algae using Two Sample T-test and one-way ANOVA with Tukey HSD test, normalized δ^{13}C and calibrated δ^{15}N values were tested for univariate normality with Shapiro-Wilks test (R package: stats). Principal component analysis (PCA, R package: FactoMineR) and Linear discriminant analysis (LDA, R package: MASS) were performed in R version 4.1.1 with RStudio interface version 1.4.1717. To examine the differences between sea ice and pelagic algae, PCA was performed on normalized δ^{13}C-AA values and calibrated δ^{15}N-AA values, respectively. To assess to what extent sea ice algae can be distinguished from pelagic algae, an LDA classification model was built based on their normalized δ^{13}C-EAA values and a leave-one-out cross validation approach was used to calculate the probability of group membership of the classifier samples. Standard ellipse areas (SEA) were plotted for the groups' bivariate means in the PCA and LDA plots, each enclosing ~40% of the data.

2.3 Results

2.3.1 Amino acid δ^{13}C and δ^{15}N patterns

The overall δ^{13}C-AA patterns for all measured algae were similar to eukaryotic microalgae reported elsewhere (Larsen et al., 2013), with relatively more positive values for NEAAs (Fig. 2.2). For EAAs, all the algae groups had normalized δ^{13}C values of -3 to -6‰ for Phe, Leu and Val, and ~2‰ for Ile. The δ^{13}C of Thr was more variable, ranging from 7.8‰ to 14.9‰. Sea ice algae collected from brash ice (B) had higher Thr values than those of pelagic algae (P) for both size groups (Two Sample T-test, $p < 0.01$) while their Val values were significantly lower than pelagic algae for the 0.2–3 μm group ($p < 0.05$).

To validate if the difference between sea ice and pelagic algae was consistent across different ice types, we compare the results from the brash ice with sea ice algae from fast ice (F) from Cambridge Bay. Similarly, sea ice algae from the fast ice (> 0.7 µm; n = 6) exhibited a higher Thr value than those of pelagic algae for both sizes (n = 9 for each size; Two Sample T-test, $p < 0.01$; Fig. 2.2). Leu and Val values from the fast ice algae were significantly different from those of pelagic algae for both sizes ($p < 0.01$). The NEAA patterns were relatively similar between all groups, except for Gly which was significantly higher in both size groups of pelagic algae ($p < 0.05$; Fig. 2.2). Variations in normalized δ^{13}C-EAA values were significantly different between different groups (one-way ANOVA, $p < 0.001$), with a higher variation in sea ice algae, ranging 21.7 ± 1.0‰ for > 0.7 µm fast ice algae, 18.3 ± 1.6‰ and 18.5 ± 3.4‰ for > 3 µm and 0.2–3 µm brash ice algae, and 15.2 ± 2.0‰ and 13.7 ± 1.5‰ for > 3 µm and 0.2–3 µm pelagic algae, respectively. The Tukey HSD test revealed that the differences between > 3 µm and 0.2–3 µm brash ice algae, > 0.7 µm fast ice algae and 0.2–3 µm brash ice algae, and > 3 µm and 0.2–3 µm pelagic algae were not significant ($p > 0.05$).

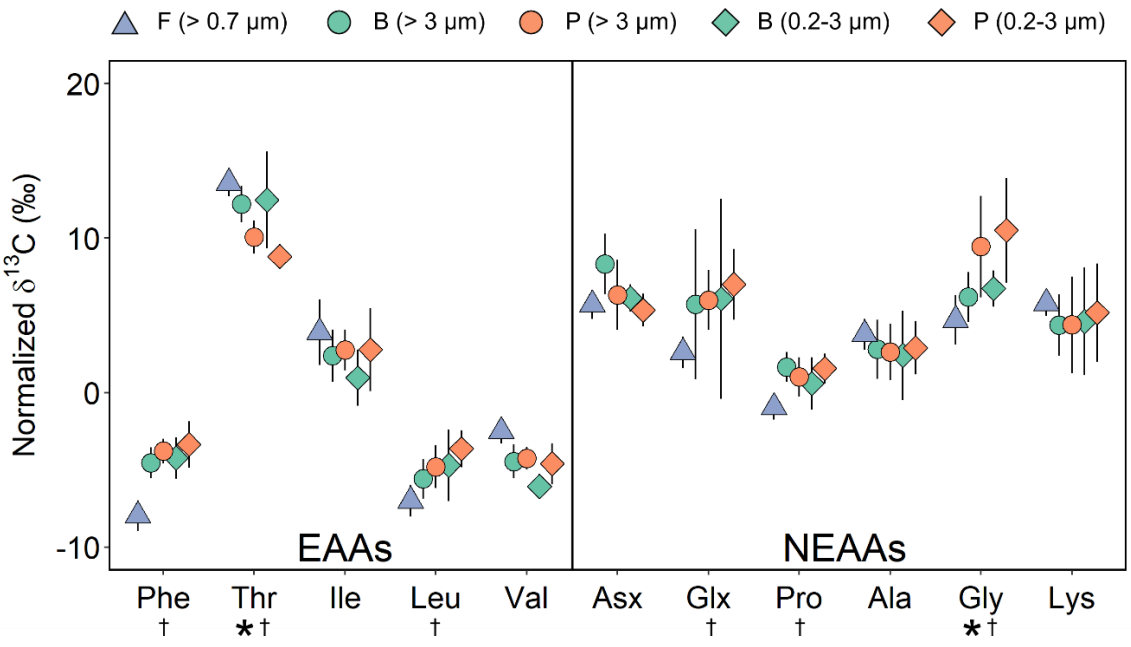

Figure 2.2 Normalized δ^{13}C-AA values of pelagic algae (P) and sea ice algae from the fast ice (F) and brash ice (B). Error bars show ±1 standard deviation for each group (n = 5-9). Asterisks indicate significant differences between brash ice algae and pelagic algae for both sizes (Two Sample T-test, $p < 0.05$). Daggers indicate significant differences between fast ice algae and

pelagic algae for both sizes (Two Sample T-test, $p < 0.05$). Abbreviations: EAAs, essential amino acid; NEAAs: non-essential amino acid.

Patterns of δ^{15}N-AA for pelagic and sea ice algae were also broadly similar to marine algae and particulate organic matter reported globally (McCarthy et al., 2007; 2013) with relatively lower values for source AAs and higher values for trophic AAs (Fig. 2.3). Note that δ^{15}N-AA in the fast ice samples from the Cambridge Bay was not analyzed due to low biomasses from small filtration volumes (see Sect. 2.2.1). Different algal and size groups shared similar calibrated δ^{15}N-AA values in Phe (mean: 5.3 ± 1.3‰) and Lys (mean: 5.5 ± 1.4‰; one-way ANOVA, $p > 0.05$; Fig. 2.3). There were significant offsets in trophic AAs between brash ice algae and pelagic algae (Two Sample T-test; Asx, Ala, and Gly for > 3 µm, $p < 0.05$; Gly and Val for 0.2–3 µm, $p < 0.05$; Fig. 2.3). Compared to Phe, which is an indicator of δ^{15}N of baseline N sources, most trophic AAs had similar or higher δ^{15}N values while Gly and Thr were lower (Fig. 2.3).

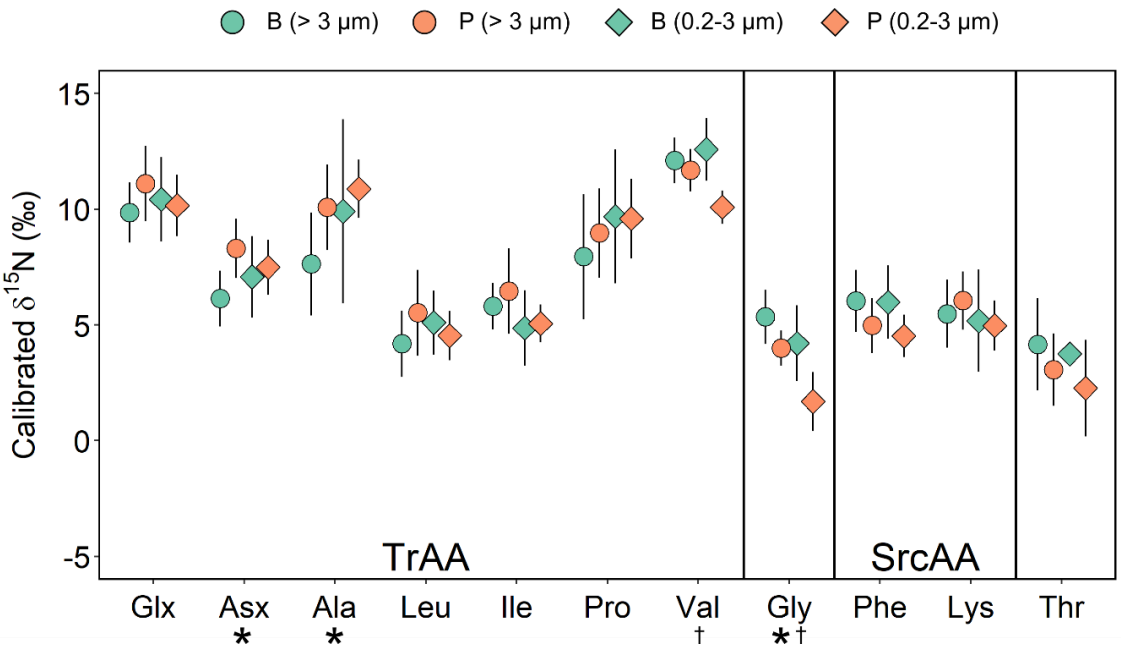

Figure 2.3 Normalized δ^{15}N-AA values of pelagic algae (P) and sea ice algae from the brash ice (B). Error bars show ±1 standard deviation for each group (n = 4-8). Asterisks indicate significant differences between > 3 µm sea ice and pelagic algae (Two Sample T-test, $p < 0.05$). Daggers indicate significant differences between 0.2–3 µm sea ice and pelagic algae (Two Sample T-test, $p < 0.05$). Abbreviations: SrcAA, source amino acid; TrAA, Trophic AA.

2.3.2 Multivariate analysis

To explore the differences in normalized δ^{13}C-AA patterns between sea ice and pelagic algae, principal component analysis (PCA) was performed on pelagic algae (P) and sea ice algae from the fast ice (F) and brash ice (B). PCA using normalized δ^{13}C values of 11 AAs explained 60.6% of the total variation between individual samples. The first principal component (PC1) accounted for 37.1% of the total variation and separated the pelagic algae from the fast ice algae (Fig. 2.4a). The standard ellipses of brash ice algae and pelagic algae showed a more constrained and separated distribution when performing PCA using only the normalized δ^{13}C values of EAAs, with variation explained by PC1 increased by 11.6% (Fig. 2.4b). Phe, Leu, and Thr contributed the most to the variation of PC1 (30.1%, 29.3%, and 23.1%, respectively). PC2 explained 24.6% of the total variation, mostly contributed by Ile (58.7%) and Thr (32.1%).

PCA was performed on brash ice and pelagic algae using δ^{15}N-SrcAAs and δ^{15}N-TrAAs respectively, and no clear separations were observed between algal groups (data not shown).

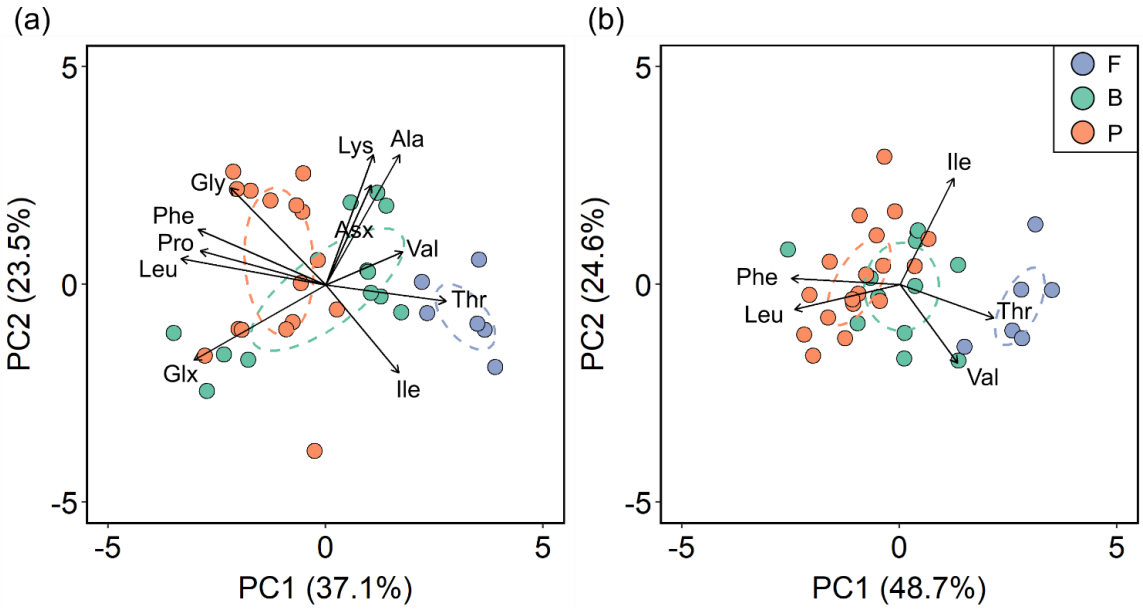

Figure 2.4 Principal Component Analysis based on normalized δ^{13}C values of (a) 11 amino acids and (b) 5 essential amino acids of pelagic algae (P) and sea ice algae from the fast ice (F) and brash ice (B). Values in parentheses of the axis titles are the percentage variation explained by

each axis. The colored ellipses represent standard ellipse area (SEA) for each corresponding group, containing ~40% of the data.

The separation between brash/fast ice algae and pelagic algae became more pronounced in the LDA classification model (Fig. 2.5). The first linear discriminant (LD1) explained 80.2% of group variation (Fig. 2.5). The re-classification using the leave-one-out cross validation approach showed that 8 out of 12 brash ice samples were classified as brash ice algae (87.0 ± 12.6%), 15 out of 18 pelagic samples were classified as pelagic algae (86.9 ± 16.1%), and all 6 fast ice algae were classified as fast ice algae (93.8 ± 15.1%; Table A3).

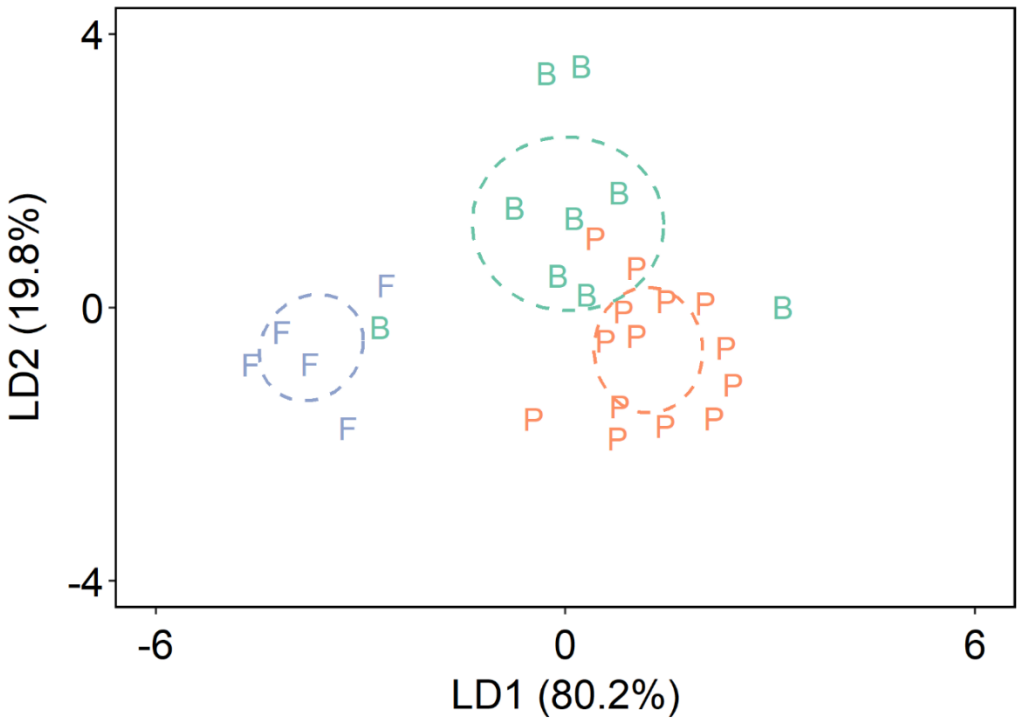

Figure 2.5 Linear discriminant analysis based on normalized $\delta^{13}C$ values of 5 essential amino acids of pelagic algae (P) and sea ice algae from the fast ice (F) and brash ice (B). Values in parentheses of the axis titles are the percentage variation explained by each axis. The colored ellipses represent standard ellipse area (SEA) for each corresponding group, containing ~40% of the data.

2.3.3 TP and ∑V, Phe-normalized $\delta^{15}N$ of Ala and Thr,

Beta (β) values calculated from the calibrated $\delta^{15}N$ of Phe and Glx averaged 3.8 ± 0.5‰ and 4.4 ± 0.9‰ for > 3 µm and 0.2–3 µm brash ice algae, and 6.1 ± 1.3‰ and 5.6 ±

0.9‰ for > 3 μm and 0.2–3 μm pelagic algae, respectively. The $\beta_{Glx/Lys}$ values were similar across different size and algal groups (one-way ANOVA, $p > 0.05$), with means of 4.4 ± 0.7‰ and 5.2 ± 0.9‰ for > 3 μm and 0.2–3 μm brash ice algae, and 5.1 ± 1.1‰ and 4.8 ± 1.0‰ for > 3 μm and 0.2–3 μm pelagic algae, respectively.

Table 2.1 Calculated $\beta_{Glx/Phe}$ and $\beta_{Glx/Lys}$ values (sample size, mean, and standard deviation) of different algal groups from published literature and this study. Asterisks indicate significant differences between > 3 μm brash ice and pelagic algae (Two Sample T-test, $p < 0.01$).

	$\beta_{Glx/Phe}$			$\beta_{Glx/Lys}$		
Group	**n**	**Mean**	**SD**	**n**	**Mean**	**SD**
Nielsen et al. (2015)						
Phytoplankton	47	2.9	1.9	–	–	–
Ramirez et al. (2021)						
Eukaryotic algae	39	3.8	1.3	8	4.6	2.6
This study						
Brash ice algae						
> 3 μm*	8	3.8	0.5	8	4.4	0.7
0.2–3 μm	4	4.4	0.9	4	5.2	0.9
Pelagic algae						
> 3 μm*	7	6.1	1.3	7	5.1	1.1
0.2–3 μm	7	5.6	0.9	6	4.8	1.0

Trophic position (TP) values estimated based on the calibrated $\delta^{15}N$ of Phe and Glx averaged 1.2 ± 0.1 (n = 12) and 1.5 ± 0.2 (n = 21) for sea ice algae from the brash ice and pelagic algae (Fig. 2.6a). Values of the ∑V parameter for microbial resynthesis were similar between the two algal groups, with means of 1.8 ± 0.5‰ and 1.9 ± 0.5‰, respectively (Two Sample T-test, $p > 0.05$; Fig. 2.6a). Both sea ice and pelagic algae showed significant differences in TP from cultured algae (0.7 ± 0.5, n = 12), and zooplankton (2.5 ± 0.4, n = 7). The ∑V values of sea ice algae were significantly different from sediment values reported in the literature (2.3 ± 0.7‰, n = 28; $p < 0.05$) while those of pelagic algae showed no difference from sediment ($p > 0.05$; Fig. 2.6a).

Another way to distinguish different end-members is to examine their Phe-normalized $\delta^{15}N$ of Ala and Thr, which have been found useful in previous studies

(Doherty et al., 2021). Sea ice algae from the brash ice and pelagic algae were examined and compared with previously published end-members (McCarthy et al., 2013; Yamaguchi & McCarthy, 2018; Doherty et al., 2021). Sea ice algae had similar Phe-normalized Ala values with cultured algae ($p > 0.05$), which were significantly different from pelagic algae, and all the other end-members ($p < 0.05$; Fig. 2.6b). Pelagic algae had higher Ala $\delta^{15}N$ than sea ice algae and cluster closer to microbial degraded POM and sediment (Fig. 2.6b).

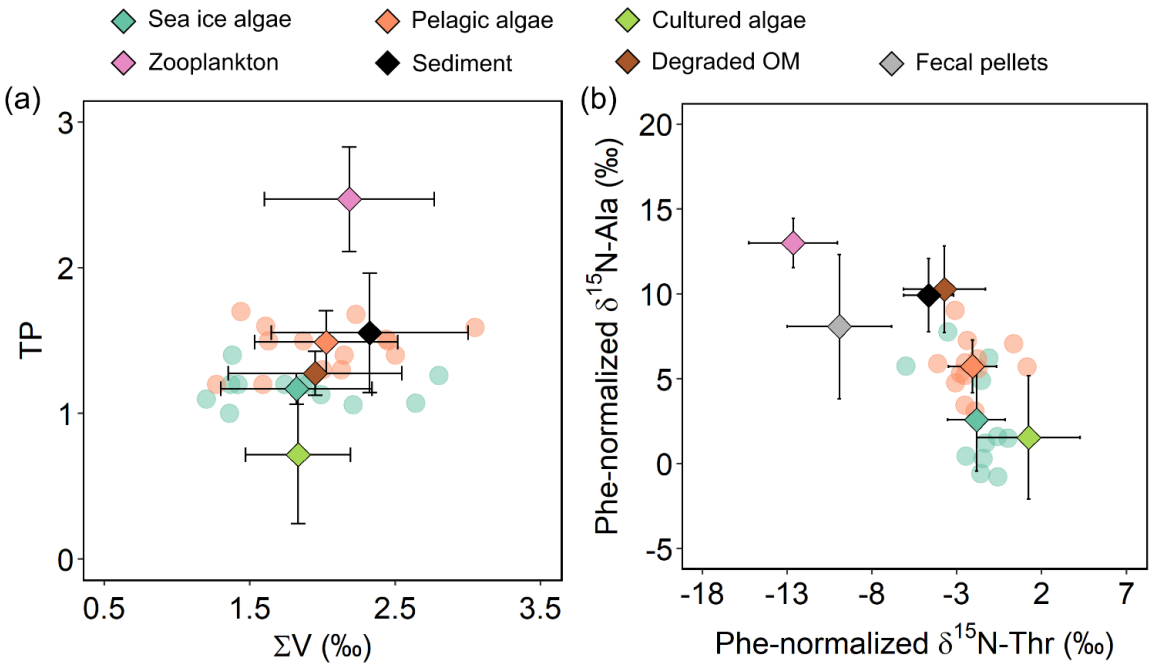

Figure 2.6 Estimation of trophic transfers and microbial reworking from $\delta^{15}N$-AA. (a) End-member trophic position (TP) and the ΣV parameter of sea ice (brash-ice) and pelagic algae were calculated based on calibrated $\delta^{15}N$-AA values (semi-transparent circles) with end-member means and ±1 standard deviations (diamonds with error bars). (b) End-member data based on Phe-normalized $\delta^{15}N$ of Ala and Thr (semi-transparent circles) are shown with end-member means and ±1 standard deviations (diamonds with error bars). Other end-member means and standard deviations are shown in diamonds with error bars from previously published studies: cultured algae, McCarthy et al., 2013; sediment, Sauthoff, 2016; degraded OM, Yamaguchi & McCarthy, 2018; fecal pellet and zooplankton, Doherty et al., 2021). Abbreviations: OM, organic matter.

2.4 Discussion

2.4.1 Distinct essential amino acid $\delta^{13}C$ fingerprints

Our study characterized for the first time, distinct $\delta^{13}C$-EAA patterns between sea ice and pelagic algae (Fig. 2.2). Despite a different size range (> 0.7 µm), this distinction

from pelagic algae was found consistent in another set of sea ice algae from the fast ice from Cambridge Bay. The distinction between sea ice and pelagic algae is further evidenced by the increase in variation explained by PC1 and PC2 and a clear separation between groups with loadings of only EAAs in the PCA (Fig. 2.4b). This finding was consistent with previous observations that EAAs were among the most informative AAs for separating different primary producers (Larsen et al., 2013). The separation between sea ice and pelagic algae became more pronounced in the LDA classification model that correctly predicted the classes of most samples (Fig. 2.5; Table A3), which is not surprising because, unlike PCA, LDA is a supervised technique that maximizes the separability between the classes. The strong classification probability in LDA demonstrated the potential to use δ^{13}C-EAA fingerprints to trace C sources from sea ice and pelagic origins. Typical sea ice and pelagic communities in Arctic/subarctic regions consist of a mixture of diatoms, dinoflagellates, and flagellates (Lizotte, 2003; Poulin et al., 2011; Harrison et al., 2013; Hop et al., 2020), which was evidenced by the similar δ^{13}C-AA patterns for all measured algae to eukaryotic microalgae reported by Larsen et al. (2013). Although the community composition of sea ice and pelagic algae from the northern Labrador Sea and Baffin Bay was not characterized in this study due to the lack of taxonomic identification, previous studies can provide some taxonomic information of sea ice and pelagic communities in Frobisher Bay (Hsiao, 1979; Hsiao & Pinkewycz, 1985; Hsiao, 1992). Ice cores, seawater and sediment trap samples revealed a dominance of diatoms in both sea ice algae in spring and phytoplankton in summer in Frobisher Bay (Hsiao, 1979; Hsiao & Pinkewycz, 1985; Hsiao, 1992). Moreover, the community composition of sea ice algae from the fast ice in Cambridge Bay was surveyed and over 80% of the total population was dominated by pennate and centric diatoms (Pogorzelec et al., in review). Hence, we speculate that the unique δ^{13}C-EAA signatures between the sea ice and pelagic communities are less likely to be driven by their similar community composition, and instead, they may be linked to the underlying biochemical and physiological differences between these two groups.

To date, unique δ^{13}C-EAA patterns have been identified in algae, seagrass, plants, fungi and bacteria (Larsen et al., 2009; 2013; Lehman, 2009; Vokhshoori et al., 2014). Distinct and consistent δ^{13}C-EAA patterns in different phylogenic groups result from

their associated biosynthetic pathways and isotopic effects (Macko et al., 1987; Abraham & Hesse, 2003; Scott et al., 2006), which can be used as "fingerprints" to trace organic C sources in consumers and detrital materials (Larsen et al., 2013; 2015; McMahon et al., 2015). Larsen et al. (2013) analyzed a wide range of field and culture samples and suggested that microalgae, such as chlorophytes and diatoms, shared similar δ^{13}C-EAA patterns and therefore should be categorized into a single group. Based on their work, one would expect similar δ^{13}C-EAA patterns between sea ice and pelagic algae, which are typically dominated by diatoms in summer (Kirst and Wiencke, 1995; Lovejoy et al., 2002; Lizotte, 2003; Hop et al., 2020). Whereas, we proposed that sea ice and pelagic algae may generate distinct δ^{13}C-EAA fingerprints based on the unique adaptations of sea ice algae to their extreme habitats. Our findings in general supported this hypothesis (Fig. 2.2), but the specific mechanisms remain unclear. There are several hypothetical explanations for their unique δ^{13}C-EAA patterns. Sea ice algae are typically selectively developed from algal cells that incorporate into sea ice during ice formation or colonize the sea ice following ice formation (Kirst & Wiencke, 1995; Lizotte, 2003; Mundy and Meiners, 2021). The sea ice assemblages are subject to large gradients of temperature, irradiance, and salinity during their life cycles. Adaptations to these special growing conditions require specific physiological and metabolic properties, e.g., changes in enzyme activities (Kirst & Wiencke, 1995; Lizotte, 2003). First, sea ice algae are adapted to low-light conditions within or beneath sea ice with higher chlorophyll to C ratios and hence require fewer photons to complete their life cycles compared to phytoplankton (Kirst & Wiencke, 1995). Sea ice algae are also found to have optimal photosynthetic rates at lower salinity during ice melting or at higher salinity during colder seasons, depending on specific species (Lizotte, 2003). Studies on sea ice prokaryotic diversity demonstrated a higher number of cultivatable species compared to planktonic communities, indicating that sea ice communities may be better adapted to large substrate gradients (Junge et al., 2002; Lizotte, 2003). In addition, anti-freeze proteins have been reported to be produced by some polar sea ice assemblages, which are characterized by their ability to influence ice formation and protect sea ice diatoms from freezing (Ewart et al, 1999; Janech et al., 2006; Bayer-Giraldi et al., 2011). Amino acid composition analysis showed a high abundance in Ala, Gly and Thr in anti-freeze proteins (Bayer-

Giraldi et al., 2011), while our study found significant differences in $\delta^{13}C$ values of Gly and Thr between sea ice and pelagic algae for both sizes (Fig. 2.2). AA mol% of sea ice and pelagic algae were well-balanced and consistent with previously reported values in marine phytoplankton (Cowie & Hedges, 1992), but significantly increased abundance of Thr was not observed in both fast-ice and brash-ice algal groups (Fig. A1). To our knowledge, it is not yet known whether expression and biosynthesis of anti-freeze proteins are associated to the C fractionation of those abundant or $\delta^{13}C$-enriched amino acids in sea ice algae. Nevertheless, the generation of unique $\delta^{13}C$ signatures in other source-specific molecules are produced by Arctic sea ice diatoms (Belt et al., 2008). Belt et al. reported that Arctic sea ice diatoms can produce a sea-ice-specific isoprenoid biomarker with distinctive $\delta^{13}C$ signatures from that originated from planktonic or terrigenous organic matter (2008). As amino acids are the building blocks of life and contribute to the majority of organic C in plankton and sinking particulate organic matter (Hedges et al., 2001), their $\delta^{13}C$ signatures controlled by biosynthetic and metabolic pathways are likely to be impacted and modified by specific adaptations to extreme living conditions in sea ice organisms. Future investigation is necessary for enhanced understanding of specific processes that control stable isotope fractionation of individual amino acids in sea ice algae.

2.4.2 N sources, trophic level, and microbial reworking

Amino acid $\delta^{15}N$ analysis is a powerful tool to trace N cycling, reconstruct trophic relationships in marine food webs and estimate the degree of microbial resynthesis in marine organic matter (Ohkouchi et al., 2017; Close, 2019). In this study, both sea ice and pelagic algae shared similar $\delta^{15}N$ values of SrcAAs (Phe: 5.3 ± 1.3‰; Lys: 5.5 ± 1.4‰), consistent with the near-surface $\delta^{15}N$ values of nitrate ($\delta^{15}N$-NO_3) in the study region (5–6‰; Sherwood et al., 2021). This similarity with near-surface $\delta^{15}N$-NO_3 has two implications. First, from a nutrient uptake perspective, the $\delta^{15}N$-SrcAAs in pelagic and sea ice algae could be interpreted to represent the accumulated product in Rayleigh isotope fractionation dynamics during algal growth on nitrate (e.g., Waser et al., 2000). Water column nutrient concentrations were not measured alongside the algae collection in 2019 and 2021, but euphotic zone nitrate (and ammonium) along the western Labrador

Sea and Baffin Bay margins is generally exhausted to < 1 μM by July each year (Harrison et al., 2013). In this regard, the algal δ^{15}N-SrcAA values appear to converge on that of δ^{15}N-NO_3 under conditions of complete nutrient utilization. Second, from a trophic processing perspective, the δ^{15}N-SrcAA values in sea ice and pelagic algae were the same, despite the indication of higher trophic position and microbial resynthesis in the pelagic algae (Fig. 2.6). This adds to the growing body of evidence that δ^{15}N-SrcAA signatures are minimally altered during trophic processing of both living and detrital biomass (e.g., Chikaraishi et al., 2009; Shen et al., 2021). Together, these interpretations lend support to the use of δ^{15}N-SrcAA values recorded in benthic organisms and sediments for tracking changes in baseline δ^{15}N variability spatially and temporally (Sherwood et al., 2014; Vokhshoori & McCarthy, 2014).

The higher TP in pelagic versus sea ice algae may be attributed to the different degrees of heterotrophic processing in these field samples (Fig. 2.6). The $\beta_{Glx/Phe}$ (2.9‰) used in the TP calculation was derived mostly from cultured marine phytoplankton (Nielsen et al., 2015). Compared to cultured samples, field-collected algae samples include varying amounts of heterotrophic bacteria, protozoa and microzooplankton. The influence of heterotrophic biomass is evident from the higher calculated $\beta_{Glx/Phe}$ values for sea ice and pelagic algae (Table 2.1). Hence, application of a smaller $\beta_{Glx/Phe}$ value from cultured samples led to slightly higher TP values in both the pelagic and sea ice algae samples as compared to cultured algae (Table 2.1; Fig. 2.6a). Recent studies revealed that $\beta_{Glx/Phe}$ values are more variable and more influential on TP estimation than typically considered while $\beta_{Glx/Lys}$ showed less variation across primary producer taxonomic groups (Ramirez et al., 2021). The smaller variability in $\beta_{Glx/Lys}$ was also reflected by the lack of significant differences between different size and algal groups in our samples (Table 2.1). To account for variability in β values and to obtain realistic TP estimation, future research should sample in-situ primary producers concurrent to sampling of consumers, establish/apply β values from in-situ primary producers, and when feasible, include estimation based on δ^{15}N-Lys for cross validation.

Although Glx is often used to compute TP for its chemical stability, high abundance, and the pronounced trophic enrichment of δ^{15}N (Chikaraishi et al., 2009),

questions have been raised on whether Glx reflects reliable trophic enrichment in plankton food webs (Gutiérrez-Rodríguez et al., 2014; Décima et al., 2017). Through a series of chemostat experiments, Décima et al. suggested that under-estimation of Glx-based TP for protistan consumers can be outstanding, and Ala instead may provide a more robust trophic signal for protistan and metazoan consumers (2017). Our results showed that Ala and Thr provide an improved separation between the primary end-members (algae, fecal pellet, zooplankton, degraded OM and sediment) from the microbial and plankton food webs compared to the TP-∑V model (Fig. 2.6). The resemblance of sea ice algae with cultured algae and the clustering of pelagic algae towards degraded OM and sediment demonstrated again the slightly higher contribution of heterotrophic reworking in pelagic algae. Previous studies have revealed that Ala has a higher trophic sensitivity to consumers involved in microbial food webs than Glx, while Thr can distinguish animal metabolism (zooplankton and fecal pellet) from microbial metabolism (microalgae and sediment; Gutiérrez-Rodríguez et al., 2014; Décima et al., 2017; Doherty et al., 2021). Combined, Phe-normalized $\delta^{15}N$ values of Ala and Thr indicated slightly higher microbial metabolism in pelagic algae and minimal impacts of animal metabolism on both sea ice and pelagic algae. Our observations provide support to the use of $\delta^{15}N$-Ala-Thr models for improved characterization of the end-member distribution and contribution in microbial food webs.

2.4.3 Uncertainties in the CSIA-AA proxies

Our results showed clear separation of pelagic and sea ice algae based on $\delta^{13}C$-EAA patterns. However, it should be emphasized that the measured $\delta^{13}C$-EAA patterns represent the integrated isotopic effects of a natural community. Previous studies characterized $\delta^{13}C$-EAA values mostly at a family/species level and explored their unique patterns for each phylogenic group (Larsen et al., 2009, 2013). Even though Canadian Arctic sea ice and pelagic assemblages are known to be often dominated by centric and pennate diatom species, among which *Atteya* spp., *Fragilariopsis cylindrus,* and *Nitzschia frigida* are the most frequently reported (Poulin et al., 2011; Szymanski and Gradinger, 2016; Hop et al., 2020; Pogorzelec et al., in review), our samples may be influenced by other C imprints including other eukaryotic and prokaryotic algae and

bacteria. Contribution from heterotrophic bacteria can be estimated from TP-∑V and δ^{15}N-Ala-Thr models (Fig. 2.6). Our results suggest the modification by heterotrophic biomass was in general insignificant.

As stated above, we hypothesized that the distinct δ^{13}C-EAA pattern in sea ice algae from pelagic algae is governed by their unique physiological adaptations to extreme conditions. Nevertheless, the distinctions in δ^{13}C-EAA patterns between sea ice and pelagic algae could be impacted by the differences in algal community composition. To assess the role community composition played in separating the algal groups, we measured different size classes of sea ice and pelagic algae. Size classes are an important functional trait for marine microalgae, and it has been previously reported that picoplankton has distinct taxonomic composition from micro- and nanophytoplankton (Lizotte, 2003; Finkel et al., 2010; Balzano et al., 2012). Hence, differences in the δ^{13}C-EAA patterns between size classes can serve as a rough proxy for δ^{13}C-EAA variations due to community composition. In our study, the differences between sizes were less pronounced compared to the differences between sea ice and pelagic origins (Fig. 2.2, 2.4), indicating community composition played a minor role in separating the algae groups. It is yet difficult to draw a conclusion based on the moderate sample size of our algae samples, especially for sea ice algae which were collected opportunistically. Hence, extensive sampling of sea ice and pelagic algae of different sizes across a wide range of geographical locations in different seasons is fundamental to test the consistency in δ^{13}C-EAA patterns of sea ice and pelagic algae across size, space, and time (Close, 2019; Whiteman et al., 2019).

It is extremely hard to build an end-member library for each phylogeny due to the difficulties in isolating substantial biomass for different species from field samples. Lab cultures require specific facilities to maintain suitable growing conditions which could be expensive and time consuming, and therefore constrain the number of species that can be grown at a time, especially for sea ice algae. To our knowledge, few facilities can simulate sea ice growth and mimic the natural sea ice environment for growing sea ice algae (Geilfus et al., 2016). Moreover, not all the species are cultivatable. Although easier to cultivate, planktonic communities are known to have a lower number of cultivatable

species compared to sea-ice communities, which may result in biases when characterizing species-specific end-members (Junge et al., 2002; Lizotte, 2003). On the other hand, field assemblages are easier to be processed and less time-consuming with less or no taxonomic identification and cultivation effort. Characterization of their δ^{13}C-EAA patterns from different types of habitats helps us obtain a general idea of contributions from different C sources to marine organic matter.

In our study, the consistency in δ^{13}C-EAA patterns and the degree of heterotrophic processing in sea ice and pelagic algae were validated by application of different multivariate analyses, linear models and comparison with published data. A tremendous advantage of using CSIA-AA proxies is the ability of amino acid δ^{13}C and δ^{15}N to provide independent evidence and information about the source contributions and heterotrophic processing in marine organic matter. However, the underlying biochemical or metabolic mechanisms remained largely unclear. For example, the $\sum$V parameter was defined as the average deviation of trophic AAs that reflects the degree of microbial resynthesis (McCarthy et al., 2007). This application has been broadly reported and yielded consistent observations across different types of samples (McCarthy et al., 2013; Batista et al., 2014; Yamaguchi & McCarthy, 2018). Yet the fundamental relationships between microbial resynthesis and the deviation of δ^{15}N values of each trophic AA are uncertain. Similar constraints can be found in the distinct δ^{13}C-EAA patterns between certain phylogenic classifications and the use of Ala and Thr to trace heterotrophic processing in microbial food webs (Larsen et al., 2013; Décima et al., 2017; Doherty et al., 2021). A thorough understanding of the amino acid δ^{13}C and δ^{15}N dynamics at molecular, cellular, and physiological levels is crucial for accurate data interpretation of CSIA-AA data in marine biogeochemistry and ecology (Whiteman et al., 2019). Lastly, amino acid δ^{13}C and δ^{15}N data have been rapidly and widely generated in the last decade. However, inter-laboratory variations across different amino acids are variable and yet, inter-laboratory comparisons of CSIA-AA data are scarce, especially for δ^{15}N-AA (Yarnes & Herszage, 2017). Future work should also consider the effects of ultrasonication and removal of supernatant on selective loss of AAs (see Sect. 2.2.2). Without accounting for such variation in CSIA-AA data due to inconsistent derivatization and calibration techniques, data generated from different laboratories may not be directly

comparable. Hence, sample preparation protocols and quality assurance procedures need to be standardized across laboratories.

2.5 Conclusion

Taken together, our study presented for the first time, distinct δ^{13}C-EAA patterns between sea ice and pelagic algae and explored the N sources, trophic transfers, and microbial resynthesis from the δ^{15}N-AA data of these samples in remote polar settings. Our observations support the hypothesis that the δ^{13}C-AA and δ^{15}N-AA patterns of sea ice algae can be distinguished from those of pelagic algae. Multivariate analyses further demonstrated the diagnostic potential of δ^{13}C-EAA to differentiate eukaryotic microalgae from sea ice and pelagic origins. These findings may enhance our understanding of C sources and transfers in ecologically important areas that are subject to sea-ice dynamics in the changing Arctic Ocean. Our study also examined the degree of trophic transfers and microbial resynthesis in the field-collected algae samples from δ^{15}N-AA. The use of Ala and Thr illustrated better relationships and separations between sea ice/pelagic algae and other end-member groups, reflecting a slightly higher degree of heterotrophic reworking in pelagic algae. These δ^{15}N-AA based proxies can provide valuable information about the general composition and purity of field samples. With the on-going sea ice decline in the coming century, it is key to understand sea ice algae production to predict future productivity and plankton community responses in the changing Arctic. Our dataset provides new insights into the differentiation in δ^{13}C-AA and δ^{15}N-AA between sea ice and pelagic algae and highlights the potential to address crucial knowledge gaps in sea ice algae dynamics using CSIA-AA.

Despite the powerful potential in CSIA-AA, limitations and challenges remain to be addressed in future research. Establishment of a larger repository of end-member data from laboratory cultures under various growing conditions and extensive sampling of marine primary producer end-members across size, space, and time are fundamental to assess the consistency in δ^{13}C-EAA patterns of different functional groups and the robustness in δ^{15}N-AA proxies to reflect N cycling processes. To improve data interpretation of the multi-dimensional CSIA-AA proxies, specific processes that control

stable isotope fractionation of individual amino acids are worth investigating. Standardization of sample processing and data calibration techniques is essential to ensure direct comparisons of cross-study datasets.

2.6 Conflict of Interest

The authors declare that the research was conducted in the absence of any commercial or financial relationships that could be construed as a potential conflict of interest.

2.7 Author Contributions

S-MC and OAS contributed to conception and design of the study. S-MC contributed to sampling. S-MC and OAS contributed to sample processing, measurements and data analysis. PM provided up-to-date references and taxonomic data from sea ice and phytoplankton studies in Frobisher Bay for comparison with our data. S-MC wrote the manuscript with input from all the co-authors.

2.8 Funding

This research was funded by NSERC Discovery Grant (RGPIN-2018-05590) and NSERC Ship Time Grant (RGPST-544990-2020) to O. Sherwood.

2.9 Acknowledgments

We would like to express our gratitude for all the officers and crew members of the Canadian Coast Guard Ship *Amundsen* for their professional support with sea ice and seawater sampling. We are grateful to C. J. Mundy from University of Manitoba for providing fast-ice algae samples and valuable insights on sea ice algae and statistics. We thank Chelsea Fougère for assistance with CSIA-AA measurements and data analysis. We thank Evan Edinger, David Cote, Blake Tibert, Nina Golombek, Amy McAllister, and Simone Booker for help at sea or in the laboratory. We thank John Gosse, Markus Kienast, Zoe Finkel, Thomas Larsen, Matthew McCarthy, and Kelton McMahon for valuable discussions about the analyses and data.

CHAPTER 3 SEA ICE ALGAE AND ZOOPLANKTON FECAL PELLETS FUEL ORGANIC PARTICLE EXPORT IN THE SEASONALLY ICE-COVERED NORTHWEST LABRADOR SEA[2]

Abstract

Ocean warming and Arctic sea ice decline are expected to affect biological pump efficiency by altering the timing, quantity, quality, and composition of export production. However, the origins and composition of sinking organic matter are still understudied for the oceans generally, and in ice-covered areas especially. Here we use compound-specific isotope analysis (CSIA) of amino acids (AAs) to investigate the sources and composition of exported organic matter from a sediment trap-derived time-series of sinking particles collected at depths of 469 m and 915 m at the edge of Saglek Bank in the northern Labrador Sea from 2017 to 2019. The outer edge of Saglek Bank is located at the confluence of cold and fresh Arctic outflow and relatively warmer Atlantic waters. The area is subject to seasonal sea ice cover and is a biological hotspot for benthic organisms including deep-sea corals and sponges. Sea ice was present for ~50–60% of the deployment days in both cycles. Primary production at our study site was initiated by sea ice breakup, which modulates light availability to under-ice algal blooms. Microalgal taxonomy indicated the presence of ice-associated diatoms in the sinking particles during the spring bloom in 2018, confirming that sea ice algae contributed to the organic particle export at our study site. Abundant copepods and copepod nauplii in the sinking particles was consistent with a high abundance of copepods in overlying epipelagic waters. Stable carbon isotopes ($\delta^{13}C$) of essential amino acids (EAAs) revealed a potentially important contribution of sea ice algae as the ultimate carbon source for sinking particles, with only minor modification by microbial resynthesis. Stable nitrogen isotopes ($\delta^{15}N$) of AAs provided independent evidence of the minor bacterial contribution and revealed dominant animal sources (4–15% zooplankton and 70–92% fecal pellets) to the sinking particles.

[2]Chen, S.M., Dezutter, T., Cote, D., Edinger, E., Lalande, C., and Sherwood, O.A. Sea ice algae and zooplankton fecal pellets fuel organic particle export in the seasonally ice-covered northwest Labrador Sea. In prep.

Student Contribution: I contributed to conception and design of the study. I contributed to sampling and sample processing, CSIA-AA and bulk stable isotope measurements, and data analysis. I wrote the manuscript with input from all the co-authors.

Together, our study demonstrates the importance of sea ice algae and fecal pellets to the biological pump in the seasonally ice-covered northwest Labrador Sea, with sea ice algae exported either directly via passive sinking or indirectly via zooplankton grazing and fecal pellets dominating the organic particle fluxes.

3.1 Introduction

The ocean's biological pump sequesters about 10 Pg of carbon per year, which represents up to one-third of anthropogenic carbon emissions to the atmosphere (Sabine et al., 2004; Sabine and Tanhua, 2010). The pump operates by exporting unrespired particulate organic matter (POM) via three pathways: passive sinking ("gravitational pump"), active transport by animals ("migrant pump"), and physical mixing ("mixing pump"; Volk and Hoffert, 1985; Turner, 2015; Nowicki et al., 2022). In deep waters, most of the POM is remineralized to CO_2 and inorganic nutrients (Martin et al., 1987); a small fraction (< 5 %) of exported POM is sedimented and buried (Middleburg, 2019). Despite its importance in global biogeochemical models, the proportional contribution of each biological pump export pathway is poorly estimated. Recent ensemble numerical modeling suggests that the gravitational pump accounts for about 70% of total carbon export, while migrating zooplankton and physical mixing account for 10% and 20%, respectively (Nowicki et al., 2022). However, biogeochemical models may overestimate the gravitational pump fluxes due to complex dependencies on factors such as the composition of sinking particles, aggregation and disaggregation processes, microbial degradation, zooplankton grazing, and fecal pellet production (De La Rocha and Passow, 2007; Turner, 2015; Durkin et al., 2016). The effects of climate change (i.e., rising temperatures, enhanced ocean stratification and acidification, and changing nutrient availability) compound the uncertainties in biological pump functioning and efficiency (Finkel et al., 2010; Passow and Carlson, 2012; Arrigo and van Dijken, 2015).

The effects of climate change are amplified in the Arctic and subarctic seas. These regions are thought to represent a globally important carbon sink (Bates and Mathis, 2009; MacGilchrist et al., 2014) due to high rates of primary productivity across the expansive continental shelves (Kaltin and Anderson, 2005; Harrison et al., 2013), high nutrient availability (Kaltin et al., 2002, Murata and Takizawa, 2003), and sea-ice and solar

dynamics (Rysgaard et al., 2007; Harrison et al., 2013). However, ongoing declines in seasonal sea ice extent and enhanced freshwater input due to global warming has affected carbon export and cycling in these regions (Steele et al., 2008; Lalande et al., 2009b; Grebmeier, 2012; Arrigo and van Dijken, 2015). An increase in primary production has been observed in the Arctic (Arrigo and van Dijken, 2015), which could lead to an increase in POM export (Lalande et al., 2009a, b). On the other hand, the loss of sea ice has also been shown to cause a reduction in surface nutrient availability and a shift in plankton community structure from larger celled plankton to picoplankton, which may decrease the POM export to the deep sea (Li et al., 2009; Finkel et al., 2010). The accelerating loss of sea ice necessitates a deeper understanding of factors controlling POM export in ice-covered ecosystems and responses to accelerating sea ice loss.

Exported sinking particles comprising the gravitational pump are typically collected, measured, and characterized using moored sediment traps (Honjo and Doherty, 1988). These tools allow for direct sampling of sinking particles in remote regions, especially where seasonal sea ice coverage constrains remote sensing of ocean colour, which does not account for widely reported under-ice algal growth and phytoplankton blooms (Strass and Nöthig, 1996; Yager et al., 2001; Fortier et al., 2002; Mundy et al., 2009; Arrigo et al., 2012, 2014). The collection of sinking particles, combined with flux measurements, plankton counts and geochemical analyses, provides information about 1) sources, cycling, and fate of key elements in the ocean, e.g., carbon and nitrogen; 2) processes and mechanisms that control the fluxes of sinking particles; and 3) biogeochemical and ecological roles of particles in the cycling of key elements. Extensive effort has led to an improved understanding of regional fluxes and composition of exported particles in Beaufort Sea (Carey, 1987; Forbes et al., 1992; Lalande et al., 2009a), Canadian Arctic Archipelago (Hargrave et al., 1989, 1994; Dezutter et al., 2021), northern Baffin Bay (Hargrave et al., 2002; Lalande et al., 2009a), Laptev Sea, and East Siberian Sea (Lalande et al., 2009a, b, 2019). Nevertheless, it is difficult to identify and quantify the main sources contributing to sinking particles collected in sediment traps. Microalgae and zooplankton taxonomy has been the traditional approach for describing and quantifying dynamics of exported communities and is critical for ground-truthing biomolecular methods that depend on cross-referencing both molecular and morphological information

(McManus and Katz, 2009; Joo et al., 2022). However, taxonomic enumeration is time-consuming and labour-intensive and is complicated by large morphological variability within and between species, lack of taxonomic expertise, and inconsistency in identification methods (McQuatters-Gollop et al., 2017). Estimates of biomass or particulate organic carbon (POC) based on composition and abundance data may also be confounded by the wide range in cell sizes within and between functional groups (e.g., diatoms, dinoflagellates, etc; Leblanc et al., 2012). An improved quantification of the composition of exported sinking particles is key to better understanding and predicting the responses of Arctic/subarctic biological pump, marine ecosystems, and benthic communities to a rapidly changing climate.

Stable isotopes of carbon ($\delta^{13}C$) and nitrogen ($\delta^{15}N$) have been widely used to investigate biogeochemical processes in marine ecosystems (Peterson and Fry, 1987; Altabet et al., 1999). Isotopic compositions of sinking organic matter collected in long-term sediment traps record information about sources and cycling of carbon and nitrogen on timescales of months to years (Nakatsuka et al., 1997; Altabet et al., 1999; Montes et al., 2013). However, traditional measurements of stable isotope values of bulk organic matter can be difficult to interpret due to confounding factors of source variability and heterotrophic modifications (Boecklen et al., 2011). Recent advances in carbon and nitrogen compound-specific isotope analysis (CSIA) of amino acids (AAs) has helped to address these complications (Larsen et al., 2009; Larsen et al., 2013; McMahon et al., 2013; Batista et al., 2014; Ohkouchi et al., 2017; Close, 2019; Shen et al., 2021). Interpretation of $\delta^{13}C$-AA analysis is based on the classification of AAs into essential and non-essential groups. Essential amino acids (EAAs) are synthesized only by autotrophs, and hence their $\delta^{13}C$ values remain unchanged with trophic transfers (Larsen et al., 2013; McMahon et al., 2013). Diverse biosynthetic pathways and associated isotopic effects result in distinct and consistent $\delta^{13}C$-EAA signatures of different primary producers, which are reflected in $\delta^{13}C$-EAA patterns of consumers (Hayes, 1993; Larsen et al., 2009). Interpretation of $\delta^{15}N$-AA, on the other hand, is based on different groupings that are independent of those based on $\delta^{13}C$. The $\delta^{15}N$ values of source AAs (SrcAAs) undergo little or no $\delta^{15}N$ enrichment during trophic transfers while those of trophic AAs (TrAAs) are enriched with increasing trophic position or modified by microbial

processing (McClelland & Montoya, 2002). Hence, the complementary but fully independent δ^{13}C-AA and δ^{15}N-AA analyses offer detailed insights about carbon and nitrogen origins, trophic changes, and microbial degradation and allow for more accurate and detailed interpretation of stable isotope data (McMahon et al., 2013; McMahon & McCarthy, 2016).

The goal of this study is to investigate the biotic carbon and nitrogen sources and trophic and microbial processing of sinking particles in a seasonally ice-covered ocean, northern Labrador Sea. Two sediment traps were deployed at different depths at the outer edge of Saglek Bank in the northern Labrador Sea from October 2017 to August 2018 and from August 2018 to July 2019, respectively. We combine traditional measurements of particle flux, phytoplankton and zooplankton taxonomy, and bulk stable isotopes, with CSIA-AA to characterize the origins, alteration, and transport mechanisms of sinking particles. Together these data help constrain the sources and proportional contributions of sinking organic matter to export flux in the northern Labrador Sea and provide valuable context for biogeochemical processes and responses in other high-latitude seas.

3.2 Material and methods

3.2.1 Study site

Located in the north-western section of the Atlantic Ocean, the Labrador Sea is a high-latitude marginal sea of the Atlantic Ocean and an important transition zone connecting Arctic and subarctic ecosystems, bounded by the Labrador and Newfoundland shelves to the west and the southern tip of Greenland to the east (Fragoso et al., 2017). The overall circulation of the Labrador Sea is cyclonic, with layers of distinct water masses in the boundary currents. The upper layer of boundary currents comprises cold and fresh Arctic waters from mixing between the water entering Baffin Bay from eastern Davis Strait, that is cooled in the winter as it circulates within the bay, and the inflow from the Arctic Ocean, that are mainly identified as the Baffin Island Current (BIC) and the Labrador Current (LC; Fig. 3.1; Tang et al., 2004). Underneath are the relatively warm and saline waters of West Greenland Current (WGC), with a dominant inflow through eastern Davis Strait and a branch deflecting westwards forming a counter-clockwise gyre (Irminger Current) while the remaining waters propagate north (Fig. 3.1; Yashayaev, 2007; Frajka-

Williams et al., 2009). In Baffin Bay, below the WGC water lies Baffin Bay Deep Water at 1200–1800 m and Baffin Bay Bottom Water below 1800 m, which have no direct access to the Arctic and Atlantic Oceans due to the relatively shallow sill depths of the Arctic channels and Davis Strait (Tang et al., 2004). The inner shelf of the Labrador Sea is covered by landfast ice with drifting pack ice cover further offshore from January to May each year (Hall et al., 1999; National Snow and Ice Data Center). The study area lies in a transitional zone between the ice-dominated Boreal Polar Province (BPLR) of the Labrador Shelf, and the largely ice-free and deeply convective Atlantic Arctic Province (ARCT) of the Atlantic Polar Biome (Longhurst, 2010), within the path of high iceberg drifts from the north (Baffin Bay) and the west (Hudson Strait; Marson et al., 2018). Differences in physical-chemical parameters shape variability in phytoplankton community composition and the seasonality of phytoplankton blooms between and within these two provinces (Fratantoni and Pickart, 2007; Yashayaev, 2007; Frajka-Williams and Rhines, 2010; Fragoso et al., 2017). Phytoplankton blooms start on the Labrador shelf from April to early May. These blooms are typically dominated by diatoms, favoured by high silicate concentrations in Arctic waters (Fragoso et al., 2018), and facilitated by vigorous tidal mixing in Hudson Strait (Drinkwater and Harding 2001). From mid-May to June, weaker blooms occur in the central Labrador Sea induced by increased light levels (Frajka-Williams and Rhines, 2010). The strong bottom currents on the Labrador shelf expose hard substrates, providing suitable habitats for deep-sea corals and sponges (Wareham & Edinger, 2007). Observations of abundant and diverse deep-sea corals and sponges are reported at Saglek Bank, forming important habitats for many fish and invertebrate species (Wareham & Edinger, 2007; Dinn et al., 2020). With ongoing global warming and sea ice decline, the ocean and ice conditions at the study site are projected to be impacted, with up to 70% decrease in winter sea ice extent and a shorter winter ice duration (Han et al., 2019), which may have cascading effects on the phytoplankton community, export fluxes, and in turn, benthic communities.

3.2.2 Environmental Data

Satellite derived daily-average sea ice concentrations were retrieved at a 12.5 km resolution from the Centre ERS d'Archivage et de Traitement (CERSAT) of the French Research Institute for the Exploration and Exploitation of the Sea (IFREMER) and

averaged for a 3° × 3° grid centred at the mooring location (59–62°N, 60–63°W; Fig. 3.1). Weekly-average chlorophyll *a* (chl *a*) concentrations for the same selected grid (59–62°N, 60–63°W) were derived from Ocean Color (Aqua MODIS, 4 × 4 km; missing data are due to obstacles in observing conditions; https://oceancolor.gsfc.nasa.gov/) and BIO remote sensing group (https://github.com/BIO-RSG). The large areal grid (333 km × 172 km) grid used for sea ice and chl *a* retrieval was necessary to smooth out data coverage gaps.

3.2.3 Sample collection and processing

Two sediment traps were deployed off Saglek Bank on the northern Labrador slope from October 2017 to August 2018 at a depth of 469 m (bottom depth: 509 m; 60.47°N, 61.26°W; denoted as trap "SB-500") and from August 2018 to July 2019 at a depth of 915 m (bottom depth: 1015 m; 60.46°N, 61.16°W; denoted as trap "SB-1000") during the annual ArcticNet expeditions of the CCGS *Amundsen* (Table 3.1; Fig. 3.1). Both sediment traps (Technicap PPS 3/3; 0.125 m^2 aperture) were equipped with a baffle sieve (diameter: 9.5 mm) covering the trap opening and 24 sampling bottles (265 ml) programmed to rotate every 14 days. Before deployment, each sampling bottle was filled with filtered seawater with a salinity > 36 PSU adjusted using sodium chloride. Sodium borate-buffered formaldehyde (2% v/v) was added to preserve the collected particles during and after deployment. In August 2018 and July 2019, both sediment traps were recovered before the final sampling bottle rotation, therefore the last sampling bottles remained open and were excluded from the study. Zooplankton were sorted from half of the volume of each trap sample under a stereomicroscope and preserved in 4% formalin solution. Zooplankton were counted and identified to the lowest taxonomic level possible (Dezutter et al., 2021). Following the removal of zooplankton, subsamples were analyzed for total particulate matter (TPM), particulate organic carbon (POC) and particulate nitrogen (PN) and converted to daily fluxes (mg m^{-2} d^{-1}) following Dezutter et al. (2021). Microalgal cells were enumerated and counted to the lowest taxonomic level possible using an inverted microscope (Wild Herbrugg) in accordance with Lund et al. (1958). For each sample, a minimum of 100 cells were enumerated along three transects (Genin et al., 2021) at a magnification of 20x for the 2017–2018 deployment and of 60x for the 2018–2019 deployment. Microalgal counts were converted to daily fluxes (cells m^{-2} d^{-1}). For bulk and

amino acid stable isotope analyses, samples were washed with Milli-Q water, freeze-dried, and homogenized prior to further analyses.

Zooplankton was opportunistically sampled with a multi-net plankton sampler (Hydrobios, mesh size 200 μm) close to the HiBio-C mooring site (60.47°N, -61.16°E) on July 25, 2021, during the annual CCGS *Amundsen* expedition. The plankton sampler was deployed with one of the nets programmed to be opened at ~ 200 m, pulled up to surface and closed. Once retrieved, zooplankton from the targeted net were gently poured into incubation chambers filled with filtered seawater (0.2 μm) to clear their gut content for 6–12 hours (Doherty et al., 2021; Stamieszkin et al., 2021). After incubation, zooplankton were transferred into a labelled plastic bag and immediately frozen and stored at -20 ℃ until further analysis.

In the laboratory, 30 to 50 copepods were subsampled from the zooplankton samples under a binocular microscope (Motic SMZ-168). The subsampled copepods were freeze-dried and homogenized until further analysis. Detritus aggregates (clumps of dark-color materials; Fig. 3.4b) that were collected along with the zooplankton from the incubation chambers were hand-picked into a Petri dish filled with Milli-Q water under the microscope. The collected detritus aggregates were then filtered onto 0.7-μm GF/F filters (Whatman) and freeze-dried until further analysis.

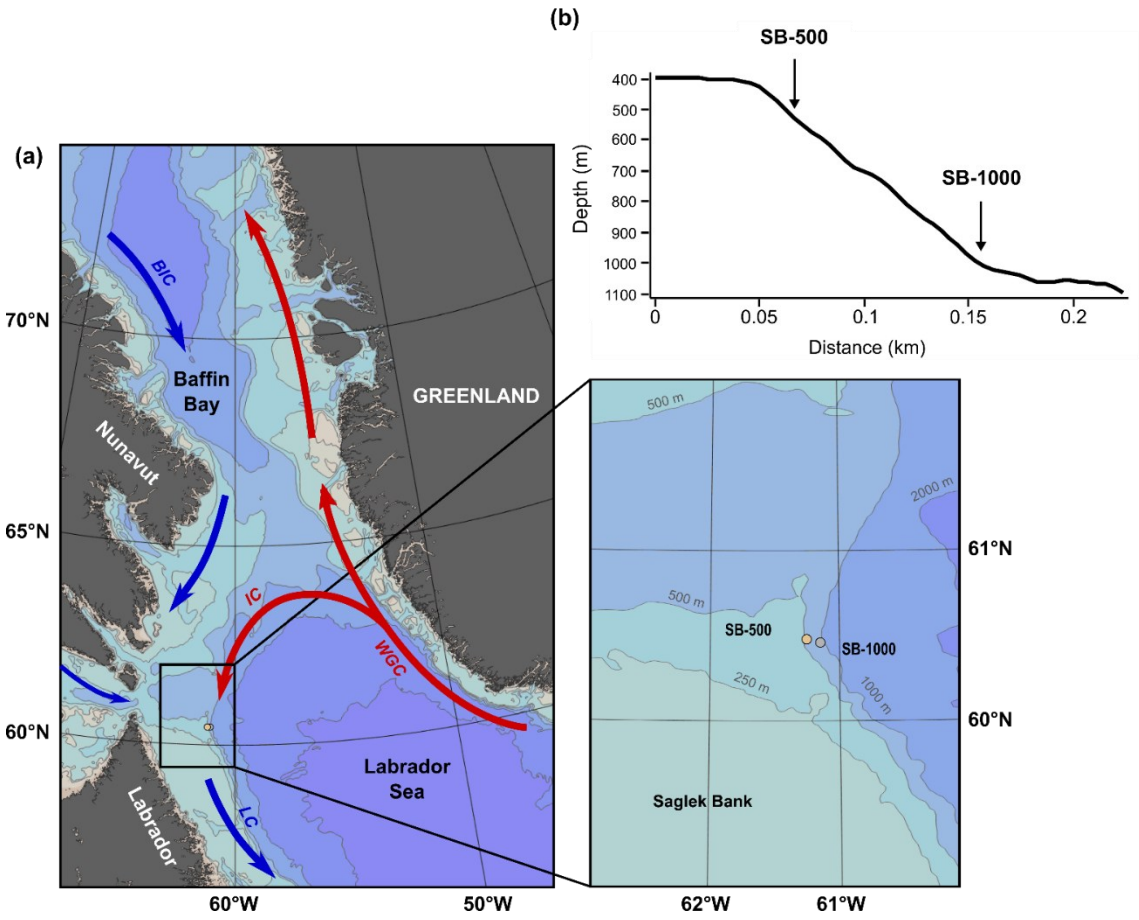

Figure 3.1 Map and inset detail of study site off Labrador and Nunavut, Canada (a) with bathymetry (grey contours), simplified representation of the main boundary currents (arrows) and sediment trap locations (circles), and (b) cross section of the continent slope where the two sediment traps (SB-500 and SB-1000) were deployed and their depth profiles. Black rectangle represents the area where sea ice concentration and surface chlorophyll *a* concentration were derived for (59–62°N, 60–63°W). Abbreviations: BIC, Baffin Island Current; LC, Labrador Current; IC, Irminger Current; WGC, West Greenland Current. Figure made with Ocean Data View, Schlitzer, 2021.

Table 3.1 Sediment trap deployment information and sea ice conditions during the deployment in the northern Labrador Sea.

Trap	Mooring	Latitude (°N)	Longitude (°E)	Trap depth (m)	Deployment date	Recovery date*	Deployment days*	Date of first ice (> 10%)	Date of last ice (>10%)	Percent of deployment days with >10% ice cover	Average areal extent of ice cover during ice-in
SB-500	HiBioA-17	60.47	-61.26	469	16-Oct-17	16-Jul-18	274	01-Jan-18	30-Jun-18	62%	44 ± 19%
SB-1000	HiBioC-18	60.46	-61.16	915	03-Aug-18	18-Jun-19	319	19-Dec-18	28-May-19	49%	42 ± 14%

*Deployment days for the final sampling bottle rotations were excluded.

3.2.4 Bulk and amino acid $\delta^{13}C$ and $\delta^{15}N$ analysis

Due to limited material in sinking particles, subsamples were taken for bulk and amino acid stable isotope analyses (Table B1, B2). Bulk $\delta^{13}C$ and $\delta^{15}N$ were measured in duplicate or triplicate (based on the available dry weight). Subsamples for bulk $\delta^{13}C$ analysis were decarbonated in 4% HCl at 80℃ for one hour and rinsed in Milli-Q water repeatedly until pH neutralized, following the method of Galy et al. (2007). Decarbonated samples were dried at 50℃ overnight. Subsamples for bulk $\delta^{15}N$ analysis were not pre-treated. Bulk $\delta^{13}C$ and $\delta^{15}N$ analysis were carried out at the Canada Excellence Research Chairs Laboratory at Dalhousie University using an Elemental Analyzer (EA; Elementar microcube) coupled with an Isotope Ratio Mass Spectrometer (IRMS; Isoprime 100). Isotopic values were calibrated to co-analyzed reference material and reported in delta notation (δ) in units of per mill "‰" relative to Vienna PeeDee Belemnite (VPDB) and air for $\delta^{13}C$ and $\delta^{15}N$, respectively. Analytical precision based on differences between sample replicates was < 0.15 ‰ for both $\delta^{13}C$ and $\delta^{15}N$.

Approximately 5 mg of organic carbon per sample was required for $\delta^{13}C$-AA and $\delta^{15}N$-AA analyses. Samples with insufficient organic carbon were combined with adjacent samples, if available. Each sample composite included not more than three samples (6 weeks) in total. Combined periods are January 31 to March 3, 2018; April 3 to May 1, 2018; and August 3 to September 18, 2018. Sample composites were hydrolyzed in 6-N HCl (Sigma-Aldrich) at 110 ℃ for 20 hours, purified and derivatized in batches of 6–7 samples following previously established protocols (Silfer et al. 1991; Larsen et al. 2013; Batista et al. 2014; McMahon et al. 2015; Chen et al. 2022). Each sample batch contained two calibration standards of AA mixtures with known $\delta^{13}C$ and $\delta^{15}N$ values and a lab standard (homogenized Chlorella powder; Organika) processed in the same way as samples. Samples were measured in triplicate for $\delta^{13}C$ and $\delta^{15}N$, bracketed by triplicate injections of calibration standards, using a Trace 1310 Gas Chromatograph (GC) coupled with a Delta V IRMS (Thermo Scientific). A total of twelve AAs were typically resolved: alanine (Ala), glycine (Gly), proline (Pro), valine (Val), leucine (Leu), isoleucine (Ile), asparagine + aspartic acid (Asx), threonine (Thr), serine (Ser), glutamine + glutamic acid (Glx), phenylalanine (Phe), and lysine (Lys). Final $\delta^{13}C$ values were corrected for the isotopic fractionation and the introduction of carbon atoms during

derivatization according to Silfer et al. (1991) and normalized against instrument drift between successive triplicate injections of the amino acid standard by applying linear regression (Yarnes and Herszage, 2017). Final $\delta^{15}N$ values were calibrated based on the offset between known and measured values of calibrated standards and normalized against instrument drift by applying linear regression. The average reproducibility of $\delta^{13}C$ was ± 0.3‰ for the internal standard Nle (n = 12), and from ± 0.3‰ (Ala, Leu, Asp, and Phe) to ± 0.8‰ (Lys) for AA standards, respectively (n = 12 for each AA). The average reproducibility of $\delta^{15}N$ was ± 0.4‰ for the internal standard Nle (n = 11), and from ± 0.2‰ (Glu) to ± 0.6‰ (Ala, Val, and Ile) for AA standards, respectively (n = 11 for each AA). The absolute (mol) and relative (mol%) abundances of amino acids were estimated by calibration of mass 44 peak areas against that of internal standard (Nle) using a relative response factor for each AA, following Kaiser and Benner (2005). Yields of total hydrolysable AAs (THAAs) were determined by dividing the total abundance of AAs by the amount of hydrolyzed material.

3.2.5 Calculations and statistical analyses

To account for the spatio-temporal variations in baseline $\delta^{13}C$ (Larsen et al. 2015; Chen et al. 2022), the $\delta^{13}C$-AA values were internally normalized by subtracting the mean of 5 EAAs (Phe, Leu, Ile, Thr and Val) for each sample (denoted as normalized $\delta^{13}C$). Normalization accounts for influences from inorganic carbon sources and other environmental parameters, whereas the internal variations between AAs reveal the underlying biochemical mechanisms (Larsen et al., 2015; McMahon et al., 2015; Stahl, 2021; Elliott Smith et al., 2022).

The $\delta^{15}N$ values for THAAs ($\delta^{15}N_{THAA}$) were calculated by summing the mol%-weighted $\delta^{15}N$ values following McCarthy et al. (2013):

$$\delta^{15}N_{THAA} = \sum(\delta^{15}N_i \times mol\%_i) \quad (1)$$

Where $\delta^{15}N_i$ is the calibrated $\delta^{15}N$ value of individual AA and $mol\%_i$ is the mol% of the corresponding AA.

The "metazoan" trophic position (TP_{met}) of samples was calculated based on calibrated $\delta^{15}N$ values of Glx and Phe, following the equation proposed by Chikaraishi et al. (2009) and modified by Nielsen et al. (2015):

$$TP_{met} = \frac{(\delta^{15}N_{Glx} - \delta^{15}N_{Phe} - 2.9‰)}{6.6‰} + 1 \quad (2)$$

The "protozoan" trophic position (TP_{pro}) was calculated based on calibrated $\delta^{15}N$ values of Ala and Phe, following Décima et al. (2017) and Décima and Landry (2020):

$$TP_{pro} = \frac{(\delta^{15}N_{Ala} - \delta^{15}N_{Phe} - 3.2‰)}{4.5‰} + 1 \quad (3)$$

Three proxies are commonly used to evaluate the degree of heterotrophic bacterial degradation in organic material, based on changes in AA composition or average deviation of $\delta^{15}N$-TrAAs. The percentage of N represented by THAA in total N (THAA-N%) is used as a degradation indicator, where THAA-N% below 38% is considered to indicate diagenetic alteration (Cowie and Hedges, 1992). THAA-N% was calculated, following:

$$THAA - N\% = \frac{\sum(mol_i \times n_i)}{DW \times TN\% \div M_N} \times 100\% \quad (4)$$

Where n is the number of N atoms in individual AA, mol_i is the absolute abundance of this AA, DW is the dry weight of hydrolyzed material, $TN\%$ is the weight percentage of total N, and M_N is the atomic mass of N. Similarly, the percentage of carbon represented by THAA in total organic carbon (THAA-C%) was calculated based on the number of carbon atoms, total organic carbon percentage, and the atomic mass of carbon.

The degradation index (DI) is based on the changes in the mol% of AAs with diagenetic alteration (Dauwe and Middelburg, 1998; Dauwe et al., 1999), and was calculated following Dauwe et al. (1999):

$$DI = \sum_i \left[\frac{var_i - AVG_i}{STD_i}\right] \times fac.coef_i \quad (5)$$

Where var_i is the mol% of each AA in this dataset (Ala, Asp, Glu, Gly, Ile, Leu, Phe, Thr, and Val), and AVG_i and STD_i are the mean and standard deviation of individual AA in the reference dataset from Dauwe et al. (1999), and $fac.coef_i$ is the factor coefficient for the corresponding AA based on the first principal component factor from Table 1 in Dauwe et al. (1999). Note that DI was calculated without Ser in this study due to unavailability of Ser data for some samples.

The degree of heterotrophic resynthesis can also be evaluated by calculating the ∑V based on the average deviation of calibrated δ^{15}N values of TrAAs from their mean, following the formula from McCarthy et al. (2007):

$$\sum V = \frac{1}{n} \sum ABS(\delta^{15}N_i - \delta^{15}N_{mean}) \quad (6)$$

Where n is the number of TrAAs used in the calculation, $\delta^{15}N_i$ are the calibrated δ^{15}N values of each TrAA (Ile, Leu, Asx, Glx, Pro, and Ala) and $\delta^{15}N_{mean}$ is the average δ^{15}N of these AAs. Higher ∑V values suggest a higher degree of heterotrophic resynthesis (McCarthy et al., 2007).

Differences in CSIA-AA patterns and parameters were tested between sediment traps, detritus, copepods, and other published end-members using Two Sample T-tests. Prior to carrying out the Two Sample T-test, the residuals of normalized δ^{13}C and calibrated δ^{15}N values were tested for univariate normality with Shapiro-Wilks test (R package: stats). To compare the normalized δ^{13}C signatures between sediment traps and sea ice and pelagic algae, principal component analysis (PCA, R package: FactoMineR) and linear discriminant analysis (LDA, R package: MASS) were performed in R version 4.1.1 with Rstudio interface version 1.4.1717. Standard ellipse areas (SEA) were plotted for each group's bivariate means in the PCA, each enclosing ~40% of the data.

Bayesian mixing models were performed in R (MixSIAR; Stock and Semmens, 2016) to estimate the proportional contributions of three end-members (phytoplankton, fecal pellets, and zooplankton) using Phe-normalized δ^{15}N-Ala and δ^{15}N-Thr to sediment traps. The models were parameterized using means and standard deviations of chosen biotracers with an uninformative prior and a MCMC chain length of 10^6 (Stock and

Semmens, 2016). Model convergence was tested with Geweke and Gelman-Rubin diagnostic tests (Stock and Semmens, 2016). We report the median of results for each end-member to account for skewed distributions of model results.

3.3 Results

3.3.1 Environmental Conditions

Sea ice in the study area began forming in early January for both sediment trap deployments and persisted until June in 2018, and May in 2019 (Table 3.1, Fig. 3.2a). The areal extent of sea ice during the ice season averaged around 40% during both deployments (Table 3.1). Due to the lower number of deployment days, SB-500 experienced a higher percentage of ice days as compared to SB-1000 (Table 3.1).

Remotely sensed chl *a* concentration showed one major bloom peak in each year, in late April 2018 and early May 2019, when ice coverage was still > 25% in areal extent (Fig 3.2a). The timing of these blooms coincided with the appearance of > 15 hours of daylight (Astronomical Applications Department of the United States Naval Observatory, "Duration of Daylight"), followed by phytoplankton blooms with a smaller magnitude (< 2 mg m^{-3}) during the open-water period (defined as sea ice concentration < 10%; Fig. 3.2a).

Table 3.2 Total particulate matter (TPM) and particulate organic carbon (POC) daily fluxes, and bulk and amino acid stable isotopes of sinking particles collected from October 2017 to July 2019 in the northern Labrador Sea (deployment days for the final sampling bottle rotations were excluded).

Trap	Cup	Date of open	Date of close	TPM (mg m^{-2} d^{-1})	POC (mg C m^{-2} d^{-1})	Bulk $\delta^{13}C$ (‰)	Bulk $\delta^{15}N$ (‰)	TP_{met}	TP_{pro}	∑V (‰)	DI	THAA yield (μmol g^{-1})	THAA-C (%)	THAA-N (%)
SB-500	1	16-Oct-17	01-Nov-17	1955	25.5	NA	NA	NA	NA	NA	NA	NA	NA	NA
	2	01-Nov-17	16-Nov-17	959	22.8	NA	NA	NA	NA	NA	NA	NA	NA	NA
	3	16-Nov-17	01-Dec-17	982	19.3	-25.3	6.8	2.1	2.3	2.2	NA	114.9	15.2	50.7
	4	01-Dec-17	16-Dec-17	1116	22.2	-25.3	6.8	2.0	2.3	1.8	-1.1	59.1	10.7	33.6
	5	16-Dec-17	01-Jan-18	591	14.3	-24.7	7.5	NA	NA	NA	NA	NA	NA	NA
	6	01-Jan-18	16-Jan-18	1007	12.9	-24.6	7.0	NA	NA	NA	NA	NA	NA	NA
	7	16-Jan-18	31-Jan-18	603	10.6	-25.0	7.2	NA	NA	NA	NA	NA	NA	NA
	8*	31-Jan-18	15-Feb-18	785	15.1	-25.6	6.3	2.1	2.9	1.8	NA	NA	NA	NA
	9*	15-Feb-18	03-Mar-18	449	10.5	NA	6.7							
	10	03-Mar-18	18-Mar-18	179	5.7	-24.6	7.2	NA	NA	NA	NA	NA	NA	NA
	11	18-Mar-18	03-Apr-18	379	7.8	NA	7.7	2.0	2.4	2.2	-0.9	69.9	NA	36.4
	12*	03-Apr-18	17-Apr-18	294	7.3	-25.4	8.1	2.1	2.6	1.9	-0.8	74.4	12.4	28.1
	13*	17-Apr-18	01-May-18	384	8.5	NA	6.3							
	14	01-May-18	16-May-18	132	4.6	-24.9	6.3	NA	NA	NA	NA	NA	NA	NA
	15	16-May-18	01-Jun-18	285	12.5	-24.3	5.9	2.0	2.0	1.8	-0.4	170.8	18.9	42.4
	16	01-Jun-18	16-Jun-18	86	4.3	-23.8	5.6	NA	NA	NA	NA	NA	NA	NA
	17	16-Jun-18	01-Jul-18	139	5.3	-25.8	6.1	NA	NA	NA	NA	NA	NA	NA
	18	01-Jul-18	16-Jul-18	167	4.4	-24.8	9.3	NA	NA	NA	NA	NA	NA	NA
	Mean ± SD			583 ± 482	11.9 ± 6.8	-24.9 ± 0.6	6.9 ± 0.9	2.0 ± 0.1	2.4 ± 0.1	2.0 ± 0.2	-0.8 ± 0.3	97.8 ± 46.0	14.3 ± 3.6	38.3 ± 8.7
	Annual flux (g m^{-2} yr^{-1})			214	4.3									

Trap	Cup	Date of open	Date of close	TPM (mg m^{-2} d^{-1})	POC (mg C m^{-2} d^{-1})	Bulk $\delta^{13}C$ (‰)	Bulk $\delta^{15}N$ (‰)	TP_{met}	TP_{pro}	$\sum V$ (‰)	DI	THAA yield (µmol g^{-1})	THAA-C (%)	THAA-N (%)
SB-1000	1*	03-Aug-18	19-Aug-18	243	8.4	NA	NA							
	2*	19-Aug-18	03-Sep-18	248	9.3	-25.9	NA	2.3	NA	1.5	0.0	120.0	NA	NA
	3*	03-Sep-18	18-Sep-18	587	16.3	-25.0	8.6							
	4	18-Sep-18	03-Oct-18	1085	23.7	-25.2	6.0	2.1	2.5	2.3	-0.7	78.2	11.5	30.3
	5	03-Oct-18	19-Oct-18	1436	30.4	-25.0	6.7	NA	NA	NA	NA	NA	NA	NA
	6	19-Oct-18	03-Nov-18	719	18.8	-25.4	NA	2.2	2.6	2.2	-0.9	86.0	11.6	NA
	7	03-Nov-18	18-Nov-18	1181	25.2	-25.5	6.7	NA	NA	NA	NA	NA	NA	NA
	8	18-Nov-18	03-Dec-18	798	16.8	-25.1	NA	2.1	2.6	2.1	-0.8	71.0	9.4	NA
	9	03-Dec-18	19-Dec-18	282	9.9	-25.4	7.6	NA	NA	NA	NA	NA	NA	NA
	10	19-Dec-18	03-Jan-19	210	5.2	-26.0	NA	NA	NA	NA	NA	NA	NA	NA
	11	03-Jan-19	19-Jan-19	1029	22.9	-24.6	7.5	2.2	2.9	2.8	-1.3	129.3	17.9	53.1
	12	19-Jan-19	02-Feb-19	223	5.9	-26.6	NA	NA	NA	NA	NA	NA	NA	NA
	13	02-Feb-19	16-Feb-19	631	11.4	-25.1	6.9	NA	NA	NA	NA	NA	NA	NA
	14	16-Feb-19	03-Mar-19	1711	24.5	-24.8	7.1	2.0	2.3	1.9	-1.0	44.6	8.4	24.8
	15	03-Mar-19	19-Mar-19	2383	28.4	-24.5	7.8	1.9	2.5	NA	0.5	17.5	1.9	11.7
	16	19-Mar-19	03-Apr-19	3017	32.0	-24.8	7.2	2.0	2.7	1.9	2.2	12.4	3.5	9.3
	17	03-Apr-19	18-Apr-19	884	13.4	-24.9	NA	2.1	2.8	1.8	-1.1	61.8	11.2	NA
	18	18-Apr-19	03-May-19	1360	19.3	-25.0	NA	NA	NA	NA	NA	NA	NA	NA
	19	03-May-19	19-May-19	2241	28.4	-24.7	4.5	1.8	2.0	1.6	NA	NA	NA	NA
	20	19-May-19	03-Jun-19	2784	35.1	-24.9	5.3	1.9	2.3	1.9	0.0	36.8	7.8	19.9
	21	03-Jun-19	18-Jun-19	2036	28.4	-25.2	6.5	NA	NA	NA	NA	NA	NA	NA
	Mean ± SD			1195 ± 871	19.7 ± 9.1	-25.2 ± 0.5	6.8 ± 1.1	2.0 ± 0.2	2.5 ± 0.3	2.0 ± 0.4	-0.3 ± 1.0	65.8 ± 39.5	9.2 ± 4.7	24.9 ± 15.9
	Annual flux (g m^{-2} yr^{-1})			438	7.2									

*CSIA-AA values were combined for adjacent sampling periods (cups).

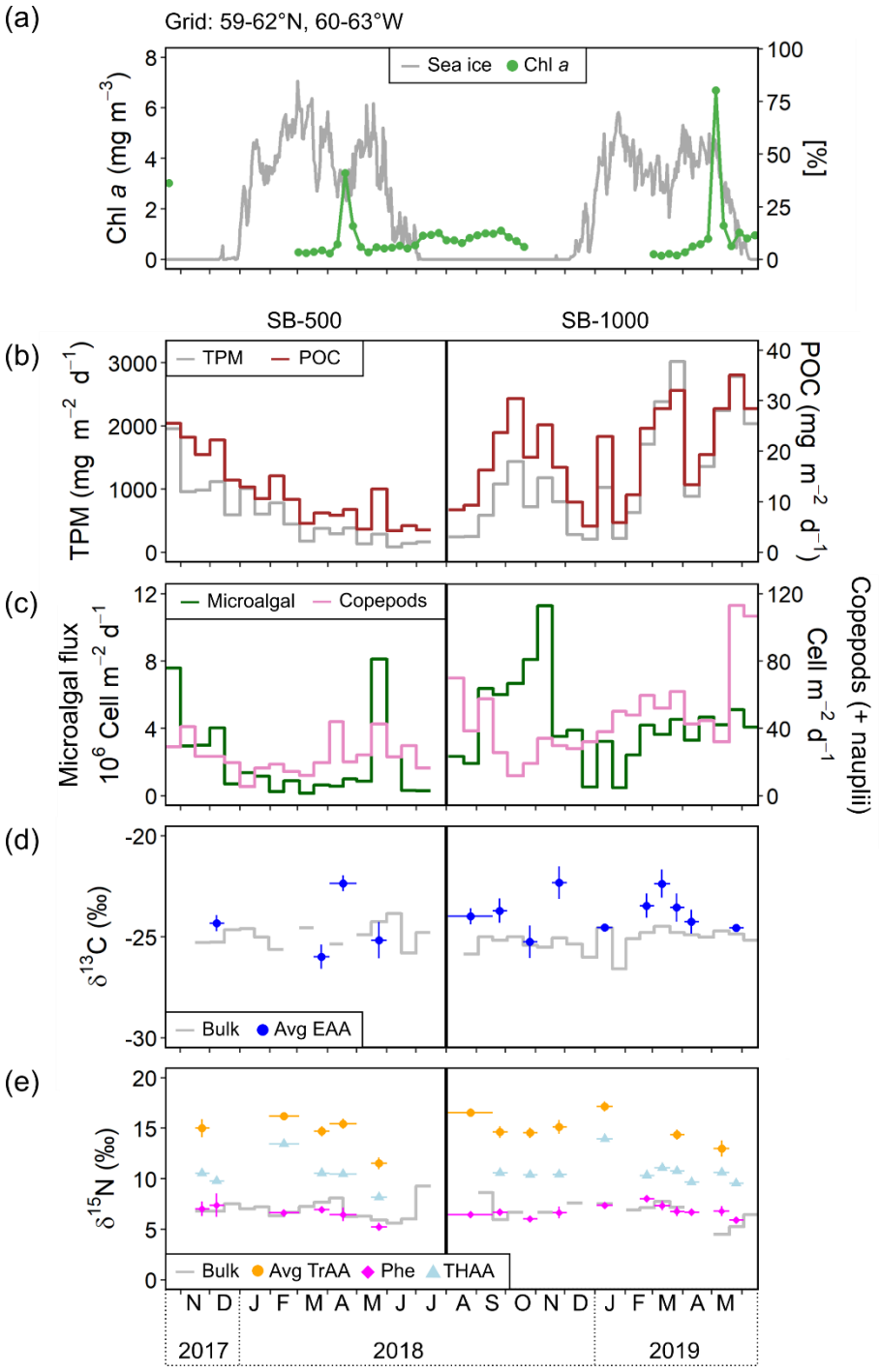

Figure 3.2 Time-series of (a) satellite derived daily sea ice concentration at a 12.5 km resolution from the Centre ERS d'Archivage et de Traitement (IFREMER) and weekly-averaged chl a concentration derived from Ocean Color (Aqua MODIS, 4 × 4 km; missing data are due to obstacles in observing conditions; https://oceancolor.gsfc.nasa.gov/) and BIO remote sensing group (https://github.com/BIO-RSG) for the 3° × 3° grid centred at the mooring site (59–62°N, 60–63°W), (b) total particulate matter (TPM) and particulate organic carbon (POC) fluxes, (c) microalgal flux (diatoms + Chlorophyceae + flagellates) and copepod flux (including copepod nauplii), (d) bulk δ^{13}C and average δ^{13}C of five essential amino acids (Avg EAA; Phe, Thr, Ile,

Leu, Val), and (e) bulk $\delta^{15}N$, average $\delta^{15}N$ of trophic AAs (Avg TrAA), Phe, and total hydrolysable AAs (THAA) of SB-500 and SB-1000 sinking particles. Vertical error bars show ±1 standard deviation for each sample (n = 3–4). Horizontal error bars show temporal ranges of individual or combined samples (see Sect. 3.2.4).

3.3.2 Particulate matter and organic carbon fluxes

The annual TPM flux (438 g m^{-2} yr^{-1}) was ~2 times higher during the 2018–2019 cycle (SB-1000) than during the 2017–2018 cycle (214 g m^{-2} yr^{-1}; SB-500 trap; Table 3.2). The POC flux of the SB-1000 trap was also ~2 times higher than at 469 m (7.2 and 3.8 g C m^{-2} yr^{-1} respectively; Table 3.1). Daily fluxes of TPM shared similar trends with POC in both cycles (Fig. 3.2b). In SB-500, TPM and POC showed an overall decreasing trend from late October 2017 to July 2018, with a small peak in May (Fig. 3.2b). In SB-1000, TPM and POC peaks were observed in early October and late March and May 2019 (Fig. 3.2b).

3.3.3 Microalgal and copepod fluxes

Diatoms, Chlorophyceae and flagellates dominated the microalgal flux in both cycles (~97%). The total fluxes of diatoms, Chlorophyceae and flagellates peaked in late October 2017 and late May 2018 in SB-500 and early November 2018 in SB-1000 (Fig. 3.2c). Peaks of diatoms were observed in late October, 2017, and from May to June, 2018 in SB-500 (Fig. 3.3a). Centric diatoms contributed the majority of the diatom export in both cycles (Fig. 3.3b). Shortly before the diatom peak in late May, 2018, surface chl *a* maximum was observed in April (Fig. 3.2a, 3.3a). During the phytoplankton bloom in late May 2018, sea ice exclusive species *Nitzschia frigida* and *Melosira arctica* were reported (Fig. 3.3). Centric and pennate diatom species that are ice-associated, for example, *Chaetoceros/Attheya* spp., *Fragilariopsis* spp., and *Nitzschia/Pseudo-Nitzschia* spp. were also reported during the spring bloom in 2018 (Fig. 3.3). High fluxes of Chlorophyceae (> 2 million cells m^{-2} d^{-1}) were observed in late October and November and early December, 2017 in SB-500 and from early September to early November, 2018 in SB-1000 (Fig. 3.3a). Dominances of flagellates were only observed in sinking particles of SB-1000, contributing to up to ~75% of the microalgal flux (Fig. 3.3b).

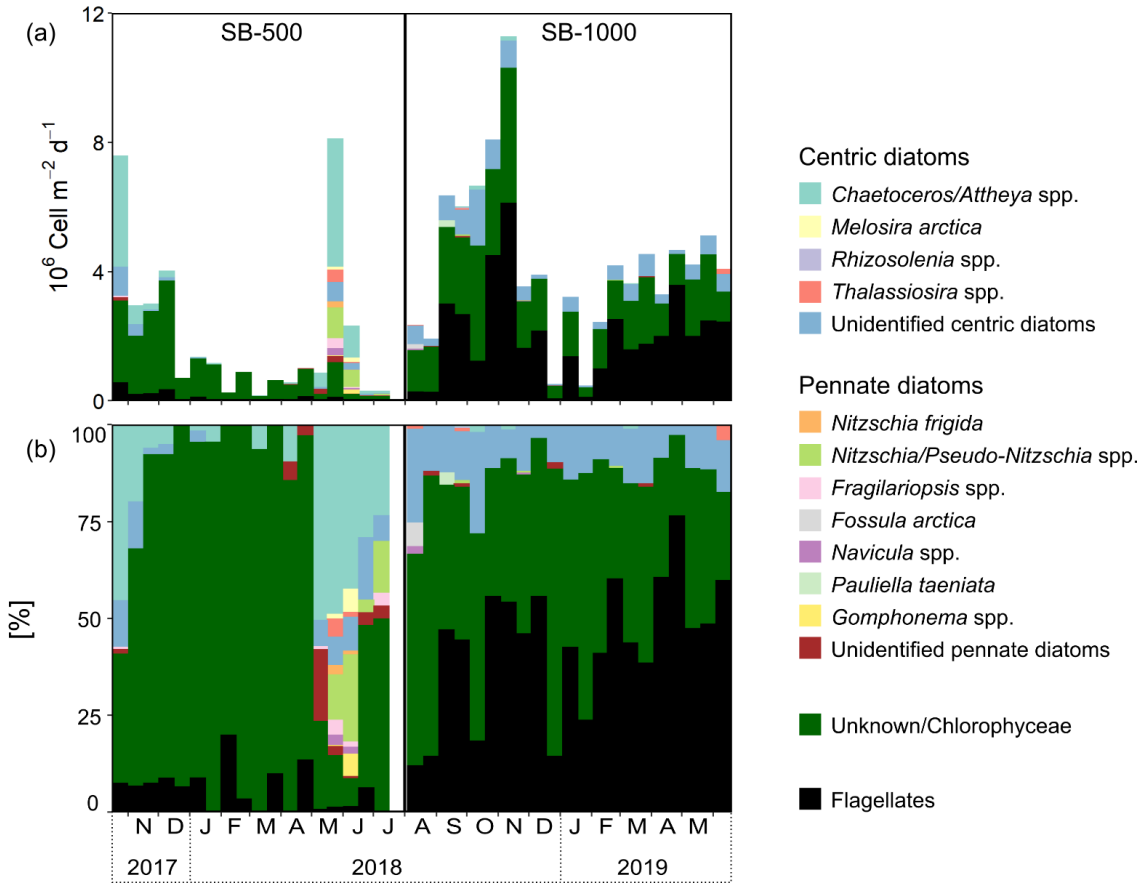

Figure 3.3 (a) Fluxes of diatoms, Chlorophyceae (listed as "unknown" in 2017–2018 cycle), and flagellates and (b) percent contribution of diatoms, Chlorophyceae, and flagellates in sinking particles collected in SB-500 and SB-1000 sediment traps.

Copepods and copepod nauplii dominated the zooplankton community for most of the deployment periods in both cycles, except when the empty shells of pteropod *Limacina spp.* were dominant in late November in 2017 and September in 2018 (data not shown). Peaks of the copepod fluxes were observed in early November, 2017, and early April and late May, 2018 in the SB-500 sinking particles and in early August, 2018, late March and late May in 2019 in the SB-1000 sinking particles (Fig. 3.4a). In July 2021, large-bodied copepods, e.g., *Calanus* sp., dominated the zooplankton community collected near HiBio-C mooring site (Fig. 3.4b, c).

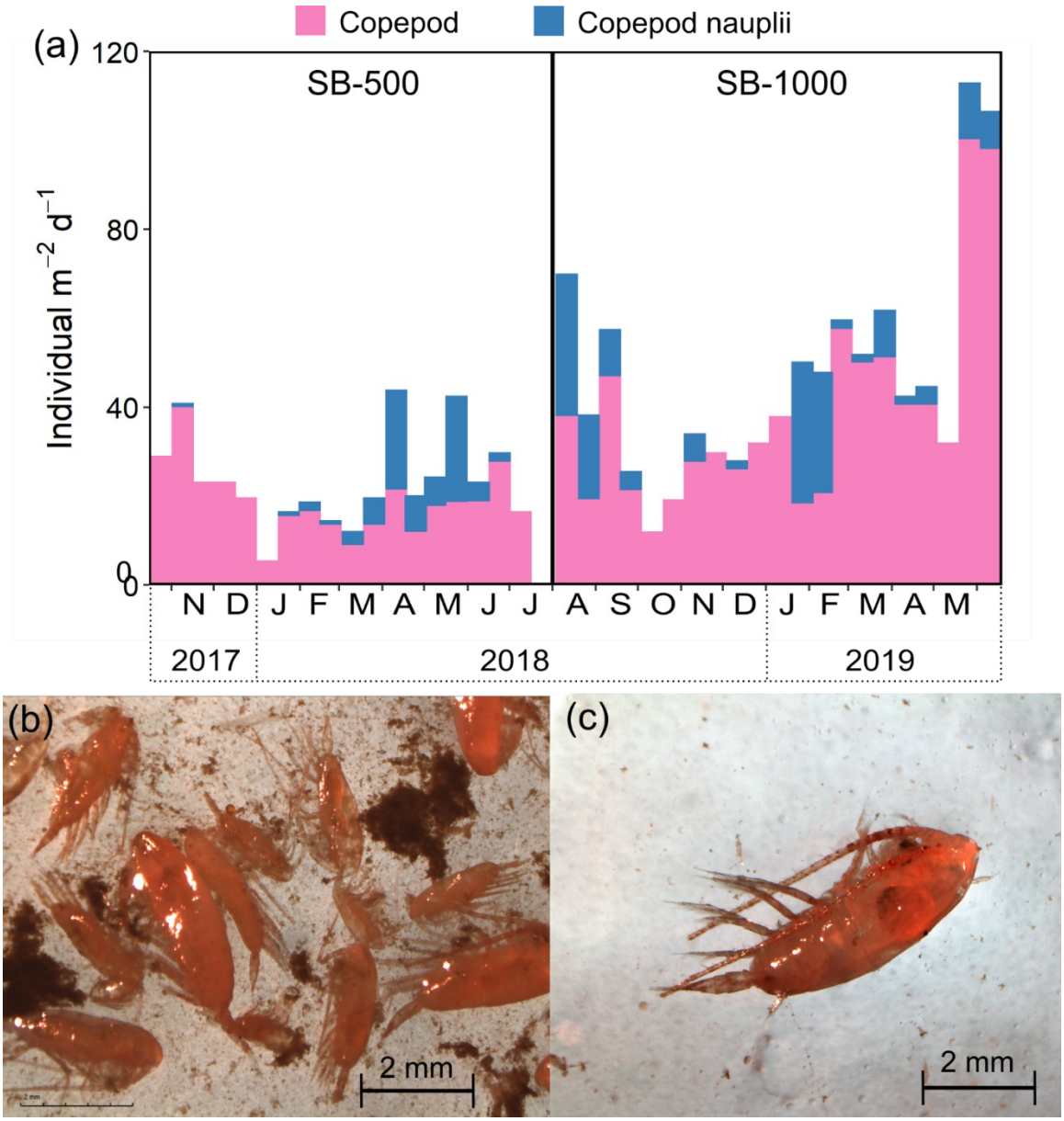

Figure 3.4 (a) Fluxes of copepods and copepod nauplii in sinking particles collected in SB-500 and SB-1000 sediment traps and example images of zooplankton collected in the northern Labrador Sea in 2021. (b) A mixture of copepods and detritus aggregates in the multi-net samples and (c) example of individual copepod subsampled for CSIA-AA analyses

3.3.4 Temporal changes in bulk and amino acid $\delta^{13}C$ and $\delta^{15}N$

Bulk $\delta^{13}C$ values for the SB-500 and SB-1000 traps were similar, varying from -25.8‰ to -23.8‰ and from -26.6‰ to -24.5‰, respectively (Fig. 3.2d). The average $\delta^{13}C$-EAA values of the sinking particles were more variable than the bulk $\delta^{13}C$ values, fluctuating from -26.0‰ to -22.3‰ with no significant difference (Fig. 3.2d). Bulk $\delta^{15}N$ values of the SB-500 and SB-1000 traps ranged from 5.6‰ to 9.3‰ and from 4.5‰ to

8.6‰, respectively (Fig. 3.2e). The δ^{15}N-Phe values, which is commonly used to indicate N source δ^{15}N value, averaged 6.6 ± 0.7‰ and 6.8 ± 0.6‰ for the SB-500 and SB-1000 traps, respectively, with both minima occurring in May shortly after the surface water chlorophyll peaks (Fig. 3.2e). The δ^{15}N-TrAA values in both sediment traps averaged ~8.0‰ more elevated than the δ^{15}N-Phe, varying from 11.5‰ to 17.2‰ (Fig. 3.2e). The δ^{15}N of total hydrolysable AAs (THAA) averaged 10.5 ± 1.7‰ and 10.7 ± 1.2‰ for the SB-500 and SB-1000 traps, respectively, ranging between δ^{15}N-Phe and δ^{15}N-TrAA (Fig. 3.2e).

3.3.5 Amino acid δ^{13}C and δ^{15}N patterns

To explore potential carbon sources to export production, we compared the normalized δ^{13}C-AA patterns with algae collected from melted brash ice and pelagic algae collected from deep chlorophyl maximum depth in the northern Labrador Sea and Baffin Bay in 2019 and 2021 (see details in Chen et al., 2022). Sinking particles obtained during both sampling periods and at both depths shared similar δ^{13}C-EAA patterns, with δ^{13}C values of ~-4.3‰ for Phe and Val, ~12.5‰ for Thr, ~2.9‰ for Ile and ~-6.8‰ for Leu (Fig. 3.5a). The δ^{13}C-EAA patterns of sinking particles were overall similar to those measured previously for sea ice algae (Two-Sample T-Test on individual EAAs, $p > 0.05$ except Leu; Chen et al., 2022) than to those of pelagic algae (< 0.05 for Phe, Thr, and Leu; Fig. 3.5a; Chen et al., 2022).

Patterns of calibrated δ^{15}N-AA (Fig. 3.5b) were broadly similar to those for sinking particles reported in other geographical locations, with more enriched δ^{15}N-TrAA and more depleted δ^{15}N-Thr compared to δ^{15}N-SrcAA (Monterey Bay, Shen et al., 2021; Gulf of Maine, Golombek et al., 2024). No significant differences were found in δ^{15}N-AA values between SB-500 and SB-1000 particles (Two Sample T-test, $p > 0.05$). The δ^{15}N values of individual TrAAs fluctuated from ~12.0‰ to ~17.0‰ (Fig. 3.5b). The δ^{15}N values of TrAAs and Thr for sinking particles showed significant distinctions from sea ice and pelagic algae ($p < 0.05$) and detritus ($p < 0.05$ except Val). No significant differences were observed in δ^{15}N-TrAAs between sediment traps and copepods (except Ala). The δ^{15}N-Phe of sinking particles was comparable with sea ice algae ($p > 0.05$) but significantly higher than pelagic algae, copepods, and detritus ($p < 0.05$; Fig. 3.5b).

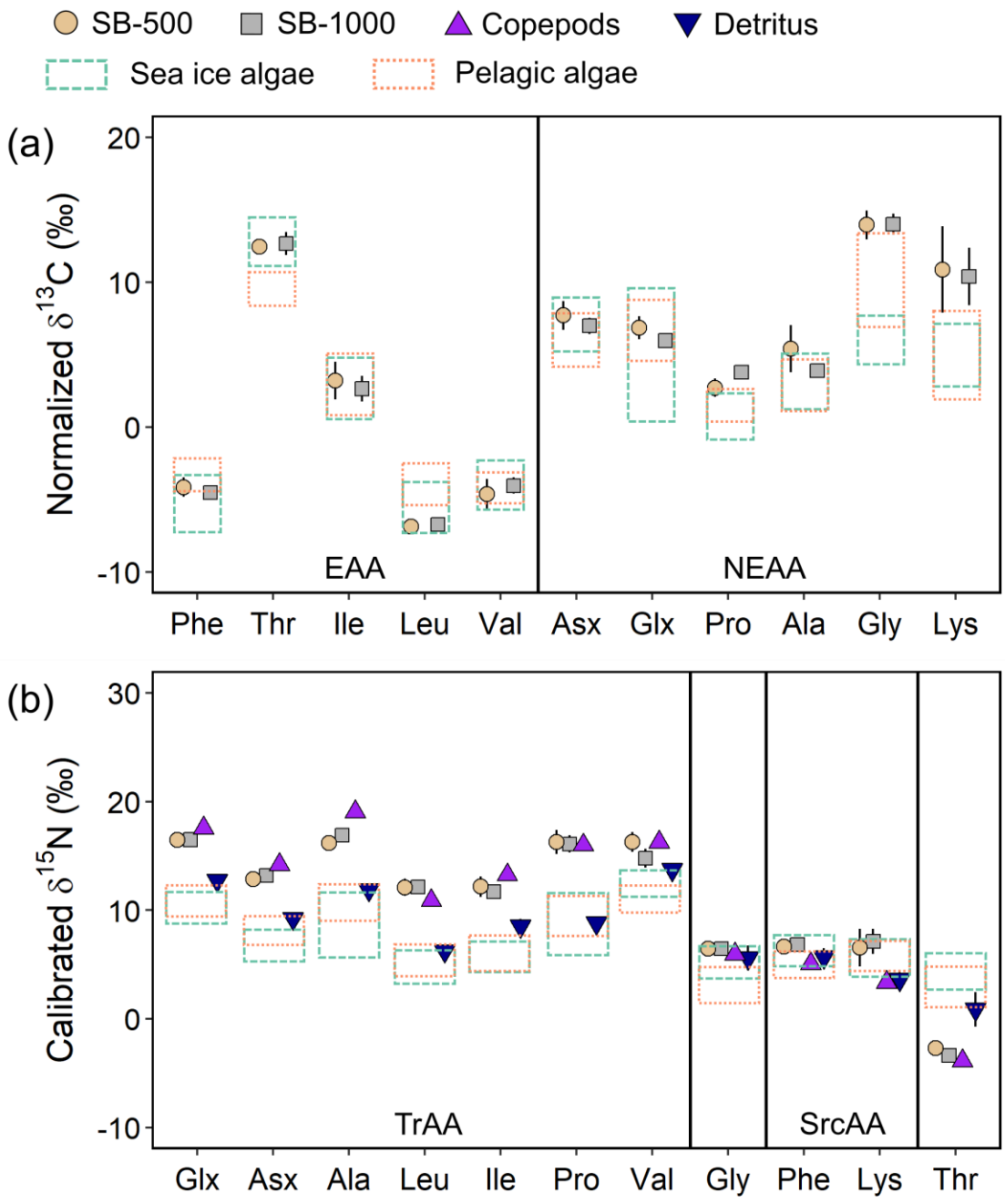

Figure 3.5 Normalized δ^{13}C-AA patterns (a) and calibrated δ^{15}N-AA patterns (b) of SB-500 and SB-1000 sinking particles, copepods and detritus collected close to the mooring site. Data are compared with normalized δ^{13}C-AA and calibrated δ^{15}N-AA patterns of > 3 µm and 0.2–3 µm sea ice and pelagic algae collected from the Northern Labrador Sea and Baffin Bay, respectively (Chen et al., 2022; dashed and dotted rectangles; range: mean ±1 stdev). Error bars show ±1 standard error for each group (SB-500: n = 4–6; SB-1000: n = 7–11; Copepods: n = 3; Detritus = 3). EAA, essential amino acid; NEAA, non-essential amino acid; TrAA, trophic amino acid; SrcAA, source amino acid.

3.3.6 Microalgal and bacterial contribution to sinking particles

To evaluate the potential contributions of sea ice and pelagic algae to the sinking particle fluxes, normalized δ^{13}C-AA patterns were compared using PCA (Fig. 3.6a). PCA based on normalized δ^{13}C-EAA explained 66.3% of the total variation, with the first two principal components (PC1 and PC2) accounting for 36.5% and 29.8%, respectively (Fig. 3.6a). The standard ellipses of sinking particles mostly overlapped with each other as well as sea ice algae while clustered apart from pelagic algae (Fig. 3.6a).

To investigate the degree of bacterial biomass in sinking particles, we performed LDA based on a training dataset comprising eukaryotic microalgae and bacteria from Larsen et al. (2009; 2013). While bacteria and eukaryotic microalgae demonstrated distinct δ^{13}C-EAA patterns from each other, 13 out of 14 sinking particle samples were classified as eukaryotic microalgae with 100% probability (one classified as bacteria with 58% probability; Fig. 3.6b).

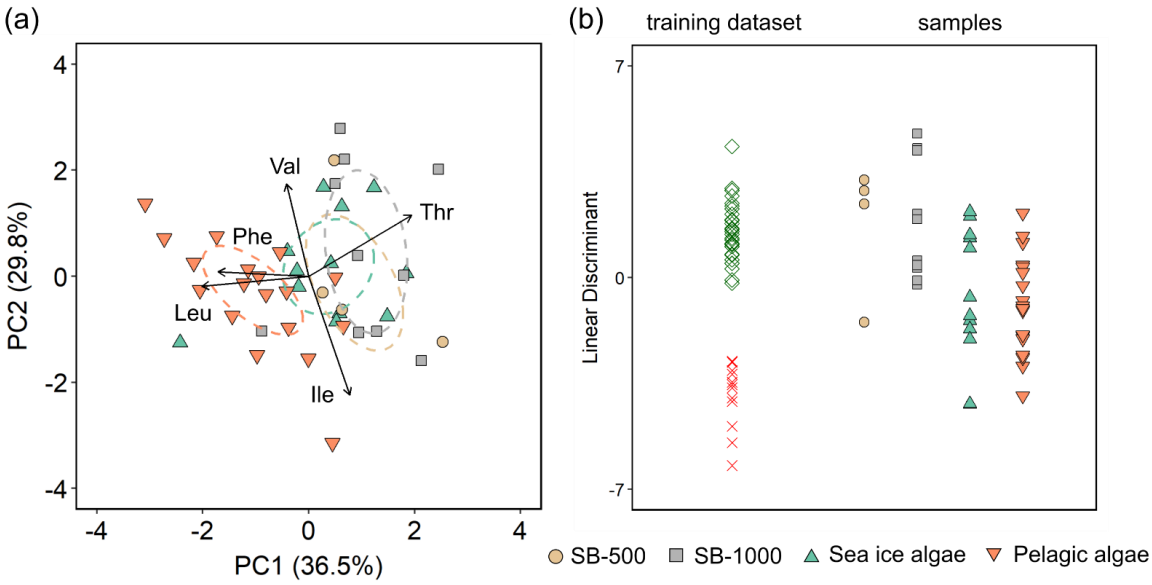

Figure 3.6 Principal component analysis (a) based on normalized δ^{13}C values of five essential amino acids of sinking particles collected in SB-500 and SB-1000 sediment traps, > 3 µm and 0.2–3 µm sea ice algae and pelagic algae and (b) linear discriminant analysis based on normalized δ^{13}C values of five essential amino acids of a training dataset comprising bacteria (open crosses) and eukaryotic microalgae (open diamonds) from Larsen et al. (2009; 2013). Values in parentheses of the axis titles are the percentage variation explained by each axis. The coloured ellipses represent standard ellipse area (SEA) for each corresponding group, containing ~40% of the data. Sea ice and pelagic algae data are from Chen et al., 2022.

The "metazoan" trophic position (TP_{met}) values of both sediment traps averaged 2.0 (Fig. 3.7a). The "protozoan" trophic position (TP_{pro}) averaged 2.4 and 2.6 for the SB-500 and SB-1000 traps, respectively, significantly different from but ranging between detritus (1.7 ± 0.3) and copepods (3.4 ± 0.3; Two Sample T-test, $p < 0.01$; Fig. 3.7b). Values of the ∑V parameter for microbial resynthesis for SB-500 and SB-1000 sediment traps ranged from 1.8 to 2.2‰ and from 1.5 to 2.8‰, respectively, similar to detritus (1.6–1.9‰; Two Sample T-test, $p > 0.1$) and slightly lower than copepods (2.2–2.7‰; $p < 0.05$; Fig. 3.7c). No significant offsets were found in TP_{met}, TP_{pro}, and ∑V values between SB-500 and SB-1000 sediment traps ($p > 0.1$).

Phe-normalized $\delta^{15}N$ of Ala and Thr has been shown to improve characterization of potential end-member contributors to sinking particles (Doherty et al., 2021; Chen et al., 2022; Wojtal et al. 2023). The Phe-normalized $\delta^{15}N$-Ala and $\delta^{15}N$-Thr values were similar between SB-500 and SB-1000 sediment traps (Two Sample T-test, $p > 0.1$), ranging around 10.0‰ and -9.5‰, respectively and overlapping with fecal pellets ($p > 0.1$; Fig. 3.7d). Copepods shared similar $\delta^{15}N$-Ala and $\delta^{15}N$-Thr values with zooplankton ($p > 0.1$). Detritus values ranged between phytoplankton, fecal pellets, and zooplankton end-members (Fig. 3.7d).

A three-end-member Bayesian mixing model based on Phe-normalized $\delta^{15}N$ of Ala and Thr demonstrated a dominant contribution (70–92%) of fecal pellets to sinking particles in both sediment traps (Fig. 3.8). Zooplankton contributed 4–15% and phytoplankton contributed 1–23% to the sinking particles (Fig. 3.8). Phytoplankton contribution peaked during the spring bloom in 2018 (Fig. 2a, 3a, 8). No significant differences were found in the modelled contributions of phytoplankton, zooplankton, and fecal pellets to the sinking particles between the SB-500 and SB-1000 traps.

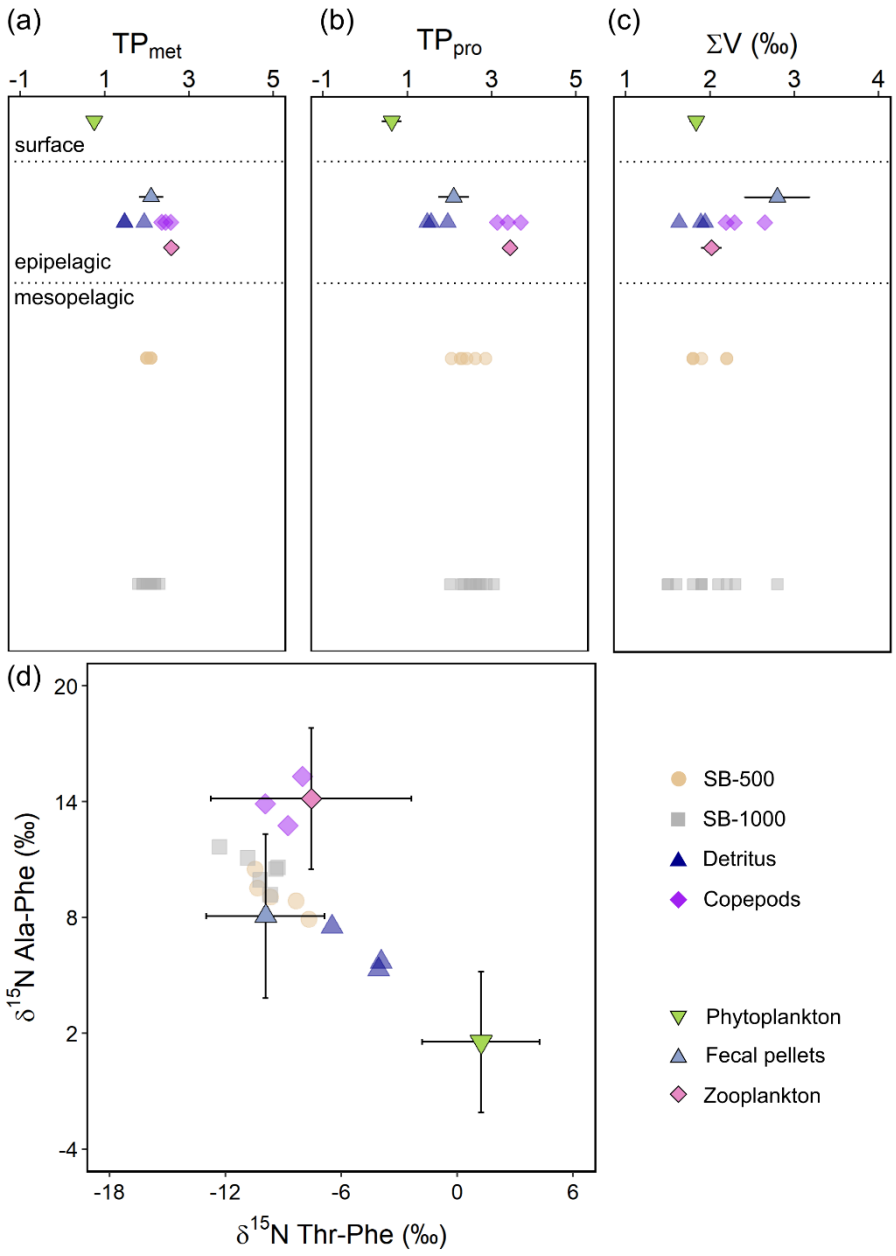

Figure 3.7 δ^{15}N-AA parameters for trophic positions and microbial resynthesis of sinking particles collected in SB-500 and SB-1000 sediment traps, detritus, and copepods (semi-transparent shapes), compared with means of phytoplankton, fecal pellets, and zooplankton end-members (shapes with error bars). (a) "metazoan" trophic position (TP_{met}), (b) "protozoan" trophic position (TP_{pro}), and (c) the $\sum V$ parameter in different water layers. (d) Phe-normalized δ^{15}N of Ala and Thr. Error bars show ±1 standard errors. End-member distributions are from previously published literature: McClelland and Montoya, 2002; Chikaraishi et al., 2009; Hannides et al., 2009, 2013; Doherty et al., 2021.

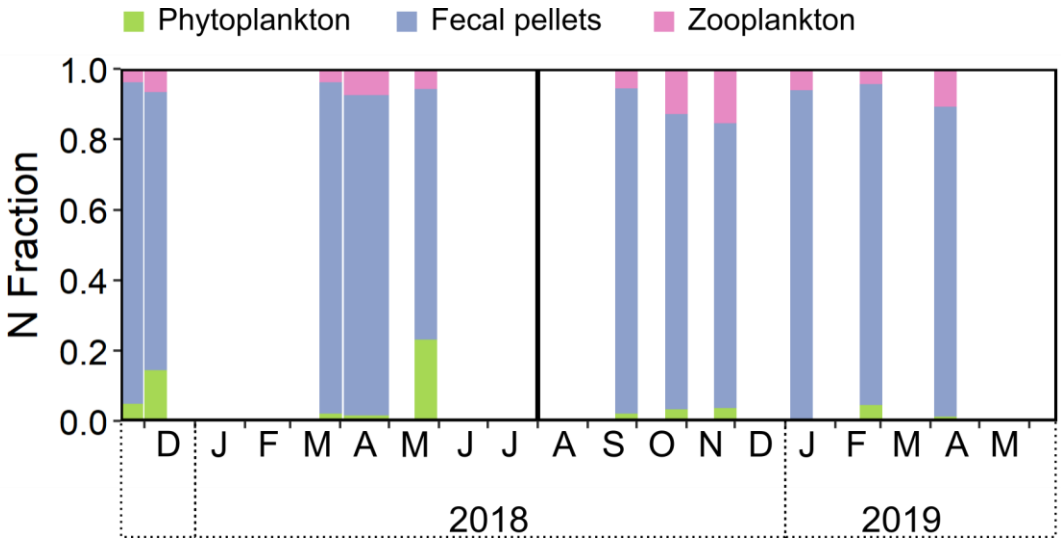

Figure 3.8 MixSIAR-derived relative contributions of different end-members in sinking particles. The relative N contributions from zooplankton, fecal pellets, and phytoplankton were estimated based on Phe-normalized $\delta^{15}N$ of Ala and Thr. End-member source data are from previously published literature: McClelland and Montoya, 2002; Chikaraishi et al., 2009; Hannides et al., 2009, 2013; Doherty et al., 2021.

3.4 Discussion

The benthic habitats of Saglek Bank area, including the Labrador Shelf slope, are known to support abundant deep-sea corals and sponges, for example, the gorgonian *Primnoa resedaeformis* and the large sponge *Geodia* spp. (Wareham and Edinger, 2007; Dinn et al., 2020). These deep-water sessile organisms rely on deposition of POM from the surface (Sherwood et al., 2005; Sherwood and Edinger, 2009; Dinn et al., 2020). Therefore, an enhanced understanding of the biotic carbon and nitrogen sources and trophic and microbial processing in the sinking particles at the Saglek Bank area is critical. In our study, $\delta^{13}C$-EAA results revealed dominance of relatively "fresh" organic matter (i.e., less microbially degraded) and a potentially high baseline contribution of sea ice algae to sinking particles (at the base of food web). The $\delta^{15}N$-AA data suggested sinking particles were dominated by animal sources, fecal pellets and zooplankton. Together, these results suggested that sea ice algae and exported zooplankton fecal pellets can be a critical source of C and N for the benthic fauna.

3.4.1 Contribution of surface primary production

Bulk $\delta^{13}C$ values of sinking particles at the study site (-26.6 to -23.8‰) fell toward the lower end of the typical range of marine particulate organic matter from

Arctic/subarctic regions (-19 to -26‰; Schubert and Calvert, 2001; Søreide et al., 2006; Belt et al., 2008). The temporal variability of bulk $\delta^{13}C$ was relatively small (~2.0‰) and was not correlated to the more variable $\delta^{13}C$-EAA (~4.0‰; $r^2 = 0.004$; Fig. 3.2d). Given the low THAA-C% (< 20%), the bulk $\delta^{13}C$ signal in the sinking particles was likely driven by other (non-EAA) carbon-containing compounds (i.e., NEAAs, amino sugars, carbohydrates, lipids, molecularly uncharacterizable organic compounds) and was therefore largely decoupled from $\delta^{13}C$-EAA due to biogeochemical and/or metabolic processing during export and sinking.

In a previous study, $\delta^{13}C$-EAA in sinking particles collected in sediment traps deployed in Monterey Bay was shown to quantitatively track the bulk $\delta^{13}C$ of surface primary production (Shen et al., 2021). If this principle applies to sinking particles generally, then the $\delta^{13}C$-EAA measured in the Saglek Bank traps would imply that the bulk $\delta^{13}C$ of surface water primary production ranges from -26.0 to -22.3‰ over an annual cycle. These values bracket a recently modelled estimate of mean annual baseline $\delta^{13}C$ (-23.5‰) at 60°N/60°W in the Labrador Sea but exceed the modelled annual variability by about 3 ‰ (Espinasse et al. 2022). Given the negligible microbial influence on $\delta^{13}C$-EAA values (discussed below), the $\delta^{13}C$-EAA results imply a potentially wider variability in primary producer $\delta^{13}C$ than currently captured in isoscape models of baseline $\delta^{13}C$.

Beyond tracking the $\delta^{13}C$ of primary production, $\delta^{13}C$-EAA signatures are potentially even more useful for quantifying the relative contributions of different primary producer functional groups in marine food webs (Lehman, 2009; Larsen et al., 2013; Schiff et al., 2014; Vokhshoori et al., 2014). Both sediment traps demonstrated similar $\delta^{13}C$-EAA patterns with sea ice and pelagic algae collected from Northern Labrador Sea and Baffin Bay (Chen et al., 2022; Fig. 3.5), suggesting that exported organic carbon primarily originated from surface primary production, assuming that sea ice and pelagic algae are the major autotrophic sources (Irwin, 1990; Gosselin et al., 1997). Sea ice algae are generally acknowledged to play an important role in primary and export production in the Arctic Ocean, especially in higher latitudes of the Arctic (Hsiao, 1980; Michel et al., 1996; Gosselin et al., 1997; Fernández-Méndez et al, 2014; Fadeev et al., 2021). In our study, a higher similarity was observed between sinking particles and

sea ice algae (Two Sample T-test, $p > 0.1$ except Leu), compared to pelagic algae ($p < 0.05$ for Phe, Thr, and Leu; Fig. 3.5a). This resemblance was further evidenced by the overlap of sinking particles with sea ice algae in the PCA (Fig. 3.6b), suggesting the carbon in EAAs of the sinking particles originates largely from sea ice algae.

The large contribution of sea ice algae to the sinking particles is operated via two pathways: direct sinking of ice algal biomass and indirect transfers via heterotrophic processing (e.g., zooplankton grazing). Sea ice algal biomass is generally composed of relatively large cells (> 5 μm; 50–100%) in the Arctic (Gosselin et al., 1997) and hence is exported more efficiently to depth, compared to pelagic algae. Sea-ice or under-ice diatoms typically form large under-ice mats and long strands; when detached from ice, the strands sink rapidly, sporadically contributing large amounts of C to the benthic ecosystem (Fernández-Méndez et al, 2014). Fast-sinking ice-associated diatom aggregates contribute to higher export efficiency and enhanced pelagic-benthic coupling, whereas smaller and slow-sinking flagellate-dominated aggregates are largely recycled in the epipelagic waters (Fadeev et al., 2021). At our study site, sea ice was present for ~50–60% of the deployment days in both cycles (Table 3.1). Both chl *a* maxima in early April, 2018 and early May, 2019 coincided with sea ice breakups (defined as sea ice concentration < 50% for more than five consecutive days), suggesting surface algal blooms induced by an increase in light availability with sea ice melt and a potential release of sea ice algae to the water column by the ice melt (Fig. 3.2a; Michel et al., 1993). Light availability for primary production in sea ice-covered Arctic and subarctic seas is largely governed by daylight periods, sea ice cover, and snow depth, controlling the timing and initiation of under-ice blooms (Mundy et al., 2009, 2014; Leu et al., 2015). In the Labrador Sea, light is the primary limiting factor to primary production for most of the year, whereas nutrients becomes co-limiting or limiting in summer/autumn as they become depleted within the mixed layer, especially for nitrate on the Labrador Shelf (Harrison and Li, 2007). Following the chl *a* maxima, the persistent phytoplankton blooms with a smaller magnitude (< 2 mg m^{-3}) during the open-water period could be governed by nutrient limitation (Fig. 3.2a; Leu et al., 2015). Nevertheless, remote-sensing of ocean color only accounted for phytoplankton blooms in open water and thus under-ice algal growth remained “invisible” and its magnitude was uncertain.

Direct sinking of sea ice algae was also evident by the microalgal taxonomy of our sinking particles. Sea ice and pelagic algae are often dominated by centric and pennate diatoms with species reported in both habitat types (Hsiao, 1980; Melnikov, 1998; Poulin et al., 2011), for example, *Chaetoceros/Attheya* spp., *Fragilariopsis* spp., and *Nitzschia/Pseudo-Nitzschia* spp, which were also observed in our samples (Fig. 3.3). Microalgal counts revealed a dominance of *Chaetoceros/Attheya* spp. in the fall diatom fluxes in 2017 and the fluxes in 2018 while unidentified centric diatoms dominated the fall fluxes in 2018 and the spring fluxes in 2019 (Fig. 3.3b). Although it is difficult to tell what fraction of the observed diatoms were originated from sea ice or pelagic habitats, the observation of sea ice exclusive species *Nitzschia frigida* and *Melosira arctica* in the sinking particles of the northern Labrador Sea confirmed the cooccurrence of sea ice algae in exported carbon (Fig. 3.3; Lalande et al., 2019a). The occurrence of *Nitzschia frigida* and *Melosira arctica* cooccurred with the dominance of *Chaetoceros/Attheya* spp. in May 2018, shortly after the surface chl *a* maximum in April associated with the ice melt, suggesting a potential sea ice algal bloom/release induced by sea ice breakup in 2018 (Fig. 3.2a, 3.3). Although the direct export of *Nitzschia frigida* and *Melosira arctica* accounted for only a small fraction, the magnitude of sea ice algal export remains unknown, given the fact that *Chaetoceros/Attheya* spp. can be either from sea ice or pelagic habitats (Fig. 3.3b). Due to an inconsistency among taxonomists for identification of the diatoms in our two sediment traps, multiple diatom species, including the sea ice exclusive species, were not identified for the 2018–2019 cycle and hence the magnitude and timing of ice algal export remained uncertain for this cycle. Further, taxonomic analysis provides a visual representation of plankton cells exported through passive sinking but does not account for other organic matter components, such as fecal pellets and detritus. Therefore, the taxonomic counts only represent a portion of exported sea ice algae whereas δ^{13}C-EAA can trace the other portion that cannot be visually identified (e.g., degraded, assimilated, or excreted).

In terms of indirect carbon export from surface primary producers, flux of fecal pellets from zooplankton grazing is an important but highly variable component, which is governed by variation in sea ice/pelagic algae and zooplankton biomass and community composition (Turner, 2015). Sea ice algae were found to have higher nutritional quality

compared to phytoplankton with an elevated essential fatty acid content and thereby may be a better food source for consumers (Park et al., 2002; Arrigo and Thomas, 2004; McMahon et al., 2006; Amiraux et al., 2021). The importance of sea ice algae as food supply for zooplankton grazers has been reported in Hudson Bay (Runge and Ingram, 1988), Frobisher Bay (Grainger and Hsiao, 1990), Canadian Arctic Archipelago (Michel et al., 1996), Barents Sea (Scott et al., 1999, 2001), and northern Baffin Bay (Michel et al., 2002). A more recent biomolecular study also revealed active feeding on sea ice algae by copepods *Calanus glacialis* under seasonal sea ice long before ice melt and the development of ice-edge blooms in the Northern Berring Sea (Durbin and Casas, 2014). Overall, δ^{13}C-EAA signatures revealed a dominance of relatively "fresh" organic matter (i.e., less microbially degraded) and a potentially high baseline contribution of sea ice algae in sinking particles (via direct or indirect export), which was consistent with previous observations that sea ice algae could be either exported via fast-sinking aggregates (e.g., in Beaufort Sea, Carey, 1987; in Eurasian Basin, Fernández-Méndez et al, 2014), or ingested by zooplankton and exported as fecal materials (e.g., in Canadian Arctic Archipelago, Michel et al., 1996). The contribution of fecal pellets to our sinking particles was further evidenced by the independent δ^{15}N-AA analyses, discussed in the section below.

3.4.2 Organic matter composition in sinking particles

The δ^{15}N-THAA values represent the mass-balanced N isotopic signature of all AAs and were 2–7‰ more elevated than bulk signals (Fig. 3.2e), suggesting a contribution of isotopically lighter non-AA compounds to the sinking particles. The changes in bulk δ^{15}N were positively correlated with δ^{15}N-THAA ($p < 0.05$). This is not surprising given the large contribution of THAA-N to total N (up to ~50%; Table 3.2). Among TrAAs, δ^{15}N of Leu, Ile, Glx, and Ala were positively correlated with bulk δ^{15}N ($p < 0.05$). δ^{15}N-Phe represents the isotopic baseline of source N while δ^{15}N-TrAA changes with heterotrophic modifications (McClelland & Montoya, 2002; Ohkouchi et al., 2017). The positive correlation with THAAs and TrAAs indicated that changes in bulk δ^{15}N were influenced by AA isotopic fractionations from trophic transfers or microbial alteration (McMahon and McCarthy, 2016). However, the discrepancy of bulk δ^{15}N from TrAA and THAA δ^{15}N values suggests other sources are also controlling the

overall bulk signal, i.e., N-containing organic compounds like nucleic acids, lipids, carbohydrates, and uncharacterizable OM (Hedges et al., 2001; Batista, 2016; McMahon and McCarthy, 2016), which made up the other half or more of total N in sinking particles (Table 3.2). For examples, N-acetyl-D-glucosamine from blue crab and lobster chitin was found to be ~9‰ lighter than the bulk $\delta^{15}N$ of the whole organisms (Macko et al., 1990) while $\delta^{15}N$ of chlorophyll was ~5‰ lighter than the bulk $\delta^{15}N$ of cultured phytoplankton, and marine sinking particles and sediments collected across different geographical locations (Sachs et al., 1999).

While $\delta^{13}C$-EAA traces the ultimate autotrophic carbon sources to the sinking particles, variations in $\delta^{15}N$-AA reflect three separate processes: baseline isotopic values of source N, trophic transfers, and microbial resynthesis (Ohkouchi et al., 2017). The $\delta^{15}N$-Phe is used as a proxy for baseline $\delta^{15}N$ because it does not undergo deamination reactions during heterotrophic metabolism (Chikaraishi et al., 2009). To investigate the degree of heterotrophic processing in consumer tissues and detrital materials, several parameters have been developed based on $\delta^{15}N$-TrAA and $\delta^{15}N$-Phe. The "metazoan" trophic position (TP_{met}) is calculated from $\delta^{15}N$-Glu while the "protozoan" trophic position (TP_{pro}) includes both trophic transfers through both metazoans and protozoans (Chikaraishi et al., 2009; Nielsen et al., 2015; Décima et al., 2017; Décima and Landry, 2020). The $\sum V$ parameter measures the degree of heterotrophic processing from the deviation of $\delta^{15}N$-TrAA (McCarthy et al., 2007). In our study, the elevated $\delta^{15}N$ of TrAAs in the sinking particles versus sea ice and pelagic algae is indicative of alteration by heterotrophic processing (Fig. 3.5b). It is hard to infer how much alteration was driven by high trophic materials or heterotrophic microbial biomass by looking at the $\delta^{15}N$-TrAA values alone. Recent studies have identified several $\delta^{15}N$-AA patterns resulting from microbial heterotrophy (McMahon and McCarthy, 2016; Fig. 14 in Ohkouchi et al., 2017): 1) algae-like pattern when microbes synthesize AAs *de novo* from inorganic N; 2) metazoan-like pattern when microbes incorporate existing AAs; 3) both Glu and Phe increase in the same way when microbes conduct extracellular protein hydrolysis; and 4) scattered pattern when only selected AAs are resynthesized. The algae-like pattern exhibits a $\delta^{15}N$-AA pattern similar to that of algae with low TP_{met} values (Ohkouchi et al., 2017), which is not consistent with our data (Fig.

3.5b, 3.7a). Patterns with high δ^{15}N-Glu and Phe from extracellular protein hydrolysis elevates the δ^{15}N of all AAs with similar amplitudes, including those of SrcAAs (Ohkouchi et al., 2017), contrary to those of our sinking particles which remained low (Fig. 3.5b) and reflected the regional nitrate δ^{15}N (Sherwood et al. 2021). The pattern linked to microbial resynthesis was similar to the metazoan-like pattern but showed more scattered changes in δ^{15}N-TrAAs with a large increase in ∑V (Ohkouchi et al., 2017). In our study, given the minimal deviations in δ^{15}N-Phe, relatively consistent elevated δ^{15}N-TrAA, a higher TP_{met} compared to phytoplankton, and a moderate ∑V overlapping with phytoplankton (except for a few values in the 915m trap), our sinking particles more likely underwent "metazoan" heterotrophy (Fig. 3.5b, 3.7a; Ohkouchi et al., 2017).

By comparing δ^{15}N-AA derived parameters with previously established end-member data of major components reported in marine POM (phytoplankton, fecal pellets, and zooplankton), we can estimate the relative contribution of these end-members to the sinking particles (Fig. 3.7). TP_{met} and ∑V did not clearly distinguish the three end-members from each other, especially for fecal pellets and zooplankton (Fig. 3.7a, c). This presumably resulted from the underestimation of Glx-based TP (TP_{met}) in plankton food webs, which was observed in experimental studies by Gutiérrez-Rodríguez et al. (2014) and Décima et al. (2017), and the confounding effects of microbial reworking (Ohkouchi et al., 2017). Previous studies suggested that Ala and Thr provide a better separation of end-members because Ala has a higher trophic sensitivity to protistan consumers while Thr can distinguish animal metabolism (zooplankton and fecal pellets) from microbial metabolism (phytoplankton; Gutiérrez-Rodríguez et al., 2014; Décima et al., 2017; Doherty et al., 2021). Using Ala to compute the trophic position (TP_{pro}) of our sinking particles, we observed a clearer separation between the three end-members (Fig. 3.7b). The improved separation of TP_{pro} was obvious between detritus and copepods samples, with detritus overlapping with the fecal pellet end-member and copepods falling within the zooplankton end-member (Fig. 3.7b). The elevated TP_{pro} compared to TP_{met} in sinking particles suggested a pronounced "protozoan" food web imprint on the exported N, that was not visible in TP_{met}. This demonstrated the important role of "protozoan" food web in exporting surface production to the depth. Plotting Phe-normalized δ^{15}N of

Ala against Thr further provides two-dimensional separation between different samples and end-members (Fig. 3.7d). Doherty et al. (2021) used microbial degraded OM as one of the end-members in the Ala-Thr model. The reason why we did not include microbial degraded OM here is that this end-member was derived from measurements of high molecular weight dissolved OM and mesopelagic ultra-filtered POM which were not likely to settle into our sediment traps (Yamaguchi and McCarthy, 2018). Nevertheless, sediment traps may be influenced by lateral transport or resuspension of aged sediment which is more degraded. Our sediment traps were deployed at the outer edge of Saglek Bank (Fig. 3.1), exposed to strong bottom currents and vertical mixing from the Hudson Strait outflow (Fig. 3.1; Hecker et al., 1980; Harding, 1998; Drinkwater and Harding, 2001; Wareham & Edinger, 2007). Continental margins are often subject to vigorous bottom currents and hence lateral transport and resuspension of sediments near the bottom (Rea and Hovan, 1995; Hwang et al., 2010). The fractional proportion of sediment resuspension versus surface production is commonly quantified using two-end-member ^{14}C mass balance (Hwang et al., 2017; Golombek et al., 2024), which was not available in this study. Nevertheless, the influence of resuspended sediments is considered minor, at least to the AA pool, as evident from $\delta^{13}C$-EAA and $\delta^{15}N$-AA serving as two independent approaches for estimating microbial POM contribution to our sediment traps (Fig. 3.6b, 3.7). The THAA-N% in our sinking particles at times exceeded 38% (Table 3.2), falling within the range for living biomass reported by Cowie and Hedges (1992) whereas degraded sediments and resuspended materials have much lower values (Cowie and Hedges, 1992; Colombo et al., 1998; Golombek et al., 2024), again evidencing the minor contribution of degraded sediments to our sinking particles.

The minimal microbial degradation of sinking particles could be attributed to rapid export of fast-sinking diatoms and fecal pellets (Turner, 2015; Lalande et al., 2019; Genin et al., 2021). There is considerable overlap between sinking particles and fecal pellets in the Ala-Thr biplots (Fig. 3.7c). We then use Bayesian mixing model based on Phe-normalized $\delta^{15}N$ of Ala and Thr to quantify contributions of end-members to sinking particles. Assuming phytoplankton, fecal pellets, and zooplankton are the major N sources to the AA pool in sinking particles, our MixSIAR mixing model suggested a dominant contribution of animal sources throughout the two years (4–15% “zooplankton” and 70–

92% “fecal pellets”; Fig. 3.8). This was consistent with the observations of sustained copepod communities in sinking particles and highly abundant large-bodied copepods caught in the plankton sampler at our study site (Fig. 3.4b, c) as well as previous observations of copepod dominance in subarctic Labrador Sea (Darnis et al., 2022). During phytoplankton blooms, the contribution of direct phytoplankton export was up to 23% (Fig. 3.8). Note that fecal pellets and zooplankton end-members used in our mixing model consist of data collected from salp, amphipod, krill and mixed community samples that involve herbivory, carnivory, and detritivory feeding (Doherty et al., 2021). We also applied the three end-member mixing model on our copepod and detritus samples to verify the accuracy of the model. Copepod samples were accurately classified within the “zooplankton” end-member (60–93%), while detritus samples were classified as “phytoplankton” (30–50%) and “fecal pellets” (30–50%). Since the detritus aggregates were collected along with the zooplankton from the plankton net (see Sect. 3.2.3), they were likely contributed by large particles (marine snow) that originate from aggregated phytoplankton (phytodetritus) and fecal matter (Turner, 2015).

3.4.3 Exported fecal pellets

The fecal-pellet-like δ^{15}N-AA signatures in our sinking particles and Bayesian mixing model outputs revealed a potential dominance of fecal pellets to exported POM at the study site (Fig. 3.7d). Sinking fecal pellets serve as an important source of organic material for benthic communities but are hard to quantify (Pilskaln and Honjo, 1987; Wilson et al., 2013). The collection of recognizable fecal pellets and its proportion in sinking particles largely vary with depth, season, location and is affected by zooplankton diets and other enhancing/inhibiting mechanisms during sedimentation (Noji, 1991; Hargrave et al., 1994; Wilson et al., 2013). Although fecal pellets are subject to bacterial degradation and/or zooplankton grazing, they may be consumed or repackaged by deep resident zooplankton (that produce larger pellets) or broken down and incorporated into sinking marine snow, and eventually have a greater chance to reach the deep sea (Noji, 1991; Wilson et al., 2013; Stamieszkin et al., 2017). For example, vertical migration of *Calanus* spp. may promote sinking of particles by feeding in the surface and egesting fecal materials in deeper waters (Noji, 1991; Passow and Carlson, 2012). During sedimentation,

fecal pellets are likely to be modified and repackaged several times and become unrecognizable as fecal pellets, making it difficult for visual identification (Noji, 1991). For example, an earlier study estimated a low fecal pellet contribution to POC in a sediment trap collected under permanent ice cover in the Arctic (< 20%), which was derived from enumeration of two types of pellets (cylindrical and ellipsoid; Hargrave et al., 1994). Nevertheless, our results agreed with more recent studies that discovered substantial contribution of fecal pellets from large copepods to vertical export (up to > 60% of the POC flux) in other polar regions; e.g., Fram Strait (Lalande et al., 2011), northern Baffin Bay (Sampei et al., 2004), Beaufort Sea (Juul-Pedersen et al., 2010), and the Southern Ocean (Dagg et al., 2003; Gleiber et al., 2012; Décima et al., 2023). Recent applications of Bayesian mixing model using Phe-normalized $\delta^{15}N$ of Ala and Thr revealed an increasing contribution of fecal pellets to both small and large particles with increasing depth in North Pacific, indicating fecal pellet production by zooplankton and disaggregation into smaller particles at mesopelagic depths (> 50% in the mid mesopelagic; Doherty, 2021; Wojtal et al. 2023). A recent model study suggested that sinking fecal pellets accounted for 50–90% of total carbon export for most low-latitude seas (Nowicki et al., 2022). Nowicki et al. (2022) found that fecal pellets from "gravitational pump" (i.e., via passive sinking) contributed less to total carbon export in high latitudes (40–50%) because of the larger contribution of "mixing pump" (i.e., via active physical transport) from deep water formation. However, the "mixing pump" in their models only includes dissolved organic carbon component and neglected the suspended POC from eddy subduction (Nowicki et al., 2022). Our study, on the other hand, only characterized the particulate portion in the sediment traps, part of which may be transported via the "mixing pump". Hence, our estimates of higher contribution of fecal pellets are reasonable. In fact, physical transport of suspended POC by vertical mixing, seasonal mixed layer detrainment, eddy subduction, and large-scale ocean circulation could play an important role in exporting POC to depth (Omand et al., 2015; Dall'Olmo et al., 2016; Nowicki et al., 2022). For example, based on mixed-layer depth data from Argo floats and satellite estimates of POC, the largest mixed-layer pump can be found in high latitude regions in the North Atlantic, Southern Ocean, and north-west Pacific, accounting for on average 23% of estimates of the biological carbon pump (Dall'Olmo et al., 2016). Glider observations complemented by high-

resolution modelling revealed that eddy-driven POC flux can contribute up to half of the total POC export during spring blooms in highly productive subpolar oceans, such as North Atlantic (Omand et al., 2015).

Overall, our findings suggested that sea ice algae and zooplankton fecal pellets fuel export productivity to the mesopelagic in a seasonally ice-covered region. This has important ecological implications for global warming and declines in sea ice in the Arctic and subarctic oceans (Pabi et al., 2008). Sea ice declines represent habitat loss and reduced fatty acid quality for sea ice-reliant species (Post et al., 2013). This reduction accompanied by younger and thinner ice, freshening surface water, and less ice-covered area in the Arctic/subarctic, may also induce changes in community structures and phenology of zooplankton, and hence impacting fecal pellet export and food supply to benthic communities (Post et al., 2013; Leu et al., 2015; Turner, 201 5). Although primary production and POC fluxes were predicted to increase in polar oceans as a result of longer ice-free periods, other mechanisms may limit the delivery of POM to benthic ecosystems (Sweetman et al., 2017). First, ocean warming accelerates remineralization and microbial degradation in the water column and hence may reduce the effectiveness of POM export to depth (Riebesell et al., 2009; Turner, 2015). Increased stratification caused by surface warming and freshwater input from sea ice melting limits deep-water ventilation and reduces nutrient supply to surface waters. The weakened deep-water intrusion may reduce the strength of mixed layer pump that acts as an important pathway for POM export in high latitude seas (Dall'Olmo et al., 2016). Reduced nutrient supply shifts the surface plankton communities from dominance by diatoms and large zooplankton towards those dominated by picoplankton and small zooplankton, thereby reducing the strength of biological pump and the sedimentation of organic particles to depth (Li et al., 2009; Finkel et al., 2010; Turner, 2015). This may further deprive benthic communities of organic matter supply, which are predicted to impact biodiversity hotspots, such as those inhabited by deep-sea corals and sponges (Levin and Le Bris, 2015; Sweetman et al., 2017). Hence, these habitats are particularly vulnerable to changes in food quality and quantity in the changing Arctic/subarctic oceans.

3.5 Conclusions

In this study, we applied CSIA-AA proxies on sinking particles time series collected in sediment traps at depths of 469 m and 915 m in the northwestern Labrador Sea (~60°N) to explore the sources and composition of organic carbon and nitrogen in sinking organic matter at the Arctic/subarctic boundary. The sinking particles δ^{13}C-EAA patterns indicated that sea ice algae are an important food source to higher trophic levels and that surface primary production was largely preserved in exported organic matter at the study site. Additionally, δ^{15}N-AA results independently verified the minor bacterial contribution to sinking particles and revealed dominant animal sources (fecal pellets and zooplankton) to the sinking flux. Overall, these results have significant implications for the use of CSIA-AA in biogeochemical and ecological studies of marine environments. The use of CSIA-AA in sinking particles time series obtained from moored sediment traps provides quantitative estimates of plankton and fecal pellet contributions to carbon export in the ocean, which may help improve the accuracy of flux estimates derived from counting methods and biogeochemical models. Combined with conventional analyses, such as plankton analyses and flux measurements, CSIA-AA may fulfil the promise of precise and high-resolution delineation of marine sinking organic matter in space and time. Climate-related ocean changes may further limit food availability for deep-water benthic assemblages, such as deep-sea corals and sponges (Levin and Le Bris, 2015; Sweetman et al., 2017). We suggest that future work should expand CSIA-AA measurements on sinking particles collected by sediment trap time series globally and establish multi-proxy data repository for vulnerable ecozones. CSIA-AA end-member data for estimating sinking particle composition should be better constrained, especially for δ^{13}C-EAA. More accurate quantitative estimates of sinking particle composition and processing are beneficial for future studies to predict the biogeochemical and ecological responses in important deep-sea ecosystems to on-going changing climate.

3.6 Data availability

Data are available in the supplementary material.

3.7 Author contribution

S-MC, DC, EE and OAS contributed to conception and design of the study. S-MC and TD contributed to sampling. TD contributed to flux measurements and microalgal and zooplankton counts. S-MC and OAS contributed to sample processing, CSIA-AA and bulk stable isotope measurements, and data analysis. DC, EE, and CL contributed to data interpretation. S-MC wrote the manuscript with input from all the co-authors.

3.8 Competing interests

The authors declare that they have no conflict of interests.

3.9 Acknowledgements

Funding for this study was provided by an NSERC Discovery Grant to OAS (RGPIN-2018-05590), NSERC Ship Time grants to OAS (544990-2020) and EE (515528-2018), and DFO funding to the Marine Conservation Targets program. Moorings were collected on board the Canadian research icebreaker *CCGS Amundsen* as part of the ArcticNet Hidden Biodiversity (HiBio) project. Logistical support was provided by the Amundsen Science program, which is supported by the Canada Foundation for Innovation through Université Laval. We would like to express our gratitude for all the officers and crew members of the Canadian Coast Guard Ship *Amundsen* for their professional support with sediment trap and zooplankton sampling. We also thank Shawn Meredyk from Amundsen Science for leading mooring deployments and recoveries, Maxime Geoffroy, Eugenie Jacobsen, and Jordan Sutton for helping with zooplankton sampling, Claire Normandeau for bulk stable isotope analyses, and Karen Stamieszkin for valuable discussion about zooplankton analyses.

CHAPTER 4 PRESERVATION OF AMINO ACID $\delta^{13}C$ AND $\delta^{15}N$ SIGNALS IN A HOLOCENE-AGED SEDIMENT CORE FROM NORTHERN BAFFIN BAY[3]

Abstract

To predict how ongoing climate-driven changes in ocean conditions will impact marine ecosystems, it is important to investigate biogeochemical and ecological responses to changing ocean conditions of the past. Here we apply compound-specific isotope analysis (CSIA) of amino acids (AA) to a marine sediment core spanning most of the Holocene period to investigate carbon (C) and nitrogen (N) sources and cycling associated with export production and microbial degradation for the past ca. 9,000 years in eastern Baffin Bay off northwest Greenland. Our results showed excellent long-term preservation of CSIA-AA isotopic information despite noticeable alteration in AA concentrations. We observed a significant shift in stable carbon isotopes ($\delta^{13}C$) of essential amino acids in the early Holocene, coherent with an overall increase in diatom fluxes and relative declines in sea-ice diatoms. We reconstructed the first baseline stable nitrogen isotope ($\delta^{15}N$) values for the Northwest Greenland shelf and observed well preserved $\delta^{15}N$ of Phenylalanine which showed slightly higher values than the inferred modern level of nitrate $\delta^{15}N$ at our study site. AA-based heterotrophic indicators (trophic position, $\delta^{15}N$-AA pattern, and $\sum V$) showed a lack of progressive microbial reworking with depth despite continuous losses of AAs and suggested that most of diagenesis may have occurred during sedimentation and early deposition. These results highlighted the potential of AAs as reliable tracers of export production and microbial degradation, and their potential to enhance the accuracy of geochemical interpretations based on traditional geochemical proxies. We suggest that future work should expand CSIA-AA applications to paleoenvironmental studies to better understand long-term changes in ocean conditions

[3]Chen, S.M., Limoges, A., and Sherwood, O.A. Preservation of amino acid $\delta^{13}C$ and $\delta^{15}N$ signals in a Holocene-aged sediment core from northern Baffin Bay. In prep.

Student Contribution: I contributed to conception and design of the study. I contributed to CSIA-AA sample processing, measurements, and data analysis. I wrote the manuscript with input from all the co-authors.

and identify ecosystem shifts. This information is key to better predict future responses of marine ecosystems to climate change.

4.1 Introduction

The accelerating loss of Arctic sea ice has been unprecedented for at least the past 1,450 years (Kinnard et al., 2011), and facilitates a positive climate feedback that amplifies Arctic warming through reducing surface albedo (Serreze and Barry, 2011; Post et al., 2013). For the past several decades, the annual minimum sea ice extent has been drastically declining with shorter sea-ice seasons, younger and thinner ice, and increasing freshwater discharge from sea ice melting (Meredith et al., 2019; Hanna et al., 2021). The decline in sea ice represents habitat loss for sea ice algae, which are a major contributor to Arctic primary production (up to 60% in the central Arctic; Legendre et al., 1992; Gosselin et al., 1997; Ardyna et al., 2020). Resulting shifts to pelagic primary production (Arrigo and van Dijken, 2015) may cause mismatches in the timing of zooplankton production and thus impact the biomass and energy transfer to higher trophic levels (Post et al., 2013; Leu et al., 2015; Tedesco et al., 2019; Limoges et al., 2023). Also, a decrease in surface nutrient availability due to surface freshening and enhanced stratification may cause a shift in plankton community composition from larger nanophytoplankton toward smaller picoplankton (Li et al., 2009; Finkel et al., 2010). Together, these changes have the potential to impact the magnitude and quality of export production, which plays a critical role fueling benthic ecological communities and is a major pathway in marine carbon sequestration (Buesseler and Boyd, 2009; Buesseler et al., 2020). To place these observations into the context of long-term climate change, it is necessary to develop new biogeochemical proxies for linking nutrient-productivity dynamics over centennial to millennial timescales.

Stable carbon and nitrogen isotopes ($\delta^{13}C$ and $\delta^{15}N$) of bulk sedimentary organic matter (OM) are widely used in marine biogeochemistry and paleoceanography (Peterson and Fry, 1987; Altabet et al., 1999). The $\delta^{13}C$ and $\delta^{15}N$ values of primary producers vary in space and time due to plankton physiology and environmental factors such as temperature and nutrient (e.g., carbon dioxide, CO_2, nitrate, NO_3) concentrations and processing histories (Peterson and Fry, 1987; Goericke and Fry, 1994). These “baseline”

isotopic values are integrated into export production and, ultimately, sedimentary OM. Isotopic analysis of the sediments may then be used for tracking long term changes in nutrient sources and/or utilization in overlying surface waters (Altabet and Francois, 1994; Galbraith and Kienast, 2013). However, sedimentary $\delta^{13}C$ and $\delta^{15}N$ records are affected by factors that may overprint baseline values, such as heterotrophic processing (i.e., zooplankton grazing and fecal pellet production) and microbial activity during particle export and burial (Macko & Estep, 1984; Altabet, 1996; Robinson et al., 2012; Hannides et al., 2013). Post-depositional diagenetic processes such as oxidation or hydrolysis may selectively remove isotopically distinct compounds from the bulk OM (Freudenthal et al., 2001, Lehmann et al., 2002; Tesdal et al., 2013). Also, sediments comprise time-varying mixtures of inorganic and organic materials of different $\delta^{13}C$ and $\delta^{15}N$ (Kienast et al. 2005). To overcome these challenges, stable isotope analysis of specific biomarker compounds such as chlorin (e.g., Junium et al., 2015) or microfossil-bound N (e.g., Sigman et al., 1999) have been used, but these represent tiny fractions of sedimentary OM and therefore may not capture information about larger scale nutrient-productivity dynamics.

Amino acids are the major form of molecularly characterizable N and organic C in living organisms and non-living OM. They thus represent important components of plankton, bacteria, and marine sediments (Cowie and Hedges, 1992; Hedges et al., 2001). Their absolute abundance and relative concentrations have been widely used as indicators of OM degradation state (Cowie and Hedges, 1992; Dauwe et al., 1999). Compound-specific isotope analysis (CSIA) of amino acids (AAs) has recently emerged to address the complications linked to the interpretation of bulk stable isotope data by providing specific information about the sources and processing of OM (Larsen et al., 2009; Larsen et al., 2013; Batista et al., 2014; McMahon et al., 2015; Ohkouchi et al., 2017; Close, 2019; Shen et al., 2021). Interpretation of $\delta^{13}C$-AA signatures is based on the classification of AAs into essential and non-essential groups. The C skeletons of essential amino acids (EAAs: phenylalanine, threonine, isoleucine, leucine, and valine) are synthesized only by primary producers. Consumers cannot synthesize EAAs in amounts adequate to support growth and maintenance, and thus EAAs in consumer tissues are acquired directly from their diet with minor changes to the C skeletons (“dietary routing”;

O'Brien et al., 2002; Wu, 2009). Thus, $\delta^{13}C$ values of EAAs remain unchanged when EAAs are entirely incorporated into consumers' tissues (McMahon et al., 2010, 2013; Larsen et al., 2013).In primary producers, the diverse biosynthetic pathways and associated isotopic effects between different phylogenic groups (e.g., terrestrial plants, fungi, and bacteria) lead to distinct and consistent $\delta^{13}C$-EAA signatures, which are passed to and preserved in consumer tissues with trophic transfers, allowing EAAs to trace sources of primary production fueling food webs (Hayes, 1993; Larsen et al., 2009; Elliott Smith et al., 2022).

The $\delta^{15}N$-AA interpretation is based on a different classification, independent of that for $\delta^{13}C$. $\delta^{15}N$-AA values in autotrophs mainly derive from transamination of individual AAs from the central glutamate pool (Macko et al., 1986). When incorporated into heterotrophs or detrital OM, the autotrophic baseline signatures undergo alteration due to trophic transfers or microbial degradation (Keil and Fogel, 2001; McCarthy et al., 2013). Different classes of AAs undergo different degrees of alteration: $\delta^{15}N$ values of "source" AAs (SrcAAs: phenylalanine and lysine) undergo little or no enrichment with trophic transfers and thus preserve baseline N values in marine OM. By contrast, those of "trophic" AAs (TrAAs: glutamine/glutamic acid, asparagine/aspartic acid, alanine, leucine, isoleucine, proline, and valine) are enriched with increasing trophic level, or altered by microbial resynthesis (McClelland & Montoya, 2002). The decoupled changes in $\delta^{15}N$ of SrcAAs and TrAAs allow for direct estimation of trophic position (TP), and the scattering of TrAA patterns has been proposed as a new proxy for the degree of microbial alteration (McClelland and Montoya, 2002; McCarthy et al., 2007, 2013; Popp et al., 2007; Chikaraishi et al., 2009; Hannides et al., 2009, 2013; Nielsen et al., 2015). Hence, $\delta^{13}C$-AA and $\delta^{15}N$-AA are complementary yet fully independent approaches for disentangling the influences from C and N sources, trophic changes, and microbial degradation, thereby allowing for more accurate interpretation of stable isotope data (McMahon & McCarthy, 2016). However, applications of CSIA-AA proxies on ancient marine sediments are still limited, from only a few selective geographical locations (Peru margin: Larsen et al., 2015; eastern tropical Pacific: Sauthoff, 2016; North Pacific: Batista et al., 2014; North Pacific and Pacific Arctic: Choi et al., 2022). Isoscapes

(mapping of isotope spatial gradients) based on δ^{15}N-Phe for sedimentary baselines remain to be constructed globally and over long time scales.

Here we present a sediment core record spanning the past ca. 9,000 years from northern Baffin Bay using existing CSIA-AA proxies, including a recently developed proxy for sea ice algae (Chen et al., 2022). Chen et al. explored the diagnostic potential of δ^{13}C-EAA to trace sea ice algae in Canadian Arctic and subarctic seas (2022) and revealed a significant contribution of sea ice algae and fecal pellets to export production in seasonally ice-covered northwest Labrador Sea (Chapter 3). As a key transition zone between the Western Arctic and North Atlantic oceans (Münchow et al., 2015), more than half of Baffin Bay is covered by sea ice for nine months per year with abundant icebergs (Tang et al., 2004). Thus, it is a good location to study long-term biogeochemical and ecological changes in response to sea ice decline in a mid-Arctic region with the use of CSIA-AA proxies.

A number of studies on sediment cores from northeastern Baffin Bay have been conducted to investigate changes in ecosystem function over the Holocene (0–11 kyrs) period (e.g., Levac et al., 2001; Mudie et al., 2005; Knudsen et al., 2008; St-Onge and St-Onge, 2014; Caron et al., 2019a, b; Giraudeau et al., 2020; Hansen et al., 2020; Limoges et al., 2020; Saini et al., 2020; Jackson et al., 2021). Here we report on the δ^{13}C-AA and δ^{15}N-AA data of a marine sediment core recovered in a deep glacial trough (water depth: 987 m) on the continental shelf of west Greenland, northeastern Baffin Bay (73°15.66'N, 57°53.98'W). We investigate Holocene δ^{15}N baselines for northeastern Baffin Bay and evaluate the fidelity of the δ^{13}C-AA and δ^{15}N-AA proxies in sediments spanning several millennia by comparing them with existing CSIA-AA data of marine OM reported elsewhere (e.g., Larsen et al., 2013, 2015; Braun et al., 2017; Choi et al., 2022) and previously published multi-proxy data from the same core (Caron et al., 2019a, b; Hansen et al., 2020; Limoges et al., 2020). Our objective is to enhance understanding of the preservation of CSIA-AA proxies in aged and degraded marine sediments to improve accuracy of geochemical data interpretation in paleoenvironmental studies. This study has important implications for reconstructing biogeochemical cycling and heterotrophic dynamics over long time scales.

4.2 Materials and Methods

4.2.1 Study site

Baffin Bay is a semi-enclosed deep basin (> 2,300 m) that connects the Arctic to the subarctic Labrador Sea and the North Atlantic. It is bounded by Greenland to the east and by Baffin Island and Devon Island to the west (Rudels, 2011). The oceanography of modern Baffin Bay is influenced by a combination of warm Atlantic and cold Pacific waters: 1) the northward flowing West Greenland Current (WGC) carries a mix of cold and fresh waters from the East Greenland Current and warm Atlantic-sourced waters from the Irminger Current along the coast of Greenland, and 2) the southward flowing Baffin Island Current (BIC) carries cold and fresh waters of Pacific origin along Baffin Island (Fig. 4.1; Lehmann et al., 2019). Although water mass exchange with the Arctic and Atlantic oceans is restricted by the presence of shallow sills in the connecting channels (< 700 m; Fig. 4.1; Lehmann et al., 2019), Baffin Bay is one of the key areas for freshwater and sea ice export to the North Atlantic (Tang et al., 2004; Münchow et al., 2015). Our study site is located in northeastern Baffin Bay and on the shelf region of Greenland that is cut by many canyons and fjords and receives meltwater and icebergs supplies from the Greenland Ice Sheet (Fig. 4.1). Baffin Bay is almost completely covered by sea ice from December to April (as of 2023, National Snow & Ice Data Center; Tang et al., 2004), but the eastern sector of the basin has the shortest sea ice season because of the influence of the warm West Greenland Current (Tang et al., 2004). Sea ice motion and thickness in the Baffin Bay are also controlled by Arctic Oscillation, described as the difference in sea-level pressure between the Arctic Ocean and the middle latitudes (Thompson and Wallace, 1998; Rigor et al., 2002; Cohen and Barlow, 2005). During the positive phase of Arctic Oscillation, cold air is trapped by low sea-level pressure, whereas wintertime surface winds and thermodynamic processes lead to an overall thinning of sea ice cover, an earlier sea-ice melt, and increased export of meltwater and drift ice in the Arctic Ocean (Rigor et al., 2002). Conversely, the negative phase results in a buildup of multiyear ice in a strong Beaufort Gyre, reduced export of freshwater and sea ice (Rigor et al., 2002). During the Holocene, sea ice dynamics and marine productivity at the core site, which were previously evaluated by diatom fluxes, sea-ice biomarkers (IP_{25} and HBI III), total organic carbon (TOC), total nitrogen (TN),

bulk $\delta^{13}C$ and $\delta^{15}N$, were closely linked to shifts in climate and ocean conditions, e.g., Arctic Oscillation, meltwater discharge from deglaciation, changes in seasonal sea ice concentrations, and balance between Arctic and Atlantic water influences (Limoges et al., 2020). The ongoing warming and loss of sea ice and glaciers may have consequences for marine productivity and biogeochemical cycling in Baffin Bay.

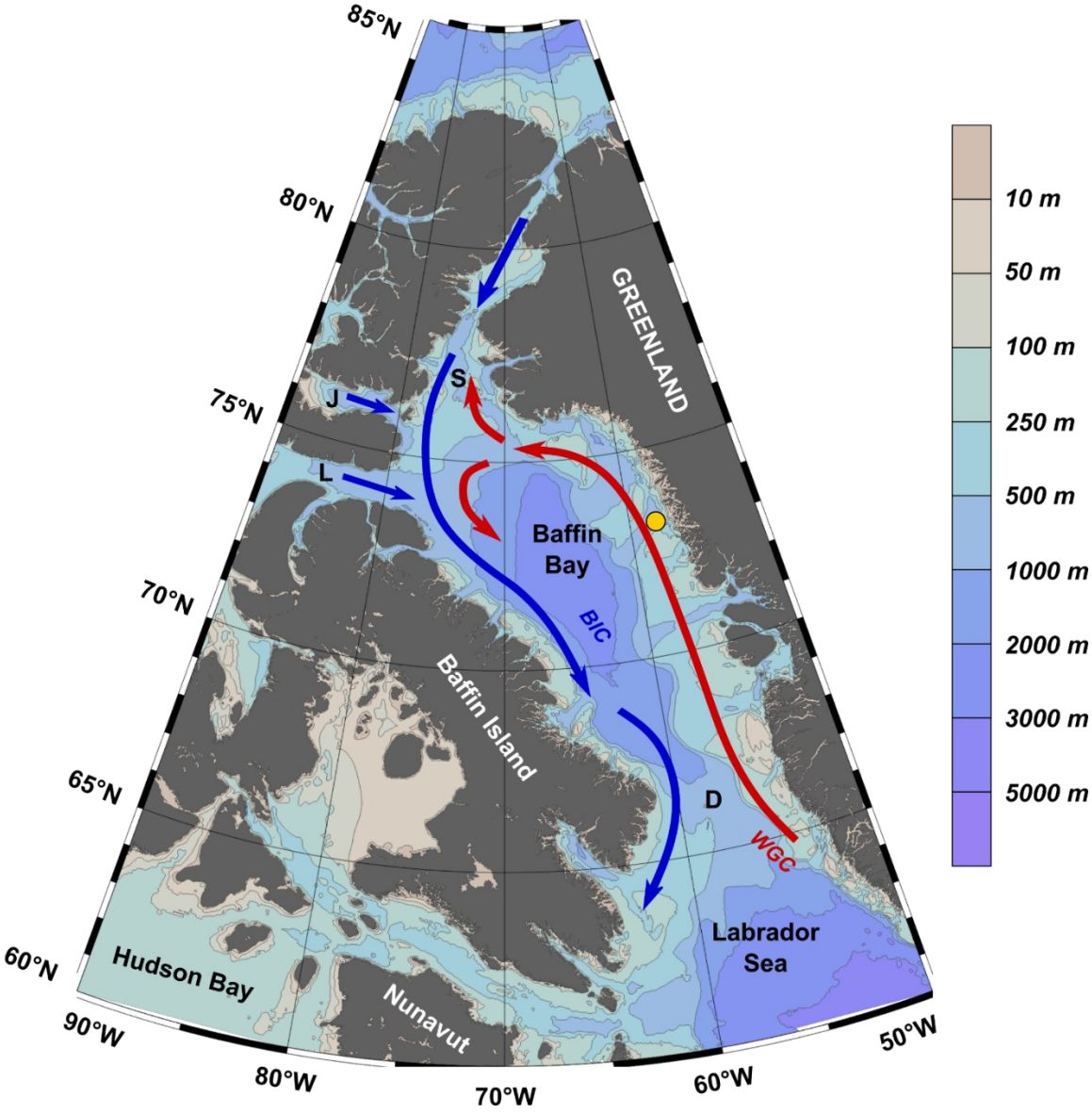

Figure 4.1 Location of sediment core AMD14-204 on the shelf off northwest Greenland (yellow circle) with bathymetry (grey contours) and major currents (arrows). Color bars indicate bottom depth (m). Abbreviations: S, Smith Sound; J, Jones Sound; L, Lancaster Sound; D, Davis

Strait; BIC, Baffin Island Current; WGC, West Greenland Current. Figure made with Ocean Data View, Schlitzer, 2022.

4.2.2 Sample collection and processing

Sediment core AMD14-204 was collected using a Calypso square gravity core in the eastern Baffin Bay (73°15.66'N, 57°53.98'W) during the ArcticNet expedition on board the CCGS Amundsen in 2014 (Fig. 4.1). The 738-cm core was retrieved at a water depth of 987 m, subsampled onboard using u-channels, and stored at 4°C during the transportation. Subsamples for biomarker analyses were stored at -80°C until analysis.

4.2.3 Age model and sedimentary proxies

The age model for AMD14-204 is based on 11 accelerator mass spectrometry ^{14}C dates from samples of planktic and mixed benthic foraminiferal assemblages and ostracods (Table C1; see details in Hansen et al., 2020). Previously published radiocarbon dates from core AMD14-204 were based on the Marine13 radiocarbon calibration curve (Reimer et al., 2013) with a reservoir age correction of $\Delta R = 140 \pm 30$ years for the west coast of Greenland (Lloyd et al., 2011; Hansen et al., 2020). Since then, the calibration curve and the reservoir age correction for the study location have been updated (Heaton et al., 2020; Pieńkowski et al., 2023). A revised age model calibrated using the CALIB 8 software (Stuiver and Reimer, 1993) and the updated calibration curve, Marine20 (Heaton et al., 2020), with a reservoir age correction of $\Delta R = -93 \pm 111$ years for the west coast of Greenland (Pieńkowski et al., 2023) is included in the supplementary material (Table C1). However, to make our results comparable to previously published multi-proxy records on core AMD14-204, we applied the earlier version of age model in this study (same as Hansen et al., 2020). Based on this age model, AMD14-204 spans the last 9.2 cal. kyr before present (hereafter expressed as kyr BP; Limoges et al., 2020).

Samples for total organic carbon (TOC), total nitrogen (TN), bulk stable carbon ($\delta^{13}C$) and nitrogen isotopes ($\delta^{15}N$) were measured at an interval of 5–20 cm, which represents an effective age resolution of c. 75–440 years (methodology and data are available in Limoges et al., 2020).

4.2.4 Amino acid $\delta^{13}C$ and $\delta^{15}N$ analysis

For CSIA-AA analyses, three subsamples were selected from six distinct periods (9.2 to 8.0, 8.0 to 7.0, 7.0 to 6.0, 5.0 to 4.5, 3.0 to 2.5, and 0.5 to 0.2 kyr BP) to capture environmentally significant variations in the primary production and sea-surface proxies (i.e., TOC, diatoms, IP_{25} and HBI III) reported from the same core in Limoges et al. (2020).

According to the results of TOC content (%), 0.7–1.7 gram of dry sediment were weighted for each subsample to meet the requirement of 10 mg organic C for CSIA-AA analyses. Samples were hydrolyzed in 6-N HCl (Sigma-Aldrich) at 110 ℃ for 20 hours, purified and derivatized into trifluoroacetyl-isopropyl ester derivatives in batches of 6 samples following previously established protocols (Silfer et al. 1991; Larsen et al. 2013; Batista et al. 2014; McMahon et al. 2015; Chen et al. 2022). Each batch included three external standards that were treated following the same protocol: duplicate of a calibration standard of AA mixtures (with known $\delta^{13}C$ and $\delta^{15}N$ values; see a list of AAs below) and a lab standard made of homogenized Chlorella powder (Organika). Samples and standards were spiked with a norleucine (Nle) internal standard (Sigma-Aldrich) prior to purification and derivatization. Derivatized samples were stored at -20℃ until analysis. On the day of analysis, samples were dried under N_2 gas, dissolved in ethyl acetate, measured in triplicate for $\delta^{13}C$ or $\delta^{15}N$, using a Trace 1310 Gas Chromatograph (GC) coupled with a Delta V IRMS (Thermo Scientific). Every 2–3 samples (including the lab standard) were bracketed by triplicate injections of calibration standards. A total of eleven AAs were typically measured in most samples with good reproducibility (same as those in the calibration standard: alanine (Ala), glycine (Gly), proline (Pro), valine (Val), leucine (Leu), isoleucine (Ile), asparagine + aspartic acid (Asx), threonine (Thr), glutamine + glutamic acid (Glx), phenylalanine (Phe), and lysine (Lys). Due to small m/z 28 peak responses, $\delta^{15}N$ of Thr was not determined in most samples (Table C2). Isotopic values were calibrated to co-analyzed reference material and reported in delta notation (δ) in units of per mill "‰" relative to Vienna PeeDee Belemnite (VPDB) and air for $\delta^{13}C$ and $\delta^{15}N$, respectively. Measured $\delta^{13}C$ values were corrected for isotopic fractionation and introduction of C atoms during the derivatization according to Silfer et al. (1991) and

normalized against instrument drift between successive triplicate injections of the calibration standard (Yarnes and Herszage, 2017; denoted as calibrated $\delta^{13}C$). Measured $\delta^{15}N$ values were calibrated based on the offset between known and measured values of calibration standards and normalized against instrument drift (denoted as calibrated $\delta^{15}N$). The average reproducibility of $\delta^{13}C$ was ± 0.3‰ for the internal standard Nle (n = 12), and from ± 0.2‰ (Phe) to ± 0.5‰ (Val, Leu, Pro, and Lys) for AA standards, respectively (n = 12 for each AA). The average reproducibility of $\delta^{15}N$ was ± 0.4‰ for the internal standard Nle (n = 11), and from ± 0.2‰ (Lys) to ± 0.5‰ (Ala and Ile) for AA standards, respectively (n = 12 for each AA). The absolute (mol) and relative (mol%) molar concentrations of AAs were calculated by calibration of mass 44 peak areas against that of the internal standard (Nle) using a relative response factor for each AA, following Kaiser and Benner (2005). Yields of total hydrolysable AAs (THAAs) were calculated by dividing the total abundance of AAs by the amount of hydrolyzed material.

4.2.5 Calculations and statistical analyses

To account for the spatial-temporal variability in source $\delta^{13}C$ (Larsen et al. 2015; Chen et al. 2022), $\delta^{13}C$-AA values were internally normalized by subtracting the $\delta^{13}C$ mean of the five commonly reported EAAs (Phe, Leu, Ile, Thr and Val) for each sample (denoted as normalized $\delta^{13}C$) using the following equation:

$$Normalized\ \delta^{13}C_i = \delta^{13}C_i - \frac{1}{5}(\delta^{13}C_{Phe} + \delta^{13}C_{Thr} + \delta^{13}C_{Ile} + \delta^{13}C_{Leu} + \delta^{13}C_{Val}) \quad (1)$$

Where $\delta^{13}C_i$ is the calibrated $\delta^{13}C$ value of individual AA. Normalization accounts for influences from inorganic C sources and other environmental parameters, whereas the internal variations between AAs reveal the underlying biochemical mechanisms (Larsen et al., 2015; McMahon et al., 2015; Stahl, 2021; Elliott Smith et al., 2022).

To account for the baseline variability in $\delta^{15}N$ (McCarthy et al., 2007), $\delta^{15}N$-AA values were normalized to the baseline N indicator $\delta^{15}N$-Phe (denoted as normalized $\delta^{15}N$):

$$Normalized\ \delta^{15}N_i = \delta^{15}N_i - \delta^{15}N_{Phe} \quad (2)$$

$\delta^{15}N_{THAA}$ refers to the molar weighted average $\delta^{15}N$ of THAA, thus representing the average $\delta^{15}N$ value of hydrolysable proteinaceous material in the sample (McCarthy et al., 2013; Batista et al. 2014):

$$\delta^{15}N_{THAA} = \sum(\delta^{15}N_i \times mol\%_i) \quad (3)$$

Where $\delta^{15}N_i$ is the calibrated $\delta^{15}N$ value of individual AA and $mol\%_i$ is the molar percentage of the corresponding AA.

Similarly, $\delta^{13}C_{THAA}$ was calculated based on the calibrated $\delta^{13}C$ value of individual AA and the mol% of the corresponding AA.

The "metazoan" trophic position (TP_{met}) represents trophic transfers through metazoans and was calculated based on calibrated $\delta^{15}N$ values of Glx and Phe, following the equation proposed by Chikaraishi et al. (2009) and modified by Nielsen et al. (2015):

$$TP_{met} = \frac{(\delta^{15}N_{Glx} - \delta^{15}N_{Phe} - 2.9‰)}{6.6‰} + 1 \quad (4)$$

The "protozoan" trophic position (TP_{pro}) includes trophic transfers through both metazoans and protozoans and was calculated based on calibrated $\delta^{15}N$ values of Ala and Phe, following Décima et al. (2017) and Décima and Landry (2020):

$$TP_{pro} = \frac{(\delta^{15}N_{Ala} - \delta^{15}N_{Phe} - 3.2‰)}{4.5‰} + 1 \quad (5)$$

Changes in AA composition and average deviation of $\delta^{15}N$-TrAAs are two common degradation indicators to evaluate the degree of microbial degradation in OM. The percentage of N represented by THAA in total N (THAA-N%; mol N in THAA over mol total N) below 38% is considered to indicate diagenetic alteration (Cowie and Hedges, 1992):

$$THAA\text{-}N\% = \frac{\sum(mol_i \times n_i)}{DW \times TN\% \div M_N} \times 100\% \quad (6)$$

Where n is the number of N atoms in individual AA, mol_i is the absolute abundance of this AA, DW is the dry weight of hydrolyzed material, $TN\%$ is the weight percentage of total N, and M_N is the atomic mass of N. Similarly, the percentage of C represented by THAA in total organic C (THAA-C%) was calculated based on the number of C atoms, total organic C percentage, and the atomic mass of C (mol C in THAA over mol total organic C).

The degree of heterotrophic resynthesis was evaluated by calculating the ∑V parameter based on the average deviation of calibrated δ^{15}N values of six TrAAs from their mean, following the formula from McCarthy et al. (2007):

$$\sum V = \frac{1}{n} \sum ABS(\delta^{15}N_i - \delta^{15}N_{mean}) \quad (7)$$

Where n is the number of TrAAs used in the calculation, $\delta^{15}N_i$ are the calibrated δ^{15}N values of each TrAA (Ile, Leu, Asx, Glx, Pro, and Ala) and $\delta^{15}N_{mean}$ is the average δ^{15}N of these AAs. A higher ∑V value suggests a higher degree of heterotrophic resynthesis (McCarthy et al., 2007).

Differences in normalized δ^{13}C and δ^{15}N values and AA mol% among different periods were tested using one-way analysis of variance (ANOVA) and posthoc Tukey HSD tests. Differences in CSIA-AA patterns and parameters were tested between 9.2–5.6 kyr BP and 5.5–0.2 kyr BP using Two Sample T-tests. Pearson correlation coefficients were calculated between all pairs of variables that pass the normality test and displayed in a correlation matrix (R package: corrplot). Statistical models were verified for univariate normality using Shapiro-Wilks test (R package: stats) and visually using QQ plots (R package: ggpubr) in R version 4.1.1 with Rstudio interface version 1.4.1717.

Table 4.1 Depth (cm), age (cal. yrs BP), total organic carbon (TOC) and nitrogen (TN) contents (%) and ratios, and total hydrolysable amino acid (THAA) contents (μmol g^{-1}, mg (100 mg TOC)$^{-1}$, and %) of core AMD14-204 (singular data).

Depth (cm)	Age* (cal. yrs BP)	TOC* (%)	TN* (%)	TOC:TN	THAA yield (μmol g^{-1})	THAA yield [mg (100 mg TOC)$^{-1}$]	THAA-C (%)	THAA-N (%)
6.5	243	1.44	0.18	8.06	20.72	14.94	6.1	16.9
11.5	319	1.41	0.18	7.79	5.92	5.00	2.4	4.6
16.5	395	1.46	0.18	8.09	5.43	3.77	1.9	4.5
138.5	2566	1.45	0.18	8.20	6.73	2.42	2.2	5.7
148.5	2764.6	1.41	0.17	8.22	3.39	3.19	1.6	2.8
158.5	2963.2	1.44	0.17	8.25	4.73	3.02	1.8	4.1
290.5	4693.6	1.35	0.16	8.39	4.58	4.90	1.7	4.4
300.5	4817.4	1.41	0.17	8.35	4.66	3.05	1.9	3.9
310.5	4941.3	1.38	0.17	8.32	5.45	3.94	2.1	5.0
462.5	6386.3	1.20	0.15	8.27	2.37	3.03	1.2	2.6
472.5	6468.5	1.22	0.15	8.35	3.17	2.52	1.4	3.5
482.5	6550.7	1.20	0.15	8.15	2.92	2.47	1.3	3.0
562.5	7305.8	1.07	0.13	7.96	2.94	4.32	1.5	3.4
582.5	7501.8	1.07	0.14	7.90	2.31	3.88	1.2	2.7
594.5	7617.2	1.01	0.13	7.87	2.57	4.61	1.5	3.1
694.5	8689	0.59	0.08	7.57	1.41	2.84	1.5	3.1
704.5	8798.6	0.60	0.08	7.59	1.16	3.08	1.2	2.5
714.5	8908.8	0.59	0.08	7.62	1.09	2.32	1.1	2.2

*Values originally reported in Limoges et al. (2020).

Table 4.2 Depth (cm), age (cal. yrs BP), bulk (singular data) and amino acid stable isotopes (‰; mean ± propagated uncertainty based on triplicate injections) of core AMD14-204.

Depth (cm)	Age* (cal. yrs BP)	Bulk $\delta^{13}C$* (‰)	Bulk $\delta^{15}N$* (‰)	THAA $\delta^{13}C$ (‰)	THAA $\delta^{15}N$ (‰)	EAA $\delta^{13}C$ (‰)	Phe $\delta^{15}N$ (‰)	TrAA $\delta^{15}N$ (‰)	TP_{met}	TP_{pro}	∑V (‰)
6.5	243	-22.64	7.05	-12.62 ± 0.1	11.10 ± 0.4	-18.29 ± 0.4	NA	NA	NA	NA	NA
11.5	319	-22.50	7.18	-19.66 ± 0.6	12.36 ± 0.2	-20.65 ± 0.4	7.61 ± 0.5	13.94 ± 0.3	1.94 ± 0.1	2.47 ± 0.2	2.10 ± 0.4
16.5	395	-22.77	7.07	-16.67 ± 0.3	10.72 ± 0.1	-23.19 ± 0.5	8.22 ± 0.3	14.07 ± 0.3	1.82 ± 0.1	2.61 ± 0.2	2.00 ± 0.3
138.5	2566	-22.18	7.02	-14.42 ± 0.2	11.33 ± 0.5	-20.04 ± 0.8	8.08 ± 0.7	13.98 ± 0.3	1.79 ± 0.1	2.27 ± 0.2	1.95 ± 0.3
148.5	2764.6	-22.35	7.11	-16.90 ± 0.1	13.16 ± 0.3	NA	8.21 ± 0.1	NA	1.86 ± 0.0	2.52 ± 0.3	NA
158.5	2963.2	-22.23	7.04	-15.42 ± 0.4	12.19 ± 0.2	-21.01 ± 0.6	8.23 ± 0.6	14.30 ± 0.2	1.82 ± 0.1	2.79 ± 0.2	2.08 ± 0.2
290.5	4693.6	-22.40	7.10	-16.94 ± 0.3	11.68 ± 0.3	-22.51 ± 0.4	8.79 ± 0.7	13.38 ± 0.3	1.64 ± 0.1	2.05 ± 0.2	2.35 ± 0.3
300.5	4817.4	-22.66	7.21	-16.99 ± 0.1	12.36 ± 0.2	-18.74 ± 0.4	8.04 ± 0.5	NA	1.83 ± 0.1	2.34 ± 0.2	NA
310.5	4941.3	-22.68	6.90	-15.24 ± 0.3	12.58 ± 0.2	-21.56 ± 0.7	8.65 ± 0.8	14.30 ± 0.4	1.62 ± 0.2	2.51 ± 0.2	1.74 ± 0.4
462.5	6386.3	-24.01	7.63	-16.95 ± 0.1	12.98 ± 0.3	-19.65 ± 0.7	8.37 ± 0.6	NA	1.81 ± 0.2	2.34 ± 0.2	NA
472.5	6468.5	-23.44	7.62	-15.95 ± 0.7	13.48 ± 0.8	NA	7.85 ± NA	NA	1.92 ± NA	2.53 ± NA	NA
482.5	6550.7	-23.63	7.79	-17.43 ± 0.5	13.05 ± 0.2	-23.92 ± 0.7	8.42 ± 0.6	14.54 ± 0.2	1.89 ± 0.2	2.55 ± 0.2	2.04 ± 0.2
562.5	7305.8	-23.55	7.82	-16.52 ± 0.1	13.46 ± 0.3	-20.23 ± 0.5	10.65 ± 1.1	14.98 ± 0.3	1.68 ± 0.2	1.98 ± 0.3	2.46 ± 0.3
582.5	7501.8	-23.61	7.74	-15.23 ± 0.2	12.18 ± 0.2	NA	7.59 ± 0.8	NA	2.08 ± 0.1	2.33 ± 0.3	NA
594.5	7617.2	-23.39	7.87	-18.05 ± 0.4	13.93 ± 0.3	-23.16 ± 0.6	9.18 ± 0.4	14.79 ± 0.2	1.87 ± 0.1	2.58 ± NA	2.35 ± NA
694.5	8689	-23.69	7.37	-17.87 ± 0.2	12.90 ± 0.3	-18.79 ± 0.3	9.08 ± 1.4	NA	1.77 ± 0.3	NA	NA
704.5	8798.6	-23.77	7.47	-14.42 ± 0.2	11.12 ± 0.3	-16.72 ± 1.3	7.85 ± 1.6	NA	2.01 ± 0.3	NA	NA
714.5	8908.8	-24.13	7.21	-19.51 ± 0.5	13.29 ± 0.1	NA	8.52 ± 0.6	NA	2.05 ± 0.1	NA	NA

*Values originally reported in Limoges et al. (2020).

4.3 Results

4.3.1 Temporal trends in bulk elemental composition, micropaleontology and biomarkers

The trends in bulk elemental composition, micropaleontology, and biomarkers were previously published in Limoges et al. (2020) and are briefly summarized here. Both TOC% and TN% remained low throughout the core, ranging 0.59–1.52% and 0.08–0.20%, respectively (Fig. 4.2a). A sharp increase in TOC% occurred at around 7.7 kyr BP (by ~1%), followed by a slow increase toward ~3 kyr BP and then a decline to the top of the core (Fig. 4.2a). TN% remained the lowest for 9.2–7.7 kyr BP and later slowly increased toward the top of the core (Fig. 4.2a).

The lowest diatom fluxes were found during 9.2–7.7 kyr BP with moderate *Chaetoceros* spores, accompanied by a high contribution of "marginal ice zone" assemblages (Fig. 4.2b, c). From around 6 kyr BP, total diatom fluxes progressively increased and peaked at 4.4 kyr BP with a decline in the "marginal ice zone" assemblages, followed by a gradual decrease in diatom fluxes and a strong increase in the "marginal ice zone" group (Fig. 4.2b, c). A sharp decline in diatom fluxes occurred at around 3 kyr BP accompanied by a sharp decline in the "marginal ice zone" group and a marked increase in the "summer subsurface" and "drift-ice/pack-ice" taxa (Fig. 4.2b, c). Thereafter, total diatom fluxes remained low for the rest of the core (Fig. 4.2b).

Fluxes of IP_{25} were detected throughout the core, with a relative high flux during 9.2–6.6 kyr BP (Fig. 4.3d). Later IP_{25} fluxes progressively decreased and reached the lowest at around 3 kyr BP before rising again to reach a maximum at 0.2 kyr BP. Both peaks in IP_{25} co-occurred with peaks of HBI III (Fig. 4.3d). The relatively low values of HBI III from 5 kyr BP are concurrent with the decline in IP_{25}, followed by a sharp increase in HBI III at 2.3 kyr BP (Fig. 4.3d).

4.3.2 THAA compositions

The trends of THAA yield, THAA-N%, and THAA-C% in the sediment core exhibited a logarithmic pattern ($r^2 \geq 0.5$; Fig. 4.2g). The THAA yield averaged for each period increased from ~1.0 μmol g^{-1} in 9.2–8.2 kyr BP to ~10 μmol g^{-1} in 0.5–0.2 kyr BP

(Fig. 4.2g). When averaged for each period, THAA-N% and THAA-C% demonstrated similar increasing trends, slowing rising from 9.2–8.0 kyr BP until 3.0–2.5 kyr BP by ~2% and then rapidly increasing to 8.7% and 3.5% in 0.5–0.2 kyr BP, respectively (Fig. 4.2g). The maxima of THAA-N% and THAA-C% occurred at 0.2 kyr BP (16.9% and 6.1%, respectively) which were ~3 times higher than the subsequently older sample (0.3 kyr BP; Fig. 4.2g).

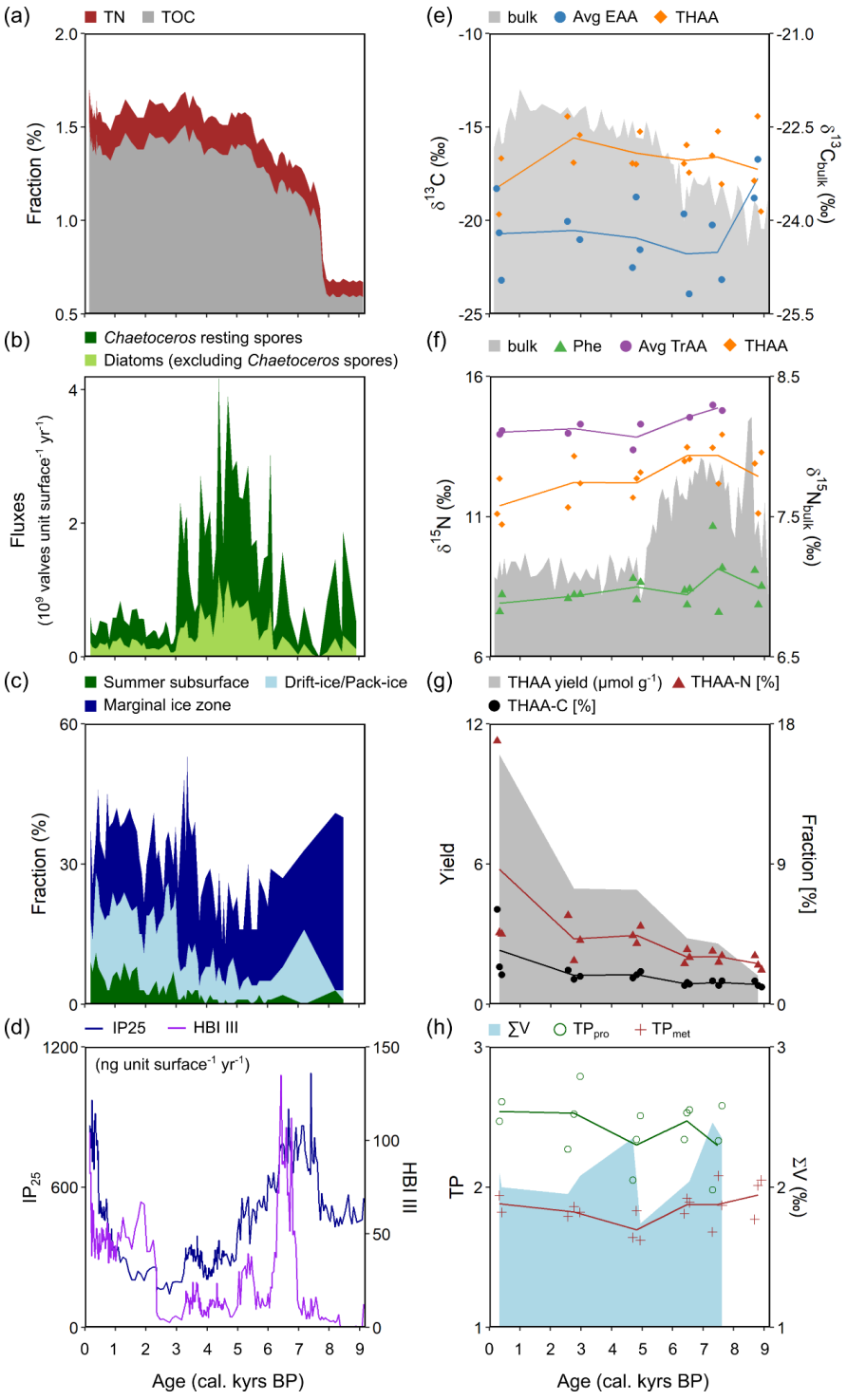

Figure 4.2 Temporal patterns in geochemical and biogenic proxies in sediment core AMD14-204 for the past c. 9,000 years BP (a-d, modified from Limoges et al., 2020): (a) total organic carbon (TOC) and total nitrogen (TN) content (wt%), (b) total diatom fluxes (dark green includes Chaetoceros spores and light green excludes Chaetoceros spores), (c) relative contribution of "summer subsurface", "drift-ice/pack-ice", and "marginal ice zone" assemblages (%), and (d) fluxes of IP_{25} (left y-axis) and HBI III (right y-axis), and bulk stable isotopes and

CSIA-AA results in this study (e-f): (e) bulk $\delta^{13}C$, average $\delta^{13}C$ of 5 essential amino acids (Avg EAA; Phe, Thr, Ile, Leu, Val) and total hydrolysable AAs (THAA), (f) bulk $\delta^{15}N$, average $\delta^{15}N$ of trophic AAs (Avg TrAA), Phe, and THAA, (g) THAA yield (averaged for each period), THAA-C%, and THAA-N%, and (h) TP_{pro}, TP_{met}, and degradation indicator ΣV of sediment core AMD14-204 for the past c. 9,000 years BP. Trend lines show averages for different periods (9.2 to 8.0, 8.0 to 7.0, 7.0 to 6.0, 5.0 to 4.5, 3.0 to 2.5, and 0.5 to 0.2 kyr BP; n = 1–3 for each period).

4.3.3 Amino acid molar concentrations

Concentrations of most AAs in the sediment core were similar between different periods, ranging from ~5.0 to ~10.0% (except Gly, Lys, and Thr; Fig. 4.3). The concentrations of Gly and Lys were relatively higher than the other AAs for most samples (Fig. 4.3). From the bottom of the core, Gly% increased from ~7.5% to ~29.0% while Lys% declined from ~18.5% to ~6.0% (Fig. 4.3). A decreasing trend was also observed in Leu%, Ile%, Pro%, and Val% (Fig. 4.3). Thr had the lowest abundance, ranging from 0.6 to 4.3 % (Fig. 4.3).

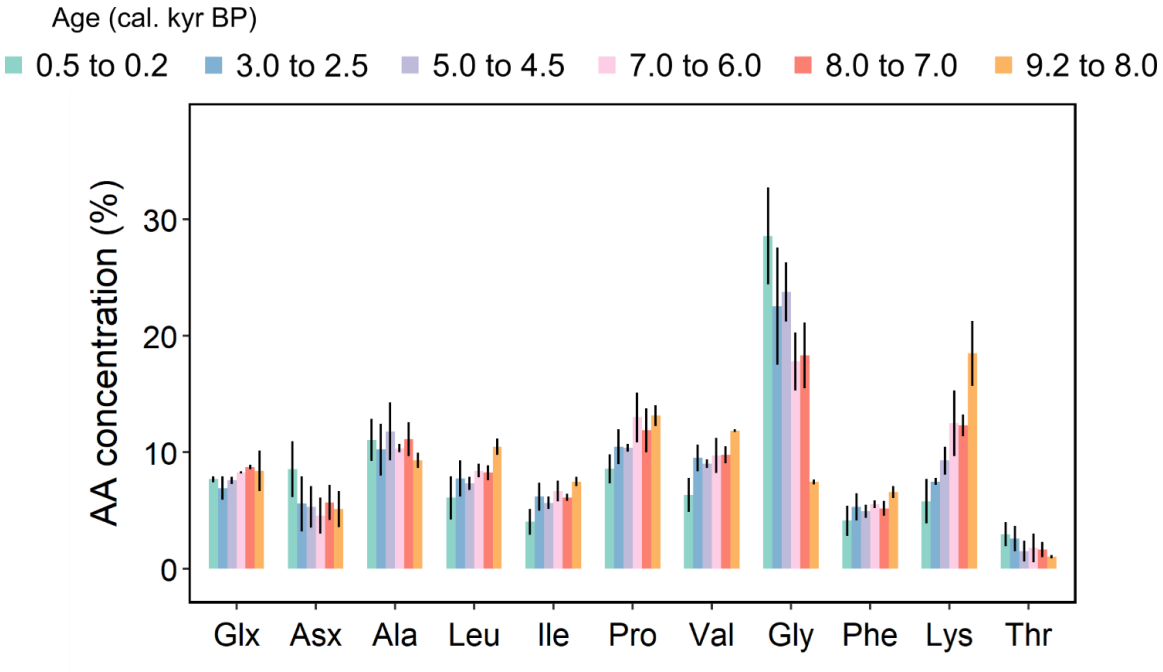

Figure 4.3 The average AA molar composition of sediment core AMD14-204 for six periods (0.5 to 0.2, 3.0 to 2.5, 5.0 to 4.5, 7.0 to 6.0, 8.0 to 7.0, and 9.2 to 8.0 kyr BP). Error bars represent ± 1 standard error for each period (n = 2–3 for Thr and n = 3 for other AAs).

4.3.4 Bulk $\delta^{13}C$ and $\delta^{15}N$ variability

The values of bulk $\delta^{13}C$ and $\delta^{15}N$ were previously published in Limoges et al. (2020) and are briefly summarized here. Bulk $\delta^{13}C$ ranged from -24.4‰ to -21.9‰,

increased from the bottom of the core until reaching a plateau at ca. 3.0 kyr BP, and later decreased to around -23‰ from ca. 1.0 kyr BP (Fig. 4.2e). Bulk $\delta^{15}N$ rapidly increased from 6.9‰ from the bottom of the core and peaked at 8.2‰ at ~8.5 kyr BP (Fig. 4.2f). Later bulk $\delta^{15}N$ progressively decreased until 5.0 kyr BP and stabilized at ~7.0‰ (Fig. 4.2f).

4.3.5 Amino acid $\delta^{13}C$ variability

The $\delta^{13}C$-THAA ranged from -19.7‰ to -12.6‰, demonstrating a higher variability with more enriched values compared to bulk $\delta^{13}C$ (Fig. 4.2e). The average $\delta^{13}C$ of five EAAs ($\delta^{13}C$-EAA) ranged from -23.9‰ to -16.7‰ and was also more variable than bulk $\delta^{13}C$. When averaged for each period, $\delta^{13}C$-EAA dropped from -17.8‰ at 9.2–8.0 kyr BP to -21.7‰ at 8.0–7.0 kyr BP, increased slightly to -20.9‰ at 5.0–4.5 kyr BP, and remained stable thereafter (Fig. 4.2e).

When internally normalized (see Eq. (1) in Sect. 2.5), the $\delta^{13}C$ patterns of EAAs were consistent between different periods (except for 9.2–8.0 kyr BP), with Phe ranging from ~-4.0 to ~-2.0‰, Thr from ~9.0 to ~11.0‰, Ile from ~-2.0 to ~-1.0‰, Leu from ~-5.0 to ~-3.0‰, and Val from ~-2.0 to ~0.0‰ (Fig. 4.4a). By contrast to Thr that showed higher values (15.8 ± 1.9‰), the $\delta^{13}C$ of Phe was lower from 9.2–8.0 kyr BP than during other periods (-6.5 ± 0.1‰; Fig. 4.4a). However, given the small sample size, such differences were not statistically significant (Table C2). The overall $\delta^{13}C$-EAA patterns of the sediment core fell between the values for sea ice algae, pelagic algae, and heterotrophic bacteria reported elsewhere (Fig. 4.4a; Larsen et al., 2013; Chen et al., 2022).

4.3.6 Amino acid $\delta^{15}N$ variability

The $\delta^{15}N$ values of Phe, a commonly used proxy for baseline N source, fluctuated between 7.6 and 10.6‰ throughout the core with a small peak in 8.0–7.0 kyr BP and a higher variability than bulk $\delta^{15}N$ (Fig. 4.2f). The average $\delta^{15}N$ values of trophic AAs ranged from 13.4 to 15.0‰ and showed a decreasing trend from 8.0–7.0 to 5.0–4.5 kyr BP, dropping from 14.9‰ to 14.5‰ before remaining constant towards the top of the core (Fig. 4.2f). The $\delta^{15}N$-THAA averaged for each period demonstrated a similar trend with the bulk $\delta^{15}N$ with more enriched values and slightly higher variability, increasing

from 12.4‰ from the bottom of the core, peaking at 13.2‰ at 8.0–7.0 kyr BP, and steadily declining to 11.4‰ until 0.5–0.2 kyr BP (Fig. 4.2f).

When normalized to the baseline proxy (δ^{15}N-Phe), the δ^{15}N of TrAAs showed elevated levels from the baseline, with Glx, Val and Ala being the most elevated (~8.0–9.0‰, ~8.0–9.0‰, and ~9.0–10.0‰, respectively; Fig. 4.4b). The δ^{15}N of Lys (the other SrcAA) showed a negligible deviation from Phe, while the δ^{15}N-Thr was depleted by 2.4 ‰ (Fig. 4.4b). With the exception of Thr, the overall Phe-normalized δ^{15}N-AA patterns fell between those for detritus and fecal pellets and were distinctly different from either cultured algae or zooplankton.

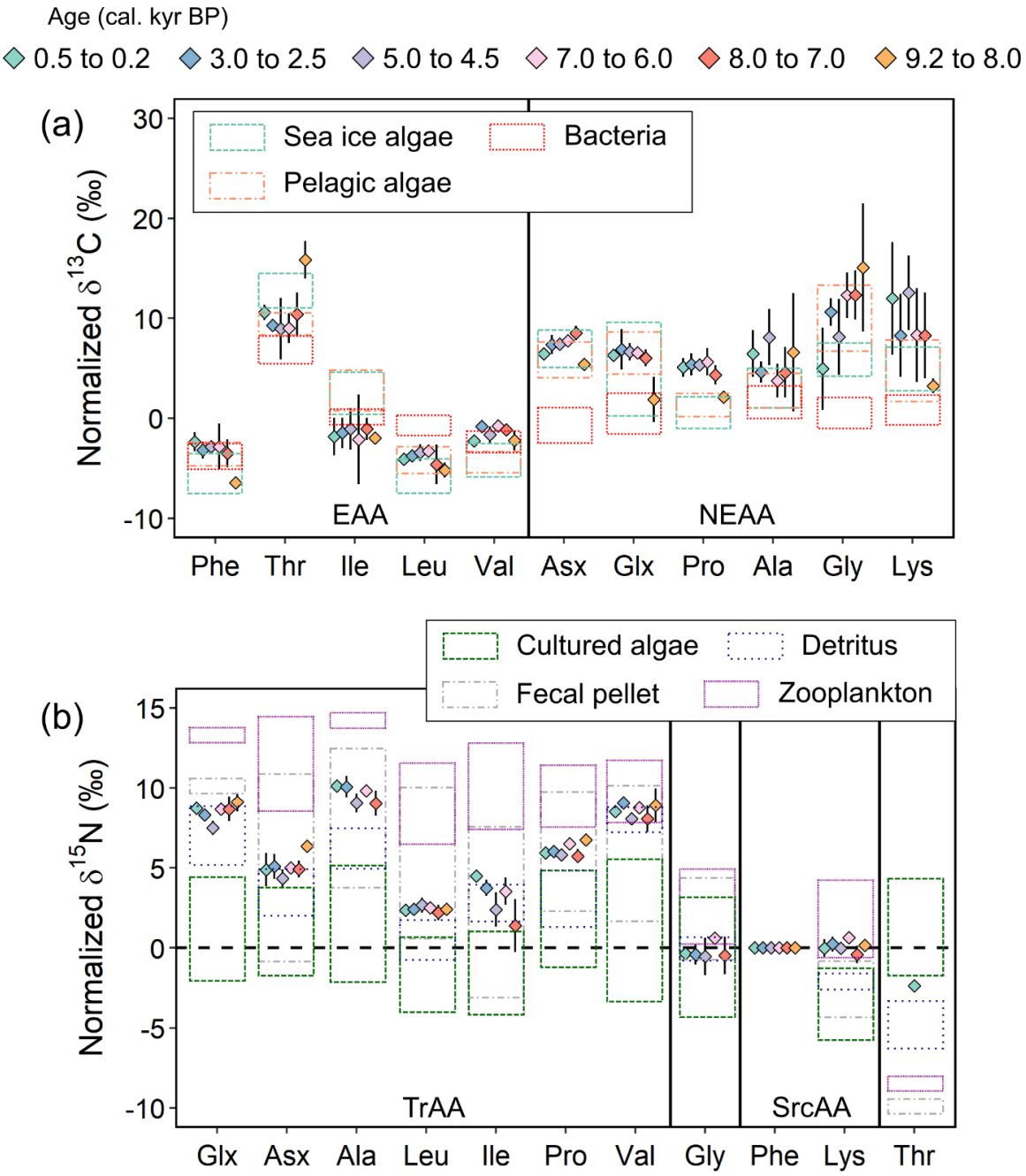

Figure 4.4 (a) δ^{13}C-AA patterns normalized to the mean of δ^{13}C of 5 essential amino acids (Phe, Thr, Ile, Leu, Val) and (b) δ^{15}N-AA patterns normalized to the baseline proxy δ^{15}N-Phe of different periods in sediment core AMD14-204 (0.5 to 0.2, 3.0 to 2.5, 5.0 to 4.5, 7.0 to 6.0, 8.0 to 7.0, and 9.2 to 8.0 kyr BP). Error bars show ±1 standard error for each period (n = 1–3). δ^{13}C-AA patterns are compared with those of sea ice algae and pelagic algae collected in Canadian Arctic/subarctic seas from Chen et al. (2022) and heterotrophic bacteria from Larsen et al. (2013). δ^{15}N-AA patterns are compared with those of cultured autotrophic algae, detritus, fecal pellets, and zooplankton from McClelland and Montoya (2002), Chikaraishi et al. (2009), Hannides et al. (2009, 2013), Doherty et al. (2021), and Chen et al. (Chapter 3). EAA, essential amino acid; NEAA, non-essential amino acid; TrAA, trophic amino acid; SrcAA, source amino acid.

4.3.7 Temporal dynamics in trophic and degradation proxies

TP_{met}, the most common proxy for metazoan trophic transfers, ranged from 1.6 to 2.1 throughout the core, mirroring the trend of the $\delta^{15}N$ values of Phe when averaged for each period (Fig. 4.2f, h). The more recently proposed proxy for protozoan trophic transfers, TP_{pro}, was ~0.5 higher than TP_{met}, ranging from 2.0 to 2.8 and mirroring the $\delta^{15}N$-Phe pattern when averaged for each period (Fig. 4.2f, d). As an indicator for the degree of heterotrophic bacterial resynthesis, values of the $\sum V$ parameter fluctuated from 1.7 to 2.5‰, dropping from 2.5 to 1.7‰ from 8.0–7.0 to 5.0–4.5 kry BP, rising and dropping again from 2.4‰ to 2.0‰ from 5.0–4.5 to 3.0–2.5 kyr BP (Fig. 4.2h).

4.4 Discussion

In this study, we presented one of the first investigations of downcore CSIA-AA variations in Holocene aged sediments. Our sediment core record spanning the past ca. 9,000 years showed significant diagenetic alteration of organic geochemical compositions, but with little apparent effect on CSIA-AA patterns or derived parameters. These results suggest that CSIA-AA signals recorded in marine sediments may help to disentangle processes affecting bulk $\delta^{13}C$ and $\delta^{15}N$ signals and thereby inform interpretations of biogeochemical cycling and heterotrophic dynamics over multimillennial timescales.

4.4.1 Diagenetic patterns

4.4.1.1 THAA losses indicate substantial OM degradation

In this study, we use THAA contents as a proxy for organic alteration and diagenesis. The decreasing downcore trends in THAA contents (Fig. 4.2g) are broadly consistent with previously reported organic degradation trends in marine sediments (Cowie and Hedges, 1992, 1994; Cowie et al., 1995; Wakeham et al., 1997; Lee et al., 2000; Hedges et al., 2001; Batista et al., 2014). The upper most analyzed interval at 6.5 cm/243 yr BP had a THAA yield of 14 mg/100 mg OC and thereafter < 5 mg/100 mg OC (Table 4.1). For reference, THAA yields range 50–100 mg/100 mg OC in fresh plankton and microbial biomass, and typically > 30 mg/100 mg OC in epipelagic layer sediment traps (Cowie and Hedges 1992). Mesopelagic-depth sinking particles collected from sediment traps deployed in the northern Labrador Sea had THAA yields of 24.7 ± 12.6

mg/100 mg OC (Chen et al., Chapter 3). Based on these reference values, the upper core sediments appear to be strongly depleted in THAA content relative to fresh plankton or exported sinking particles. THAA-N%, which is a widely used organic degradation proxy, was 17% in the upper core interval, also considerably lower than that of fresh biomass (> 50%, Cowie and Hedges, 1992; Wakeham et al., 1997) and sediment traps (> 38%, Cowie and Hedges 1992; > 20%, Chen et al., Chapter 3). The THAA losses continued downcore. If the uppermost interval from 6.5 cm/243 yr BP is included, the downcore decreases follow logarithmic relationships with age (THAA yield = -1.51ln(yr) + 16.4 mg/100 mg OC, $r^2 = 0.56$; THAA-C% = 0.70ln(yr) + 7.56 %, $r^2 = 0.53$; THAA-N% = -1.90ln(yr) + 19.78 %, $r^2 = 0.46$). However, the uppermost interval appeared to be an outlier relative to the other more recent intervals and could represent fresher material that was worked downward by bioturbation. Given the depths and resolution of the analysed samples, it is not possible to determine if the THAA losses happened before, or just after, initial sedimentation and burial. Regardless, all the sediments analyzed in the present study appeared to be substantially degraded with respect to THAA contents.

The downcore decrease in THAA-C% and THAA-N% suggested a preferential degradation of AAs over total OM (Fig. 4.2g; Braun et al., 2017). Reactive proteins and carbohydrates are preferentially degraded during early diagenesis which concentrates refractory materials that can only be significantly degraded in the presence of O_2 (Burdige, 2007). The preferential consumption of AAs was evident by the much faster decrease in THAA contents compared to TOC and TN (Fig 4.2a, g), indicating that AAs were converted into other non-AA or uncharacterizable OM compounds that were consumed at a much slower rate in the deeper and more oxygen deficient buried sediments (Henrichs, 1992; Hedges and Keil, 1995; Burdige, 2007).

The downcore THAA losses were notably decoupled from the sediment grain size, which was fine to medium silt throughout the core (Caron et al., 2020), and TOC and TN contents, which were stable over most of the core record, except for the abrupt shift in 7.7 kyr BP (Fig. 4.2a). The shift in TOC% and TN% coincides with a change in sediment provenance associated with a hypothesized reorganization in paleoceanography (Caron et al., 2019, 2020; Limoges et al., 2020). Earlier than 7.7 kyr BP, the sediments

were supplied mainly by meltwater discharge from the Upernavik ice stream on the west Greenland, which would have had very low organic contents. Afterwards, sediments were supplied by hemipelagic sedimentation from relatively warmer and presumably more biologically productive waters of the West Greenland Current (Caron et al., 2019). The lack of any corresponding changes in TOC:TN ratios (Table 4.1) indicated that the 7.7 kyr shift in TOC and TN was driven by changing proportions of organic to inorganic sediment inputs and was unrelated to organic diagenesis.

While THAA yields, THAA-C%, and THAA-N% in marine sediments vary across different time scales, geographical locations, and oceanic conditions, the values in core AMD14-204 are comparable to previously reported values. For example, Colombo et al. (1998), Braun et al. (2017), and Choi et al. (2022) reported sedimentary THAA yields of < 40 μmol g^{-1}, THAA-C% of < 20%, and THAA-N% of < 40% below the first few centimeters from the surface. The variations in THAA contents may be linked to different parameters including temperature, current influences, water depths, sedimentation rates, bottom O_2 conditions, and other environmental factors (Canfield, 1993; Burdige, 2007; Braun et al., 2017). In sediments from shallower waters on the southwest Greenland margin near Davis Strait (389 and 498 m), higher THAA contents were measured for the past 10,000 years, with THAA yields of ~20–40 μmol g^{-1} and THAA-N% of ~20–40% (Braun et al., 2017). Temperature data showed that surface temperature at Davis Strait was ~4°C warmer than that near our core site in the northeastern Baffin Bay (73.86°N) in August (averaged for 1948–1999, Tang et al., 2004). The lower THAA contents at our study site may thus potentially be attributed to a stronger influence of cold Arctic waters, lower marine productivity, greater sea-ice cover, less incident radiation, and a deeper water depth (987 m at our study site), where less of the produced OM reaches the seafloor.

4.4.1.2 Changes in AA molar concentrations and implications for Degradation Index (DI)

With a decreasing trend in THAA contents, AA molar concentration (AA mol%) showed pronounced trends with increasing age (Fig. 4.2g, 4.3). We were not able to resolve Thr and Ser in most of our samples, especially for $\delta^{15}N$ measurements, and thus a

commonly used diagenesis proxy, degradation index (DI; Cowie and Hedges, 1992; Dauwe and Middelburg, 1998; Dauwe et al., 1999), was not determined in this study. However, our observations have important implications for the use of DI in sediments.

In contrast to previous studies reporting increasing Gly mol% with increasing degradation in marine sediments (Cowie and Hedges, 1992; Dauwe and Middelburg, 1998; Dauwe et al., 1999), we observed a significant decrease in Gly mol% with depth (Fig. 4.3, 4.5). This decrease was balanced by increases in the relative concentrations of Ile, Leu, Val, Pro, and Lys (Fig. 4.3, 4.5). Enrichment in Gly mol% is generally interpreted as an indicator for microbial degradation (Cowie and Hedges, 1992; Dauwe et al., 1999; Choi et al., 2022). The preferential accumulation of Gly mol% in marine sediments during sinking and deposition is linked to newly synthesized Gly from microbial production or selective preservation of Gly-concentrated diatom cell walls (Hecky et al., 1973; Cowie and Hedges, 1992; Dauwe and Middelburg, 1998). Cell wall amino acids are less susceptible to enzymatic degradation in comparison to intracellular elements that have relatively higher reactivities (Cowie and Hedges, 1992; Dauwe and Middelburg, 1998). The mechanism of the Gly decline in our core is uncertain, yet the relatively high Gly concentrations in most of the core (~18–30% except for 9.2–8.0 kyr BP) compared to that in fresh plankton (< 15%; Cowie and Hedges, 1992; Dauwe and Middelburg, 1998; Gaye et al., 2022), was consistent with values reported for degraded sediments (Fig. 4.3; Cowie and Hedges, 1992; Dauwe and Middelburg, 1998; Gaye et al., 2022). Therefore, these sediments must be subject to certain degrees of microbial degradation that had preferentially preserved Gly by the time they reached the seafloor or shortly after burial, as also indicated by elevated TP_{pro} and ΣV values (see discussion in the section below). Pantoja and Lee (2003) observed a lack of difference in degradation status with depth in deep sediments because the organic matter deposited on the seafloor surface were already degraded after travelling though the ~1,000-m water column, a depth that is similar to our study site. Hence, we suggest that there may be other processes leading to the post-depositional loss of Gly, following the initial enrichment driven by degradation.

The downcore loss of Gly may be an indication of structural changes in the sedimentary OM. Glynn et al. (2022) documented Gly losses in subfossil (~9.6–11.6 kyr BP) coral skeletons and proposed a mechanism of abiotic Gly decarboxylation (Catão and López-Castillo, 2018), where proton transfer assisted by water molecules cleaves the C-N bond of free Gly, leading to its degradation. They pointed out that this abiotic decarboxylation was consistent with physical structural changes in the coral skeletons, which may have allowed for sea-water penetration and thus enhanced both biotic and abiotic degradation. Similarly, a decrease in Gly mol% was observed in subfossil mollusc shells, which was most likely driven by physical leaching and abiotic chemical reactions (Vokhshoori et al., 2023). Therefore, we hypothesize that abiotic decarboxylation may explain the downcore decrease in Gly mol%. This possibility raises questions for the applicability of DI for evaluating the relative degradation state of OM in downcore sediments, specifically, where degradation is partly abiotically controlled, the use of DI may not reflect the true degradation state of OM.

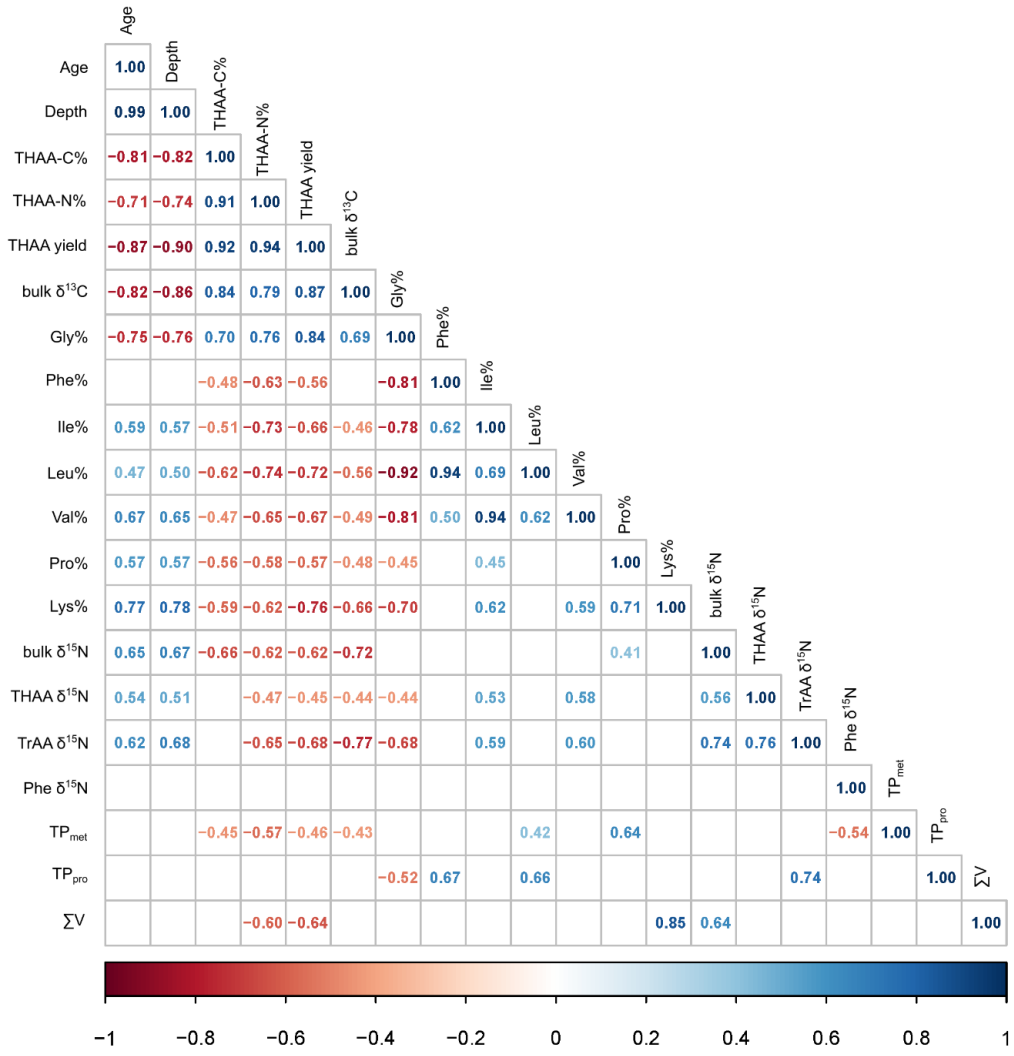

Figure 4.5 Correlation matrix of age, depth, THAA contents, AA mol%, bulk $\delta^{13}C$ and $\delta^{15}N$, and amino acid $\delta^{13}C$ and $\delta^{15}N$ parameters in sediment core AMD14-204. Positive values show significant positive correlation and negative values show significant negative correlation ($p < 0.05$). Blank space shows insignificant correlation. Color bars indicate correlation coefficients.

4.4.2 Isotopic patterns

4.4.2.1 Temporal shifts in bulk $\delta^{13}C$ and $\delta^{15}N$ signals

Bulk $\delta^{13}C$ values of the whole sediment core (ca. -24 to -22‰) fell within the typical range of marine particulate organic matter (POM) reported in Arctic/subarctic regions (Schubert and Calvert, 2001; Søreide et al., 2006; Belt et al., 2008). Bulk $\delta^{15}N$

values (ca. +7 to +8‰) fell within the isotopic range of modern surface and subsurface nitrates in central and western Baffin Bay (~6–8‰) but were heavier than those from more Atlantic-water influenced sectors of eastern Baffin Bay (Fig. 4.2f; Lehmann et al., 2019; Sherwood et al., 2021). An abrupt shift at ~5 kyr BP separated the core into two significantly different clusters (Two-Sample T-test, $p < 0.001$) with relatively lower $\delta^{13}C$ and higher $\delta^{15}N$ from 9.2–5.1 and relatively higher $\delta^{13}C$ and lower $\delta^{15}N$ from 5.1–0.2 kyr BP (Fig. 4.6). Terrestrially derived OM is generally more depleted in both $\delta^{13}C$ and $\delta^{15}N$ compared to marine OM (Hoefs, 2018), so it is unlikely that the opposing trends in bulk $\delta^{13}C$ and $\delta^{15}N$ were due to changes in terrestrial inputs. The isotopic shift also appeared to be unrelated to OM accumulation or preservation as there were no corresponding changes in sediment grain size, TOC, TN, OC:N ratios, or AA-based degradation indices at 5.1 kyr. Limoges et al. (2020) noted that the shift in bulk coincided with a transition from marginal ice zone to more temperate micropaleontological assemblages (Fig 4.2b–d). They proposed that the elevated bulk $\delta^{15}N$ in the earlier Holocene may have been linked to more complete surface-water nitrate assimilation due to enhanced stratification caused by meltwater input from the Greenland Ice Sheet. They also interpreted the bulk $\delta^{13}C$ record as a proxy for ice (higher $\delta^{13}C$) vs pelagic (lower $\delta^{13}C$) sources particulate OM; however, this interpretation of $\delta^{13}C$ was difficult to reconcile with divergent trends in IP_{25} and HBI III ice algae biomarkers (Fig 4.2d).

The temporal shift in bulk $\delta^{13}C$ was decoupled from changes in AA-specific $\delta^{13}C$ (Fig. 4.2e). $\delta^{13}C$-THAA was uncorrelated with age or bulk $\delta^{13}C$ and there was no difference before versus after the step change at 5.1 kyr (Two-Sample T-test, $p > 0.1$). This decoupling between bulk $\delta^{13}C$ and $\delta^{13}C$-THAA (Fig. 4.2e) may be explained by the very low contribution ($1.9 \pm 1.1\%$) that AAs made to the TOC. The bulk $\delta^{13}C$ signal must instead be driven by more abundant compounds comprising the TOC, such as lipids, carbohydrates and, in particular, “uncharacterizable” OM (Wakeham et al., 1997). Solid-phase nuclear magnetic resonance data have revealed that non-protein alkyl carbon and black carbon comprise most of the uncharacterizable OM in marine sediments (up to 60% of TOC; Gélinas et al., 2001; Arndt et al., 2013; Middelburg, 2019).

In comparison to carbon, the bulk and AA-specific $\delta^{15}N$ records were more coupled. $\delta^{15}N$-THAA was positively correlated with age and bulk $\delta^{15}N$ (Fig. 4.5) and exhibited a ~-1‰ step change from higher to lower values at 5.1 kyr (Two-Sample T-test, $p < 0.05$). As with carbon, AAs accounted for a small percentage (4.3 ± 3.2%) of TN; the rest must be represented by other N-bearing organic compounds, uncharacterizable OM, as well as N-bearing clays (Kienast et al., 2005; Batista et al., 2014). It is unclear why the bulk and AA-specific stable isotopes were more coupled for $\delta^{15}N$ than for $\delta^{13}C$ despite the similarly low AA contributions to TOC and TN. Downcore analysis of the relative concentrations and compound-specific isotopes of different non-AA organic and inorganic fractions would help deconvolve the bulk isotopic records.

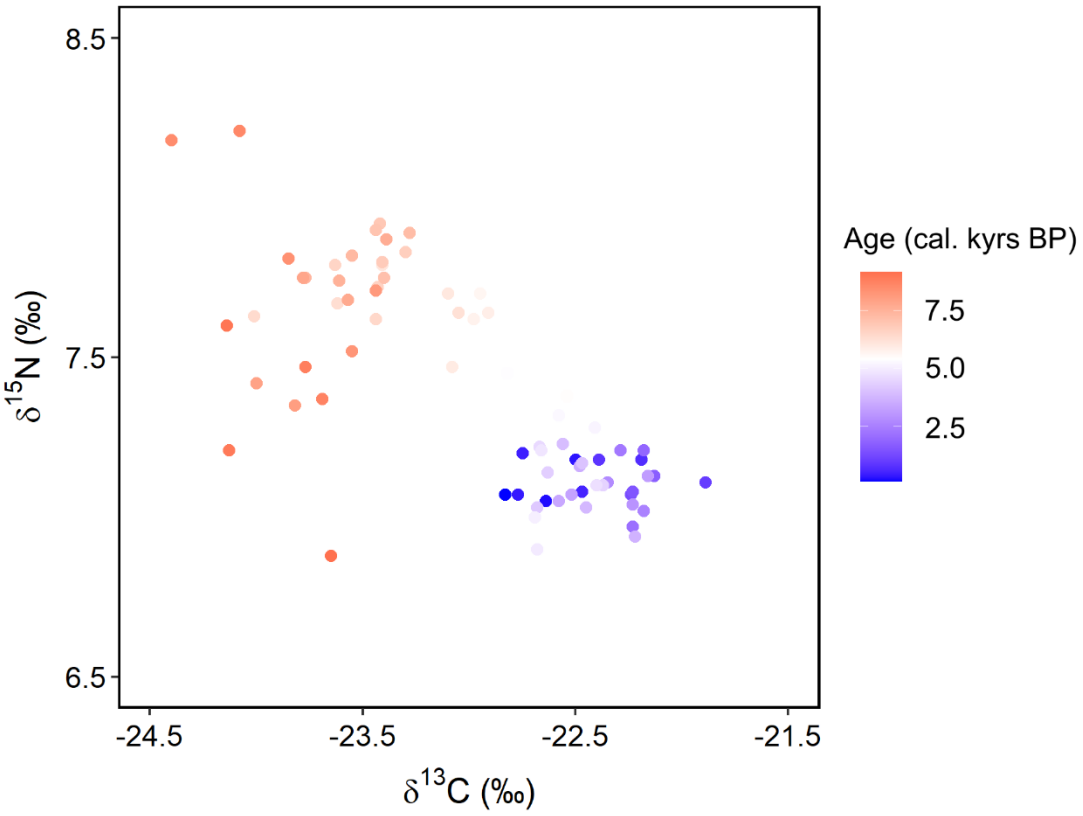

Figure 4.6 Bulk $\delta^{15}N$ against bulk $\delta^{13}C$ of core AMD14-204. Color bar indicates the age of samples. Note the temporal separation in bulk $\delta^{13}C$ and $\delta^{15}N$ signals of sediments before and after ~5.5 kyr.

4.4.2.2 Reconstruction of primary producer carbon sources from δ^{13}C-EAA signals

Patterns of d^{13}C-EAA in marine OM have proven to be a robust proxy for the baseline isotopic signatures of surface primary producers (Larsen et al., 2009; Larsen et al., 2013; Vokhshoori et al., 2014; Larsen et al., 2015; Elliott Smith et al., 2022). δ^{13}C-EAA of primary producers are transferred to higher trophic levels or detrital materials with little or no isotopic fractionation (McMahon et al., 2013; Schiff et al., 2014; Larsen et al., 2015; Shen et al. 2021). In the present study, internally normalized sediment core δ^{13}C-EAA values fell within the ranges for sea ice algae, pelagic algae, and heterotrophic bacteria reported elsewhere (Larsen et al., 2013, 2015; Chen et al., 2022), suggesting the ultimate source of sedimentary carbon in the AAs is from these sources, and revealing remarkable long-term preservation of primary production and microbial resynthesis signatures in sedimentary δ^{13}C-EAA (Fig. 4.4a).

Average δ^{13}C-EAA for the earliest 9.2–8.0 kyr period was 3.4 ± 0.5‰ higher than the rest of the period averages, driven primarily by the +8‰ offset in δ^{13}C-Thr (Fig. 4.2e). Together with the corresponding decrease in δ^{13}C-Phe, the resulting δ^{13}C-EAA pattern most closely resembled that of sea ice algae. The separation between 9.2–8.0 kyr and the other periods became more pronounced in the LDA classification model (Fig. 4.7). Samples from 9.2–8.0 kyr clustered apart from the other periods and were classified as sea ice algae with probabilities of > 99% (Table C4), while samples from the other periods clustered together with heterotrophic bacteria and pelagic algae. This suggests that AAs from the earliest period were generated largely from sea ice algae with relatively less bacterial reworking, while AAs from < 8 kyr were generated from pelagic algae with relatively more bacterial reworking.

Previous sedimentological and micropaleontological studies on the same sediment core revealed distinct paleoceanographic periods and associated sources of primary production over the 9.2 kyr record (Caron et al., 2019a, b; Hansen et al., 2020; Limoges et al., 2020). In the early Holocene (Greenlandian; 9.2–8.0 kyr), the northwest Greenland margin was subject to deglacial conditions with extended sea ice cover and high meltwater discharge (Caron et al., 2019b; Hansen et al., 2020). The prevalence of sea ice

algae δ^{13}C-EAA signatures during this period agrees with high relative abundance of ice-associated diatom assemblages and relatively high fluxes of IP_{25} and HBI III (Fig. 4.2c, d). Similarly, the shift to more pelagic algae like δ^{13}C-EAA signatures after 8 kyr (Northgrippian and Meghalayan) agrees with micropaleontological evidence (relative decrease in sea-ice diatoms and dinoflagellate cysts and increase in warm-water diatoms and benthic foraminifera) for warmer conditions associated with northward intrusion of the West Greenland Current (Hansen et al., 2020; Limoges et al., 2020). From 4 kyr onward, micropaleontological records indicate a return to cooler, seasonally ice-covered conditions associated with neoglacial cooling (Limoges et al., 2020). While the δ^{13}C-EAA signatures from the youngest intervals trend back toward sea ice algae, LDA outputs for all intervals < 8 kyr were indistinguishable within analytical uncertainties (Fig. 4.7). This suggests that the analytical methods employed here were not sensitive enough to capture the relatively more subtle changes in primary productivity following the major paleoceanographic reorganization at 8 kyr. Alternatively, we note that micropaleontological proxies are highly source specific, whereas the δ^{13}C-EAA records integrate and therefore smooth out the geochemical signatures from all sources of AAs, which may be less sensitive to the taxa-specific changes apparent in the micropaleontological records.

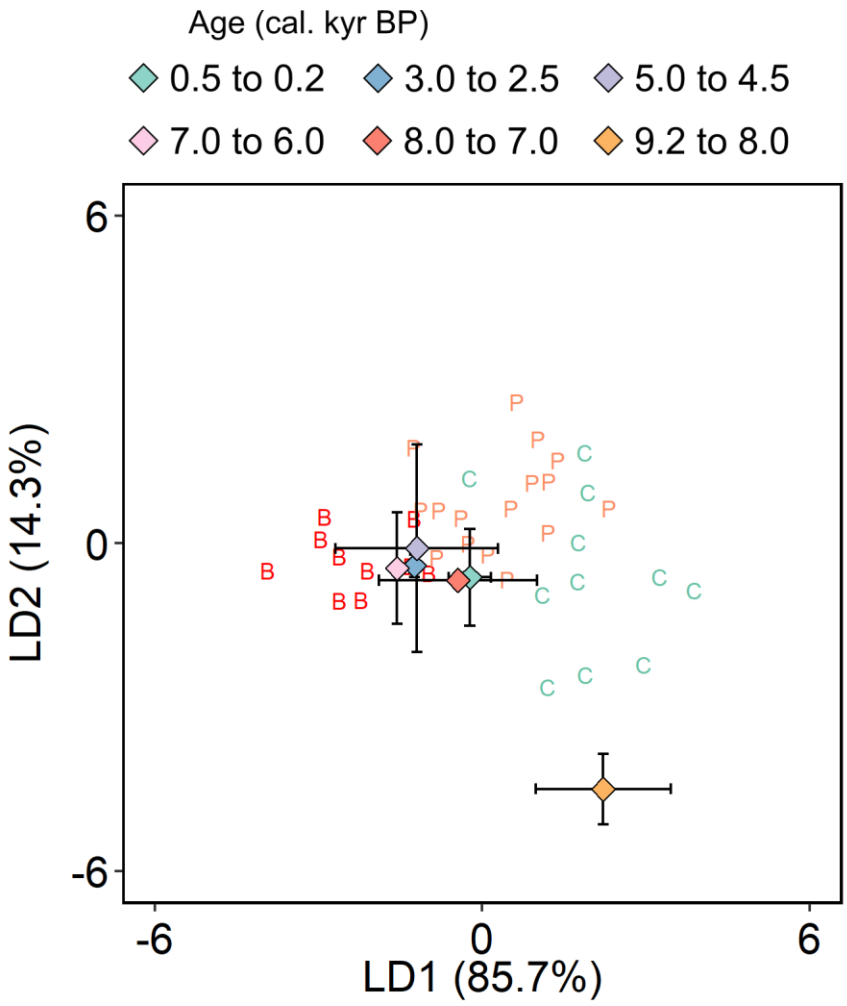

Figure 4.7 Linear discriminant analysis based on normalized $\delta^{13}C$ values of five essential amino acids of core AMD14-204. The model was trained on three categorical variables: (B) heterotrophic bacteria from Larsen et al. (2013); (P) pelagic algae and (C) sea ice algae from Chen et al. (2022). Values in parentheses of the axis titles are the percentage variation explained by each axis. Linear discriminants are averaged for each period and shown with means and ±1 standard errors (diamonds with error bars).

4.4.2.3 Apparent stability of the baseline $\delta^{15}N$ record

In this and the following section we deconvolve the $\delta^{15}N$-THAA record into the source nitrogen (or "baseline") and heterotrophic components. In isotope ecology and paleoceanography studies, "baseline" $\delta^{15}N$ usually refers to $\delta^{15}N$ of primary producers, which reflects the combined influences of inorganic N isotopes and the degree of N utilization (Altabet and Francois, 1994; Waser et al., 1998; Altabet et al., 1999; Needoba et al., 2003). Owing to minimal fractionation during heterotrophic processing, $\delta^{15}N$-Phe

has proven to be a reliable baseline N proxy for not only animals (McClelland & Montoya, 2002; Chikaraishi et al., 2009; Vokhshoori and McCarthy 2014; McMahon and McCarthy 2018), but also heterotrophic protists (Gutiérrez-Rodríguez et al., 2014; Décima et al., 2017), bacteria, fungi, archaea (Yamaguchi et al., 2017), and plants (Fogel and Tuross, 1999). In the present study, sedimentary δ^{15}N-Phe remained stable over the length of the record (linear regression: δ^{15}N-Phe vs age, $p > 0.1$). The relatively poor analytical uncertainty (± 0.5‰) of the δ^{15}N-Phe measurements may conceal an underlying trend: the slope of the δ^{15}N vs age relationship (-0.08 ‰/1000 yr) is in fact similar to that of the bulk δ^{15}N record (-0.07 ‰/1000 yr) and would likely be statistically significant with tighter analytical precision and/or a larger number of downcore measurements. Even so, the magnitude of these changes (-0.7 ‰ for δ^{15}N-bulk; -0.9 ‰ for δ^{15}N-Phe) is relatively small. For comparison, Kienast et al. (2019) reported a -2‰ decrease in δ^{15}N-bulk over a ~8 kyr core collected further south on the western Greenland margin (64°21.680'N, 52°57.70'W, 483 m water depth).

The average δ^{15}N-Phe (8.4 ± 0.7‰) in core AMD14-204 falls toward the higher end of the isotopic range of modern surface and subsurface nitrates (Lehmann et al., 2019, 2022; Sherwood et al., 2021) and POM (Fox et al., 2022) in Baffin Bay. At present, mixed layer waters of Baffin Bay have two main sources. Pacific water, which becomes isotopically enriched in nitrate (δ^{15}N-NO_3: ~7–8‰) as it crosses the Bering and Chukchi shelves (Granger et al., 2011, 2018; Brown et al., 2015; Fripiat et al., 2018), transits through the Canadian Artic Archipelago and enters Baffin Bay via Lancaster, Jones, and Smith Sounds or via Nares Strait (Fig. 4.1; Jones et al., 2003; Tang et al, 2004; Münchow et al., 2015; Carmack et al., 2016; Hu et al., 2019). The Pacific water extends to a depth of ~300 m in western Baffin Bay and shallows to ~100 m in eastern Baffin Bay, below which lay warmer and isotopically lighter (δ^{15}N-NO_3: ~5‰) Atlantic-sourced waters flowing into Baffin Bay via the West Greenland Current (Melling et al., 2001; Jones et al., 2003; Tang et al., 2004; Sherwood et al. 2021).

Inferring from present-day conditions, the relatively high δ^{15}N-Phe in core may result from complete utilization of largely Pacific-derived nitrogen. Tremblay et al. (2006) observed an increase in δ^{15}N of pelagic OM with decreasing fraction of

unassimilated nitrate in the northern Baffin Bay, converging toward the estimated initial $\delta^{15}N$ of nitrate (8.4 ± 0.2‰). Our $\delta^{15}N$-Phe values are consistent with these values. However, the data in Tremblay et al. (2006) were collected in the North Water Polynya of Smith Sound (76–79ºN; Fig. 4.1), where the influence of Pacific water should be greater than at the AMD14-204 core site. It is difficult to reconcile this interpretation with the presumed influence of isotopically lighter Atlantic waters at the study site, especially as multi-proxy records from core AMD14-204 indicate an onset of Atlantic water in the early Holocene (Hansen et al., 2020; Limoges et al., 2020). Improved delineation of the $\delta^{15}N$-NO_3 isoscape in northeastern Baffin Bay, using direct measurements (or inferred from seawater nitrate to phosphate ratios; Sherwood et al. 2021) could help resolve this problem.

Regardless of the mechanisms of baseline $\delta^{15}N$ enrichment, the overall record suggests relatively stable oceanographic conditions with respect to nitrate sources and assimilation efficiency over the 9.2 kyr length of the record. Sedimentological, foraminiferal, and geochemical records revealed flooding of Bering Strait and Chukchi shelf by rapid sea level rise ca. 12–7 kyr BP (Elias et al., 1992, 1996; Keigwin et al., 2006; Smith et al., 2011) and complete opening of Nares Strait due to glacial retreat ca. 9–8 kyr BP (Georgiadis et al., 2018; Jennings et al., 2019), evidencing a supply of Pacific waters to the Arctic Ocean and an establishment of a new gateway for Pacific waters into the Baffin Bay by early Holocene time. Observational and modelling results suggested that the distribution of Pacific-sourced water in the upper Arctic Ocean, together with river runoff and ice melt, was relatively fast (years to decades) before exiting through the Canadian Archipelago and Fram Strait (Becker and Björk, 1996; Jones et al., 1998; Ekwurzel et al., 2001; Jones, 2001; Hu et al., 2019). Further, recent foraminifera-bound $\delta^{15}N$ records indicate that the coupled nitrification-denitrification mechanism for $\delta^{15}N$-NO_3 enrichment of Pacific water over the Bering and Chukchi shelves was in place by 11 kyr (Farmer et al. 2021). Our baseline $\delta^{15}N$-Phe record is largely consistent with this paleoceanographic framework.

4.4.2.4 Heterotrophic processing

The heterotrophic component of THAA record is represented by trophic AAs. Because trophic AAs account for a larger share of THAA relative to Phe (Fig. 4.3), the δ^{15}N-TrAA record paralleled the δ^{15}N-THAA record, with a statistically significantly (linear regression: δ^{15}N-TrAA vs. age, $p < .05$) but relatively small magnitude decrease (-0.9 ‰) in values from 9.2 kyr to present. When normalized to δ^{15}N-Phe, the δ^{15}N-TrAA patterns were consistent between different periods, suggesting similar degrees of heterotrophic processing over the 9.2 kyr record (Fig. 4.4b).

The overlapping δ^{15}N-TrAA patterns of our core with values for fecal pellets degraded OM, but with less depleted δ^{15}N-Thr value, indicated that core sediments mainly contained microbially-modified OM (e.g., detritus) and not fresh algal or zooplankton biomass. Previous studies proposed four δ^{15}N-AA patterns shaped by microbial metabolisms (McMahon and McCarthy, 2016; Fig. 14 in Ohkouchi et al., 2017): 1) algae-like pattern when microbes synthesize AAs *de novo* from inorganic N with low TP_{met} and $\sum V$ values; 2) metazoan-like pattern when microbes incorporate existing AAs from the environment with an increase in TP_{met} values; 3) consistent isotopic enrichment across all AAs, possibly by extracellular protein hydrolysis; and 4) scattered pattern when only selected AAs are resynthesized with a large increase in $\sum V$ values. The δ^{15}N-TrAA patterns in our core showed more similarity with those of metazoan-like pattern (Ohkouchi et al., 2017) with moderate $\sum V$ values (~2‰) that were comparable to those in sinking particles collected in northern Labrador Sea (Chen et al., Chapter 3).

TP proxies have been developed based on δ^{15}N values from two different groupings of AAs: TP_{met} which is calculated from δ^{15}N of Phe and Glx, reflects metazoan trophic steps, while TP_{pro} which is based on Phe and Ala, includes trophic steps from both metazoan and protozoan grazing (Chikaraishi et al., 2009; Nielsen et al., 2015; Décima et al., 2017; Décima and Landry, 2020). Glx has been widely used in CSIA-AA studies for TP estimates for its chemical stability and high abundance in most organisms (Chikaraishi et al., 2009). Gutiérrez-Rodríguez et al. (2013) observed a lack of enrichment in protistan δ^{15}N-Glx relative to their prey with increasing trophic steps,

raising questions on whether Glx-based TP (later called TP_{met}) may underestimate protistan trophic transfers (2014). Through chemostat experiments, Décima et al. proposed Ala-based TP (later referred as TP_{pro}) provides a more robust trophic signal for both protistan and metazoan consumers (2017).

Here, TP_{met} values were comparable to that of primary consumers (2.0), suggesting limited trophic transfers from metazoan grazing, most likely by zooplankton (Doherty et al., 2021). Furthermore, the elevated TP_{pro} (by ~0.5) revealed the "invisible" protozoan or bacterial signatures (Fig. 4.2h; Décima et al., 2017; Décima and Landry, 2020; Doherty et al., 2021). Together these results revealed that the sediments were modified by both trophic grazing and microbial resynthesis. The ∑V parameter is a complementary proxy to TP_{pro} that reflects the degree of heterotrophic processing by calculating the deviation from the "baseline" δ^{15}N-AA patterns in marine algae (McCarthy et al., 2007; McCarthy et al., 2013). Elevated ∑V values suggest incorporation of microbial-derived organic N proteinaceous materials (McCarthy et al., 2007). The sediment core ∑V (1.7–2.5‰) fell within the typical range of that for sinking particles and sediments (~1.0–3.0‰) reported elsewhere (McCarthy et al., 2007; Shen et al., 2021). TP_{pro} calculated from δ^{15}N-Ala and Phe in previously reported sinking POM and sediments typically ranged from ~1.0 to ~3.0, varying between different geographical locations, water depths, and oxygen conditions (McCarthy et al., 2007; Batista et al., 2014; Yamaguchi and McCarthy, 2018; Sabadel et al., 2019; Choi et al., 2022; Yoshikawa et al., 2022). Ianiri and McCarthy (2023) reported high TP_{pro} (~3) and ∑V (> 2‰) values in high-molecular-weight dissolved organic matter (DOM) and lower values in low-molecular-weight DOM collected in the North Atlantic Subtropical Gyre (2023). They proposed that the high-molecular-weight DOM was mainly derived from continual heterotrophic bacterial and protozoan production while the low-molecular-weight DOM was directly produced via de novo synthesis (Ianiri and McCarthy, 2023). Our TP_{pro} and ∑V fell toward the higher end of the typical range for marine POM and similar to those of highly degraded (high-molecular-weight) DOM, suggesting a considerable degree of microbial production during sedimentation (McCarthy et al., 2007; Batista et al., 2014; Yamaguchi and McCarthy, 2018; Sabadel et al., 2019; Choi et al., 2022; Yoshikawa et al., 2022; Ianiri and McCarthy, 2023).

4.4.2.5 Multi-millennial preservation of CSIA signals

Various organic geochemical proxies have been developed based on either AA concentrations (THAA yields, AA mol%) or AA isotopic values (δ^{15}N-AA patterns, $\sum$V) to evaluate the degree of microbial alteration of marine OM (McCarthy et al., 2007). While THAA contents give an overview of AA losses during the OM degradation in marine sediments, proxies based on δ^{15}N-AA patterns provide more detailed information in terms of trophic transfers and microbial alteration of OM.

The relatively invariant TP_{pro} and $\sum$V throughout the core did not show significant correlations with depth, indicating a lack of progressive microbial reworking after OM burial despite the continuous THAA losses (Fig. 4.2g, h; Fig. 4.5). Consistent with TP_{pro} and $\sum$V, no significant differences were observed in Phe-normalized δ^{15}N-TrAA patterns between different periods (Fig. 4.4b). The discrepancy in temporal changes between the two types of degradation indicators, THAA contents and δ^{15}N-AA proxies (TP_{pro}, $\sum$V, and δ^{15}N-TrAA), was consistent with previous observations and may be driven by different degradation mechanisms (Batista et al., 2014; Sauthoff, 2016; Choi et al., 2022; Golombek et al., 2024). Batista et al. (2014) suggested that declining THAA contents was caused by AA remineralization and removals. The labile AAs are either converted into more refractory materials or CO_2, and hence their absolute and relative amounts are lowered, which is fundamentally different from microbial resynthesis that induces isotopic changes in individual AAs (Dauwe 1999; McCarthy et al., 2007). While OM remineralization leads to a decrease in the absolute amount of OM and the relative amount of reactive components (e.g., AAs), part of OM is re-assimilated and repackaged into bacterial biomass (Burdige, 2007). Isotopic changes of N are induced by enzymatic degradation processes, such as deamination and transamination (Macko and Estep, 1984; Macko et al., 1986; Ohkouchi et al., 2017). It has been shown that organic matter preservation in marine sediments is linked to organic matter sorption to mineral surfaces in protected coatings (Hedges and Keil, 1995). The organic sorption to mineral surface is strongly protective of liable organic compounds, such as AAs and simple sugars, slowing remineralization rates by up to five orders of magnitude. (Keil et al., 1994; Mayer, 1994a, b; Hedges and Keil, 1995). Recent research suggested geopolymerization of simple sugar and AAs catalyzed by dissolved Fe and Mn under anoxic conditions, or Fe and Mn

oxides under oxic conditions, may play a key role in absorptive protection of OM against remineralization (Moore et al., 2023). Combined with protective sorption to mineral surface, geopolymerization could transform liable reactants into recalcitrant organics and promote OM preservation in marine sediments (Hedges and Keil, 1995; Burdige, 2007; Moore et al., 2023). This may explain the lack of continuous microbial resynthesis with a decelerating decline in THAA contents in our sediment core. Instead of being assimilated into heterotrophic bacterial biomass with N isotopic changes, AAs may be protected by organic sorption from microbial degradation and converted into large refractory molecules, e.g., the uncharacterizable OM, by geoploymerization or other formation pathways (Moore et al., 2023).

Taken together, these results provided insights into the degree of diagenesis in ~9 kyr sediments collected from deep water on the coast of Northwest Greenland. When sediments traveled through the 987-m water column before deposition, they had already been modified by processes such as trophic transfers, remineralization, and resynthesis. This is evidenced by the low THAA contents, high Gly mol%, scattered δ^{15}N-AA patterns and elevated TP_{met}, TP_{pro}, and $\sum V$ (Fig. 4.2, 4.3, 4.4). Microbial modification that led to isotopic changes plateaued immediately after burial of the sediments in the upper centimeters (likely due to the decrease in bacterial activity or mineral protection), and hence recorded the pre-burial signatures of δ^{15}N-AA proxies. Meanwhile, AA losses from remineralization or removal processes, which may be linked to structural changes in the OM or transformation into recalcitrant organics, continued to slowly reduce the absolute number of AAs as well as the relative contribution of selected AAs (e.g., Gly) to OM, without inducing noticeable isotopic fractionations in the AA pool (Fig. 4.2, 4.3, 4.4).

4.5 Summary and Conclusion

This study presented the first coupled records of AA-specific δ^{13}C and δ^{15}N in a marine sediment core spanning most of the Holocene period. We documented detailed information on C and N baseline signatures, and trophic and microbial processing through a 9.2 kyr sediment core collected in northeastern Baffin Bay. Comparison of our measurements with existing CSIA-AA data and other multi-proxy records shows robust

long-term preservation of AA $\delta^{13}C$ and $\delta^{15}N$ proxies despite significant downcore loss in AA concentrations. $\delta^{13}C$-EAA patterns preserved signals from primary production and captured an early Holocene shift from largely sea ice algae signatures to those of pelagic algae and heterotrophic bacteria, coherent with previous micropaleontological evidence for plankton community shifts (Hansen et al., 2020; Limoges et al., 2020). $\delta^{15}N$-Phe was relatively well preserved, demonstrating the potential to serve as a reliable proxy $\delta^{15}N$ baseline in aged marine sediments. AA-based trophic and bacterial indicators showed a lack of progressive microbial reworking after OM burial, suggesting that most of the diagenesis occurred during sinking and early deposition. These results expand the limited existing CISA-AA data on multi-millennial sediments and highlight the potential of AAs as reliable tracers complementary to other geochemical proxies. We suggest that CSIA-AA provide complementary information about export production and microbial degradation for more specific and reliable geochemical interpretations.

Together, these new data strongly support the potential to extend the biogeochemical time series for longer-term paleo-reconstruction and disentangle short-term variability for periods of interest using CSIA-AA. Long-term preservation of CSIA-AA information in marine sediments may be governed by the protective mechanisms of organics against microbial degradation. Future controlled experiments coupled with CSIA-AA measurements on preservation mechanisms in marine sediments, such as geopolymerization, can help interpret CSIA-AA records in natural sediments.

4.6 Conflict of Interest

The authors declare that the research was conducted in the absence of any commercial or financial relationships that could be construed as a potential conflict of interest.

4.7 Author Contributions

S-MC and OAS contributed to conception and design of the study. AL contributed to measurements of bulk OM stable isotope analyses, diatoms, and sea-ice biomarkers. S-MC and OAS contributed to CSIA-AA sample processing, measurements, and data analysis. S-MC wrote the manuscript with input from all the co-authors.

4.8 Funding

This study was funded by an NSERC Discovery Grant to OAS (RGPIN-2018-05590).

4.9 Acknowledgments

Core AMD14-204 was collected as part of the GREENEDGE project funded by ANR and the Total Foundation. Ship-time was funded by the ERC-STG-ICEPROXY project. This work was supported by an NSERC Discovery Grant to OAS. We thank Amundsen Science which is supported by the Canada Foundation for Innovation and NSERC. We are grateful to the captain, officers, crew, and scientists on board the *CCGS Amundsen* 2014 expedition for the recovery of core AMD14-204.

CHAPTER 5 CONCLUSION

Recent advances in CSIA-AA offer new opportunities to enhance our understanding of biogeochemical and ecological responses in vulnerable polar ecosystems to changing climate. This thesis applies the novel CSIA-AA techniques to investigate marine export production in the Canadian Arctic and subarctic seas. Our study demonstrated that:

For the first time, δ^{13}C-AA and δ^{15}N-AA patterns of sea ice algae were distinguished from those of pelagic algae, which highlighted the diagnostic potential of CSIA-AA to differentiate microalgal assemblages from sea ice and pelagic origins in future studies. The δ^{13}C-EAA signature of sea ice algae may serve as a new indicator for sea ice algae contribution in exported sinking particles and archived marine sediments. To enhance our understanding of C and N sources and cycling in exported OM and their impacts on biological pump efficiency in ice-covered Arctic and subarctic seas, characterization and quantification of sea ice algae contribution are essential. These findings help enhance the accuracy of quantitative estimates of sinking particle composition and processing.

Building on the findings in Chapter 2 and previous work of CSIA-AA proxies, we investigated the OM fluxes and composition in northwest Labrador Sea, an important transition zone connecting Arctic and subarctic ecosystems. The δ^{13}C-EAA patterns of exported sinking particles indicated that sea ice algae are an important food source to higher trophic levels, consistent with the observations of lengthy sea-ice cover (50-60% of each annual cycle) and ice-associated diatoms during the spring bloom following ice breakup in 2018. δ^{15}N-AA results revealed dominant animal sources (fecal pellets and zooplankton) to the sinking fluxes, consistent with the observations of sustained copepod communities throughout both annual cycles. These findings revealed the importance of sea ice algae and fecal pellets in the biological pump in seasonally ice-covered northwest Labrador Sea, with sea ice algae exported either directly via passive sinking or indirectly via zooplankton grazing and fecal pellets dominating the organic particle fluxes. These findings have important implications for the ongoing decline in sea-ice extent and early sea ice melt in Arctic and subarctic seas, given the important roles sea ice algae and

zooplankton fecal pellets play in controlling the timing, quantity, and quality of primary, secondary and export production.

We carried out the first CSIA-AA measurements on Holocene sediments in northeastern Baffin Bay. δ^{13}C-AA and δ^{15}N-AA sediment core records spanning most of the Holocene period in northeastern Baffin Bay showed excellent long-term preservation of CSIA-AA proxies despite noticeable alteration in AA concentrations. δ^{13}C-EAA patterns preserved integrated signals from primary production and microbial resynthesis. A shift in baseline C values was captured in the early Holocene using the δ^{13}C-EAA end-member of sea ice algae from Chapter 2, coherent with an overall increase in diatom fluxes and a relative decline in sea-ice diatoms. Baseline N values indicated that surface water may be fueled by regenerated Pacific-derived nutrients via complete utilization, consistent with modern observations of N limitation in Pacific-sourced waters in Baffin Bay. AA-based trophic and bacterial indicators showed a lack of progressive microbial reworking with depth despite continuous losses of AAs and suggested that most of diagenesis may have occurred during sedimentation and early deposition. These results expand the limited existing CISA-AA data on multi-millennial sediments and highlighted the potential of CISA-AA proxies as reliable tracers of export production and microbial degradation for longer-term paleo-reconstruction.

Despite the powerful potential in CSIA-AA demonstrated in this thesis, methodological limitations and application challenges remain to be addressed in future research. In Chapter 2, we hypothesized that the distinct δ^{13}C-EAA pattern in sea ice algae from pelagic algae is governed by their unique physiological adaptations to extreme conditions. Nevertheless, we should acknowledge that this distinction in δ^{13}C-EAA patterns could be impacted by the differences in algal community composition and heterotrophic bacterial biomass. The measured δ^{13}C-EAA values of sea ice algae and pelagic algae represent the integrated isotopic values of natural communities. Thus, our samples conceivably contain multiple species, some of which can be found in both habitats (e.g., *Chaetoceros/Attheya* spp., *Fragilariopsis* spp., and *Nitzschia/Pseudo-Nitzschia* spp; Hsiao, 1980; Melnikov, 1998; Poulin et al., 2011), as well as heterotrophic biomass, whereas previous studies characterized δ^{13}C-EAA values mostly at a

family/species level (Larsen et al., 2009, 2013). The distinction in δ^{13}C-EAA from pelagic algae was found more pronounced in fast ice algae (> 80% were pennate and centric diatoms; Pogorzelec et al., 2022) than brash ice algae. It remains unclear if this was driven by distinct physiological responses of similar communities (e.g., diatom-dominated) or distinct community compositions between the ice habitats. We measured different size classes, an important trait of community composition, of sea ice and pelagic algae and found that the differences between sizes were less pronounced compared to the those between sea ice and pelagic origins, indicating community composition played a minor role in separating the algal groups. Nevertheless, a lack of taxonomic resolution is a major limitation in this study. Although we included past surveys on species composition of sea ice algae and pelagic algae from the sampling sites as well as other Arctic regions (Hsiao, 1979; Hsiao & Pinkewycz, 1985; Hsiao, 1992; Hargrave et al., 1994; Hop et al., 2020; Dhifallah et al., 2022), a description of species for each size class and algal group in this study would be helpful to constrain the differences in community composition and their potential impacts on the distinct δ^{13}C-EAA patterns between sea ice algae and pelagic algae.

In Chapter 3, the resolution of OM fluxes and stable isotope data was mainly compromised by methodological limitations. First, the two sediment traps were deployed at different depths on the outer edge of Saglek Bank and thus OM fluxes and composition of sinking particles may be biased by the differences in exported depths. Due to low OM content in some sampling bottles (and only half volume was processed), we were not able to measure the bulk and CSIA-AA stable isotopes for each integrated period (15-16 days/bottle) and some CSIA-AA data during the spring/summer blooms were missing (e.g., June and July in 2018). Further, grouping and taxonomic resolution of microalgae and zooplankton counts were inconsistent between the two annual cycle due to an inconsistency among taxonomists. For example, Chlorophyceae were listed as "unknown" in 2017-2018 cycle while multiple diatom species, including the ice associated species, were not identified for the 2018-2019 cycle, which posed challenges in estimating the magnitude and timing of ice algal export in the 2018-2019 cycle. In this study, we estimated fecal pellet contribution to exported sinking particles using an end-member based on published data. The impact of the study would have been significantly

enhanced if we sampled and measured fecal pellets at our study site during the deployment periods.

In Chapter 4, OM content in Holocene sediments was extremely low compared to fresher materials (e.g., sea ice algae in Chapter 2 and exported sinking particles in Chapter 3). Therefore, the biggest limitation issue in this study comes from the resolution of AA peaks in GC-IRMS. For fresher materials with relatively consistent AA profiles (similar AA mol%), most hydrolysable AAs can be resolved with good reproducibility. For Holocene sediments with more variable AA profiles in this study, we were not able to resolve all the AAs in sufficient peak sizes in the chromatographs, especially for Thr and Ser in $\delta^{15}N$ measurements. Thus, a commonly used diagenesis proxy, degradation index (DI), was not determined and Phe-normalized $\delta^{15}N$ of Ala and Thr model was not applicable in this study. To capture long-term CSIA-AA trends concurrent with significant variations in primary production and sea-ice dynamics (Limoges et al., 2020), three subsamples were selected from six distinct periods for CSIA-AA analyses. Despite the relatively consistent inter-millennial trends in AA $\delta^{13}C$ and $\delta^{15}N$ proxies when averaged for each period, there appeared to be shorter-term variations within each period. The shorter-term CSIA-AA variability may be hidden by the low sampling resolution. A lack of studies on the effects of sources and $\delta^{15}N$ of inorganic N on $\delta^{15}N$-Phe values made it difficult to interpret the baseline variability in our core. Similarly, the effects of OM preservation mechanisms (e.g., geopolymerization) on CSIA-AA proxies in natural sediments remain unclear, confounding our interpretation of the diagenesis processes in ~9,000 years old sediments.

To test the fidelity of $\delta^{13}C$-EAA proxy for sea ice algae, establishment of a large repository of end-member data from laboratory cultures and extensive sampling of sea-ice and pelagic algae across size, space, and time are fundamental. It is difficult to isolate substantial biomass for different species from field samples or maintain lab cultures for a diverse list of species, especially for sea ice algae (Geilfus et al., 2016). Nevertheless, culture experiments comparing $\delta^{13}C$-EAA signatures of the same species growing in sea water versus sea ice is necessary to fully test our hypothesis. Field samples are easier to be collected and less time-consuming with less or no cultivation effort, so a detailed

description of species composition coupled with CSIA-AA measurements on field assemblages collected from seawater and sea ice is of great importance, particularly for different types of sea ice (e.g., first-year ice versus multiyear ice, landfast ice versus brash ice; Leu et al., 2015; Mundy and Meiners, 2021).

It would be beneficial to continue CSIA-AA measurements on sinking particles collected from moored sediment traps deployed at the same location and water depth in the northern Labrador Sea to constrain OM fluxes and composition from the same exported depths. More materials should be processed for an improved sampling resolution for CSIA-AA and effort should be made to make sure taxonomic identification is consistent between different deployment cycles. When feasible, sampling of in-situ end-members (e.g., phytoplankton, zooplankton, and fecal pellets), concurrent to the sampling of exported sinking particles, would greatly improve the accuracy of the mixing model estimation of end-member relative contributions.

We also suggest that future work should expand CSIA-AA measurements on Holocene marine sediments globally and establish multi-proxy data repository for vulnerable ecozones. To improve data interpretation of the multi-dimensional CSIA-AA proxies, specific processes that control stable isotope fractionation of individual AAs, especially for baseline proxy δ^{15}N-Phe, are worth investigating. In future studies, it would be interesting to investigate short-term variabilities in CSIA-AA proxies during periods of interest (e.g., Little Ice Age, McMahon et al., 2015; early Holocene deglaciation, Limoges et al., 2020) from long-term paleo-archives. Controlled experiments on the underlying biochemical or metabolic mechanisms between inorganic N and SrAA δ^{15}N and between microbial activities and TrAA δ^{15}N is crucial for accurate data interpretation of CSIA-AA information preserved in marine OM and ancient sediments (Whiteman et al., 2019). Finally, to fulfil the diagnostic potential of CSIA-AA proxies, standardization of sample processing and data calibration techniques is essential to ensure direct comparisons of cross-study datasets.

Overall, the work presented in this thesis has significant implications for the use of CSIA-AA in future biogeochemical and ecological studies. First, we demonstrated the ability to differentiate natural sea-ice and pelagic assemblages using CSIA-AA, which

provides the potential to address crucial knowledge gaps in sea ice algae dynamics. Second, we revealed that sea ice algae and fecal pellets are critical C and N sources in exported sinking particles in the northern Labrador Sea, which are subject to climate-related ocean changes that are expected to alter the timing, quantity and quality of food sources for deep-water benthic assemblages. Finally, the robust long-term preservation of CSIA-AA information in Baffin Bay Arctic marine sediments allows for more specific and reliable geochemical interpretations to understand changes in past ocean conditions and ecosystem shifts. Together, this thesis paves the way for the use of a newly developed biomarker for sea ice algae and other existing CSIA-AA proxies that are proven to be reliable OM tracers across different sedimentary regimes and time scales in ice-covered Arctic and subarctic seas, which is essential for predicting future responses of Arctic/subarctic ecosystems to long-term climate change.

REFERENCES

Aagaard, K. and Carmack, E.C., 1989. The role of sea ice and other fresh water in the Arctic circulation. Journal of Geophysical Research: Oceans, 94(C10), pp.14485-14498.

Abelson, P.H. and Hoering, T., 1961. Carbon isotope fractionation in formation of amino acids by photosynthetic organisms. Proceedings of the National Academy of Sciences, 47(5), pp.623-632.

Abraham, W.R. and Hesse, C., 2003. Isotope fractionations in the biosynthesis of cell components by different fungi: a basis for environmental carbon flux studies. *FEMS Microbiology Ecology*, *46*(1), pp.121-128.

Altabet, M.A. and Francois, R., 1994. Sedimentary nitrogen isotopic ratio as a recorder for surface ocean nitrate utilization. Global Biogeochemical Cycles, 8(1), pp.103-116.

Altabet, M.A., 1996. Nitrogen and carbon isotopic tracers of the source and transformation of particles in the deep sea. Particle Flux in the Ocean, pp.155-184.

Altabet, M.A., Pilskaln, C., Thunell, R., Pride, C., Sigman, D., Chavez, F. and Francois, R., 1999. The nitrogen isotope biogeochemistry of sinking particles from the margin of the Eastern North Pacific. Deep Sea Research Part I: Oceanographic Research Papers, 46(4), pp.655-679.

Amiraux, R., Archambault, P., Moriceau, B., Lemire, M., Babin, M., Memery, L., Massé, G. and Tremblay, J.E., 2021. Efficiency of sympagic-benthic coupling revealed by analyses of n-3 fatty acids, IP25 and other highly branched isoprenoids in two filter-feeding Arctic benthic molluscs: Mya truncata and Serripes groenlandicus. Organic Geochemistry, 151, p.104160.

Anderson, L.G., Falck, E., Jones, E.P., Jutterström, S. and Swift, J.H., 2004. Enhanced uptake of atmospheric CO2 during freezing of seawater: A field study in Storfjorden, Svalbard. Journal of Geophysical Research: Oceans, 109(C6).

Ardyna, M., Mundy, C.J., Mills, M.M., Oziel, L., Grondin, P.L., Lacour, L., Verin, G., Van Dijken, G., Ras, J., Alou-Font, E. and Babin, M., 2020. Environmental drivers of under-ice phytoplankton bloom dynamics in the Arctic Ocean. Elementa: Science of the Anthropocene, 8, p.30.

Arndt, S., Jørgensen, B.B., LaRowe, D.E., Middelburg, J.J., Pancost, R.D. and Regnier, P., 2013. Quantifying the degradation of organic matter in marine sediments: A review and synthesis. Earth-Science Reviews, 123, pp.53-86.

Arrigo, K.R. and Thomas, D.N., 2004. Large scale importance of sea ice biology in the Southern Ocean. Antarctic Science, 16(4), pp.471-486.

Arrigo, K.R., van Dijken, G. and Pabi, S., 2008. Impact of a shrinking Arctic ice cover on marine primary production. Geophysical Research Letters, 35(19).

Arrigo, K.R., Perovich, D.K., Pickart, R.S., Brown, Z.W., Van Dijken, G.L., Lowry, K.E., Mills, M.M., Palmer, M.A., Balch, W.M., Bahr, F. and Bates, N.R., 2012. Massive phytoplankton blooms under Arctic sea ice. Science, 336(6087), pp.1408-1408.

Arrigo, K.R., 2014. Sea ice ecosystems. Annual Review of Marine Science, 6, pp.439-467.

Arrigo, K.R., Perovich, D.K., Pickart, R.S., Brown, Z.W., Van Dijken, G.L., Lowry, K.E., Mills, M.M., Palmer, M.A., Balch, W.M., Bates, N.R. and Benitez-Nelson, C.R., 2014. Phytoplankton blooms beneath the sea ice in the Chukchi Sea. Deep Sea Research Part II: Topical Studies in Oceanography, 105, pp.1-16.

Arrigo, K.R. and van Dijken, G.L., 2015. Continued increases in Arctic Ocean primary production. Progress in Oceanography, 136, pp.60-70.

Astronomical Applications Department of the United States Naval Observatory (no date) Duration of Daylight/Darkness Table for One Year. Available at: https://aa.usno.navy.mil/data/Dur_OneYear (Accessed: 06 November 2023).

Balzano, S., Marie, D., Gourvil, P. and Vaulot, D., 2012. Composition of the summer photosynthetic pico and nanoplankton communities in the Beaufort Sea assessed by T-RFLP and sequences of the 18S rRNA gene from flow cytometry sorted samples. The ISME journal, 6(8), pp.1480-1498.

Bates, N.R. and Mathis, J.T., 2009. The Arctic Ocean marine carbon cycle: evaluation of air-sea CO 2 exchanges, ocean acidification impacts and potential feedbacks. Biogeosciences, 6(11), pp.2433-2459.

Batista, F.C., Ravelo, A.C., Crusius, J., Casso, M.A. and McCarthy, M.D., 2014. Compound specific amino acid δ15N in marine sediments: A new approach for studies of the marine nitrogen cycle. Geochimica et Cosmochimica Acta, 142, pp.553-569.

Batista, F.C., 2016. An examination of the marine nitrogen cycle: insights from novel stable nitrogen isotopic approaches. Doctoral dissertation. University of California, Santa Cruz.

Bayer-Giraldi, M., Weikusat, I., Besir, H. and Dieckmann, G., 2011. Characterization of an antifreeze protein from the polar diatom Fragilariopsis cylindrus and its relevance in sea ice. Cryobiology, 63(3), pp.210-219.

Becker, P. and Björk, G., 1996. Residence times in the upper Arctic Ocean. Journal of Geophysical Research: Oceans, 101(C12), pp.28377-28396.

Bélanger, S., Ehn, J.K. and Babin, M., 2007. Impact of sea ice on the retrieval of water-leaving reflectance, chlorophyll a concentration and inherent optical properties from satellite ocean color data. Remote Sensing of Environment, 111(1), pp.51-68.

Belt, S.T., Massé, G., Rowland, S.J., Poulin, M., Michel, C. and LeBlanc, B., 2007. A novel chemical fossil of palaeo sea ice: IP25. Organic Geochemistry, 38(1), pp.16-27.

Belt, S.T., Massé, G., Vare, L.L., Rowland, S.J., Poulin, M., Sicre, M.A., Sampei, M. and Fortier, L., 2008. Distinctive 13C isotopic signature distinguishes a novel sea ice biomarker in Arctic sediments and sediment traps. Marine Chemistry, 112(3-4), pp.158-167.

Belt, S.T. and Müller, J., 2013. The Arctic sea ice biomarker IP25: a review of current understanding, recommendations for future research and applications in palaeo sea ice reconstructions. Quaternary Science Reviews, 79, pp.9-25.

Berge, J., Renaud, P.E., Darnis, G., Cottier, F., Last, K., Gabrielsen, T.M., Johnsen, G., Seuthe, L., Weslawski, J.M., Leu, E. and Moline, M., 2015. In the dark: a review of ecosystem processes during the Arctic polar night. Progress in Oceanography, 139, pp.258-271.

Boecklen, W.J., Yarnes, C.T., Cook, B.A. and James, A.C., 2011. On the use of stable isotopes in trophic ecology. Annual Review of Ecology, Evolution, and Systematics, 42, pp.411-440.

Braun, S., Mhatre, S.S., Jaussi, M., Røy, H., Kjeldsen, K.U., Pearce, C., Seidenkrantz, M.S., Jørgensen, B.B. and Lomstein, B.A., 2017. Microbial turnover times in the deep seabed studied by amino acid racemization modelling. Scientific Reports, 7(1), p.5680.

Broughton, R.C.I., Newsham, K.K., Hill, P.W., Stott, A. and Jones, D.L., 2015. Differential acquisition of amino acid and peptide enantiomers within the soil microbial community and its implications for carbon and nitrogen cycling in soil. Soil Biology and Biochemistry, 88, pp.83-89.

Brown, T.A., Belt, S.T., Tatarek, A. and Mundy, C.J., 2014. Source identification of the Arctic sea ice proxy IP25. Nature Communications, 5(1), p.4197.

Brown, Z.W., Casciotti, K.L., Pickart, R.S., Swift, J.H. and Arrigo, K.R., 2015. Aspects of the marine nitrogen cycle of the Chukchi Sea shelf and Canada Basin. Deep Sea Research Part II: Topical Studies in Oceanography, 118, pp.73-87.

Budge, S.M., Wooller, M.J., Springer, A.M., Iverson, S.J., McRoy, C.P. and Divoky, G.J., 2008. Tracing carbon flow in an arctic marine food web using fatty acid-stable isotope analysis. Oecologia, 157, pp.117-129.

Burdige, D.J., 2007. Preservation of organic matter in marine sediments: controls, mechanisms, and an imbalance in sediment organic carbon budgets?. Chemical reviews, 107(2), pp.467-485.

Buesseler, K.O., 1998. The decoupling of production and particulate export in the surface ocean. Global Biogeochemical Cycles, 12(2), pp.297-310.

Buesseler, K.O. and Boyd, P.W., 2009. Shedding light on processes that control particle export and flux attenuation in the twilight zone of the open ocean. Limnology and Oceanography, 54(4), pp.1210-1232.

Buesseler, K.O., Boyd, P.W., Black, E.E. and Siegel, D.A., 2020. Metrics that matter for assessing the ocean biological carbon pump. Proceedings of the National Academy of Sciences, 117(18), pp.9679-9687.

Calvert, S.E., 2004. Beware intercepts: interpreting compositional ratios in multi-component sediments and sedimentary rocks. Organic Geochemistry, 35(8), pp.981-987.

Campbell, K., Mundy, C.J., Barber, D.G. and Gosselin, M., 2015. Characterizing the sea ice algae chlorophyll a–snow depth relationship over Arctic spring melt using transmitted irradiance. Journal of Marine Systems, 147, pp.76-84.

Canfield, D.E., 1993. Organic matter oxidation in marine sediments. In Interactions of C, N, P and S biogeochemical cycles and global change (pp. 333-363). Berlin, Heidelberg: Springer Berlin Heidelberg.

Carey Jr, A.G., 1987. Particle flux beneath fast ice in the shallow southwestern Beaufort Sea, Arctic Ocean. Marine Ecology Progress Series, pp.247-257.

Carmack, E.C., Yamamoto‐Kawai, M., Haine, T.W., Bacon, S., Bluhm, B.A., Lique, C., Melling, H., Polyakov, I.V., Straneo, F., Timmermans, M.L. and Williams, W.J., 2016. Freshwater and its role in the Arctic Marine System: Sources, disposition, storage, export, and physical and biogeochemical consequences in the Arctic and global oceans. Journal of Geophysical Research: Biogeosciences, 121(3), pp.675-717.

Caron, M., St-Onge, G., Montero-Serrano, J.C., Rochon, A., Georgiadis, E., Giraudeau, J. and Massé, G., 2019a. Holocene chronostratigraphy of northeastern Baffin Bay based on radiocarbon and palaeomagnetic data. Boreas, 48(1), pp.147-165.

Caron, M., Rochon, A., Montero-Serrano, J.C. and St-Onge, G., 2019b. Evolution of sea-surface conditions on the northwestern Greenland margin during the Holocene. Journal of Quaternary Science, 34(7), pp.569-580.

Carstens, D., Lehmann, M.F., Hofstetter, T.B. and Schubert, C.J., 2013. Amino acid nitrogen isotopic composition patterns in lacustrine sedimenting matter. Geochimica et Cosmochimica Acta, 121, pp.328-338.

Catão, A.J.L. and López-Castillo, A., 2018. On the degradation pathway of glyphosate and glycine. Environmental Science: Processes & Impacts, 20(8), pp.1148-1157.

Chen, S.M., Mudie, P. and Sherwood, O.A., 2022. Amino acid δ13C and δ15N fingerprinting of sea ice and pelagic algae in Canadian Arctic and Subarctic Seas. Frontiers in Marine Science, 9, p.976908.

Chikaraishi, Y., Ogawa, N.O., Kashiyama, Y., Takano, Y., Suga, H., Tomitani, A., Miyashita, H., Kitazato, H. and Ohkouchi, N., 2009. Determination of aquatic food-web structure based on compound-specific nitrogen isotopic composition of amino acids. Limnology and Oceanography: methods, 7(11), pp.740-750.

Choi, H., Choi, B., Chikaraishi, Y., Takano, Y., Kim, H., Lee, K., Lim, D. and Shin, K.H., 2022. Microbial alteration in marine sediments: Insights from compound-specific isotopic compositions of amino acids in subseafloor environments. Frontiers in Marine Science, 9, p.1030669.

Close, H.G., 2019. Compound-specific isotope geochemistry in the ocean. Annual Review of Marine Science, 11, pp.27-56.

Coachman, L.K. and Aagaard, K., 1974. Physical oceanography of Arctic and subarctic seas. In Marine Geology and Oceanography of the Arctic seas (pp. 1-72). Berlin, Heidelberg: Springer Berlin Heidelberg.

Cohen, J. and Barlow, M., 2005. The NAO, the AO, and global warming: how closely related?. Journal of Climate, 18(21), pp.4498-4513.

Colombo, J.C., Silverberg, N. and Gearing, J.N., 1998. Amino acid biogeochemistry in the Laurentian Trough: vertical fluxes and individual reactivity during early diagenesis. Organic Geochemistry, 29(4), pp.933-945.

Cowie, G.L. and Hedges, J.I., 1992. Sources and reactivities of amino acids in a coastal marine environment. Limnology and Oceanography, 37(4), pp.703-724.

Cowie, G.L. and Hedges, J.I., 1994. Biochemical indicators of diagenetic alteration in natural organic matter mixtures. Nature, 369(6478), pp.304-307.

Cowie, G.L., Hedges, J.I., Prahl, F.G. and De Lange, G.J., 1995. Elemental and major biochemical changes across an oxidation front in a relict turbidite: an oxygen effect. Geochimica et Cosmochimica Acta, 59(1), pp.33-46.

Dagg, M.J., Urban-Rich, J. and Peterson, J.O., 2003. The potential contribution of fecal pellets from large copepods to the flux of biogenic silica and particulate organic carbon in the Antarctic Polar Front region near 170 W. Deep Sea Research Part II: Topical Studies in Oceanography, 50(3-4), pp.675-691.

Dall'Olmo, G., Dingle, J., Polimene, L., Brewin, R.J. and Claustre, H., 2016. Substantial energy input to the mesopelagic ecosystem from the seasonal mixed-layer pump. Nature Geoscience, 9(11), pp.820-823.

Darnis, G., Geoffroy, M., Dezutter, T., Aubry, C., Massicotte, P., Brown, T., Babin, M., Cote, D. and Fortier, L., 2022. Zooplankton assemblages along the North American Arctic: Ecological connectivity shaped by ocean circulation and bathymetry from the Chukchi Sea to Labrador Sea. Elem Sci Anth, 10(1), p.00053.

Dauwe, B. and Middelburg, J.J., 1998. Amino acids and hexosamines as indicators of organic matter degradation state in North Sea sediments. Limnology and oceanography, 43(5), pp.782-798.

Dauwe, B., Middelburg, J.J., Herman, P.M. and Heip, C.H., 1999. Linking diagenetic alteration of amino acids and bulk organic matter reactivity. Limnology and Oceanography, 44(7), pp.1809-1814.

Décima, M., Landry, M.R., Bradley, C.J. and Fogel, M.L., 2017. Alanine δ15N trophic fractionation in heterotrophic protists. Limnology and Oceanography, 62(5), pp.2308-2322.

Décima, M. and Landry, M.R., 2020. Resilience of plankton trophic structure to an eddy-stimulated diatom bloom in the North Pacific Subtropical Gyre. Marine Ecology Progress Series, 643, pp.33-48.

Décima, M., Stukel, M.R., Nodder, S.D., Gutiérrez-Rodríguez, A., Selph, K.E., Dos Santos, A.L., Safi, K., Kelly, T.B., Deans, F., Morales, S.E. and Baltar, F., 2023. Salp blooms drive strong increases in passive carbon export in the Southern Ocean. Nature communications, 14(1), p.425.

De La Rocha, C. and Passow, U., 2007. Factors influencing the sinking of POC and the efficiency of the biological carbon pump. Deep Sea Research Part II: Topical Studies in Oceanography, 54(5-7), pp.639-658.

De La Vega, C., Jeffreys, R.M., Tuerena, R., Ganeshram, R. and Mahaffey, C., 2019. Temporal and spatial trends in marine carbon isotopes in the Arctic Ocean and implications for food web studies. Global change biology, 25(12), pp.4116-4130.

DeNiro, M.J. and Epstein, S., 1977. Mechanism of carbon isotope fractionation associated with lipid synthesis. Science, 197(4300), pp.261-263.

De Troch, M., Boeckx, P., Cnudde, C., Van Gansbeke, D., Vanreusel, A., Vincx, M. and Caramujo, M.J., 2012. Bioconversion of fatty acids at the basis of marine food webs: insights from a compound-specific stable isotope analysis. Marine Ecology Progress Series, 465, pp.53-67.

Dezutter, T., Lalande, C., Darnis, G. and Fortier, L., 2021. Seasonal and interannual variability of the Queen Maud Gulf ecosystem derived from sediment trap measurements. Limnology and Oceanography, 66, pp.S411-S426.

Dhifallah, F., Schiffrine, N., Rochon, A., Gosselin, M., 2022. Temporal changes of dinoflagellate communities in inner Frobisher Bay, Nunavut, Canada. International Conference on Modern and Fossil Dinoflagellates (DINO12), July 2-8, 2022, Las Palmas de, Grand Canarias, Spain, Extended Abstract 5.04, https://dino12conference.com/, available on request.

Dinn, C., Zhang, X., Edinger, E. and Leys, S.P., 2020. Sponge communities in the eastern Canadian Arctic: species richness, diversity and density determined using targeted benthic sampling and underwater video analysis. Polar Biology, 43(9), pp.1287-1305.

Doherty, S., 2021. Stable Isotope Signatures of Zooplankton Fecal Pellets in Particulate Organic Matter (Doctoral dissertation, University of Miami).

Doherty, S.C., Maas, A.E., Steinberg, D.K., Popp, B.N. and Close, H.G., 2021. Distinguishing zooplankton fecal pellets as a component of the biological pump using compound‐specific isotope analysis of amino acids. Limnology and oceanography, 66(7), pp.2827-2841.

Drinkwater, K.F. and Harding, G.C., 2001. Effects of the Hudson Strait outflow on the biology of the Labrador Shelf. Canadian Journal of Fisheries and Aquatic Sciences, 58(1), pp.171-184.

Durbin, E.G. and Casas, M.C., 2014. Early reproduction by Calanus glacialis in the Northern Bering Sea: the role of ice algae as revealed by molecular analysis. Journal of Plankton Research, 36(2), pp.523-541.

Durkin, C.A., Van Mooy, B.A., Dyhrman, S.T. and Buesseler, K.O., 2016. Sinking phytoplankton associated with carbon flux in the Atlantic Ocean. Limnology and Oceanography, 61(4), pp.1172-1187.

Ekwurzel, B., Schlosser, P., Mortlock, R.A., Fairbanks, R.G. and Swift, J.H., 2001. River runoff, sea ice meltwater, and Pacific water distribution and mean residence times in the Arctic Ocean. Journal of Geophysical Research: Oceans, 106(C5), pp.9075-9092.

Elias, S.A., Short, S.K. and Phillips, R.L., 1992. Paleoecology of late-glacial peats from the Bering Land Bridge, Chukchi Sea shelf region, northwestern Alaska. Quaternary Research, 38(3), pp.371-378.

Elias, S.A., Short, S.K., Nelson, C.H. and Birks, H.H., 1996. Life and times of the Bering land bridge. Nature, 382(6586), pp.60-63.

Elliott Smith, E.A., Fox, M.D., Fogel, M.L. and Newsome, S.D., 2022. Amino acid δ13C fingerprints of nearshore marine autotrophs are consistent across broad spatiotemporal scales: An intercontinental isotopic dataset and likely biochemical drivers. Functional Ecology, 36(5), pp.1191-1203.

Espinasse, B., Sturbois, A., Basedow, S.L., Hélaouët, P., Johns, D.G., Newton, J. and Trueman, C.N., 2022. Temporal dynamics in zooplankton δ13C and δ15N isoscapes for the North Atlantic Ocean: Decadal cycles, seasonality, and implications for predator ecology. Frontiers in Ecology and Evolution, 10, p.986082.

Ewart, K.V., Lin, Q. and Hew, C.L., 1999. Structure, function and evolution of antifreeze proteins. Cellular and Molecular Life Sciences CMLS, 55, pp.271-283.

Fábián, V., Morvai, M., Pintér-Szakács, M. and Molnár-Perl, I., 1991. Standardization of cation-exchange clean-up prior to gas chromatography of amino acids. Journal of Chromatography A, 553, pp.87-92.

Fadeev, E., Rogge, A., Ramondenc, S., Nöthig, E.M., Wekerle, C., Bienhold, C., Salter, I., Waite, A.M., Hehemann, L., Boetius, A. and Iversen, M.H., 2021. Sea ice presence is linked to higher carbon export and vertical microbial connectivity in the Eurasian Arctic Ocean. Communications biology, 4(1), p.1255.

Farmer, J.R., Sigman, D.M., Granger, J., Underwood, O.M., Fripiat, F., Cronin, T.M., Martínez-García, A. and Haug, G.H., 2021. Arctic Ocean stratification set by sea level and freshwater inputs since the last ice age. *Nature Geoscience*, *14*(9), pp.684-689.

Fernández-Méndez, M., Wenzhöfer, F., Peeken, I., Sørensen, H.L., Glud, R.N. and Boetius, A., 2014. Composition, buoyancy regulation and fate of ice algal aggregates in the Central Arctic Ocean. PLoS One, 9(9), p.e107452.

Fetterer, F., K. Knowles, W. N. Meier, M. Savoie, and A. K. Windnagel. Sea Ice Index, Version 3. 2017, Distributed by National Snow and Ice Data Center. https://doi.org/10.7265/N5K072F8. Date Accessed 10-31-2023.

Finkel, Z.V., Beardall, J., Flynn, K.J., Quigg, A., Rees, T.A.V. and Raven, J.A., 2010. Phytoplankton in a changing world: cell size and elemental stoichiometry. Journal of Plankton Research, 32(1), pp.119-137.

Fogel, M.L. and Tuross, N., 1999. Transformation of plant biochemicals to geological macromolecules during early diagenesis. Oecologia, 120, pp.336-346.

Forbes, J.R., Macdonald, R.W., Carmack, E.C., Iseki, K. and O'Brien, M.C., 1992. Zooplankton retained in sequential sediment traps along the Beaufort Sea shelf break during winter. Canadian Journal of Fisheries and Aquatic Sciences, 49(4), pp.663-670.

Fortier, M., Fortier, L., Michel, C. and Legendre, L., 2002. Climatic and biological forcing of the vertical flux of biogenic particles under seasonal Arctic sea ice. Marine Ecology Progress Series, 225, pp.1-16.

Fox, A. and Walker, B.D., 2022. Sources and Cycling of Particulate Organic Matter in Baffin Bay: A Multi-Isotope δ13C, δ15N, and Δ14C Approach. Frontiers in Marine Science, 9, p.846025.

Fragoso, G.M., Poulton, A.J., Yashayaev, I.M., Head, E.J. and Purdie, D.A., 2017. Spring phytoplankton communities of the Labrador Sea (2005–2014): pigment signatures, photophysiology and elemental ratios. Biogeosciences, 14(5), pp.1235-1259.

Fragoso, G.M., Poulton, A.J., Yashayaev, I.M., Head, E.J., Johnsen, G. and Purdie, D.A., 2018. Diatom biogeography from the Labrador Sea revealed through a trait-based approach. Frontiers in Marine Science, 5, p.297.

Frajka-Williams, E., Rhines, P.B. and Eriksen, C.C., 2009. Physical controls and mesoscale variability in the Labrador Sea spring phytoplankton bloom observed by Seaglider. Deep Sea Research Part I: Oceanographic Research Papers, 56(12), pp.2144-2161.

Frajka-Williams, E. and Rhines, P.B., 2010. Physical controls and interannual variability of the Labrador Sea spring phytoplankton bloom in distinct regions. Deep Sea Research Part I: Oceanographic Research Papers, 57(4), pp.541-552.

Fratantoni, P.S. and Pickart, R.S., 2007. The western North Atlantic shelfbreak current system in summer. Journal of Physical Oceanography, 37(10), pp.2509-2533.

Freudenthal, T., Wagner, T., Wenzhöfer, F., Zabel, M. and Wefer, G., 2001. Early diagenesis of organic matter from sediments of the eastern subtropical Atlantic: evidence from stable nitrogen and carbon isotopes. Geochimica et Cosmochimica Acta, 65(11), pp.1795-1808.

Fripiat, F., Declercq, M., Sapart, C.J., Anderson, L.G., Brüchert, V., Deman, F., Fonseca‐Batista, D., Humborg, C., Roukaerts, A., Semiletov, I.P. and Dehairs, F., 2018. Influence of the bordering shelves on nutrient distribution in the Arctic halocline inferred from water column nitrate isotopes. Limnology and Oceanography, 63(5), pp.2154-2170.

Fry, B., 1988. Food web structure on Georges Bank from stable C, N, and S isotopic compositions. Limnology and Oceanography, 33(5), pp.1182-1190.

Galbraith, E.D. and Kienast, M., 2013. The acceleration of oceanic denitrification during deglacial warming. Nature Geoscience, 6(7), pp.579-584.

Galy, V., Bouchez, J. and France-Lanord, C., 2007. Determination of total organic carbon content and δ13C in carbonate-rich detrital sediments. Geostandards and Geoanalytical research, 31(3), pp.199-207.

Gaye, B., Lahajnar, N., Harms, N., Paul, S.A.L., Rixen, T. and Emeis, K.C., 2022. What can we learn from amino acids about oceanic organic matter cycling and degradation?. Biogeosciences, 19(3), pp.807-830.

Geilfus, N.X., Galley, R.J., Else, B.G., Campbell, K., Papakyriakou, T., Crabeck, O., Lemes, M., Delille, B. and Rysgaard, S., 2016. Estimates of ikaite export from sea ice to the underlying seawater in a sea ice–seawater mesocosm. The Cryosphere, 10(5), pp.2173-2189.

Gélinas, Y., Baldock, J.A. and Hedges, J.I., 2001. Organic carbon composition of marine sediments: Effect of oxygen exposure on oil generation potential. Science, 294(5540), pp.145-148.

Genin, F., Lalande, C., Galbraith, P.S., Larouche, P., Ferreyra, G.A. and Gosselin, M., 2021. Annual cycle of biogenic carbon export in the Gulf of St. Lawrence. Continental Shelf Research, 221, p.104418.

Georgiadis, E., Giraudeau, J., Martinez, P., Lajeunesse, P., St-Onge, G., Schmidt, S. and Massé, G., 2018. Deglacial to postglacial history of Nares Strait, Northwest Greenland: a marine perspective from Kane Basin. Climate of the Past, 14(12), pp.1991-2010.

Gérikas Ribeiro, C., dos Santos, A.L., Gourvil, P., Le Gall, F., Marie, D., Tragin, M., Probert, I. and Vaulot, D., 2020. Culturable diversity of Arctic phytoplankton during pack ice melting. Elementa: Science of the Anthropocene, 8, p.6.

Giraudeau, J., Georgiadis, E., Caron, M., Martinez, P., St-Onge, G., Billy, I., Lebleu, P., Ther, O. and Massé, G., 2020. A high-resolution elemental record of post-glacial lithic sedimentation in Upernavik Trough, western Greenland: History of ice-sheet dynamics and ocean circulation changes over the last 9100 years. Global and Planetary Change, 191, p.103217.

Gleiber, M.R., Steinberg, D.K. and Ducklow, H.W., 2012. Time series of vertical flux of zooplankton fecal pellets on the continental shelf of the western Antarctic Peninsula. Marine Ecology Progress Series, 471, pp.23-36.

Glud, R.N., 2008. Oxygen dynamics of marine sediments. Marine Biology Research, 4(4), pp.243-289.

Glynn, D.S., McMahon, K.W., Sherwood, O.A., Guilderson, T.P. and McCarthy, M.D., 2022. Investigating preservation of stable isotope ratios in subfossil deep-sea proteinaceous coral skeletons as paleo-recorders of biogeochemical information over multimillennial timescales. Geochimica et Cosmochimica Acta, 338, pp.264-277.

Goericke, R. and Fry, B., 1994. Variations of marine plankton δ13C with latitude, temperature, and dissolved CO2 in the world ocean. Global Biogeochemical Cycles, 8(1), pp.85-90.

Golombek, N.Y., Kienast, M., Pilskaln, C.H., Algar, C. and Sherwood, O., 2024. Origin and alteration of sinking and resuspended organic matter on a benthic nepheloid layer influenced continental shelf. Geochimica et Cosmochimica Acta, 366, pp.31-47.

Gosselin, M., Levasseur, M., Wheeler, P.A., Horner, R.A. and Booth, B.C., 1997. New measurements of phytoplankton and ice algal production in the Arctic Ocean. Deep Sea Research Part II: Topical Studies in Oceanography, 44(8), pp.1623-1644.

Gradinger, R.R. and Bluhm, B.A., 2004. In-situ observations on the distribution and behavior of amphipods and Arctic cod (*Boreogadus saida*) under the sea ice of the High Arctic Canada Basin. Polar Biology, 27, pp.595-603.

Grainger, E.H. and Hsiao, S.I., 1990. Trophic relationships of the sea ice meiofauna in Frobisher Bay, Arctic Canada. Polar Biology, 10(4), pp.283-292.

Granger, J., Prokopenko, M.G., Sigman, D.M., Mordy, C.W., Morse, Z.M., Morales, L.V., Sambrotto, R.N. and Plessen, B., 2011. Coupled nitrification‐denitrification in sediment of the eastern Bering Sea shelf leads to 15N enrichment of fixed N in shelf waters. Journal of Geophysical Research: Oceans, 116(C11).

Granger, J., Sigman, D.M., Gagnon, J., Tremblay, J.E. and Mucci, A., 2018. On the properties of the Arctic halocline and deep water masses of the Canada Basin from nitrate isotope ratios. Journal of Geophysical Research: Oceans, 123(8), pp.5443-5458.

Grebmeier, J.M., 2012. Shifting patterns of life in the Pacific Arctic and sub-Arctic seas. Annual review of marine science, 4, pp.63-78.

Gruber, N.I.C.O.L.A.S. and Sarmiento, J.L., 2002. Large-scale biogeochemical-physical interactions in elemental cycles. The Sea, 12, pp.337-399.

Gutiérrez-Rodríguez, A., Décima, M., Popp, B.N. and Landry, M.R., 2014. Isotopic invisibility of protozoan trophic steps in marine food webs. Limnology and oceanography, 59(5), pp.1590-1598.

Hall, F.R., Andrews, J.T., Jennings, A., Vilks, G. and Moran, K., 1999. Late Quaternary sediments and chronology of the northeast Labrador Shelf (Karlsefni Trough, Saglek Bank): links to glacial history. Geological Society of America Bulletin, 111(11), pp.1700-1713.

Han, G., Ma, Z., Long, Z., Perrie, W. and Chassé, J., 2019. Climate change on Newfoundland and Labrador shelves: Results from a regional downscaled ocean and sea-ice model under an A1B forcing scenario 2011–2069. Atmosphere-Ocean, 57(1), pp.3-17.

Hanna, E., Nolan, J.E., Overland, J.E. and Hall, R.J., 2021. Climate change in the Arctic. Arctic Ecology, pp.57-79.

Hannides, C.C., Popp, B.N., Landry, M.R. and Graham, B.S., 2009. Quantification of zooplankton trophic position in the North Pacific Subtropical Gyre using stable nitrogen isotopes. Limnology and Oceanography, 54(1), pp.50-61.

Hannides, C.C., Popp, B.N., Choy, C.A. and Drazen, J.C., 2013. Midwater zooplankton and suspended particle dynamics in the North Pacific Subtropical Gyre: A stable isotope perspective. Limnology and Oceanography, 58(6), pp.1931-1946.

Hansen, K.E., Giraudeau, J., Wacker, L., Pearce, C. and Seidenkrantz, M.S., 2020. Reconstruction of Holocene oceanographic conditions in eastern Baffin Bay. Climate of the Past, 16(3), pp.1075-1095.

Harding, G.C., 1998. 6.4 Submarine Canyons: Deposition Centres for Detrital Organic Matter?. Deep-Sea Res, 2(41), pp.231-252.

Hargrave, B.T., Von Bodungen, B., Conover, R.J., Fraser, A.J., Phillips, G. and Vass, W.P., 1989. Seasonal changes in sedimentation of particulate matter and lipid content of zooplankton collected by sediment trap in the Arctic Ocean off Axel Heiberg Island. Polar biology, 9, pp.467-475.

Hargrave, B.T., Von Bodungen, B., Stoffyn-Egli, P. and Mudie, P.J., 1994. Seasonal variability in particle sedimentation under permanent ice cover in the Arctic Ocean. Continental Shelf Research, 14(2-3), pp.279-293.

Hargrave, B.T., Walsh, I.D. and Murray, D.W., 2002. Seasonal and spatial patterns in mass and organic matter sedimentation in the North Water. Deep Sea Research Part II: Topical Studies in Oceanography, 49(22-23), pp.5227-5244.

Harrison, W.G. and Li, W.K., 2007. Phytoplankton growth and regulation in the Labrador Sea: light and nutrient limitation. Journal of Northwest Atlantic Fishery Science, 39.

Harrison, W.G., Børsheim, K.Y., Li, W.K., Maillet, G.L., Pepin, P., Sakshaug, E., Skogen, M.D. and Yeats, P.A., 2013. Phytoplankton production and growth regulation in the Subarctic North Atlantic: A comparative study of the Labrador Sea-Labrador/Newfoundland shelves and Barents/Norwegian/Greenland seas and shelves. Progress in Oceanography, 114, pp.26-45.

Harvey, H.R. and Macko, S.A., 1997. Catalysts or contributors? Tracking bacterial mediation of early diagenesis in the marine water column. Organic Geochemistry, 26(9-10), pp.531-544.

Hayes, J.M., 1993. Factors controlling 13C contents of sedimentary organic compounds: Principles and evidence. Marine Geology, 113(1-2), pp.111-125.

Hayes, J.M., 2018. 3. Fractionation of carbon and hydrogen isotopes in biosynthetic processes. In Stable isotope geochemistry (pp. 225-278). Published by De Gruyter, 2018.

Heaton, T.J., Köhler, P., Butzin, M., Bard, E., Reimer, R.W., Austin, W.E., Ramsey, C.B., Grootes, P.M., Hughen, K.A., Kromer, B. and Reimer, P.J., 2020. Marine20—the marine radiocarbon age calibration curve (0–55,000 cal BP). Radiocarbon, 62(4), pp.779-820.

Hecker, B., Blechschmidt, G. and Gibson, P., 1980. Canyon assessment study in the Mid and North Atlantic areas of the US Outer Continental Shelf: epifaunal zonation and community structure in three mid and north Atlantic canyons. Final Report, US Department of the Interior, Bureau of Land Management. Washington, DC.

Hecky, R.E., Mopper, K., Kilham, P. and Degens, E.T., 1973. The amino acid and sugar composition of diatom cell-walls. Marine biology, 19(4), pp.323-331.

Hedges, J.I. and Keil, R.G., 1995. Sedimentary organic matter preservation: an assessment and speculative synthesis. Marine chemistry, 49(2-3), pp.81-115.

Hedges, J.I., Baldock, J.A., Gélinas, Y., Lee, C., Peterson, M. and Wakeham, S.G., 2001. Evidence for non-selective preservation of organic matter in sinking marine particles. Nature, 409(6822), pp.801-804.

Henrichs, S.M., 1992. Early diagenesis of organic matter in marine sediments: progress and perplexity. Marine Chemistry, 39(1-3), pp.119-149.

Hoefs, J., 2018. Stable isotope geochemistry. 8th edition: Springer International Publishing AG, part of Springer Nature.

Honjo, S. and Doherty, K.W., 1988. Large aperture time-series sediment traps; design objectives, construction and application. Deep Sea Research Part A. Oceanographic Research Papers, 35(1), pp.133-149.

Hop, H., Poltermann, M., Lønne, O.J., Falk-Petersen, S., Korsnes, R. and Budgell, W.P., 2000. Ice amphipod distribution relative to ice density and under-ice topography in the northern Barents Sea. Polar Biology, 23, pp.357-367.

Hop, H., Vihtakari, M., Bluhm, B.A., Assmy, P., Poulin, M., Gradinger, R., Peeken, I., von Quillfeldt, C., Olsen, L.M., Zhitina, L. and Melnikov, I.A., 2020. Changes in sea-ice protist diversity with declining sea ice in the Arctic Ocean from the 1980s to 2010s. Frontiers in Marine Science, 7, p.243.

Hsiao, S.I., 1979. Phytoplankton and Sea Ice: Microalgal Data from Frobisher Bay, 1971 to 1978. Department of Fisheries and Oceans.

Hsiao, S.I., 1980. Quantitative composition, distribution, community structure and standing stock of sea ice microalgae in the Canadian Arctic. Arctic, pp.768-793.

Hsiao, S.I. and Pinkewycz, N., 1985. Arctic marine phytoplankton contributed to the sediments in Frobisher Bay. Arctic Biological Station, Department of Fisheries and Oceans.

Hsiao, S.I., 1992. Dynamics of ice algae and phytoplankton in Frobisher Bay. Polar Biology, 12(6-7), pp.645-651.

Hu, X., Myers, P.G. and Lu, Y., 2019. Pacific Water pathway in the Arctic Ocean and Beaufort Gyre in two simulations with different horizontal resolutions. Journal of Geophysical Research: Oceans, 124(8), pp.6414-6432.

Hwang, J., Druffel, E.R. and Eglinton, T.I., 2010. Widespread influence of resuspended sediments on oceanic particulate organic carbon: Insights from radiocarbon and aluminum contents in sinking particles. Global Biogeochemical Cycles, 24(4).

Hwang, J., Manganini, S.J., Park, J., Montluçon, D.B., Toole, J.M. and Eglinton, T.I., 2017. Biological and physical controls on the flux and characteristics of sinking particles on the N orthwest A tlantic margin. Journal of Geophysical Research: Oceans, 122(6), pp.4539-4553.

Ianiri, H.L. and McCarthy, M.D., 2023. Compound specific δ15N analysis of amino acids reveals unique sources and differential cycling of high and low molecular weight marine dissolved organic nitrogen. Geochimica et Cosmochimica Acta, 344, pp.24-39.

Irwin, B.D., 1990. Primary production of ice algae on a seasonally-ice-covered, continental shelf. Polar biology, 10, pp.247-254.

Jackson, R., Kvorning, A.B., Limoges, A., Georgiadis, E., Olsen, S.M., Tallberg, P., Andersen, T.J., Mikkelsen, N., Giraudeau, J., Massé, G. and Wacker, L., 2021. Holocene polynya dynamics and their interaction with oceanic heat transport in northernmost Baffin Bay. Scientific Reports, 11(1), p.10095.

Janech, M.G., Krell, A., Mock, T., Kang, J.S. and Raymond, J.A., 2006. Ice-binding proteins from sea ice diatoms (bacillariophyceae) 1. Journal of Phycology, 42(2), pp.410-416.

Jennings, A.E., Andrews, J.T., Oliver, B., Walczak, M. and Mix, A., 2019. Retreat of the Smith Sound ice stream in the Early Holocene. Boreas, 48(4), pp.825-840.

Jónasdóttir, S.H., 2019. Fatty acid profiles and production in marine phytoplankton. Marine Drugs, 17(3), p.151.

Jones, E.P., Anderson, L.G. and Swift, J.H., 1998. Distribution of Atlantic and Pacific waters in the upper Arctic Ocean: Implications for circulation. Geophysical Research Letters, 25(6), pp.765-768.

Jones, E.P., 2001. Circulation in the arctic ocean. Polar Research, 20(2), pp.139-146.

Jones, E.P., Swift, J.H., Anderson, L.G., Lipizer, M., Civitarese, G., Falkner, K.K., Kattner, G. and McLaughlin, F., 2003. Tracing Pacific water in the North Atlantic ocean. Journal of Geophysical Research: Oceans, 108(C4).

Joo, H.M., Kim, K.E., Park, J.S., Kim, H.J., Yang, E.J., Lee, T.K., Cho, K.H., Jung, J., Lee, Y., Kang, S.H. and Jung, S.W., 2022. Ecological Responses of Core Phytoplankton by Latitudinal Differences in the Arctic Ocean in Late Summer Revealed by 18S rDNA Metabarcoding. Frontiers in Marine Science, 9, p.879911.

Junge, K., Imhoff, F., Staley, T. and Deming, J.W., 2002. Phylogenetic diversity of numerically important Arctic sea-ice bacteria cultured at subzero temperature. Microbial Ecology, pp.315-328.

Junium, Christopher K., Michael A. Arthur, and Katherine H. Freeman. "Compound-specific δ15N and chlorin preservation in surface sediments of the Peru Margin with implications for ancient bulk δ15N records." Geochimica et Cosmochimica Acta 160 (2015): 306-318.

Juul-Pedersen, T., Michel, C. and Gosselin, M., 2010. Sinking export of particulate organic material from the euphotic zone in the eastern Beaufort Sea. Marine Ecology Progress Series, 410, pp.55-70.

Kaiser, K. and Benner, R., 2005. Hydrolysis‐induced racemization of amino acids. Limnology and Oceanography: Methods, 3(8), pp.318-325.

Kaltin, S., Anderson, L.G., Olsson, K., Fransson, A. and Chierici, M., 2002. Uptake of atmospheric carbon dioxide in the Barents Sea. Journal of Marine Systems, 38(1-2), pp.31-45.

Kaltin, S. and Anderson, L.G., 2005. Uptake of atmospheric carbon dioxide in Arctic shelf seas: evaluation of the relative importance of processes that influence pCO2 in water transported over the Bering–Chukchi Sea shelf. Marine Chemistry, 94(1-4), pp.67-79.

Karasov, W.H. and Martínez del Rio, C., 2007. Physiological ecology: how animals process energy, nutrients, and toxins. Princeton University Press.

Keigwin, L.D., Donnelly, J.P., Cook, M.S., Driscoll, N.W. and Brigham-Grette, J., 2006. Rapid sea-level rise and Holocene climate in the Chukchi Sea. Geology, 34(10), pp.861-864.

Keil, R.G., Montluçon, D.B., Prahl, F.G. and Hedges, J.I., 1994. Sorptive preservation of labile organic matter in marine sediments. Nature, 370(6490), pp.549-552.

Keil, R.G. and Fogel, M.L., 2001. Reworking of amino acid in marine sediments: Stable carbon isotopic composition of amino acids in sediments along the Washington coast. Limnology and Oceanography, 46(1), pp.14-23.

Kienast, M., Higginson, M.J., Mollenhauer, G., Eglinton, T.I., Chen, M.T. and Calvert, S.E., 2005. On the sedimentological origin of down‐core variations of bulk sedimentary nitrogen isotope ratios. Paleoceanography, 20(2).

Kinnard, C., Zdanowicz, C.M., Fisher, D.A., Isaksson, E., de Vernal, A. and Thompson, L.G., 2011. Reconstructed changes in Arctic sea ice over the past 1,450 years. Nature, 479(7374), pp.509-512.

Kirst, G.O. and Wiencke, C., 1995. Ecophysiology of polar algae. Oceanographic Literature Review, 12(42), p.1094.

Knudsen, K.L., Stabell, B., Seidenkrantz, M.S., Eiriksson, J. and Blake Jr, W., 2008. Deglacial and Holocene conditions in northernmost Baffin Bay: sediments, foraminifera, diatoms and stable isotopes. Boreas, 37(3), pp.346-376.

Kohlbach, D., Graeve, M., A. Lange, B., David, C., Peeken, I. and Flores, H., 2016. The importance of ice algae-produced carbon in the central Arctic Ocean ecosystem: Food web relationships revealed by lipid and stable isotope analyses. Limnology and Oceanography, 61(6), pp.2027-2044.

Lalande, C., Forest, A., Barber, D.G., Gratton, Y. and Fortier, L., 2009a. Variability in the annual cycle of vertical particulate organic carbon export on Arctic shelves: Contrasting the Laptev Sea, Northern Baffin Bay and the Beaufort Sea. Continental Shelf Research, 29(17), pp.2157-2165.

Lalande, C., Bélanger, S. and Fortier, L., 2009b. Impact of a decreasing sea ice cover on the vertical export of particulate organic carbon in the northern Laptev Sea, Siberian Arctic Ocean. Geophysical Research Letters, 36(21).

Lalande, C., Bauerfeind, E. and Nöthig, E.M., 2011. Downward particulate organic carbon export at high temporal resolution in the eastern Fram Strait: influence of Atlantic Water on flux composition. Marine Ecology Progress Series, 440, pp.127-136.

Lalande, C., Nöthig, E.M. and Fortier, L., 2019. Algal export in the Arctic Ocean in times of global warming. Geophysical Research Letters, 46(11), pp.5959-5967.

Larsen, T., Taylor, D.L., Leigh, M.B. and O'Brien, D.M., 2009. Stable isotope fingerprinting: a novel method for identifying plant, fungal, or bacterial origins of amino acids. Ecology, 90(12), pp.3526-3535.

Larsen, T., Ventura, M., Andersen, N., O'Brien, D.M., Piatkowski, U. and McCarthy, M.D., 2013. Tracing carbon sources through aquatic and terrestrial food webs using amino acid stable isotope fingerprinting. PloS one, 8(9), p.e73441.

Larsen, T., Bach, L.T., Salvatteci, R., Wang, Y.V., Andersen, N., Ventura, M. and McCarthy, M.D., 2015. Assessing the potential of amino acid 13 C patterns as a carbon source tracer in marine sediments: effects of algal growth conditions and sedimentary diagenesis. Biogeosciences, 12(16), pp.4979-4992.

Leblanc, K., Arístegui, J., Armand, L., Assmy, P., Beker, B., Bode, A., Breton, E., Cornet, V., Gibson, J., Gosselin, M.P. and Kopczynska, E., 2012. A global diatom database–abundance, biovolume and biomass in the world ocean. Earth System Science Data, 4(1), pp.149-165.

Lee, C., Wakeham, S.G. and Hedges, J.I., 2000. Composition and flux of particulate amino acids and chloropigments in equatorial Pacific seawater and sediments. Deep Sea Research Part I: Oceanographic Research Papers, 47(8), pp.1535-1568.

Legendre, L., Ackley, S.F., Dieckmann, G.S., Gulliksen, B., Horner, R., Hoshiai, T., Melnikov, I.A., Reeburgh, W.S., Spindler, M. and Sullivan, C.W., 1992. Ecology of sea ice biota: 2. Global significance. Polar Biology, 12, pp.429-444.

Lehman, J., 2009. Compound-specific amino acid isotopes as tracers of algal central metabolism: developing new tools for tracing prokaryotic vs. eukaryotic primary production and organic nitrogen in the ocean. University of California, Santa Cruz, CA, Santa Cruz, CA.

Lehmann, M.F., Bernasconi, S.M., Barbieri, A. and McKenzie, J.A., 2002. Preservation of organic matter and alteration of its carbon and nitrogen isotope composition during simulated and in situ early sedimentary diagenesis. Geochimica et Cosmochimica Acta, 66(20), pp.3573-3584.

Lehmann, N., Kienast, M., Granger, J., Bourbonnais, A., Altabet, M.A. and Tremblay, J.É., 2019. Remote western Arctic nutrients fuel remineralization in deep Baffin Bay. Global Biogeochemical Cycles, 33(6), pp.649-667.

Lehmann, N., Kienast, M., Granger, J. and Tremblay, J.É., 2022. Physical and biogeochemical influences on nutrients through the Canadian Arctic Archipelago: Insights from nitrate isotope ratios. Journal of Geophysical Research: Oceans, 127(3), p.e2021JC018179.

Leu, E., Søreide, J.E., Hessen, D.O., Falk-Petersen, S. and Berge, J., 2011. Consequences of changing sea-ice cover for primary and secondary producers in the European Arctic shelf seas: timing, quantity, and quality. Progress in Oceanography, 90(1-4), pp.18-32.

Leu, E., Mundy, C.J., Assmy, P., Campbell, K., Gabrielsen, T.M., Gosselin, M., Juul-Pedersen, T. and Gradinger, R., 2015. Arctic spring awakening–Steering principles behind the phenology of vernal ice algal blooms. Progress in Oceanography, 139, pp.151-170.

Levac, E., Vernal, A.D. and Blake Jr, W., 2001. Sea-surface conditions in northernmost Baffin Bay during the Holocene: Palynological evidence. Journal of Quaternary Science: Published for the Quaternary Research Association, 16(4), pp.353-363.

Levin, L.A. and Le Bris, N., 2015. The deep ocean under climate change. Science, 350(6262), pp.766-768.

Li, W.K., McLaughlin, F.A., Lovejoy, C. and Carmack, E.C., 2009. Smallest algae thrive as the Arctic Ocean freshens. Science, 326(5952), pp.539-539.

Limoges, A., Weckström, K., Ribeiro, S., Georgiadis, E., Hansen, K.E., Martinez, P., Seidenkrantz, M.S., Giraudeau, J., Crosta, X. and Massé, G., 2020. Learning from the past: Impact of the Arctic Oscillation on sea ice and marine productivity off northwest Greenland over the last 9,000 years. Global Change Biology, 26(12), pp.6767-6786.

Limoges, A., Ribeiro, S., Van Nieuwenhove, N., Jackson, R., Juggins, S., Crosta, X. and Weckström, K., 2023. Marine diatoms record Late Holocene regime shifts in the Pikialasorsuaq ecosystem. Global Change Biology, 29(23), pp.6503-6516.

Lizotte, M.P., 2003. The microbiology of sea ice. In Sea ice: an introduction to its physics, chemistry, biology and geology, pp.184-210. Thomas, D.N. and Dieckmann, G.S. eds., 2008.

Lloyd, J., Moros, M., Perner, K., Telford, R.J., Kuijpers, A., Jansen, E. and McCarthy, D., 2011. A 100 yr record of ocean temperature control on the stability of Jakobshavn Isbrae, West Greenland. Geology, 39(9), pp.867-870.

Longhurst, A.R., 2010. Ecological geography of the sea. Elsevier.

Lønne, O.J. and Gulliksen, B., 1991. On the distribution of sympagic macro-fauna in the seasonally ice covered Barents Sea. Polar Biology, 11, pp.457-469.

Lovejoy, C., Legendre, L., Martineau, M.J., Bâcle, J. and Von Quillfeldt, C.H., 2002. Distribution of phytoplankton and other protists in the North Water. Deep Sea Research Part II: Topical Studies in Oceanography, 49(22-23), pp.5027-5047.

Lund, J.W.G., Kipling, C. and Le Cren, E.D., 1958. The inverted microscope method of estimating algal numbers and the statistical basis of estimations by counting. Hydrobiologia, 11, pp.143-170.

MacGilchrist, G.A., Garabato, A.N., Tsubouchi, T., Bacon, S., Torres-Valdés, S. and Azetsu-Scott, K., 2014. The arctic ocean carbon sink. Deep Sea Research Part I: Oceanographic Research Papers, 86, pp.39-55.

Mackin, J.E. and Aller, R.C., 1984. Ammonium adsorption in marine sediments 1. Limnology and Oceanography, 29(2), pp.250-257.

Macko, S.A. and Estep, M.L., 1984. Microbial alteration of stable nitrogen and carbon isotopic compositions of organic matter. Organic Geochemistry, 6, pp.787-790.

Macko, S.A., Estep, M.L.F., Engel, M.H. and Hare, P.E., 1986. Kinetic fractionation of stable nitrogen isotopes during amino acid transamination. Geochimica et Cosmochimica Acta, 50(10), pp.2143-2146.

Macko, S.A., Fogel, M.L., Hare, P.E. and Hoering, T.C., 1987. Isotopic fractionation of nitrogen and carbon in the synthesis of amino acids by microorganisms. Chemical Geology: Isotope Geoscience section, 65(1), pp.79-92.

Macko, S.A., Helleur, R., Hartley, G. and Jackman, P., 1990. Diagenesis of organic matter—a study using stable isotopes of individual carbohydrates. Organic Geochemistry, 16(4-6), pp.1129-1137.

Marson, J.M., Myers, P.G., Hu, X. and Le Sommer, J., 2018. Using vertically integrated ocean fields to characterize Greenland icebergs' distribution and lifetime. Geophysical Research Letters, 45(9), pp.4208-4217.

Martin, J.H., Knauer, G.A., Karl, D.M. and Broenkow, W.W., 1987. VERTEX: carbon cycling in the northeast Pacific. Deep Sea Research Part A. Oceanographic Research Papers, 34(2), pp.267-285.

Mayer, L.M., 1994a. Surface area control of organic carbon accumulation in continental shelf sediments. Geochimica et Cosmochimica Acta, 58(4), pp.1271-1284.

Mayer, L.M., 1994b. Relationships between mineral surfaces and organic carbon concentrations in soils and sediments. Chemical Geology, 114(3-4), pp.347-363.

McCarthy, M.D., Benner, R., Lee, C. and Fogel, M.L., 2007. Amino acid nitrogen isotopic fractionation patterns as indicators of heterotrophy in plankton, particulate, and dissolved organic matter. Geochimica et Cosmochimica Acta, 71(19), pp.4727-4744.

McCarthy, M.D., Lehman, J. and Kudela, R., 2013. Compound-specific amino acid δ15N patterns in marine algae: Tracer potential for cyanobacterial vs. eukaryotic organic nitrogen sources in the ocean. Geochimica et cosmochimica Acta, 103, pp.104-120.

McClelland, J.W. and Montoya, J.P., 2002. Trophic relationships and the nitrogen isotopic composition of amino acids in plankton. Ecology, 83(8), pp.2173-2180.

McMahon, K.W., Ambrose Jr, W.G., Johnson, B.J., Sun, M.Y., Lopez, G.R., Clough, L.M. and Carroll, M.L., 2006. Benthic community response to ice algae and phytoplankton in Ny Ålesund, Svalbard. Marine Ecology Progress Series, 310, pp.1-14.

McMahon, K.W., Fogel, M.L., Elsdon, T.S. and Thorrold, S.R., 2010. Carbon isotope fractionation of amino acids in fish muscle reflects biosynthesis and isotopic routing from dietary protein. Journal of animal ecology, 79(5), pp.1132-1141.

McMahon, K.W., Hamady, L.L. and Thorrold, S.R., 2013. Ocean ecogeochemistry: A review. In: Oceanography and marine biology: An annual review.McMahon, K.W., McCarthy, M.D., Sherwood, O.A., Larsen, T. and Guilderson, T.P., 2015. Millennial-scale plankton regime shifts in the subtropical North Pacific Ocean. Science, 350(6267), pp.1530-1533.

McMahon, K.W. and McCarthy, M.D., 2016. Embracing variability in amino acid δ15N fractionation: mechanisms, implications, and applications for trophic ecology. Ecosphere, 7(12), p.e01511.

McManus, G.B. and Katz, L.A., 2009. Molecular and morphological methods for identifying plankton: what makes a successful marriage?. Journal of Plankton Research, 31(10), pp.1119-1129.

McQuatters-Gollop, A., Johns, D.G., Bresnan, E., Skinner, J., Rombouts, I., Stern, R., Aubert, A., Johansen, M., Bedford, J. and Knights, A., 2017. From microscope to management: the critical value of plankton taxonomy to marine policy and biodiversity conservation. Marine Policy, 83, pp.1-10.

Meier-Augenstein, W., 1999. Applied gas chromatography coupled to isotope ratio mass spectrometry. Journal of Chromatography A, 842(1-2), pp.351-371.

Melling, H., Gratton, Y. and Ingram, G., 2001. Ocean circulation within the North Water polynya of Baffin Bay. Atmosphere-Ocean, 39(3), pp.301-325.

Melnikov, I.A., 1998. Winter production of sea ice algae in the western Weddell Sea. Journal of Marine Systems, 17(1-4), pp.195-205.

Meredith, M., Sommerkorn, M., Cassotta, S., Derksen, C., Ekaykin, A., Hollowed, A., Kofinas, G., Mackintosh, A., Melbourne-Thomas, J., Muelbert, M.M.C. and Ottersen, G., 2019. Polar regions. Chapter 3, IPCC Special Report on the Ocean and Cryosphere in a Changing Climate.

Michel, C., Legendre, L., Therriault, J.C., Demers, S. and Vandevelde, T., 1993. Springtime coupling between ice algal and phytoplankton assemblages in southeastern Hudson Bay, Canadian Arctic. Polar Biology, 13, pp.441-449.

Michel, C., Legendre, L., Ingram, R.G., Gosselin, M. and Levasseur, M., 1996. Carbon budget of sea‐ice algae in spring: Evidence of a significant transfer to zooplankton grazers. Journal of Geophysical Research: Oceans, 101(C8), pp.18345-18360.

Michel, C., Nielsen, T.G., Nozais, C. and Gosselin, M., 2002. Significance of sedimentation and grazing by ice micro-and meiofauna for carbon cycling in annual sea ice (northern Baffin Bay). Aquatic Microbial Ecology, 30(1), pp.57-68.

Middelburg, J.J., 2019. Marine carbon biogeochemistry: a primer for earth system scientists (p. 118). Springer Nature.

Montes, E., Thunell, R., Muller-Karger, F.E., Lorenzoni, L., Tappa, E., Troccoli, L., Astor, Y. and Varela, R., 2013. Sources of δ15N variability in sinking particulate nitrogen in the Cariaco Basin, Venezuela. Deep Sea Research Part II: Topical Studies in Oceanography, 93, pp.96-107.

Moore, O.W., Curti, L., Woulds, C., Bradley, J.A., Babakhani, P., Mills, B.J.W., Homoky, W.B., Xiao, K.-Q., Bray, A.W., Fisher, B.J., Kazemian, M., Kaulich, B., Dale, A.W. and Peacock, C.L., 2023. Long-term organic carbon preservation enhanced by iron and manganese. *Nature*, 621(7978), pp.312–317.

Mudie, P.J., Rochon, A. and Levac, E., 2005. Decadal-scale sea ice changes in the Canadian Arctic and their impacts on humans during the past 4,000 years. Environmental Archaeology, 10(2), pp.113-126.

Müller, P.J., 1977. CN ratios in Pacific deep-sea sediments: Effect of inorganic ammonium and organic nitrogen compounds sorbed by clays. Geochimica et Cosmochimica Acta, 41(6), pp.765-776.

Münchow, A., Falkner, K.K. and Melling, H., 2015. Baffin island and west Greenland current systems in northern Baffin bay. Progress in Oceanography, 132, pp.305-317.

Mundy, C.J., Barber, D.G. and Michel, C., 2005. Variability of snow and ice thermal, physical and optical properties pertinent to sea ice algae biomass during spring. Journal of Marine Systems, 58(3-4), pp.107-120.

Mundy, C.J., Gosselin, M., Ehn, J., Gratton, Y., Rossnagel, A., Barber, D.G., Martin, J., Tremblay, J.É., Palmer, M., Arrigo, K.R. and Darnis, G., 2009. Contribution of under-ice primary production to an ice-edge upwelling phytoplankton bloom in the Canadian Beaufort Sea. Geophysical Research Letters, 36(17).

Mundy, C.J., Gosselin, M., Gratton, Y., Brown, K., Galindo, V., Campbell, K., Levasseur, M., Barber, D., Papakyriakou, T. and Bélanger, S., 2014. Role of environmental factors on phytoplankton bloom initiation under landfast sea ice in Resolute Passage, Canada. Marine Ecology Progress Series, 497, pp.39-49.

Mundy, C.J. and Meiners, K.M., 2021. Ecology of Arctic Sea Ice. Arctic Ecology, pp.261-288.

Murata, A. and Takizawa, T., 2003. Summertime CO2 sinks in shelf and slope waters of the western Arctic Ocean. Continental Shelf Research, 23(8), pp.753-776.

Nakatsuka, T., Handa, N., Harada, N., Sugimoto, T. and Imaizumi, S., 1997. Origin and decomposition of sinking particulate organic matter in the deep water column inferred from the vertical distributions of its δ15N, δ13 and δ14. Deep Sea Research Part I: Oceanographic Research Papers, 44(12), pp.1957-1979.

Needoba, J.A., Waser, N.A., Harrison, P.J. and Calvert, S.E., 2003. Nitrogen isotope fractionation in 12 species of marine phytoplankton during growth on nitrate. Marine Ecology Progress Series, 255, pp.81-91.

Nielsen, J.M., Popp, B.N. and Winder, M., 2015. Meta-analysis of amino acid stable nitrogen isotope ratios for estimating trophic position in marine organisms. Oecologia, 178, pp.631-642.

Noji, T.T., 1991. The influence of macrozooplankton on vertical particulate flux. Sarsia, 76(1-2), pp.1-9.

Nowicki, M., DeVries, T. and Siegel, D.A., 2022. Quantifying the carbon export and sequestration pathways of the ocean's biological carbon pump. Global Biogeochemical Cycles, 36(3), p.e2021GB007083.

O'Brien, D.M., Fogel, M.L. and Boggs, C.L., 2002. Renewable and nonrenewable resources: amino acid turnover and allocation to reproduction in Lepidoptera. Proceedings of the National Academy of Sciences, 99(7), pp.4413-4418.

Ohkouchi, N., Chikaraishi, Y., Close, H.G., Fry, B., Larsen, T., Madigan, D.J., McCarthy, M.D., McMahon, K.W., Nagata, T., Naito, Y.I. and Ogawa, N.O., 2017. Advances in the application of amino acid nitrogen isotopic analysis in ecological and biogeochemical studies. Organic Geochemistry, 113, pp.150-174.

Omand, M.M., D'Asaro, E.A., Lee, C.M., Perry, M.J., Briggs, N., Cetinić, I. and Mahadevan, A., 2015. Eddy-driven subduction exports particulate organic carbon from the spring bloom. Science, 348(6231), pp.222-225.

Pabi, S., van Dijken, G.L. and Arrigo, K.R., 2008. Primary production in the Arctic Ocean, 1998–2006. Journal of Geophysical Research: Oceans, 113(C8).

Pantoja, S. and Lee, C., 2003. Amino acid remineralization and organic matter lability in Chilean coastal sediments. Organic Geochemistry, 34(8), pp.1047-1056.

Park, S., Brett, M.T., MÜLLER‐NAVARRA, D.C. and Goldman, C.R., 2002. Essential fatty acid content and the phosphorus to carbon ratio in cultured algae as indicators of food quality for Daphnia. Freshwater Biology, 47(8), pp.1377-1390.

Passow, U. and Carlson, C.A., 2012. The biological pump in a high CO2 world. Marine Ecology Progress Series, 470, pp.249-271.

Peterson, B.J. and Fry, B., 1987. Stable isotopes in ecosystem studies. Annual Review of Ecology and Systematics, 18(1), pp.293-320.

Pieńkowski, A.J., Coulthard, R.D. and Furze, M.F., 2023. Revised marine reservoir offset (ΔR) values for molluscs and marine mammals from Arctic North America. Boreas, 52(2), pp.145-167.

Pilskaln, C.H. and Honjo, S., 1987. The fecal pellet fraction of biogeochemical particle fluxes to the deep sea. Global Biogeochemical Cycles, 1(1), pp.31-48.

Pineault, S., Tremblay, J.É., Gosselin, M., Thomas, H. and Shadwick, E., 2013. The isotopic signature of particulate organic C and N in bottom ice: Key influencing factors and applications for tracing the fate of ice-algae in the Arctic Ocean. Journal of Geophysical Research: Oceans, 118(1), pp.287-300.

Pogorzelec, N.M., Gough, K.M., Ha, S.Y., Campbell, K., Else, B., Kim, K., Lee, S.H. and Mundy, C.J., 2022. FTIR autecological analysis of bottom-ice diatom taxa across a tidal strait in the Canadian Arctic. Elementa: Science of the Anthropocene, 10(1), p.00094.

Popp, B.N., Graham, B.S., Olson, R.J., Hannides, C.C., Lott, M.J., López-Ibarra, G.A., Galván-Magaña, F. and Fry, B., 2007. Insight into the trophic ecology of yellowfin tuna, Thunnus albacares, from compound-specific nitrogen isotope analysis of proteinaceous amino acids. Terrestrial Ecology, 1, pp.173-190.

Post, D.M., 2002. Using stable isotopes to estimate trophic position: models, methods, and assumptions. Ecology, 83(3), pp.703-718.

Post, E., Forchhammer, M.C., Bret-Harte, M.S., Callaghan, T.V., Christensen, T.R., Elberling, B., Fox, A.D., Gilg, O., Hik, D.S., Høye, T.T. and Ims, R.A., 2009. Ecological dynamics across the Arctic associated with recent climate change. Science, 325(5946), pp.1355-1358.

Post, E., Bhatt, U.S., Bitz, C.M., Brodie, J.F., Fulton, T.L., Hebblewhite, M., Kerby, J., Kutz, S.J., Stirling, I. and Walker, D.A., 2013. Ecological consequences of sea-ice decline. Science, 341(6145), pp.519-524.

Poulin, M., Daugbjerg, N., Gradinger, R., Ilyash, L., Ratkova, T. and von Quillfeldt, C., 2011. The pan-Arctic biodiversity of marine pelagic and sea-ice unicellular eukaryotes: a first-attempt assessment. Marine Biodiversity, 41, pp.13-28.

Rahman, M.M. and Lamsal, B.P., 2021. Ultrasound‐assisted extraction and modification of plant‐based proteins: Impact on physicochemical, functional, and nutritional properties. Comprehensive Reviews in Food Science and Food Safety, 20(2), pp.1457-1480.

Ramirez, M.D., Besser, A.C., Newsome, S.D. and McMahon, K.W., 2021. Meta‐analysis of primary producer amino acid δ15N values and their influence on trophic position estimation. Methods in Ecology and Evolution, 12(10), pp.1750-1767.

Rea, D.K. and Hovan, S.A., 1995. Grain size distribution and depositional processes of the mineral component of abyssal sediments: Lessons from the North Pacific. Paleoceanography, 10(2), pp.251-258.

Reid, P.C., Fischer, A.C., Lewis-Brown, E., Meredith, M.P., Sparrow, M., Andersson, A.J., Antia, A., Bates, N.R., Bathmann, U., Beaugrand, G. and Brix, H., 2009. Impacts of the oceans on climate change. Advances in Marine Biology, 56, pp.1-150.

Reimer, P.J., Bard, E., Bayliss, A., Beck, J.W., Blackwell, P.G., Ramsey, C.B., Buck, C.E., Cheng, H., Edwards, R.L., Friedrich, M. and Grootes, P.M., 2013. IntCal13 and Marine13 radiocarbon age calibration curves 0–50,000 years cal BP. Radiocarbon, 55(4), pp.1869-1887.

Renaud, P.E., Riedel, A., Michel, C., Morata, N., Gosselin, M., Juul-Pedersen, T. and Chiuchiolo, A., 2007. Seasonal variation in benthic community oxygen demand: a response to an ice algal bloom in the Beaufort Sea, Canadian Arctic?. Journal of Marine Systems, 67(1-2), pp.1-12.

Riebesell, U., Körtzinger, A. and Oschlies, A., 2009. Sensitivities of marine carbon fluxes to ocean change. Proceedings of the National Academy of Sciences, 106(49), pp.20602-20609.

Rigor, I.G., Wallace, J.M. and Colony, R.L., 2002. Response of sea ice to the Arctic Oscillation. Journal of Climate, 15(18), pp.2648-2663.

Robinson, R.S., Kienast, M., Luiza Albuquerque, A., Altabet, M., Contreras, S., De Pol Holz, R., Dubois, N., Francois, R., Galbraith, E., Hsu, T.C. and Ivanochko, T., 2012. A review of nitrogen isotopic alteration in marine sediments. Paleoceanography, 27(4).

Rudels, B., 2011. Volume and freshwater transports through the Canadian Arctic Archipelago–Baffin Bay system. Journal of Geophysical Research: Oceans, 116(C8).

Runge, J.A. and Ingram, R.G., 1988. Underice grazing by planktonic, calanoid copepods in relation to a bloom of ice microalgae in southeastern Hudson Bay. Limnology and Oceanography, 33(2), pp.280-286.

Rysgaard, S., Glud, R.N., Sejr, M.K., Bendtsen, J. and Christensen, P.B., 2007. Inorganic carbon transport during sea ice growth and decay: A carbon pump in polar seas. Journal of Geophysical Research: Oceans, 112(C3).

Sabadel, A.J.M., Van Oostende, N., Ward, B.B., Woodward, E.M.S., Van Hale, R. and Frew, R.D., 2019. Characterization of particulate organic matter cycling during a summer North Atlantic phytoplankton bloom using amino acid C and N stable isotopes. Marine Chemistry, 214, p.103670.

Sabine, C.L., Feely, R.A., Gruber, N., Key, R.M., Lee, K., Bullister, J.L., Wanninkhof, R., Wong, C.S.L., Wallace, D.W., Tilbrook, B. and Millero, F.J., 2004. The oceanic sink for anthropogenic CO2. science, 305(5682), pp.367-371.

Sabine, C.L. and Tanhua, T., 2010. Estimation of anthropogenic CO2 inventories in the ocean. Annual Review of Marine Science, 2, pp.175-198.

Sachs, J.P., Repeta, D.J. and Goericke, R., 1999. Nitrogen and carbon isotopic ratios of chlorophyll from marine phytoplankton. Geochimica et Cosmochimica Acta, 63(9), pp.1431-1441.

Saini, J., Stein, R., Fahl, K., Weiser, J., Hebbeln, D., Hillaire-Marcel, C. and de Vernal, A., 2020. Holocene variability in sea ice and primary productivity in the northeastern Baffin Bay. Arktos, 6, pp.55-73.

Sampei, M., Sasaki, H., Hattori, H., Fukuchi, M. and Hargrave, B.T., 2004. Fate of sinking particles, especially fecal pellets, within the epipelagic zone in the North Water (NOW) polynya of northern Baffin Bay. Marine Ecology Progress Series, 278, pp.17-25.

Sauthoff, W., 2016. Nitrogen isotopes of amino acids in marine sediment: a burgeoning tool to assess organic matter quality and changes in supplied nitrate δ 15 N. Doctoral dissertation. University of California, Santa Cruz.

Schiff, J.T., Batista, F.C., Sherwood, O.A., Guilderson, T.P., Hill, T.M., Ravelo, A.C., McMahon, K.W. and McCarthy, M.D., 2014. Compound specific amino acid δ13C patterns in a deep-sea proteinaceous coral: Implications for reconstructing detailed δ13C records of exported primary production. Marine Chemistry, 166, pp.82-91.

Schlitzer, R., 2021. Ocean Data View, v. 5.5. 1-64 bit (Windows). 2021. https://odv. awi. de.

Schubert, C.J. and Calvert, S.E., 2001. Nitrogen and carbon isotopic composition of marine and terrestrial organic matter in Arctic Ocean sediments:: implications for nutrient utilization and organic matter composition. Deep Sea Research Part I: Oceanographic Research Papers, 48(3), pp.789-810.

Scott, C.L., Falk-Petersen, S., Sargent, J.R., Hop, H., Lønne, O.J. and Poltermann, M., 1999. Lipids and trophic interactions of ice fauna and pelagic zooplankton in the marginal ice zone of the Barents Sea. Polar Biology, 21, pp.65-70.

Scott, C.L., Falk-Petersen, S., Gulliksen, B., Lønne, O.J. and Sargent, J.R., 2001. Lipid indicators of the diet of the sympagic amphipod Gammarus wilkitzkii in the Marginal Ice Zone and in open waters of Svalbard (Arctic). Polar Biology, 24, pp.572-576.

Scott, J.H., O'Brien, D.M., Emerson, D., Sun, H., McDonald, G.D., Salgado, A. and Fogel, M.L., 2006. An examination of the carbon isotope effects associated with amino acid biosynthesis. Astrobiology, 6(6), pp.867-880.

Serreze, M.C. and Barry, R.G., 2011. Processes and impacts of Arctic amplification: A research synthesis. Global and planetary change, 77(1-2), pp.85-96.

Shen, Y., Guilderson, T.P., Sherwood, O.A., Castro, C.G., Chavez, F.P. and McCarthy, M.D., 2021. Amino acid δ13C and δ15N patterns from sediment trap time series and deep-sea corals: Implications for biogeochemical and ecological reconstructions in paleoarchives. Geochimica et Cosmochimica Acta, 297, pp.288-307.

Sherwood, O.A., Heikoop, J.M., Scott, D.B., Risk, M.J., Guilderson, T.P. and McKinney, R.A., 2005. Stable isotopic composition of deep-sea gorgonian corals Primnoa spp.: a new archive of surface processes. Marine Ecology Progress Series, 301, pp.135-148.

Sherwood, O.A. and Edinger, E.N., 2009. Ages and growth rates of some deep-sea gorgonian and antipatharian corals of Newfoundland and Labrador. Canadian Journal of Fisheries and Aquatic Sciences, 66(1), pp.142-152.

Sherwood, O.A., Guilderson, T.P., Batista, F.C., Schiff, J.T. and McCarthy, M.D., 2014. Increasing subtropical North Pacific Ocean nitrogen fixation since the Little Ice Age. Nature, 505(7481), pp.78-81.

Sherwood, O.A., Davin, S.H., Lehmann, N., Buchwald, C., Edinger, E.N., Lehmann, M.F. and Kienast, M., 2021. Stable isotope ratios in seawater nitrate reflect the influence of Pacific water along the northwest Atlantic margin. Biogeosciences, 18(15), pp.4491-4510.

Sigman, D.M., Altabet, M.A., Francois, R., McCorkle, D.C. and Gaillard, J.F., 1999. The isotopic composition of diatom‐bound nitrogen in Southern Ocean sediments. Paleoceanography, 14(2), pp.118-134.

Silfer, J.A., Engel, M.H., Macko, S.A. and Jumeau, E.J., 1991. Stable carbon isotope analysis of amino acid enantiomers by conventional isotope ratio mass spectrometry and combined gas chromatography/isotope ratio mass spectrometry. Analytical Chemistry, 63(4), pp.370-374.

Silfer, J.A., Engel, M.H. and Macko, S.A., 1992. Kinetic fractionation of stable carbon and nitrogen isotopes during peptide bond hydrolysis: experimental evidence and geochemical implications. Chemical Geology: Isotope Geoscience Section, 101(3-4), pp.211-221.

Smith, R.E., Harrison, W.G., Harris, L.R. and Herman, A.W., 1990. Vertical fine structure of particulate matter and nutrients in sea ice of the high Arctic. Canadian Journal of Fisheries and Aquatic Sciences, 47(7), pp.1348-1355.

Smith, D.E., Harrison, S., Firth, C.R. and Jordan, J.T., 2011. The early Holocene sea level rise. Quaternary Science Reviews, 30(15-16), pp.1846-1860.

Søreide, J.E., Hop, H., Carroll, M.L., Falk-Petersen, S. and Hegseth, E.N., 2006. Seasonal food web structures and sympagic–pelagic coupling in the European Arctic revealed by stable isotopes and a two-source food web model. Progress in Oceanography, 71(1), pp.59-87.

Søreide, J.E., Leu, E.V., Berge, J., Graeve, M. and Falk-Petersen, S.T.I.G., 2010. Timing of blooms, algal food quality and Calanus glacialis reproduction and growth in a changing Arctic. Global Change Biology, 16(11), pp.3154-3163.

Søreide, J.E., Carroll, M.L., Hop, H., Ambrose Jr, W.G., Hegseth, E.N. and Falk-Petersen, S., 2013. Sympagic-pelagic-benthic coupling in Arctic and Atlantic waters around Svalbard revealed by stable isotopic and fatty acid tracers. Marine Biology Research, 9(9), pp.831-850.

Stahl, A., 2021. Identifying Novel Isotopic Tracers of Marine Primary Producers to Study Food Web Carbon Cycles. University of Rhode Island.

Stamieszkin, K., Poulton, N.J. and Pershing, A.J., 2017. Zooplankton grazing and egestion shifts particle size distribution in natural communities. Marine Ecology Progress Series, 575, pp.43-56.

Stamieszkin, K., Steinberg, D.K. and Maas, A.E., 2021. Fecal pellet production by mesozooplankton in the subarctic Northeast Pacific Ocean. Limnology and Oceanography, 66(7), pp.2585-2597.

Steele, M., Ermold, W. and Zhang, J., 2008. Arctic Ocean surface warming trends over the past 100 years. Geophysical Research Letters, 35(2).

Stock, B. and Semmens, B., 2016. MixSIAR GUI user manual v3. 1. Scripps Institution of Oceanography, UC San Diego, San Diego, California, USA.

St-Onge, M.-P., and St-Onge, G., 2014. Environmental changes in Baffin Bay during the Holocene based on the physical and magnetic properties of sediment cores. Journal of Quaternary Science, 29(1), pp.41-56.

Strass, V.H. and Nöthig, E.M., 1996. Seasonal shifts in ice edge phytoplankton blooms in the Barents Sea related to the water column stability. Polar Biology, 16, pp.409-422.

Stuiver, M. and Reimer, P.J., 1993. Extended 14C data base and revised CALIB 3.0 14C age calibration program. Radiocarbon, 35(1), pp.215-230.

Sweetman, A.K., Thurber, A.R., Smith, C.R., Levin, L.A., Mora, C., Wei, C.L., Gooday, A.J., Jones, D.O., Rex, M., Yasuhara, M. and Ingels, J., 2017. Major impacts of climate change on deep-sea benthic ecosystems. Elementa: Science of the Anthropocene, 5, p.4.

Szymanski, A. and Gradinger, R., 2016. The diversity, abundance and fate of ice algae and phytoplankton in the Bering Sea. Polar Biology, 39(2), pp.309-325.

Takano, Y., Kashiyama, Y., Ogawa, N.O., Chikaraishi, Y. and Ohkouchi, N., 2010. Isolation and desalting with cation‐exchange chromatography for compound‐specific nitrogen isotope analysis of amino acids: Application to biogeochemical samples. Rapid Communications in Mass Spectrometry, 24(16), pp.2317-2323.

Tang, C.C., Ross, C.K., Yao, T., Petrie, B., DeTracey, B.M. and Dunlap, E., 2004. The circulation, water masses and sea-ice of Baffin Bay. Progress in Oceanography, 63(4), pp.183-228.

Tedesco, L., Vichi, M. and Scoccimarro, E., 2019. Sea-ice algal phenology in a warmer Arctic. Science Advances, 5(5), p.eaav4830.

Tesdal, J.E., Galbraith, E.D. and Kienast, M., 2013. Nitrogen isotopes in bulk marine sediment: linking seafloor observations with subseafloor records. Biogeosciences, 10(1), pp.101-118.

Thompson, D.W. and Wallace, J.M., 1998. The Arctic Oscillation signature in the wintertime geopotential height and temperature fields. Geophysical research letters, 25(9), pp.1297-1300.

Top, Z., Clarke, W.B., Eismont, W.C. and Jones, E.P., 1980. Radiogenic helium in Baffin Bay bottom water.

Tremblay, J.É., Michel, C., Hobson, K.A., Gosselin, M. and Price, N.M., 2006. Bloom dynamics in early opening waters of the Arctic Ocean. Limnology and Oceanography, 51(2), pp.900-912.

Turner, J.T., 2015. Zooplankton fecal pellets, marine snow, phytodetritus and the ocean's biological pump. Progress in Oceanography, 130, pp.205-248.

Ueda, K., Morgan, S.L., Fox, A., Gilbart, J., Sonesson, A., Larsson, L. and Odham, G., 1989. D-alanine as a chemical marker for the determination of streptococcal cell wall levels in mammalian tissues by gas chromatography/negative ion chemical ionization mass spectrometry. Analytical Chemistry, 61(3), pp.265-270.

Vokhshoori, N.L., Larsen, T. and McCarthy, M.D., 2014. Reconstructing δ13C isoscapes of phytoplankton production in a coastal upwelling system with amino acid isotope values of littoral mussels. Marine Ecology Progress Series, 504, pp.59-72.

Vokhshoori, N.L. and McCarthy, M.D., 2014. Compound-specific δ15N amino acid measurements in littoral mussels in the California upwelling ecosystem: a new approach to generating baseline δ15N isoscapes for coastal ecosystems. PloS one, 9(6), p.e98087.

Vokhshoori, N.L., Rick, T.C., Braje, T.J. and McCarthy, M.D., 2023. Preservation of stable isotope signatures of amino acids in diagenetically altered Middle to Late Holocene archaeological mollusc shells. Geochimica et Cosmochimica Acta, 352, pp.36-50.

Volk, T. and Hoffert, M.I., 1985. Ocean carbon pumps: Analysis of relative strengths and efficiencies in ocean-driven atmospheric CO2 changes. The carbon cycle and atmospheric CO2: Natural Variations Archean to Present, 32, pp.99-110.

Wakeham, S.G., Lee, C., Hedges, J.I., Hernes, P.J. and Peterson, M.J., 1997. Molecular indicators of diagenetic status in marine organic matter. Geochimica et Cosmochimica Acta, 61(24), pp.5363-5369.

Wareham, V.E. and Edinger, E.N., 2007. Distribution of deep-sea corals in the Newfoundland and Labrador region, Northwest Atlantic Ocean. Bulletin of Marine Science, 81(3), pp.289-313.

Waser, N.A.D., Harrison, P.J., Nielsen, B., Calvert, S.E. and Turpin, D.H., 1998. Nitrogen isotope fractionation during the uptake and assimilation of nitrate, nitrite, ammonium, and urea by a marine diatom. Limnology and Oceanography, 43(2), pp.215-224.

Waser, N.A., Harrison, W.G., Head, E.J., Nielsen, B., Lutz, V.A. and Calvert, S.E., 2000. Geographic variations in the nitrogen isotope composition of surface particulate nitrogen and new production across the North Atlantic Ocean. Deep Sea Research Part I: Oceanographic Research Papers, 47(7), pp.1207-1226.

Wassmann, P., 2011. Arctic marine ecosystems in an era of rapid climate change. Progress in Oceanography, 90(1-4), pp.1-17.

Werner, I., 1997. Grazing of Arctic under-ice amphipods on sea-ice algae. Marine Ecology Progress Series, 160, pp.93-99.

Whiteman, J.P., Elliott Smith, E.A., Besser, A.C. and Newsome, S.D., 2019. A guide to using compound-specific stable isotope analysis to study the fates of molecules in organisms and ecosystems. Diversity, 11(1), p.8.

Wilson, S.E., Ruhl, H.A. and Smith, Jr, K.L., 2013. Zooplankton fecal pellet flux in the abyssal northeast Pacific: A 15 year time‐series study. Limnology and oceanography, 58(3), pp.881-892.

Wojtal, P.K., Doherty, S.C., Shea, C.H., Popp, B.N., Benitez‐Nelson, C.R., Buesseler, K.O., Estapa, M.L., Roca‐Martí, M. and Close, H.G., 2023. Deconvolving mechanisms of particle flux attenuation using nitrogen isotope analyses of amino acids. Limnology and oceanography, 68(9), pp.1965-1981.

Wu, G., 2009. Amino acids: metabolism, functions, and nutrition. Amino Acids, 37, pp.1-17.

Yager, P.L., Connelly, T.L., Mortazavi, B., Wommack, K.E., Bano, N., Bauer, J.E., Opsahl, S. and Hollibaugh, J.T., 2001. Dynamic bacterial and viral response to an algal bloom at subzero temperatures. Limnology and Oceanography, 46(4), pp.790-801.

Yamaguchi, Y.T., Chikaraishi, Y., Takano, Y., Ogawa, N.O., Imachi, H., Yokoyama, Y. and Ohkouchi, N., 2017. Fractionation of nitrogen isotopes during amino acid metabolism in heterotrophic and chemolithoautotrophic microbes across Eukarya, Bacteria, and Archaea: Effects of nitrogen sources and metabolic pathways. Organic Geochemistry, 111, pp.101-112.

Yamaguchi, Y.T. and McCarthy, M.D., 2018. Sources and transformation of dissolved and particulate organic nitrogen in the North Pacific Subtropical Gyre indicated by compound-specific δ15N analysis of amino acids. Geochimica et Cosmochimica Acta, 220, pp.329-347.

Yarnes, C.T. and Herszage, J., 2017. The relative influence of derivatization and normalization procedures on the compound-specific stable isotope analysis of nitrogen in amino acids. Rapid Communications in Mass Spectrometry, 31(8), pp.693-704.

Yashayaev, I., 2007. Hydrographic changes in the Labrador Sea, 1960–2005. Progress in Oceanography, 73(3-4), pp.242-276.

Yashayaev, I., Peterson, I. and Wang, Z., 2021. Meteorological, Sea Ice and Physical Oceanographic Conditions in the Labrador Sea during 2018. Canadian Science Advisory Secretariat = Secrétariat canadien de consultation scientifique.

Yoshikawa, C., Ogawa, N.O., Chikaraishi, Y., Makabe, A., Matsui, Y., Sasai, Y., Wakita, M., Honda, M.C., Mino, Y., Aita, M.N. and Fujiki, T., 2022. Nitrogen isotopes of sinking particles reveal the seasonal transition of the nitrogen source for phytoplankton. Geophysical Research Letters, 49(17), p.e2022GL098670.

APPENDIX A SUPPLEMENTARY MATERIAL FOR CHAPTER 2

A.1 Supplementary Discussion

A1.1 Effects of ultrasonication

To avoid contamination peaks introduced by hydrolyzing nylon filters, biomass was extracted from the nylon filters by ultrasonicating the filters in Milli-Q water at 40 kHz before hydrolysis. It is important to note that ultrasonic extraction may induce cell disruption which releases a portion of water-soluble proteins and free AAs (Rahman & Lamsal, 2021). The removal of the supernatant following the ultrasonication may lead to an overall smaller AA yield from the biomasses on the filters. While it is possible to selectively lose some AAs, the loss of AAs is unlikely to isotopically fractionate the AAs (Matthew D. McCarthy, personal communication, August 4, 2022). In fact, different AAs are subject to different degrees of losses during filtration through a peristaltic pump, acid hydrolysis and cation exchange clean-up, and yet minimal isotope fractionation was found despite the AA loss (Silverman et al., 2021). This is evidenced by the consistent δ^{13}C-EAA and δ^{15}N-SrcAA values of > 3 μm brash ice algae between the 2019 (non-ultrasonicated) and 2021 (ultrasonicated) collections (Fig. 2.2, 2.3). We found that the relative abundance (mol%) of amino acids were also consistent between different algal groups and size classes, suggesting the loss of AAs may play a minor role in affecting the isotopic values (Fig. A1). Nevertheless, it is important to acknowledge that this extra extraction step may pose challenges for future studies to replicate or compare with our findings.

A.2 Supplementary Tables and Figures

Table A1 Sampling locations and depth, size, and biomass analyzed of sea ice and pelagic algae samples.

Sample ID	Year	Location	Station	Algae type	Samples	Size (µm)	Depth (m)	Biomass (mg)
IC1-H-Apr	2017	Cambridge Bay	CB	Sea ice	Fast ice	> 0.7	NA	NA
IC1-H-May	2017	Cambridge Bay	CB	Sea ice	Fast ice	> 0.7	NA	NA
IC2-L-Apr	2017	Cambridge Bay	CB	Sea ice	Fast ice	> 0.7	NA	NA
IC2-L-May	2017	Cambridge Bay	CB	Sea ice	Fast ice	> 0.7	NA	NA
IC4-L-Apr	2017	Cambridge Bay	CB	Sea ice	Fast ice	> 0.7	NA	NA
IC4-L-May	2017	Cambridge Bay	CB	Sea ice	Fast ice	> 0.7	NA	NA
ICEn1a	2019	Frobisher Bay	FB	Sea ice	Brash ice	> 3	0	4.8
ICEn1b	2019	Frobisher Bay	FB	Sea ice	Brash ice	> 3	0	4.8
ICEn2a	2019	Frobisher Bay	FB	Sea ice	Brash ice	> 3	0	7.6
ICEn2b	2019	Frobisher Bay	FB	Sea ice	Brash ice	> 3	0	7.6
ICEn3a	2019	Frobisher Bay	FB	Sea ice	Brash ice	> 3	0	14.9
ICEn3b	2019	Frobisher Bay	FB	Sea ice	Brash ice	> 3	0	14.9
ICEp1	2019	Frobisher Bay	FB	Sea ice	Brash ice	0.2-3	0	2.2
ICEp2	2019	Frobisher Bay	FB	Sea ice	Brash ice	0.2-3	0	2.5
ICEp3	2019	Frobisher Bay	FB	Sea ice	Brash ice	0.2-3	0	3.9
1-15-0-N	2019	Labrador Shelf	IC	Pelagic	Seawater	> 3	0	11.7
1-15-1-N	2019	Labrador Shelf	IC	Pelagic	Seawater	> 3	30	9.1
1-15-0.5-P	2019	Labrador Shelf	IC	Pelagic	Seawater	0.2-3	15	5.1
1-15-0-P	2019	Labrador Shelf	IC	Pelagic	Seawater	0.2-3	0	1.9
1-15-1-P	2019	Labrador Shelf	IC	Pelagic	Seawater	0.2-3	30	3.4
NS3-0.5-N	2019	Labrador Shelf	NS	Pelagic	Seawater	> 3	10	11.8
NS3-0-N	2019	Labrador Shelf	NS	Pelagic	Seawater	> 3	4	5.0
NS3-1-N	2019	Labrador Shelf	NS	Pelagic	Seawater	> 3	20	7.4

Sample ID	Year	Location	Station	Algae type	Samples	Size (µm)	Depth (m)	Biomass (mg)
NS3-0.5-P	2019	Labrador Shelf	NS	Pelagic	Seawater	0.2-3	10	2.7
NS3-0-P	2019	Labrador Shelf	NS	Pelagic	Seawater	0.2-3	4	6.1
NS3-1-P	2019	Labrador Shelf	NS	Pelagic	Seawater	0.2-3	20	5.3
CF-Sm1	2021	Baffin Bay	CF	Sea ice	Brash ice	> 3	0	NA
CF-Sp1	2021	Baffin Bay	CF	Sea ice	Brash ice	0.2-3	0	NA
CF0-Pm1	2021	Baffin Bay	CF	Pelagic	Seawater	> 3	0	NA
CF1-Pm1	2021	Baffin Bay	CF	Pelagic	Seawater	> 3	27	NA
CF0-Pp1	2021	Baffin Bay	CF	Pelagic	Seawater	0.2-3	0	NA
CF1-Pp1	2021	Baffin Bay	CF	Pelagic	Seawater	0.2-3	27	NA
SF-Sm1	2021	Baffin Bay	SF	Sea ice	Brash ice	> 3	0	NA
SF-Sp1	2021	Baffin Bay	SF	Sea ice	Brash ice	0.2-3	0	NA
SF0-Pm1	2021	Baffin Bay	SF	Pelagic	Seawater	> 3	0	NA
SF1-Pm1	2021	Baffin Bay	SF	Pelagic	Seawater	> 3	42	NA
SF0-Pp1	2021	Baffin Bay	SF	Pelagic	Seawater	0.2-3	0	NA
SF1-Pp1	2021	Baffin Bay	SF	Pelagic	Seawater	0.2-3	42	NA

Table A2 δ^{13}C-AA values of fast ice, brash ice, and pelagic algae.

Sample ID	Samples	Phe	Thr	Ile	Leu	Val	Asx	Glx	Pro	Ala	Gly	Lys
IC1-H-Apr	Fast ice	-26.5	-7.3	-14.8	-27.7	-21.3	-13.6	-17.6	-21.3	-16.8	-16.8	-13.4
IC1-H-May	Fast ice	-30.1	-9.4	-22.3	-29.0	-26.5	-18.4	-20.2	-24.2	-19.0	-19.3	-17.2
IC2-L-Apr	Fast ice	-31.2	-9.1	-20.9	-30.7	-25.4	-16.7	-21.8	-23.9	-18.0	-18.6	-16.7
IC2-L-May	Fast ice	-30.6	-8.7	-14.7	-29.1	-25.5	-16.7	-20.3	-23.9	-18.5	-18.2	-16.3
IC4-L-Apr	Fast ice	-32.7	-10.4	-18.6	-31.5	-25.6	-17.0	-19.9	-24.5	-20.8	-18.1	-18.0
IC4-L-May	Fast ice	-31.3	-8.3	-20.0	-28.7	-25.3	-18.1	-19.4	-22.7	-19.1	-15.5	-18.3
ICEn1a	Brash ice	-33.2	-13.5	-25.1	-31.4	-28.4	-14.0	-23.4	-23.3	-21.5	-17.3	-22.3
ICEn1b	Brash ice	-28.5	-9.8	-20.5	-31.1	-28.8	-15.8	-21.9	-23.4	-22.1	-18.6	-19.5
ICEn2a	Brash ice	-28.7	-12.8	-22.0	-30.7	-28.9	-15.9	-20.8	-23.4	-21.7	-20.9	-18.6
ICEn2b	Brash ice	-28.4	-14.0	-20.0	-31.6	-29.5	-16.1	-22.2	-23.8	-23.0	-19.8	-18.7
ICEn3a	Brash ice	-30.0	-11.8	-26.1	-30.3	-29.6	-17.0	-21.1	-23.8	-19.7	-19.0	-19.9
ICEn3b	Brash ice	-27.2	-12.0	-18.9	-29.5	-28.1	-15.0	-19.7	-22.2	-19.6	-17.1	-17.2
ICEp1	Brash ice	-28.8	-10.3	-21.6	-31.0	-32.0	-17.9	-22.6	-24.7	-21.7	-19.6	-18.7
ICEp2	Brash ice	-31.5	-12.9	-28.2	-33.3	-33.1	-20.8	-25.0	-28.1	-21.9	-21.8	-19.6
ICEp3	Brash ice	-29.3	NA	-24.4	-30.6	-29.7	-17.2	-24.0	-24.8	-19.3	-16.1	-19.1
1-15-0-N	Seawater	-30.8	-16.5	-26.1	-33.0	-32.0	-19.5	-22.5	-24.7	-22.2	-16.0	-19.4
1-15-1-N	Seawater	-30.1	-16.6	-24.0	-32.6	-31.6	-19.4	-22.0	-24.5	-22.1	-13.4	-20.6
1-15-0.5-P	Seawater	-28.7	-15.5	-19.0	-30.2	-29.6	-19.7	-20.3	-23.1	-22.3	-11.4	-18.2
1-15-1-P	Seawater	-28.4	-19.5	-27.6	-31.5	-29.6	-22.2	-22.8	-25.6	-23.6	-12.4	-21.6
NS3-0.5-N	Seawater	-27.0	-13.6	-20.5	-27.7	-27.8	-16.2	-19.8	-24.4	-22.0	-11.3	-16.6
NS3-0-N	Seawater	-28.3	-15.3	-21.4	-27.4	-27.6	-17.6	-19.8	-23.4	-22.3	NA	-18.9
NS3-1-N	Seawater	-28.0	-14.2	-22.2	-27.3	-28.1	-16.2	-19.7	-23.7	-20.6	-12.2	-16.5
NS3-0.5-P	Seawater	-28.2	-16.8	-23.2	-27.4	-27.9	-18.3	-19.4	-23.7	-21.0	-13.0	-16.1

Sample ID	Samples	Phe	Thr	Ile	Leu	Val	Asx	Glx	Pro	Ala	Gly	Lys
NS3-0-P	Seawater	-27.5	-16.9	-25.4	-28.3	-29.2	-19.4	-18.9	-23.5	-20.4	-11.8	-17.7
NS3-1-P	Seawater	-29.2	-16.9	-24.6	-28.1	-31.0	-18.7	-20.6	-24.4	-21.9	-13.4	-17.6
CF-Sm1	Brash ice	-25.6	-9.6	-19.1	-24.8	-25.7	-15.4	-9.2	-18.9	-20.9	-14.2	-18.5
CF-Sp1	Brash ice	-24.8	-14.3	-19.8	-24.6	-28.5	-17.1	-10.8	-19.4	-23.2	-15.3	-16.8
CF0-Pm1	Seawater	-26.2	-13.0	-19.2	-28.7	-28.5	-17.6	-16.3	-21.6	-20.6	-15.1	-21.0
CF1-Pm1	Seawater	-23.2	-7.9	-17.1	-26.9	-24.9	-11.3	-12.0	-18.6	-16.8	-15.4	-17.6
CF0-Pp1	Seawater	-25.4	-13.0	-20.0	-25.9	-28.1	-17.8	-13.4	-20.7	-21.9	-16.5	-16.9
CF1-Pp1	Seawater	-25.2	-14.2	-17.7	-28.0	-27.8	-17.4	-14.6	-22.2	-18.9	-15.2	-19.2
SF-Sm1	Brash ice	-25.7	-9.9	-19.9	-26.1	-27.6	-15.2	-6.9	-18.9	-20.1	-14.5	-21.2
SF-Sp1	Brash ice	-25.2	-7.7	-19.8	-22.4	-25.5	-15.0	-5.8	-18.5	-20.4	-12.0	-21.3
SF0-Pm1	Seawater	-28.2	-15.3	-23.2	-26.9	-27.0	-20.4	-15.4	-23.0	-22.9	-15.7	-22.2
SF1-Pm1	Seawater	-26.5	-11.3	-15.7	-26.8	-24.9	-19.2	-13.1	-21.1	-21.2	-15.4	-21.9
SF0-Pp1	Seawater	-30.5	-15.5	-16.5	-27.5	-30.7	-19.5	-14.2	-23.7	NA	-17.6	-24.7
SF1-Pp1	Seawater	-27.6	-13.0	-21.6	-26.4	-28.0	-19.5	-13.3	-19.7	-23.1	-14.9	-21.9

Table A3 δ^{15}N-AA values of brash ice and pelagic algae.

Sample ID	Samples	Phe	Thr	Ile	Leu	Val	Asx	Glx	Pro	Ala	Gly	Lys
ICEn1a	Brash ice	7.0	5.4	5.8	4.4	12.0	6.2	11.5	8.3	6.4	5.4	6.8
ICEn1b	Brash ice	4.9	3.6	5.6	2.4	10.9	4.6	8.8	6.2	6.1	4.4	4.7
ICEn2a	Brash ice	6.5	5.0	4.8	3.9	12.5	6.2	11.0	7.5	6.8	5.3	6.6
ICEn2b	Brash ice	6.0	3.5	6.6	3.7	11.7	5.5	9.5	6.7	6.4	5.1	4.9
ICEn3a	Brash ice	8.0	7.4	6.3	4.7	13.7	7.1	11.1	6.3	7.2	6.2	7.5
ICEn3b	Brash ice	5.0	5.0	5.4	2.8	12.6	5.3	9.0	5.1	6.5	6.2	5.6
ICEp1	Brash ice	4.6	4.0	4.4	5.2	12.8	5.7	10.0	6.9	6.2	5.1	5.0
ICEp3	Brash ice	7.4	NA	4.7	4.5	13.5	6.8	11.7	8.1	7.5	5.6	7.6
1-15-0-N	Seawater	4.7	2.2	8.3	3.8	NA	6.8	8.7	7.5	8.2	3.5	4.7
1-15-1-N	Seawater	2.6	0.8	NA	5.1	NA	7.1	10.0	6.9	8.8	2.8	4.2
1-15-0.5-P	Seawater	5.1	0.9	NA	3.8	NA	7.2	10.2	8.7	11.0	0.9	4.3
1-15-1-P	Seawater	3.0	-0.1	4.9	3.6	9.4	6.6	9.5	8.2	12.1	1.8	3.6
1-15-0-P	Seawater	4.1	2.4	6.0	3.5	9.8	6.5	8.3	7.6	9.7	2.5	4.3
NS3-0.5-N	Seawater	6.1	3.0	7.5	7.1	10.2	8.9	12.2	10.1	10.8	4.3	7.2
NS3-0-N	Seawater	5.4	2.6	7.7	7.8	12.2	9.1	12.1	11.4	10.7	3.8	7.6
NS3-1-N	Seawater	5.2	3.2	3.7	3.9	11.3	7.5	10.2	7.3	8.3	3.9	6.2
NS3-0.5-P	Seawater	5.5	3.0	6.0	5.8	10.0	8.0	11.3	10.0	11.4	0.2	6.4
NS3-0-P	Seawater	4.3	NA	4.3	3.9	10.2	7.1	9.5	10.9	10.0	1.2	5.8
NS3-1-P	Seawater	4.1	1.5	4.9	5.3	9.7	7.0	10.0	9.2	9.3	1.1	5.4
CF-Sm1	Brash ice	6.9	0.9	7.5	7.1	12.7	8.5	10.2	13.5	12.7	6.9	4.7
CF-Sp1	Brash ice	7.3	3.8	7.1	7.0	13.4	9.6	11.9	13.5	15.1	4.3	5.8
CF0-Pm1	Seawater	7.7	NA	NA	6.9	NA	11.2	12.6	11.3	NA	6.7	7.0
CF1-Pm1	Seawater	4.8	5.9	4.6	3.5	12.1	8.5	11.1	8.2	10.5	4.8	5.9

Sample ID	Samples	Phe	Thr	Ile	Leu	Val	Asx	Glx	Pro	Ala	Gly	Lys
CF0-Pp1	Seawater	5.6	5.9	4.2	5.9	11.4	9.9	12.4	12.6	12.7	4.1	NA
CF1-Pp1	Seawater	6.0	NA	NA	6.7	NA	11.3	15.8	12.6	NA	6.6	7.4
SF-Sm1	Brash ice	4.0	2.4	4.4	4.5	10.7	5.7	7.7	10.0	8.9	3.2	3.0
SF-Sp1	Brash ice	4.6	3.5	3.3	3.8	10.6	6.1	8.0	10.1	10.9	1.9	2.3
SF0-Pm1	Seawater	4.8	NA	NA	5.0	NA	8.0	9.8	10.1	NA	3.6	5.2
SF1-Pm1	Seawater	6.1	3.7	7.0	7.4	12.5	10.4	13.5	11.3	13.4	4.9	6.4
SF0-Pp1	Seawater	NA	NA	NA	NA	NA	NA	NA	NA	NA	NA	NA
SF1-Pp1	Seawater	5.4	NA	NA	7.1	NA	9.4	13.3	11.5	NA	NA	5.8

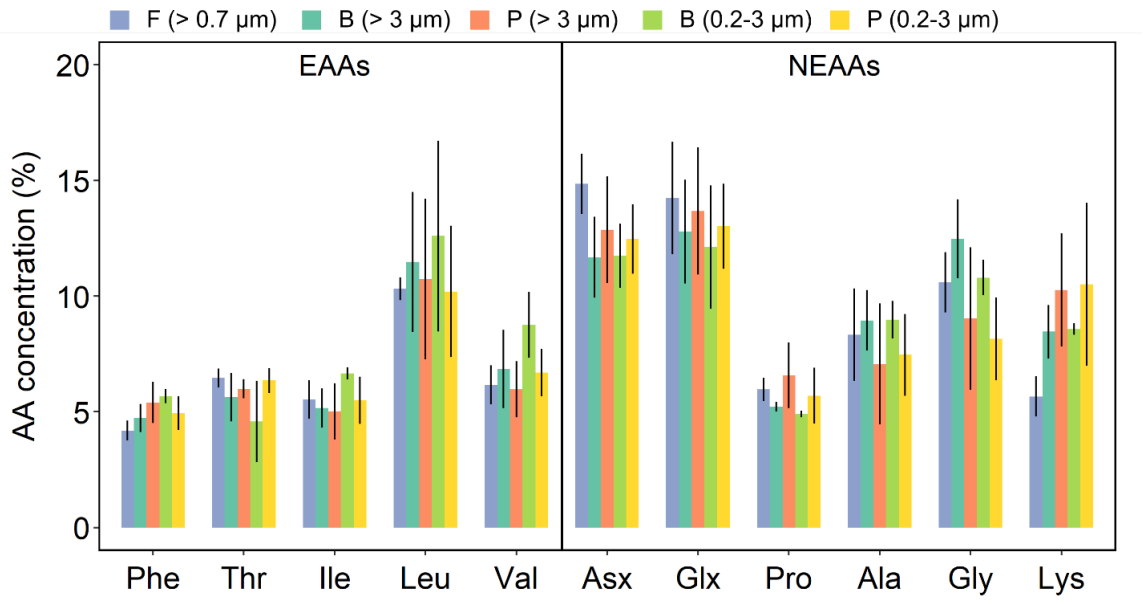

Figure A1 The AA molar composition of pelagic algae (P) and sea ice algae from the fast ice (F) and brash ice (B). Error bars represent ± 1 s.d. of averages of samples (n = 5-9).

Table A4 Principal component analysis output for Fig. 2.4b.

Importance of components

	PC1	PC2	PC3	PC4	PC5
Eigenvalue	2.43	1.23	0.86	0.47	0.00
Cumulative portion	0.49	0.73	0.91	1.00	1.00

Vector scores

	PC1	PC2	PC3	PC4	PC5
Phe	-0.56	0.04	-0.20	-0.66	0.46
Leu	-0.54	-0.18	0.16	0.69	0.42
Thr	0.48	-0.24	-0.64	0.14	0.53
Ile	0.28	0.77	0.32	0.05	0.48
Val	0.30	-0.57	0.65	-0.26	0.33

Sample scores

Sample ID	PC1	PC2	PC3	PC4	Group
ICEp1a	0.42	1.19	-2.55	0.09	B
ICEp2a	0.12	-1.12	-2.25	-0.15	B
ICEn1a	1.36	-1.75	0.52	0.40	B
ICEn2a	0.36	-0.04	-0.37	-0.55	B
ICEn3a	0.11	-1.70	-1.18	0.08	B
ICEn1b	1.35	0.45	-1.29	-0.54	B
ICEn3b	0.38	1.00	-0.30	-0.57	B
ICEn2b	0.43	1.24	-0.11	-0.95	B
CF-Sp1	-2.56	0.80	0.03	0.52	B
CF-Sm1	-0.48	-0.29	-0.33	0.59	B
SF-Sp1	-0.96	-0.89	-1.00	1.48	B
SF-Sm1	-0.66	0.15	-1.09	0.36	B
IC1-H-May	1.50	-1.43	-0.35	0.41	F
IC4-L-May	2.60	-1.06	0.18	0.87	F
IC2-L-May	3.13	1.38	0.61	0.69	F
IC1-H-Apr	2.80	-0.12	1.17	-0.80	F
IC2-L-Apr	2.82	-1.24	0.23	-0.03	F
IC4-L-Apr	3.51	-0.13	1.10	0.14	F
NS3L-0-N	-0.94	-0.21	1.12	0.25	P
NS3L-0.5-N	-0.76	0.22	0.29	-0.09	P
NS3L-1-N	-1.06	-0.45	0.39	0.35	P
NS3L-0-P	-2.19	-1.15	0.51	-0.37	P
NS3L-0.5-P	-1.64	-0.76	1.35	0.12	P
NS3L-1-P	-2.07	-0.24	0.13	0.66	P
1-15-1-N	-0.37	0.43	-0.14	-0.73	P

Sample scores

Sample ID	PC1	PC2	PC3	PC4	Group
1-15-0_5-P	-0.10	1.68	0.58	-0.32	P
1-15-0-N	-0.45	-0.38	-0.40	-0.67	P
1-15-1-P	-1.98	-1.64	1.14	-1.55	P
CF1-Pp1	-0.91	1.58	0.45	-0.75	P
CF1-Pm1	0.35	0.42	-0.90	-1.04	P
CF0-Pp1	-1.60	0.52	-0.24	0.20	P
CF0-Pm1	-0.52	1.13	-0.26	-0.59	P
SF1-Pp1	-1.08	-0.34	-0.02	0.68	P
SF1-Pm1	0.67	1.04	1.06	-0.09	P
SF0-Pp1	-0.34	2.93	0.76	1.66	P
SF0-Pm1	-1.25	-1.24	1.16	0.24	P

Table A5 Linear discriminant analysis output for Fig. 2.5.

Coefficients of linear discriminants

	LD1	LD2
Phe	-2.22	58.2
Thr	-3.11	58.6
Ile	-2.84	57.9
Leu	-2.69	58.2
Val	-3.19	57.5

Proportion of trace

	LD1	LD2
	0.80	0.20

Posterior probabilities with leave-one-out cross validation of the classifier samples

Sample ID	Actual	Predicted (% probability)		
		Brash ice algae (B)	Fast ice algae (F)	Pelagic algae (P)
ICEp1a	B	**99.8**	0.0	0.2
ICEp2a	B	**99.9**	0.0	0.1
ICEn1a	B	0.0	**100.0**	0.0
ICEn2a	B	**61.7**	0.1	38.2
ICEn3a	B	**94.9**	0.2	4.8
ICEn1b	B	**91.0**	1.5	7.4
ICEn2b	B	21.5	0.0	**78.5**
ICEn3b	B	32.5	0.0	**67.5**
CF-Sp1	B	0.0	0.0	**100.0**
CF-Sm1	B	**81.5**	0.0	18.5
SF-Sp1	B	**82.4**	0.0	17.6
SF-Sm1	B	**84.4**	0.0	15.6
IC1-H-May	F	35.8	**62.9**	1.3
IC4-L-May	F	0.0	**100.0**	0.0
IC2-L-May	F	0.1	**99.9**	0.0
IC1-H-Apr	F	0.1	**99.8**	0.1
IC2-L-Apr	F	0.1	**99.9**	0.0
IC4-L-Apr	F	0.0	**100.0**	0.0
NS3L-0-N	P	2.5	0.0	**97.5**
NS3L-0.5-N	P	10.8	0.0	**89.2**
NS3L-1-N	P	15.8	0.0	**84.2**
NS3L-0-P	P	2.0	0.0	**98.0**
NS3L-0.5-P	P	0.6	0.0	**99.4**

Posterior probabilities with cross validation of the classifier samples

Sample ID	Actual	Predicted (% probability)		
		Brash ice algae (B)	Fast ice algae (F)	Pelagic algae (P)
NS3L-1-P	P	10.1	0.0	**89.9**
1-15-1-N	P	**57.5**	0.0	42.5
1-15-0_5-P	P	1.2	0.0	**98.8**
1-15-0-N	P	28.7	0.0	**71.3**
1-15-1-P	P	0.4	0.0	**99.6**
CF1-Pp1	P	0.2	0.0	**99.8**
CF1-Pm1	P	**89.6**	0.0	10.4
CF0-Pp1	P	5.5	0.0	**94.5**
CF0-Pm1	P	17.9	0.0	**82.1**
SF1-Pp1	P	43.2	0.0	**56.8**
SF1-Pm1	P	9.6	1.1	**89.3**
SF0-Pp1	P	**67.1**	0.1	32.8
SF0-Pm1	P	1.1	0.0	**98.9**

APPENDIX B SUPPLEMENTARY MATERIAL FOR CHAPTER 3

B.1 Supplementary Tables and Figures

Table B1 Sampling date and depth, fluxes, and bulk $\delta^{13}C$ and $\delta^{15}N$ of 469-m and 915-m sediment traps. TPM, total particulate matter; POC, particulate organic carbon; PN, particulate nitrogen.

Sample ID	Depth (m)	Date open (mm/dd/yyyy)	Date close (mm/dd/yyyy)	TPM (mg m^{-2} d^{-1})	POC (mg C m^{-2} d^{-1})	PN (mg N m^{-2} d^{-1})	C:N ratio	Bulk $\delta^{13}C$ (‰)	Bulk $\delta^{15}N$ (‰)
HB17-A3	469	11/16/2017	12/1/2017	981.6	19.3	2.8	6.9	-25.3	6.8
HB17-A4	469	12/1/2017	12/16/2017	1116.4	22.2	3.2	6.9	-25.3	6.8
HB17-A5	469	12/16/2017	1/1/2018	590.9	14.3	2.4	6.0	-24.7	7.5
HB17-A6	469	1/1/2018	1/16/2018	1006.9	12.9	1.8	7.2	-24.6	7.0
HB17-A7	469	1/16/2018	1/31/2018	602.8	10.6	1.5	7.0	-25.0	7.2
HB17-A8	469	1/31/2018	2/15/2018	785.0	15.1	1.9	7.9	-25.6	6.3
HB17-A9	469	2/15/2018	3/3/2018	448.5	10.5	1.5	7.1	NA	6.7
HB17-A10	469	3/3/2018	3/18/2018	178.6	5.7	0.9	6.3	-24.6	7.2
HB17-A11	469	3/18/2018	4/3/2018	379.4	7.9	1.2	6.7	NA	7.7
HB17-A12	469	4/3/2018	4/17/2018	294.5	7.3	1.0	7.8	-25.4	8.1
HB17-A13	469	4/17/2018	5/1/2018	383.8	8.6	1.3	6.8	NA	6.3
HB17-A14	469	5/1/2018	5/16/2018	132.1	4.6	0.7	7.1	-24.9	6.3
HB17-A15	469	5/16/2018	6/1/2018	284.7	12.5	1.9	6.6	-24.3	5.9
HB17-A16	469	6/1/2018	6/16/2018	85.9	4.3	0.6	6.8	-23.8	5.6
HB17-A17	469	6/16/2018	7/1/2018	139.3	5.3	0.9	6.0	-25.8	6.1
HB17-A18	469	7/1/2018	7/16/2018	167.2	4.4	0.7	6.6	-24.8	9.3
HB18-A1	915	8/3/2018	8/19/2018	242.8	8.4	1.3	6.4	NA	NA
HB18-A2	915	8/19/2018	9/3/2018	248.5	9.3	1.4	6.9	-25.9	NA

Sample ID	Depth (m)	Date open (mm/dd/yyyy)	Date close (mm/dd/yyyy)	TPM (mg m^{-2} d^{-1})	POC (mg C m^{-2} d^{-1})	PN (mg N m^{-2} d^{-1})	C:N ratio	Bulk $\delta^{13}C$ (‰)	Bulk $\delta^{15}N$ (‰)
HB18-A3	915	9/3/2018	9/18/2018	586.6	16.3	2.3	7.0	-25.0	8.6
HB18-A4	915	9/18/2018	10/3/2018	1084.6	23.7	3.3	7.2	-25.2	6.0
HB18-A5	915	10/3/2018	10/19/2018	1435.9	30.4	4.2	7.2	-25.0	6.7
HB18-A6	915	10/19/2018	11/3/2018	718.9	18.8	2.8	6.7	-25.4	NA
HB18-A7	915	11/3/2018	11/18/2018	1180.7	25.2	3.8	6.6	-25.5	6.7
HB18-A8	915	11/18/2018	12/3/2018	797.9	16.8	2.4	7.1	-25.1	NA
HB18-A9	915	12/3/2018	12/19/2018	282.2	9.9	1.5	6.5	-25.4	7.6
HB18-A10	915	12/19/2018	1/3/2019	209.6	5.2	0.8	6.4	-26.0	NA
HB18-A11	915	1/3/2019	1/19/2019	1029.1	22.9	3.6	6.3	-24.6	7.5
HB18-A12	915	1/19/2019	2/2/2019	222.9	5.9	1.0	6.1	-26.6	NA
HB18-A13	915	2/2/2019	2/16/2019	630.5	11.4	1.7	6.7	-25.1	6.9
HB18-A14	915	2/16/2019	3/3/2019	1711.2	24.5	3.6	6.8	-24.8	7.1
HB18-A15	915	3/3/2019	3/19/2019	2383.3	28.4	4.2	6.8	-24.5	7.8
HB18-A16	915	3/19/2019	4/3/2019	3017.3	32.0	4.3	7.5	-24.8	7.2
HB18-A17	915	4/3/2019	4/18/2019	883.9	13.4	1.9	7.0	-24.9	NA
HB18-A18	915	4/18/2019	5/3/2019	1360.2	19.3	2.8	6.8	-25.0	NA
HB18-A19	915	5/3/2019	5/19/2019	2241.3	28.4	4.2	6.8	-24.7	4.5
HB18-A20	915	5/19/2019	6/3/2019	2783.7	35.1	5.2	6.8	-24.9	5.3
HB18-A21	915	6/3/2019	6/18/2019	2036.5	28.4	4.1	6.9	-25.2	6.5

Table B2 δ^{13}C-AA values of 469m and 915m sediment traps.

Sample ID	Depth (m)	Date open (mm/dd/yyyy)	Date close (mm/dd/yyyy)	Phe (‰)	Thr (‰)	Ile (‰)	Leu (‰)	Val (‰)	Asx (‰)	Glx (‰)	Pro (‰)	Ala (‰)	Gly (‰)	Lys (‰)
HB17-C1	469	11/16/2017	12/1/2017	7.0	-2.6	10.9	12.7	17.0	13.6	17.0	17.6	16.1	6.1	11.5
HB17-C2	469	12/1/2017	12/16/2017	7.4	-1.0	NA	12.6	NA	13.1	16.8	16.7	16.3	6.9	8.8
HB17-C4	469	1/31/2018	3/3/2018	6.6	NA	14.6	13.8	18.3	13.7	17.0	17.8	18.2	8.1	4.5
HB17-C5	469	3/18/2018	4/3/2018	6.9	-3.4	12.1	12.4	15.1	12.7	16.4	17.7	16.5	6.6	8.6
HB17-C6	469	4/3/2018	5/1/2018	6.5	-4.0	13.7	12.8	17.7	13.1	16.8	17.1	17.0	6.6	6.5
HB17-C7	469	5/16/2018	6/1/2018	5.2	-2.4	9.5	8.3	13.4	10.8	14.7	10.8	13.2	4.5	-0.6
HB18-C1	915	8/3/2018	9/18/2018	6.5	-4.8	15.7	14.7	18.5	13.7	17.7	16.7	18.9	6.9	5.5
HB18-C2	915	9/18/2018	10/3/2018	6.7	-3.5	10.8	11.6	15.5	14.0	17.1	16.7	16.6	6.5	7.7
HB18-C3	915	10/19/2018	11/3/2018	6.0	-3.4	11.8	12.1	15.2	12.8	17.0	16.5	16.5	6.4	8.0
HB18-C4	915	11/18/2018	12/3/2018	6.7	-2.6	12.3	12.8	17.1	12.9	16.9	16.6	17.3	6.6	6.8
HB18-C5	915	1/3/2019	1/19/2019	7.4	-4.9	12.9	14.8	18.5	14.6	18.3	22.0	19.0	7.1	12.3
HB18-C6	915	2/16/2019	3/3/2019	8.0	-1.7	NA	12.7	9.2	13.4	17.2	16.2	17.2	6.8	8.9
HB18-C7	915	3/3/2019	3/19/2019	7.4	NA	NA	12.6	17.0	13.9	16.3	15.3	17.3	6.3	6.9
HB18-C8	915	3/19/2019	4/3/2019	6.8	NA	12.2	12.2	15.6	12.5	16.0	14.5	17.7	6.7	-1.8
HB18-C9	915	4/3/2019	4/18/2019	6.7	-4.1	NA	13.3	11.8	13.5	16.9	16.6	17.8	5.8	8.8
HB18-C11	915	5/3/2019	5/19/2019	6.8	NA	10.1	10.6	14.3	12.7	14.7	13.8	14.6	7.0	5.4
HB18-C12	915	5/19/2019	6/3/2019	5.9	NA	NA	8.5	13.8	11.6	14.6	12.7	15.0	5.3	8.2

Table B3 δ^{15}N-AA values of 469m and 915m sediment traps.

Sample ID	Depth (m)	Date open (mm/dd/yyyy)	Date close (mm/dd/yyyy)	Phe (‰)	Thr (‰)	Ile (‰)	Leu (‰)	Val (‰)	Asx (‰)	Glx (‰)	Pro (‰)	Ala (‰)	Gly (‰)	Lys (‰)
HB17-C1	469	11/16/2017	12/1/2017	7.0	-2.6	10.9	12.7	17.0	13.6	17.0	17.6	16.1	6.1	11.5
HB17-C2	469	12/1/2017	12/16/2017	7.4	-1.0	NA	12.6	NA	13.1	16.8	16.7	16.3	6.9	8.8
HB17-C4	469	1/31/2018	3/3/2018	6.6	NA	14.6	13.8	18.3	13.7	17.0	17.8	18.2	8.1	4.5
HB17-C5	469	3/18/2018	4/3/2018	6.9	-3.4	12.1	12.4	15.1	12.7	16.4	17.7	16.5	6.6	8.6
HB17-C6	469	4/3/2018	5/1/2018	6.5	-4.0	13.7	12.8	17.7	13.1	16.8	17.1	17.0	6.6	6.5
HB17-C7	469	5/16/2018	6/1/2018	5.2	-2.4	9.5	8.3	13.4	10.8	14.7	10.8	13.2	4.5	-0.6
HB18-C1	915	8/3/2018	9/18/2018	6.5	-4.8	15.7	14.7	18.5	13.7	17.7	16.7	18.9	6.9	5.5
HB18-C2	915	9/18/2018	10/3/2018	6.7	-3.5	10.8	11.6	15.5	14.0	17.1	16.7	16.6	6.5	7.7
HB18-C3	915	10/19/2018	11/3/2018	6.0	-3.4	11.8	12.1	15.2	12.8	17.0	16.5	16.5	6.4	8.0
HB18-C4	915	11/18/2018	12/3/2018	6.7	-2.6	12.3	12.8	17.1	12.9	16.9	16.6	17.3	6.6	6.8
HB18-C5	915	1/3/2019	1/19/2019	7.4	-4.9	12.9	14.8	18.5	14.6	18.3	22.0	19.0	7.1	12.3
HB18-C6	915	2/16/2019	3/3/2019	8.0	-1.7	NA	12.7	9.2	13.4	17.2	16.2	17.2	6.8	8.9
HB18-C7	915	3/3/2019	3/19/2019	7.4	NA	NA	12.6	17.0	13.9	16.3	15.3	17.3	6.3	6.9
HB18-C8	915	3/19/2019	4/3/2019	6.8	NA	12.2	12.2	15.6	12.5	16.0	14.5	17.7	6.7	-1.8
HB18-C9	915	4/3/2019	4/18/2019	6.7	-4.1	NA	13.3	11.8	13.5	16.9	16.6	17.8	5.8	8.8
HB18-C11	915	5/3/2019	5/19/2019	6.8	NA	10.1	10.6	14.3	12.7	14.7	13.8	14.6	7.0	5.4
HB18-C12	915	5/19/2019	6/3/2019	5.9	NA	NA	8.5	13.8	11.6	14.6	12.7	15.0	5.3	8.2

Table B4 Principal component analysis output for Fig. 4a.

Importance of components

	PC1	PC2	PC3	PC4	PC5
Eigenvalue	1.83	1.49	0.91	0.78	0.00
Cumulative portion	0.37	0.66	0.84	1.00	1.00

Vector scores

	PC1	PC2	PC3	PC4	PC5
Phe	-0.50	0.03	-0.38	0.72	0.28
Leu	0.57	0.38	-0.45	-0.08	0.57
Thr	0.23	-0.73	0.33	0.15	0.54
Ile	-0.59	-0.06	-0.14	-0.66	0.44
Val	-0.12	0.57	0.72	0.14	0.34

Sample scores

Sample ID	PC1	PC2	PC3	PC4	Group
HB17-C2	0.63	-0.63	0.16	1.53	469m
HB17-C5	0.48	2.19	1.02	0.39	469m
HB17-C6	2.53	-1.24	0.52	-0.21	469m
HB17-C7	0.27	-0.31	-1.88	0.39	469m
HB18-C1	0.59	2.79	0.43	-0.81	915m
HB18-C2	0.68	2.21	1.61	1.13	915m
HB18-C3	1.80	0.02	1.14	0.57	915m
HB18-C4	2.13	-1.59	0.08	-0.30	915m
HB18-C5	2.45	2.02	-2.30	-0.26	915m
HB18-C6	0.95	-1.06	-1.00	0.56	915m
HB18-C7	1.29	-1.04	1.12	-0.68	915m
HB18-C8	0.50	1.75	-0.30	0.08	915m
HB18-C9	0.93	0.39	1.31	1.62	915m
HB18-C12	-0.89	-1.03	0.26	0.48	915m

Sample scores

Sample ID	PC1	PC2	PC3	PC4	Group
ICEp1	1.48	-0.76	-1.97	0.05	Sea ice algae
ICEp2	0.63	1.31	-1.71	-0.11	Sea ice algae
ICEn1	1.24	1.67	1.67	-1.77	Sea ice algae
ICEn2	0.42	0.24	0.09	0.27	Sea ice algae
ICEn3	0.28	1.68	-0.63	-0.71	Sea ice algae
ICEn1b	1.84	0.05	-0.30	0.22	Sea ice algae
ICEn3b	0.58	-0.70	0.09	0.50	Sea ice algae
ICEn2b	0.52	-0.86	0.25	0.99	Sea ice algae
CF-Sp1	-2.43	-1.25	-0.98	-0.17	Sea ice algae
CF-Sm1	-0.22	0.10	-0.17	-1.02	Sea ice algae
SF-Sp1	-0.40	0.47	-0.92	-2.06	Sea ice algae
SF-Sm1	-0.19	-0.20	-1.04	-0.46	Sea ice algae
NS3L-0-N	-1.22	-0.14	0.93	-0.68	Pelagic algae
NS3L-0.5-N	-0.81	-0.34	0.17	-0.06	Pelagic algae
NS3L-1-N	-1.15	0.13	0.20	-0.71	Pelagic algae
NS3L-0-P	-2.73	0.71	-0.29	0.37	Pelagic algae
NS3L-0.5-P	-2.17	0.25	0.82	-0.47	Pelagic algae
NS3L-1-P	-2.06	-0.26	-0.55	-0.72	Pelagic algae
1-15-1-N	-0.42	-0.29	-0.11	0.77	Pelagic algae
1-15-0.5-P	-0.01	-1.55	0.67	0.31	Pelagic algae
1-15-0-N	-0.54	0.45	-0.35	0.58	Pelagic algae
1-15-1-P	-3.09	1.37	0.33	1.63	Pelagic algae
CF1-Pp1	-0.98	-1.49	0.09	1.09	Pelagic algae
CF1-Pm1	0.50	-0.02	-0.50	1.08	Pelagic algae
CF0-Pp1	-1.45	-0.74	-0.76	-0.04	Pelagic algae
CF0-Pm1	-0.38	-0.97	-0.34	0.80	Pelagic algae
SF1-Pp1	-0.95	0.00	-0.17	-1.03	Pelagic algae
SF1-Pm1	0.65	-0.94	1.58	-0.42	Pelagic algae
SF0-Pp1	0.45	-3.15	0.83	-1.94	Pelagic algae
SF0-Pm1	-1.74	0.75	0.88	-0.81	Pelagic algae

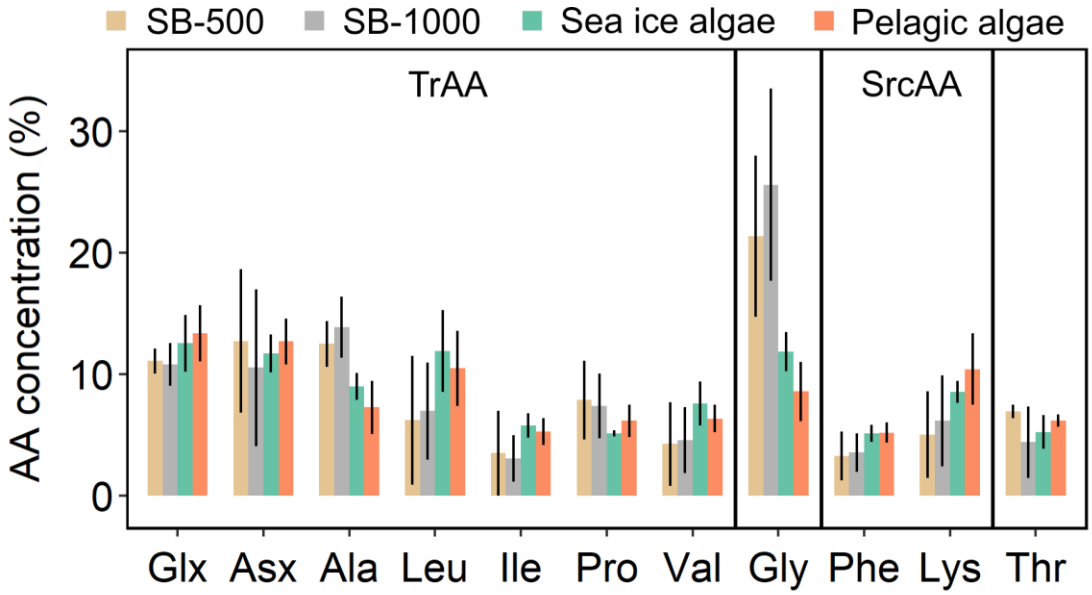

Figure B1 The AA molar composition of sinking particles from SB-500 and SB-1000 sediment traps, sea ice algae, and pelagic algae. Error bars represent ± 1 s.d. of averages of samples (n = 5-18).

APPENDIX C SUPPLEMENTARY MATERIAL FOR CHAPTER 4

C.1 Supplementary Tables and Figures

Table C1 Radiocarbon dates and modelled age for core AMD14-204

Sample depth midpoint (cm)	Lab. ID	Material	^{14}C age (yr BP)	Calibrated age range (cal. yr BP), 1σ	Modeled median age (cal. yr BP)
4.5	ETH-92277	Mixed benthic foraminifera	705 ± 50	167-276	213
70.5	ETH-92279	Mixed benthic foraminifera	1,795 ± 50	1,175-1,270	1,216
70.5	ETH-92278	Mixed planktonic foraminifera	1,710 ± 50	1,032-1,175	1,101
170	SacA 46004	Mixed benthic and planktonic foraminifera	3,555 ± 35	3,139-3,260	3,192
250.5	BETA 467785	Mixed benthic and planktonic foraminifera	4,300 ± 30	4,133-4,254	4,199
310.5	ETH-92281	Mixed benthic foraminifera	4,950 ± 60	4,860-4,992	4,941
310.5	ETH-92280	Mixed planktonic foraminifera	4,940 ± 70	4,930-5,188	5,043
410.5	ETH-92283	Mixed benthic foraminifera	5,805 ± 60	5,905-6,005	5,959
410.5	ETH-92282	Mixed planktonic foraminifera	5,825 ± 60	5,984-6,155	6,063
501.5	BETA 488641	Mixed benthic foraminifera	6,400 ± 30	6,656-6,751	6,707
580.5	ETH-92285	Mixed benthic foraminifera	7,155 ± 70	7,430-7,531	7,483
580.5	ETH-92284	Mixed planktonic foraminifera	7,005 ± 60	7,298-7,417	7,356
610	SacA 46005	Mixed benthic foraminifera and ostracods	7,445 ± 50	7,712-7,822	7,766
700.5	ETH-92286	Mixed benthic foraminifera	8,270 ± 389	8,639-8,885	8,755
737.5	ETH-92287	Mixed benthic foraminifera	8,489 ± 154	9,017-9,302	9,162

Table C2 δ^{13}C-AA values of AMD14-204 sediment core.

Depth (cm)	Age (cal. yrs BP)	Group (cal. kyrs BP)	Phe (‰)	Thr (‰)	Ile (‰)	Leu (‰)	Val (‰)	Asx (‰)	Glx (‰)	Pro (‰)	Ala (‰)	Gly (‰)	Lys (‰)
6.5	243	0.5 to 0.2	-22.55	-7.29	-17.33	-23.40	-20.87	-10.87	-11.05	-14.95	-15.75	-12.84	-16.87
11.5	319	0.5 to 0.2	-22.27	-8.98	-26.03	-23.51	-22.47	-14.49	-14.20	-14.18	-9.98	-23.06	NA
16.5	395	0.5 to 0.2	-24.39	-14.07	-24.28	-27.58	-25.64	-17.50	-17.91	-17.75	-17.00	-11.41	-9.34
138.5	2566	3.0 to 2.5	-24.09	-11.38	-19.99	-23.40	-21.35	-11.73	-11.13	-13.52	-16.47	-10.82	-15.92
148.5	2764.6	3.0 to 2.5	-21.64	NA	-22.74	-21.30	-19.54	-9.39	-9.16	-12.99	-5.27	-15.72	NA
158.5	2963.2	3.0 to 2.5	-23.38	-11.10	-23.99	-25.21	-21.38	-14.63	-16.15	-16.73	-15.34	-9.00	-8.57
290.5	4693.6	5.0 to 4.5	-25.04	-19.51	-20.64	-24.73	-22.62	-14.69	-14.15	-16.19	-17.45	-12.17	-16.63
300.5	4817.4	5.0 to 4.5	-21.95	-5.58	-23.80	-21.75	-20.64	-11.92	-12.68	-13.63	-5.02	-18.00	NA
310.5	4941.3	5.0 to 4.5	-24.29	-10.86	-21.58	-26.60	-24.49	-13.93	-16.03	-16.98	-16.04	-8.23	-8.52
462.5	6386.3	7.0 to 6.0	-24.76	-12.14	-17.32	-23.06	-21.00	-12.27	-12.81	-15.40	-17.60	-9.66	-16.04
472.5	6468.5	7.0 to 6.0	-23.48	NA	-16.56	-22.99	-20.11	-8.93	-11.56	-14.77	-8.97	-17.46	-15.05
482.5	6550.7	7.0 to 6.0	-24.46	-13.41	-30.52	-27.10	-24.09	-15.83	-17.69	-16.91	-18.46	-9.30	-10.92
562.5	7305.8	8.0 to 7.0	-25.15	-12.03	-20.18	-22.90	-20.88	-10.98	-13.35	-16.88	-18.17	-10.33	-16.23
582.5	7501.8	8.0 to 7.0	-23.18	NA	-17.66	-22.91	-19.90	-10.80	-15.76	-15.01	-7.55	-13.10	-14.25
594.5	7617.2	8.0 to 7.0	-25.26	-10.60	-25.33	-29.77	-24.86	-15.35	-17.98	-17.85	-16.03	-8.37	-10.60
694.5	8689	9.2 to 8.0	-25.34	-4.85	-20.48	-23.23	-20.04	-13.92	-14.63	-16.59	-18.10	-10.12	-16.30
704.5	8798.6	9.2 to 8.0	-23.07	1.01	-18.97	-22.65	-19.94	-10.79	-17.10	-14.66	-4.19	4.73	-12.74
714.5	8908.8	9.2 to 8.0	-25.17	NA	-23.10	-28.68	-25.91	-16.89	-18.11	-19.63	-18.55	-8.18	-11.11

Table C3 δ^{15}N-AA values of AMD14-204 sediment core.

Depth (cm)	Age (cal. yrs BP)	Group (cal. kyrs BP)	Phe (‰)	Thr (‰)	Ile (‰)	Leu (‰)	Val (‰)	Asx (‰)	Glx (‰)	Pro (‰)	Ala (‰)	Gly (‰)	Lys (‰)
6.5	243	0.5 to 0.2	NA	4.53	NA	11.75	18.64	12.02	14.82	14.63	17.63	7.17	11.70
11.5	319	0.5 to 0.2	7.61	NA	11.92	10.24	16.37	13.55	16.75	13.74	17.42	7.65	8.16
16.5	395	0.5 to 0.2	8.22	5.83	12.88	10.30	16.51	12.08	16.56	13.94	18.67	7.47	7.64
138.5	2566	3.0 to 2.5	8.08	NA	11.11	11.01	17.56	13.94	16.18	14.60	17.00	6.40	9.24
148.5	2764.6	3.0 to 2.5	8.21	NA	11.71	10.60	17.06	NA	16.79	13.98	18.23	8.32	7.98
158.5	2963.2	3.0 to 2.5	8.23	NA	12.95	10.20	17.10	12.55	16.53	14.06	19.49	8.58	8.01
290.5	4693.6	5.0 to 4.5	8.79	NA	10.11	10.71	16.32	12.28	15.93	14.52	16.72	6.01	8.86
300.5	4817.4	5.0 to 4.5	8.04	NA	NA	10.64	15.94	13.44	16.42	14.00	17.26	8.01	8.21
310.5	4941.3	5.0 to 4.5	8.65	NA	12.11	12.16	17.45	12.80	15.64	14.43	18.65	9.84	8.39
462.5	6386.3	7.0 to 6.0	8.37	NA	11.05	10.87	17.31	NA	16.61	15.65	17.58	8.76	9.07
472.5	6468.5	7.0 to 6.0	7.85	NA	NA	10.84	NA	NA	16.82	13.82	17.95	8.28	8.98
482.5	6550.7	7.0 to 6.0	8.42	NA	12.82	10.48	17.03	13.43	17.20	14.71	18.59	9.44	8.55
562.5	7305.8	8.0 to 7.0	10.65	NA	10.38	12.19	17.87	15.02	18.03	15.98	18.26	7.88	9.29
582.5	7501.8	8.0 to 7.0	7.59	NA	NA	10.72	NA	13.58	17.62	14.21	16.79	8.56	8.09
594.5	7617.2	8.0 to 7.0	9.18	NA	12.24	11.15	18.11	13.60	17.82	14.45	19.50	9.56	8.79
694.5	8689	9.2 to 8.0	9.08	NA	NA	11.11	16.94	NA	17.03	15.49	NA	NA	9.28
704.5	8798.6	9.2 to 8.0	7.85	NA	NA	10.49	NA	NA	17.40	14.43	NA	NA	7.96
714.5	8908.8	9.2 to 8.0	8.52	NA	NA	11.06	18.49	14.88	18.36	15.81	NA	NA	8.73

Table C4 Linear discriminant analysis output for Fig. 4.7.

Coefficients of linear discriminants

	LD1	LD2
Phe	0.49	5.05
Thr	0.92	4.15
Ile	0.59	4.89
Leu	0.25	4.26
Val	0.20	4.59

Proportion of trace

LD1	LD2
0.86	0.14

Posterior probabilities of the sediment samples

Age	Period	Predicted (% probability)		
		Heterotrophic bacteria (B)	Sea ice algae (C)	Pelagic algae (P)
243	0.5 to 0.2	1.2	36.6	**62.3**
319	0.5 to 0.2	**53.1**	28.7	18.3
395	0.5 to 0.2	10.0	1.1	**88.9**
2566	3.0 to 2.5	**70.3**	0.7	29.0
2963.2	3.0 to 2.5	**69.9**	1.6	28.6
4693.6	5.0 to 4.5	**99.3**	0.0	0.7
4817.4	5.0 to 4.5	4.9	**91.9**	3.2
4941.3	5.0 to 4.5	1.2	18.8	**79.9**
6386.3	7.0 to 6.0	**65.7**	0.2	34.1
6550.7	7.0 to 6.0	**94.7**	0.5	4.8
7305.8	8.0 to 7.0	**95.2**	0.1	4.7
7617.2	8.0 to 7.0	0.2	**61.0**	38.8
8689	9.2 to 8.0	0.1	**99.3**	0.5
8798.6	9.2 to 8.0	0.0	**100.0**	0.0